Stochastic dynamics of biological populations in changing environments

A thesis submitted to the University of Manchester
for the degree of Doctor of Philosophy
in the Faculty of Science and Engineering

2021

Ernesto Berríos-Caro

School of Natural Sciences

Contents

Abstract 10

Declaration 11

Copyright Statement 12

Acknowledgements 13

1 Introduction **15**

1.1 The classical physicist's approach to modelling biological systems . . . 15

1.2 Changing environments in biology 17

1.3 Thesis structure and format 18

1.4 List of works included in this thesis 23

1.5 List of works not included in this thesis 23

Bibliography 24

2 Theoretical Background **27**

Abstract 27

2.1 Markov processes 27

2.1.1 Definition and notation 27

2.1.2 Kolmogorov equations 28

2.1.3 Generating functions 29

2.2 Homogeneous birth-death processes 30

2.2.1 General birth-death process 30

2.2.2 Poisson process 33

2.2.3 Pure birth process (Yule–Furry process) 34

2.2.4 Simple birth-death process 35

2.2.5 Birth-death process with non-linear growth rates 37

2.3 Non-homogeneous birth-death process 40

2.4 Fluctuating environments . . . 42
2.4.1 Discrete space: switching environments . . . 43
2.4.2 Continuous space . . . 46
2.5 Further computational and mathematical tools . . . 49
2.5.1 Numerical methods to simulate stochastic systems . . . 49
2.5.2 Partitions of integer numbers . . . 54
Bibliography . . . 56

3 Mutators drive evolution of multi-resistance to antibiotics 59
Preface . . . 59
Abstract . . . 61
3.1 Introduction . . . 61
3.2 Results . . . 64
3.2.1 Mutators facilitate double resistance evolution by sequential acquisition of independent mutations . . . 64
3.2.2 No evidence for a growth advantage of double resistance in single-drug treatments . . . 66
3.2.3 Effect of mutator frequency on growth . . . 67
3.2.4 Stochastic simulations reveal evolutionary mechanisms of multi-resistance evolution . . . 68
3.3 Discussion . . . 73
3.4 Conclusion . . . 76
3.5 Data availability . . . 76
3.6 Methods . . . 76
3.6.1 Strains and media . . . 76
3.6.2 Selection experiment under single-drug and combination treatments 77
3.6.3 Detection and analysis of resistance . . . 78
3.6.4 Growth parameters of single- and double-resistant clones . . . 80
3.6.5 Mutation rate estimates . . . 81
3.6.6 Stochastic population dynamics model . . . 82
3.7 Extended data . . . 84
3.8 Appendix A: Stochastic population dynamics model of resistance evolution 84

3.8.1 Description of the model 84
3.8.2 Binomial approximation for stochastic growth processes 86
3.8.3 Growth of bacteria 89
3.8.4 Mutations 91
3.8.5 Estimating growth parameters from experimental data 92
3.8.6 Relationship between optical density and bacterial population size 98
3.8.7 Simulating the experiments 100
3.9 Appendix B: Bayesian statistical analysis of experiments and simulations 102
3.9.1 Model M1: Detection of resistance arising during experimental evolution 102
3.9.2 Model M2: Growth of strains derived from fluctuation tests . . 111
3.9.3 Model M3: Growth of double resistant strains from selection experiment 113
3.9.4 Model M4: Detection of resistance arising during simulation . . 115
Bibliography 117

4 Competition delays multi-drug resistance evolution during combination therapy 125
Preface 125
Abstract 126
4.1 Introduction 126
4.2 Stochastic Model 129
4.2.1 General definitions 129
4.2.2 Mean growth laws and production rates of mutants 131
4.2.3 Specific growth laws 132
4.2.4 Effect of drug treatment on growth rates 137
4.3 Probability of single and double resistance 139
4.3.1 Extinction probability of single strains 139
4.3.2 Single resistance 140
4.3.3 Double resistance 141
4.3.4 Numerical integration of the probabilities of resistance 141
4.4 Probability of resistance for growth with constant coefficients 144

4.4.1 Setup, and comparison of theory and simulation 144
4.4.2 Single resistance 146
4.4.3 Double resistance 149
4.5 Time-dependent drug concentrations 153
4.5.1 Sinusoidal drug concentrations 154
4.5.2 Pulsing drug concentrations 155
4.5.3 Probability of double resistance for time-dependent dosing schedules 156
4.6 Limitations of deterministic approximation and possible extensions of the model 158
4.7 Conclusions 160
4.8 Appendix A: Derivation of the probabilities of single and double resistance for general birth and death rates 162
4.8.1 Extinction probability for single cell and its lineage 163
4.8.2 Probability of no resistance 163
4.9 Appendix B: Probabilities of resistance for the exponential growth model (EG) with constant growth coefficients 166
4.10 Appendix C: Probabilities of resistance for the logistic growth model without competition between strains (LG) 168
4.10.1 Constant coefficients 168
4.10.2 Time-dependent rates 171
4.11 Appendix D: Probabilities of resistance for the logistic model with between-strain competition (CLG) 172
4.12 Appendix E: Further supplementary results 173
4.12.1 Probability of double resistance for constant growth rates 173
4.12.2 Further tests of theoretical predictions for resistance against numerical simulations 175
4.12.3 Probability of single and double resistance for time-dependent dosing schedules 176
4.13 Appendix F: Limitations of the analytical approach 179
Bibliography 179

5 Switching environments, synchronous sex, and the evolution of mating types **185**

Preface . . . 185

Abstract . . . 186

5.1 Introduction . . . 186

5.2 Model definitions . . . 189

5.2.1 Population dynamics . . . 189

5.2.2 Environmental dynamics . . . 192

5.2.3 Reduced model . . . 192

5.3 Stationary distribution for the number of mating types under environmental switching . . . 196

5.3.1 Slow environmental switching . . . 198

5.3.2 Fast environmental switching . . . 200

5.3.3 Transition between slow and fast switching regimes . . . 201

5.4 Selective sweeps in the switching environmental model . . . 212

5.5 Conclusions . . . 216

5.6 Appendix A: Effective rates $T^{-}_{M|\sigma}$ and $T^{+}_{M|\sigma}$ as function of $P^{\mathrm{st}}_{\mathbf{n}|\sigma}$ . . . 220

5.6.1 Calculation of the effective rate $T^{-}_{M|p_S}$ . . . 221

5.6.2 Calculation of the effective rate $T^{+}_{M|p_S}$ . . . 224

5.7 Appendix B: Closed-form solutions of $T^{-}_{M|p_S}$, $T^{+}_{M|p_S}$, and $P^{st}_{M|p_S}$ . . . 225

5.7.1 Asexual environment ($p_S = 0$) . . . 226

5.7.2 Facultative sex ($0 < p_S < 1$) and sexual environment ($p_S = 1$) . 228

5.7.3 Alternative expressions of rates $T^{-}_{M|p_S}$ and $T^{+}_{M|p_S}$ for cases $0 < p_S \leq 1$ . . . 233

5.7.4 Comparison against numerical simulations with fixed environment 235

5.7.5 Comparison against numerical simulations with switching environments . . . 235

5.8 Appendix C: Markov chain generator matrix approach . . . 237

5.8.1 Comparison against simulations . . . 238

5.8.2 Theoretical prediction of $P^{\mathrm{st}}_{M,\sigma}$ for each environment . . . 239

5.8.3 Transition between slow and fast switching regimes for low and high p_S . . . 239

5.8.4 Analytical results from the generator-matrix approach 240
5.9 Appendix D: Selective sweeps 244
5.9.1 Switching environments 245
5.9.2 Fixed asexual environment 248
Bibliography 248

6 Beyond the adiabatic limit in systems with fast environments: a τ-leaping algorithm 253

Preface 253
Abstract 254
6.1 Model setup and general principles of the algorithm 258
6.1.1 Model definitions and notation 258
6.1.2 General principles of the τ-leaping algorithm for systems in fast environments 259
6.2 Construction of the τFE algorithm for systems with discrete environments 261
6.2.1 Preliminary analysis of the environmental process 261
6.2.2 Time-averaged reaction rates as random variables 263
6.2.3 Description of the algorithm 264
6.3 Application of the τFE algorithm to models with discrete environmental states 265
6.3.1 Genetic circuit: two system-independent environments, two species 266
6.3.2 Birth-death process: three environments, two species 268
6.3.3 Bimodal genetic switch: three system-state dependent environments, two species 272
6.4 Numerical simulation of continuous-environmental systems 277
6.4.1 Setup 277
6.4.2 Implementation of the τFE algorithm for continuous environments 278
6.4.3 Conventional simulation approaches for discrete populations in continuous environments 278
6.5 Application of the τFE to continuous-environmental models 281

6.5.1 Toy model: Population dynamics with production and removal rates proportional to σ^2 . . . 281
6.5.2 Genetic switch with Hill-like regulatory function . . . 285
6.6 Discussion and conclusions . . . 287
6.7 Appendix A: Second moments of rates . . . 290
6.8 Appendix B: Further details for systems with two species and two environmental states . . . 291
6.9 Appendix C: Birth-death process with two species and three environmental states . . . 292
6.10 Appendix D: Bimodal genetic switch . . . 294
6.11 Appendix E: Gillespie algorithm with discretised environmental dynamics (GADE) . . . 295
6.12 Appendix F: Additional examples of production-removal processes in continuous environments . . . 295
6.12.1 Rates $R_{r,\sigma}(n) = \alpha_r \sigma \Theta(\sigma)$ . . . 296
6.12.2 Rates $R_{r,\sigma}(n) = \alpha_r |\sigma|$ . . . 296
Bibliography . . . 297

7 Conclusions **301**
7.1 Overview of the thesis . . . 301
7.2 Summary of results . . . 302
7.3 Future research and final remarks . . . 305
Bibliography . . . 307

Word count 70030

The University of Manchester

Stochastic dynamics of biological populations in changing environments

Ernesto Berríos-Caro

Doctor of Philosophy

January 20, 2021

Abstract

The focus of this thesis is the study of biological populations subject to external changing environments exploring a number of theoretical, numerical, and experimental approaches. We study different classes of environments, considering cases whose evolution over time is deterministic or stochastic.

The first class of environments we consider vary deterministically. Here we focus on the study of microbial resistance in bacterial populations subject to therapies of one or two antibiotics. The environment specifies the drug concentration administered to the population, so it is determined by the type of dosing schedules. We investigate how subpopulations with higher mutation rates drive the emergence of multi-drug resistance. We approach this problem analysing experimental data (obtained by Dr. Danna Gifford), comparing their observations against stochastic simulations of a multi-type branching model we design.

In separate work related to the previous one, we explore the delaying effect of competition on the emergence of single and double resistance through theoretical predictions of a similar stochastic model. We calculate the probability of having at least one resistant cell for dosing schedules with constant and time-dependent drug concentrations using a theoretical approach based on branching processes.

The second class of environments we consider vary stochastically. The first system we study is a Moran-type model, describing a population subject to a switching environment that determines the type of reproduction, namely sexual or asexual. The population can exhibit several number of 'mating types' (analog to male/female sexes, but not restricted to two) that depends on the rate of reproduction, as well as the mutation rate (i.e., inclusion of new types). We investigate the stationary distribution of the number of mating types for different switching regimes. We show that for slow switching regimes the distribution can become bimodal, while for fast switching the system behaves as if there was one single effective environment. Our approach exploits properties of branching processes and integer partitions in number theory.

Lastly, we study and design an algorithm based on the so-called τ-leaping algorithm, focusing on systems with fast fluctuating environments. Our algorithm treats the input rates for the τ-leaping as (clipped) Gaussian random variables with first and second moments constructed from the environmental process. Several biological examples are explored, such as genetic circuits, birth-death processes, and genetic switches. We consider cases with discrete and continuous environmental spaces. The algorithm can produce results for macroscopic observables in fluctuating regimes beyond the adiabatic limit (i.e., infinitely fast switching) that are in good agreement with measurements from other simulation methods, but with a significantly reduced computing time.

Declaration

No portion of the work referred to in the thesis has been submitted in support of an application for another degree or qualification of this or any other university or other institute of learning.

Copyright Statement

i. The author of this thesis (including any appendices and/or schedules to this thesis) owns certain copyright or related rights in it (the "Copyright") and s/he has given The University of Manchester certain rights to use such Copyright, including for administrative purposes.

ii. Copies of this thesis, either in full or in extracts and whether in hard or electronic copy, may be made **only** in accordance with the Copyright, Designs and Patents Act 1988 (as amended) and regulations issued under it or, where appropriate, in accordance with licensing agreements which the University has from time to time. This page must form part of any such copies made.

iii. The ownership of certain Copyright, patents, designs, trade marks and other intellectual property (the "Intellectual Property") and any reproductions of copyright works in the thesis, for example graphs and tables ("Reproductions"), which may be described in this thesis, may not be owned by the author and may be owned by third parties. Such Intellectual Property and Reproductions cannot and must not be made available for use without the prior written permission of the owner(s) of the relevant Intellectual Property and/or Reproductions.

iv. Further information on the conditions under which disclosure, publication and commercialisation of this thesis, the Copyright and any Intellectual Property and/or Reproductions described in it may take place is available in the University IP Policy (see http://documents.manchester.ac.uk/DocuInfo.aspx?DocID=487), in any relevant Thesis restriction declarations deposited in the University Library, The University Library's regulations (see http://www.manchester.ac.uk/library/aboutus/regulations) and in The University's Policy on Presentation of Theses.

Acknowledgements

I am very much thankful for the support of my supervisor Tobias Galla over the course of my Ph.D. The work presented in this thesis would not have been possible without his patience, dedication, and enthusiasm in doing science. I am also very thankful to Danna Gifford, my co-supervisor, for her support, dedication, and all her effort in explaining biology to physicists.

I would also like to thank the people with whom I have collaborated in the different projects that compose this thesis, to Christopher Knight, Marc Suñé, George Constable, and Yen Ting. Thank you for all the stimulating discussions and instructive feedback on my work. I would also like to mention my office mates: Joe, Laura, Francisco, Peter, Annie, Pierre, Rory, Henry, and Gabriel, for making my Ph.D. a more fun and less stressful experience. Thank you all for the good memories in room 7.26. My thanks to Niels Walet as well for his willingness to solve any technical issue, to Iván Vera for his support as advisor, and to The University of Manchester PDS award for making this research possible.

I am also deeply grateful for the unconditional support of my parents, sister, and grandparents, who constantly encouraged me despite the distance. My thanks as well to the people from City Church Manchester and my Connect group for caring about me. I should also mention sensei David Castán de Amo from Bujinkan Senki Dojo, and my French teachers Mathilde Savary and Amani Lowey from The University of Manchester. Thank you all for being such an inspiration.

Finally, I would like to thank the support of my friends from Chile and the friends I made in Manchester who are too numerous to mention. My deepest thanks to all of you for your constant encouragement during these years.

Chapter 1

Introduction

1.1 The classical physicist's approach to modelling biological systems

The last century brought a considerable increase in the interest of scientists in the mathematical modelling of biological systems. To a great extent, this has been due to the substantial development of experimental techniques, such as microscopic or blotting techniques, which have enlightened us about the complexity of the world of living organisms. Biologists, on the one hand, have realised the need to quantify the behaviour of biological systems in order to make predictions. Physicists and mathematicians, on the other hand, are trying to expand their self-centred circle of inquisitiveness, realising the interesting complexity of biological problems and the usefulness of mathematical and physical techniques to approach them.

Mathematical modelling in biology has a rich and varied history. Early examples can be found in the 13th century when Fibonacci used his famous series to study the growth of populations of rabbits [1]. Since then, and particularly from the 18th century onwards, the modelling has been focused on different areas of study, such as cell biology, genetics, population dynamics, ecology, to name a few [2–5]. Physicists' modelling of biology often apply methods (although not exclusively) from statistical physics [6–8] and non-linear dynamics [9]. Whichever approach used, the biological system under study is considered as a dynamical system comprised of interacting parts, often being individuals such as microbes or plants, that can exchange matter and

energy. The approach used to model the behaviour of such system will depend on what kind of description one wants to develop. In many cases, randomness will not play an important role and one can treat the system as *deterministic*, describing it using differential equations. This is the case, for example, of prey-predator models [10], Turing patterns in vegetation clusters [11], neural models [12], tumour growth models [13], among many others [2, 3]. When randomness cannot be ignored, the approach to model the system will be *stochastic*.

Stochastic processes are often used in biology when the dynamics of the system are driven by randomness. Such is the case, for example, of systems with small populations in which fluctuations cannot be neglected. Common examples from *evolutionary biology* include cancer modelling [14], antibiotic resistance [15], population genetics [16], evolutionary rescue [17], among others. In these scenarios the stochasticity is *intrinsic*, i.e., it is inherent to the system. This can arise, for instance, through mutations within a population that occur at random or the stochastic sequence of reproduction events in small populations. In other situations, the stochasticity is present in an *extrinsic* way when external sources that affect the system vary randomly, e.g., in presence of an external fluctuating environment [18]. Independently of the nature of the stochasticity of the system, often two methods are used to approach modelling randomness in populations. The first consists in performing analysis of experimental data, applying statistical methods to characterise the complexity of the system under study. The focus on these approaches is usually of producing reliable data and gaining useful information that can enlighten about the behaviour the system. The second approach consists in constructing theoretical models that can capture the main features of the system, such that they are able to predict their evolution over time. As often is the case in physics, these models rely on simplifications and idealisations of the interactions between the different agents within the system.

When constructing stochastic theoretical models to understand the dynamics of a biological population, the system is treated as interacting individuals (or agents) following certain rules determined by the conditions to which they are subject. These models are usually termed as *individual-based models* (IBM) [19, 20]. In some way, this is similar to the classical physics problem of considering interacting particles subject to forces with given constraints. For the study of IBM, well-known tools from

stochastic processes are often employed, such as master equations, generating functions, Kramers–Moyal expansions, Fokker–Planck equations, [21], among others. Cases in which the analytical tractability of the system is limited, one can resort to stochastic *numerical simulations*, such as Monte Carlo methods [22]. Simulations act as virtual realisations of experiments from which we can make observations of the system and verify the theoretical predicts of toy models as done in classical physics. The main difference from the classical physicist's perspective, however, is that when studying biology, one has to deal with a living world composed of unpredictable active agents that do not necessarily act in the same way. Quotting words of the celebrated physicist Erwin Schrödinger from his book *What is Life*? [23], when modelling biology the classical physicist will wonder:

> *"How can the events in space and time which take place within the spatial boundary of a living organism be accounted for by physics and chemistry?".*

The present thesis does not try to answer this question. This thesis, instead, is an attempt to illustrate the usefulness of stochastic processes for understanding biological phenomena. Our attempt is to explore different relevant biological scenarios from the point of view of physics by applying a number of mathematical and numerical tools, combined with experiments carried out by my collaborators to investigate them.

1.2 Changing environments in biology

The central theme of this thesis is the study of how external changing environments affect biological populations. We understand environment as any external condition, such as temperature, pressure, drug concentrations, resources, etc., that can affect the dynamics of a biological system. Environments play a fundamental role in the evolution of a population due to their coupling to different parameters of the system. Environments can, for example, increase abundance fluctuations [24] or alter mutation rates within a population [25]. Environments can even drive a population to extinction and cause biological systems to adapt in order to survive, an effect called *evolutionary rescue* [26].

Given the relevance of environments to biological populations, there has been an increasing interest in proposing different mathematical schemes to approach them. In

many cases, environments are best characterised as deterministic. Such cases include, for example, seasonal variations in models of epidemic spread [27], periodic variations in population dynamics [28], pulsed administration strategies in cancer therapies [29], treatment protocols in antibiotic resistance [30], among others. It is common for such cases to treat the environment as a dynamical system and employ methods from non-linear dynamics to study them [31].

In other cases, the unpredictability of changes in environments makes it more suitable to use a stochastic description. Depending on the nature of the environment, in some situations it will be more appropriate to consider a continuous space to model the environmental dynamics. Such cases can be studied by incorporating the effect of fluctuating environments as extrinsic noise [32]. A continuous space may be suitable to model environmental fluctuations in ecology and evolutionary biology when there are changes in abundance of resources, presence of detrimental substances, variations in temperature, etc [24, 33–35].

For many scenarios, it is more suitable to consider a discrete space to model the environmental dynamics. Such cases are often called *switching environments*, as the environmental state switches between certain collection of discrete states determined by the biological system. This can be the case of switching between phenotypical states in cell populations [36, 37], fitness variations in genotypes [38], binding of promoter sites in proteins [39], abrupt changes in carrying capacities [40], among others.

A system in a fluctuating environments is not only subject to the external noisy effect of its surroundings, but can also be driven by the intrinsic noise from the stochasticity within the system. In such cases, it is of interest to mathematically understand the effect of coupling on the system of these two sources of stochasticity [32, 41].

1.3 Thesis structure and format

This thesis explores systems subject to different types of environments, such that some of them will vary deterministically, and others stochastically. Both discrete and continuous environmental spaces are investigated, as well as different types of effects on the individual-based model under study. The methods used include theoretical, numerical, and experimental approaches, providing thus different perspectives of how

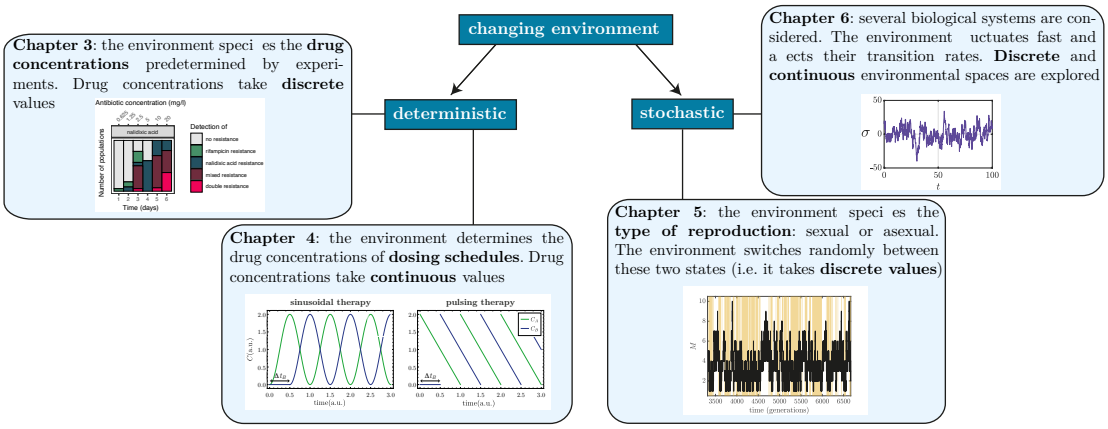

Figure 1.1: Schematic representation of the chapters in this thesis. Each chapter considers different types of external environments: in Chapters 3 and 4 the environment varies deterministically, while in Chapters 5 and 6 it varies stochastically.

stochastic processes can be employed in the modelling of biological phenomena. The experiments are performed by my co-supervisor Dr. Danna R. Gifford from the Division of Evolution and Genomic Sciences, School of Biological Sciences, The University of Manchester.

We proceed now to briefly explain how this thesis is structured, providing an overview of the main contents of each chapter and the main features of the system under study, and the role of the changing environment.

This thesis is written following the journal format of The University of Manchester, built around 4 articles presented in Chapters 3-6. Each of these chapters encloses the content of the papers, with typeset modifications to fit the requirements of the thesis' format from The University of Manchester. The paper in Chapter 4 is published in *Journal of Theoretical Biology*, while the papers in Chapters 3, 5, and 6 are under review at *Nature Ecology*, *Theoretical Population Biology*, and *Physical Review E*, respectively. The preface of each chapter contains a journal or preprint reference of the respective paper.

Figure 1.1 shows a schematic representation of the structure of this thesis, illustrating how the environment acts in the model studied in each chapter. This thesis is structured as follows:

Chapter 1: Theoretical Background. In this chapter, we provide some theoretical background of stochastic processes, including definitions of concepts such as Markov chains and master equations; we also describe birth-death processes, changing

environments, the numerical schemes used throughout this thesis, and some methods of number theory about partitions of integer numbers (these will be only used in Chapter 5).

Chapter 3: Mutators drive evolution of multi-drug resistance to antibiotics. In this chapter, we study an experimental setup developed by Dr. Danna R. Gifford of a bacterial population subject to antibiotic therapies of one and two antibiotics. The experiment consists of a number of days of growth with drug concentrations that are doubled daily, in which the population is diluted (i.e., reduced) by a certain factor at the end of each day. The drug concentration remains constant each day. We investigate the role of subpopulations with higher mutation rates on the emergence of single and double resistant cells. Our approach in this chapter is to develop a stochastic model that incorporates growth parameters measured from experiments, such that it can capture the evolution of the proportion of resistant cells throughout the experiment. The growth parameters used in the model are measured by fitting growth curves to experimental data of the bacterial populations. The bacteria exhibit a *diauxic growth* (i.e., growth with two phases) that is taken into account in our model. The model incorporates competition as well, based on the competitive Lotka–Volterra equations [42]. The environment here determines the drug concentration applied, and is coupled to the growth rate and carrying capacity of the bacterial population. Since the concentration is constant in each day of the experiment, the environmental space is discrete.

Given the large number of parameters present in the system and the complexity of the population growth, we do not focus on trying to deduce theoretical predictions of the evolution of resistance. Instead, we perform stochastic numerical simulations of our model, employing a numerical scheme that we design. This scheme uses binomial distributions to model the distribution of the number of offspring of each strain present in the system. Using binomial distributions allows us to reduce the computational running time to simulate the experiment, and to incorporate dilutions in a simple way. We find that the predictions of our model are in good agreement with the experimental observations.

Chapter 4: Competition delays multi-drug resistance evolution during combination therapy. This chapter focuses on a model similar to that in Chapter 3.

In contrast to the previous chapter, the work here is analytical and computational, and does not include laboratory experiments. Here we consider a cell population subject to a combination therapy of two drugs, in which the environment is determined by the concentrations of the drugs applied. The environment also determines the concentrations of the drugs applied. However, this time we allow the concentration to vary continuously over time. The focus of this study is on calculating the probabilities of having at least one resistant individual to one or both drugs, and compare the evolution over time of this probability for different types of growth models and drug treatments. The theoretical framework we employ is an extension of the work by Michor and Foo [43]. We consider three growth models: one with exponential growth, another with logistic growth with no competition between strains, and another with logistic growth and competition between strains. The latter is based on the competitive Lotka–Volterra equations [42].

We first test our predictions by allowing one growth parameter to vary while keeping the rest as constant. We find that the inclusion of competition can considerably delay the emergence of single resistance when resources are scarce, and can delay the emergence of double resistance for both scarce and abundant resources. We also test our predictions assuming time-dependent drug therapies (dosing schedules) that incorporate some features of clinical treatments. We find again that competition delays the emergence of resistance, and that it can alter the optimum treatment, i.e., the one that best delays the emergence of resistance.

Chapter 5: Switching environments, synchronous sex, and the evolution of mating types. In this chapter, we consider a finite population whose dynamics is driven by a Moran-like model, in which its individuals are allowed to reproduce either sexually or asexually. The environment here specifies the type of reproduction and switches stochastically between the sexual and asexual modes of reproduction. This model is an extension of the work done by Constable and Kokko [44]. Each individual in the population is of a certain *mating type*, which is analog to the male/female sexes but not restricted to two. The number of mating types represented in the population of N individuals can range from one to N. In the former case, all individuals are of the same mating type. In the latter, each member of the population represents a different mating type. This number depends on the reproduction rate of the population, as

well as the mutation rate (i.e., inclusion of new types). Our focus here is to study the stationary distribution of the number of mating types for different switching regimes of the environment.

The method we employ to calculate the distribution of the number of mating types is based on techniques from number theory, in which we exploit properties of partitions of integer numbers. This method allows us to obtain analytical solutions of the distribution for cases with non-switching environments. These solutions are then used to approximate the distribution in switching environments using methods from branching processes. We find that when the environmental switching is fast, the system behaves as if it was in a single effective environment. However, when the environment switches slowly, we see some differences such as a lower number of mating types at equilibrium and bimodality in the stationary distribution of mating types. We also demonstrate how additional biological processes such as selective sweeps can be accounted for in this switching-environment framework.

Chapter 6: Beyond the adiabatic limit in systems with fast environments: a τ-leaping algorithm. In this chapter, we focus on the design of an algorithm based on the so-called τ-leaping algorithm [45] for systems subject to a fast fluctuating environment. Our algorithm works in discrete time and treats the input rates for the τ-leaping as (clipped) Gaussian random variables with first and second moments constructed from a fast environmental process. Several biological scenarios are explored, such as genetic circuits, birth-death processes, and genetic switches, in which we explore both discrete and continuous environments. The environment is coupled to different transition rates in each system under study.

We test our algorithm by comparing the outcome of relevant stochastic quantities, such as stationary distribution and mean switching times, against predictions of standard algorithms. For discrete environmental cases we compare our predictions against the continuous-time Gillespie algorithm [46, 47]. For continuous environmental cases we construct a number of algorithms based on well-known approaches such as the Gillespie algorithm, and the Euler-Maruyama method [48]. We demonstrate that our algorithm can capture features of the system for switching regimes beyond the adiabatic limit (i.e., the limit of infinitely fast switching systems).

Chapter 7: Conclusions. Lastly, in this chapter we present final remarks, possible

future research directions, and general conclusions of this thesis.

1.4 List of works included in this thesis

The present thesis is based on the following manuscripts:

- D. R. Gifford, E. Berríos-Caro, C. Joerres, T. Galla, and C. G. Knight, "Mutators drive evolution of multi-resistance to antibiotics", bioRxiv preprint, bioRxiv: 643585 (2019). [**Under review at *Nature Ecology and Evolution***]

- E. Berríos-Caro, D. R. Gifford, and T. Galla, "Competition delays multi-drug resistance evolution during combination therapy", Journal of Theoretical Biology 509, 110524 (2021).

- E. Berríos-Caro, T. Galla, and George W. A. Constable, "Switching environments, synchronous sex, and the evolution of mating types", bioRxiv preprint, bioRxiv 2020.07.31.230482 (2020). [**Under review at *Theoretical Population Biology***]

- E. Berríos-Caro and T. Galla, "Beyond the adiabatic limit in systems with fast environments: a τ-leaping algorithm", arXiv preprint, arXiv 2011.10748 (2020). [**Under review at *Physical Review E***]

1.5 List of works not included in this thesis

Some works done in parallel are listed below. These are not included in this thesis:

- E. Berríos-Caro, M. G. Clerc, M. A. Ferre, and A. O. Leon. "Oscillating decorated interfaces in parametrically driven systems". Phys. Rev. E **97(1)**, 012207 (2018).

- E. Berríos-Caro, M. G. Clerc, D. Escaff, C. Sandivari, and M. Tlidi. "On the repulsive interaction between localised vegetation patches in scarce environments". Scientific Reports, **10(1)**, 1-8 (2020).

- A. J. Alvarez-Socorro, E. Berríos-Caro, M. G. Clerc, and A. O. Leon. "Transition from nonradiative to radiative oscillons in parametrically driven systems". Phys. Rev. E **101(5)**, 052209 (2020).

- M. Tlidi, E. Berríos-Caro, D. Pinto-Ramos, A.G. Vladimirov, and M. G. Clerc. "Interaction between vegetation patches and gaps: A self-organized response to water scarcity". Physica D: Nonlinear Phenomena **414**, 132708 (2020).

- M. Messaoudi, M. G. Clerc, E. Berríos-Caro, D. Pinto-Ramos, M. Khaffou, A. Makhoute, and M. Tlidi. "Patchy landscapes in arid environments: Nonlinear analysis of the interaction-redistribution model". Chaos **30**, 093136 (2020).

Bibliography

[1] J. C. Pierce, "The Fibonacci Series", The Scientific Monthly **73**, 224–228 (1951).

[2] J. D. Murray, *Mathematical Biology I. An Introduction*, 3rd ed., Vol. 17, Interdisciplinary Applied Mathematics (Springer, New York, 2002).

[3] J. D. Murray, *Mathematical Biology II: Spatial Models and Biomedical Applications*, Vol. 18, Interdisciplinary Applied Mathematics (Springer, New York, 2003).

[4] L. Edelstein-Keshet, *Mathematical models in biology* (SIAM, Vancouver, 2005).

[5] E. Renshaw, *Modelling biological populations in space and time*, Vol. 11 (Cambridge University Press, Cambridge, 1993).

[6] N. S. Goel, and N. Richter-Dyn, *Stochastic models in biology* (Elsevier, New York, 2016).

[7] N. T. Bailey, *The elements of stochastic processes with applications to the natural sciences*, Vol. 25 (John Wiley & Sons, New York, 1990).

[8] E. Parzen, *Stochastic processes* (SIAM, San Francisco, 1999).

[9] S. H. Strogatz, *Nonlinear dynamics and chaos: with applications to physics, biology, chemistry, and engineering* (Perseus Books, New York, 1994).

[10] A. A. Berryman, "The orgins and evolution of predator-prey theory", Ecology **73**, 1530–1535 (1992).

[11] M. Tlidi, R. Lefever, and A. Vladimirov, "On vegetation clustering, localized bare soil spots and fairy circles", in *Dissipative Solitons: From Optics to Biology and Medicine* (Springer, Berlin, 2008), pp. 1–22.

[12] S. W. Ellacott, J. C. Mason, and I. J. Anderson, *Mathematics of neural networks: models, algorithms and applications*, Vol. 8 (Springer Science & Business Media, New York, 2012).

[13] J. A. Adam, "A simplified mathematical model of tumor growth", Mathematical Biosciences **81**, 229–244 (1986).

[14] P. M. Altrock, L. L. Liu, and F. Michor, "The mathematics of cancer: integrating quantitative models", Nature Reviews Cancer **15**, 730–745 (2015).

[15] E. Massad, S. Lundberg, and H. M. Yang, "Modeling and simulating the evolution of resistance against antibiotics", International Journal of Bio-medical Computing **33**, 65–81 (1993).

[16] T. Maruyama, *Stochastic problems in population genetics*, Vol. 17 (Springer Science & Business Media, Berlin, 2013).

[17] H. Uecker, "Evolutionary rescue in randomly mating, selfing, and clonal populations", Evolution **71**, 845–858 (2017).

[18] W. Horsthemke, "Noise induced transitions", in *Non-Equilibrium Dynamics in Chemical Systems* (Springer, Berlin, 1984), pp. 150–160.

[19] V. Grimm, and S. F. Railsback, *Individual-based modeling and ecology*, Vol. 8 (Princeton University Press, New Jersey, 2005).

[20] A. J. Black, and A. J. McKane, "Stochastic formulation of ecological models and their applications", Trends in ecology & evolution **27**, 337–345 (2012).

[21] N. V. Kampen, *Stochastic processes in physics and chemistry* (North Holland, 2007).

[22] D. P. Kroese, T. Brereton, T. Taimre, and Z. I. Botev, "Why the Monte Carlo method is so important today", Wiley Interdisciplinary Reviews: Computational Statistics **6**, 386–392 (2014).

[23] E. Schrödinger, *What is life?* (Cambridge University Press, Cornwall, 2012).

[24] M. Danino, N. M. Shnerb, S. Azaele, W. E. Kunin, and D. A. Kessler, "The effect of environmental stochasticity on species richness in neutral communities", Journal of Theoretical Biology **409**, 155–164 (2016).

[25] C. Saint-Ruf, and I. Matic, "Environmental tuning of mutation rates", Environmental Microbiology **8**, 193–199 (2006).

[26] S. M. Carlson, C. J. Cunningham, and P. A. Westley, "Evolutionary rescue in a changing world", Trends in Ecology & Evolution **29**, 521–530 (2014).

[27] J. L. Aron, and I. B. Schwartz, "Seasonality and period-doubling bifurcations in an epidemic model", Journal of Theoretical Biology **110**, 665–679 (1984).

[28] R. Nisbet, and W. Gurney, "Population dynamics in a periodically varying environment", Journal of Theoretical Biology **56**, 459–475 (1976).

[29] J. Foo, and F. Michor, "Evolution of resistance to targeted anti-cancer therapies during continuous and pulsed administration strategies", PLoS Computational Biology **5**, e1000557 (2009).

[30] S. Bonhoeffer, M. Lipsitch, and B. R. Levin, "Evaluating treatment protocols to prevent antibiotic resistance", Proceedings of the National Academy of Sciences **94**, 12106–12111 (1997).

[31] X.-Q. Zhao, *Dynamical systems in population biology*, Vol. 16 (Springer, New York, 2003).

[32] M. Assaf, M. Mobilia, and E. Roberts, "Cooperation dilemma in finite populations under fluctuating environments", Physical Review Letters **111**, 238101 (2013).

[33] A. Melbinger, and M. Vergassola, "The impact of environmental fluctuations on evolutionary fitness functions", Scientific Reports **5**, 15211 (2015).

[34] N. Takahata, K. Ishii, and H. Matsuda, "Effect of temporal fluctuation of selection coefficient on gene frequency in a population", Proceedings of the National Academy of Sciences **72**, 4541–4545 (1975).

[35] S. Yachi, and M. Loreau, "Biodiversity and ecosystem productivity in a fluctuating environment: the insurance hypothesis", Proceedings of the National Academy of Sciences **96**, 1463–1468 (1999).

[36] M. Acar, J. T. Mettetal, and A. Van Oudenaarden, "Stochastic switching as a survival strategy in fluctuating environments", Nature Genetics **40**, 471–475 (2008).

[37] E. Kussell, and S. Leibler, "Phenotypic diversity, population growth, and information in fluctuating environments", Science **309**, 2075–2078 (2005).

[38] J. Travis, and E. Travis, "Mutator dynamics in fluctuating environments", Proceedings of the Royal Society of London. Series B: Biological Sciences **269**, 591–597 (2002).

[39] Y. T. Lin, P. G. Hufton, E. J. Lee, and D. A. Potoyan, "A stochastic and dynamical view of pluripotency in mouse embryonic stem cells", PLoS Computational Biology **14**, e1006000 (2018).

[40] K. Wienand, E. Frey, and M. Mobilia, "Evolution of a Fluctuating Population in a Randomly Switching Environment", Physical Review Letters **119**, 158301 (2017).

[41] P. Ashcroft, P. M. Altrock, and T. Galla, "Fixation in finite populations evolving in fluctuating environments", Journal Royal Society Interface **11**, 20140663 (2014).

[42] T. W. Schoener, "Alternatives to Lotka-Volterra competition: models of intermediate complexity", Theoretical Population Biology **10**, 309–333 (1976).

[43] J. Foo, and F. Michor, "Evolution of resistance to anti-cancer therapy during general dosing schedules", Journal of Theoretical Biology **263**, 179–188 (2010).

[44] G. W. Constable, and H. Kokko, "The rate of facultative sex governs the number of expected mating types in isogamous species", Nature Ecology & Evolution **2**, 1168 (2018).

[45] D. T. Gillespie, "Approximate accelerated stochastic simulation of chemically reacting systems", The Journal of Chemical Physics **115**, 1716–1733 (2001).

[46] D. T. Gillespie, "A general method for numerically simulating the stochastic time evolution of coupled chemical reactions", Journal of Computational Physics **22**, 403–434 (1976).

[47] D. T. Gillespie, "Exact stochastic simulation of coupled chemical reactions", Journal of Physical Chemistry **81**, 2340–2361 (1977).

[48] G. Maruyama, "Continuous Markov processes and stochastic equations", Rendiconti del Circolo Matematico di Palermo **4**, 48 (1955).

Chapter 2

Theoretical Background

Abstract

In this chapter, I will present the fundamental theoretical aspects that will serve as basis for the work presented in this thesis. Throughout the following chapters, the study will be focused on *Markov processes*, i.e., stochastic processes that have no memory of the past. One particular case that we will study are so-called *birth-death processes* used to model population dynamics. After giving a general overview of the main properties of Markov processes, I will describe different types of birth-death processes that will play a fundamental role in the following chapters. Then I will turn to describing basic properties of *changing environments*, both in discrete and continuous space. Finally, I will present some useful mathematical and numerical tools that will be used later.

2.1 Markov processes

2.1.1 Definition and notation

A continuous-time Markov process[1] (or Markov chain) is a stochastic process X_t that takes values from a set $\mathcal{S}$ over a continuous parameter space $t \in \mathbb{R}_+$ (typically time), characterised by being *memoryless*. The memoryless condition means that the transition probability from any state $X_t = n$ depends solely on state n, and not on the

[1]Markov processes are named after the Russian mathematician Andrey Andreyevich Markov (1856 – 1922).

trajectory X_t takes to reach n. Mathematically, X_t fulfils

$$\mathbb{P}\left(X_{t_{k+1}} = n_{k+1} | X_{t_k} = n_k, \ldots, X_{t_0} = n_0\right) = \mathbb{P}\left(X_{t_{k+1}} = n_{k+1} | X_{t_k} = n_k\right), \tag{2.1}$$

where $n_k \in \mathcal{S}$ represents a trajectory of the process X_t at times t_k with $k \geq 0$. The space $\mathcal{S}$ can be discrete or continuous; here we focus on the former case.

Any Markov process X_t is completely determined by the *generator matrix* $\underline{\underline{Q}}$, whose entries are defined as

$$\begin{aligned} q_{nm} &= \lim_{\Delta t \to 0} \frac{\mathbb{P}\left(X_{t+\Delta t} = m | X_t = n\right)}{\Delta t} \quad (n \neq m), \\ q_{nn} &= -\sum_{m \neq n} q_{nm}. \end{aligned} \tag{2.2}$$

In this way, the sum of the entries of each row of $\underline{\underline{Q}}$ is zero. The value $|q_{nn}|$ represents the rate at which the system leaves state n, whilst q_{nm} correspond to the probability per unit time, or *transition rate*, of transitioning from state n to state m. The generator matrix $\underline{\underline{Q}}$ is often called as the *infinitesimal generator* of the Markov chain as it fulfils

$$p_{nm} = \delta_{nm} + q_{nm}\Delta t + o(\Delta t), \tag{2.3}$$

with δ_{nm} the Kronecker delta, and $p_{nm} \equiv \mathbb{P}\left(X_{t+\Delta t} = m | X_t = n\right)$, the *transition probabilities*. In other words, the matrix $\underline{\underline{Q}}$ defines the dynamics of the Markov chain over an infinitesimal time step.

As we will see below in Section 1.5.1, a time-continuous Markov process can be numerically simulated by means of the *Gillespie algorithm*. Any time-continuous Markov chain can be defined in discrete-time by constructing the so-called *embedded* Markov chain.

2.1.2 Kolmogorov equations

The generator matrix characterises the time evolution of the probability of being at a certain state at a given time. The row vector probability $\underline{P}(t)$, whose entries are given by $P_n(t) \equiv \mathbb{P}(X_t = n)$, satisfies

$$\frac{\mathrm{d}\underline{P}}{\mathrm{d}t}(t) = \underline{P}(t) \cdot \underline{\underline{Q}}, \tag{2.4}$$

or, in summation form,

$$\frac{\mathrm{d}P_n}{\mathrm{d}t}(t) = \sum_{m \in \mathcal{S}} P_m(t) q_{mn}. \tag{2.5}$$

This equation is usually referred to as the *Kolmogorov* or *master equation*. From this equation, one can deduce $\underline{P}(t)$ given an initial condition. By using Eq. (1.2), one can express Eq. (1.5) as

$$\frac{\mathrm{d}P_n}{\mathrm{d}t}(t) = \sum_{m\neq n} P_m(t)q_{mn} - \sum_{m\neq n} P_n(t)q_{nm}, \tag{2.6}$$

for $m \in \mathcal{S}$. From this equation, it is easy to see that the first term on the right-hand side represents the net probability flux from any state m to state n, while the second one from state n to any state m. The master equation then describes the balance of the flux probabilities entering and leaving the Markov chain states.

If one is interested in the long-term evolution of $\underline{P}(t)$, i.e. the stationary distribution $\underline{P}^{\mathrm{st}}$, one sets the left-hand side of Eq. (1.4) equal to zero, so that

$$0 = \underline{P}^{\mathrm{st}} \cdot \underline{\underline{Q}}, \tag{2.7}$$

i.e., $\underline{P}^{\mathrm{st}}$ is equal to the kernel of $\underline{\underline{Q}}^T$.

2.1.3 Generating functions

In general, Kolmogorov equations are difficult to handle analytically, and can be considerably difficult to solve. This can be alleviated by using *generating functions*, which can turn the Kolmogorov equations into a single partial differential equation.

Given a distribution $P_n(t)$, we define the generating function

$$F(z,t) = \sum_{n\in\mathcal{S}} z^n P_n(t). \tag{2.8}$$

Naturally, for $n \notin \mathcal{S}$ the distribution P_n vanishes. Defining functions $f_l(X_t)$ through

$$\mathbb{P}(X_{t+\Delta t} = m + l | X_t = m) = f_l(X_t)\Delta t, \quad (l \neq 0) \tag{2.9}$$

one finds that $F(z,t)$ satisfies [1]

$$\frac{\partial F(z,t)}{\partial t} = \sum_{l\neq 0}(z^l - 1) f_l\left(z\frac{\partial}{\partial z}\right) F(z,t). \tag{2.10}$$

If the functions f_l are simple, this equation may be easy to solve. Note that l can be positive or negative. In later chapters we will provide some applications of this equation.

First and second moments

Knowing the generating function $F(z,t)$ allows us to calculate some relevant quantities through simple formulas. For instance, the kth moment defined as

$$\left\langle X_t^k \right\rangle = \mathrm{E}[X_t^k] = \sum_{n\in\mathcal{S}} n^k P_n(t), \tag{2.11}$$

can be calculated from

$$\left\langle X_t^k \right\rangle = \left.\frac{\partial^k F(z,t)}{\partial(\ln z)^k}\right|_{z=1}. \tag{2.12}$$

Often one is interested in obtaining the first two moments. The mean value of X_t takes the form

$$\langle X_t \rangle \equiv \mathrm{E}[X_t] = \left.\frac{\partial F(z,t)}{\partial z}\right|_{z=1}, \tag{2.13}$$

while the variance

$$\mathrm{Var}[X_t] \equiv \left\langle X_t^2 \right\rangle - \langle X_t \rangle^2 = \left.\frac{\partial^2 F(z,t)}{\partial z^2}\right|_{z=1} + \left.\frac{\partial F(z,t)}{\partial z}\right|_{z=1} - \left(\left.\frac{\partial F(z,t)}{\partial z}\right|_{z=1}\right)^2. \tag{2.14}$$

2.2 Homogeneous birth-death processes

Birth-death processes are a crucial topic in this thesis. Throughout the following chapters, we will look at different biological scenarios in which birth-death processes appear. This section is intended to give an overview of the main *homogeneous* birth-death processes that will be later explored. Homogeneous processes are those in which the transition rates are independent of time, which means the entries of the generator matrix $\underline{\underline{Q}}$ remain constant.

2.2.1 General birth-death process

Definition

Let us consider a population in which the number individuals is given by a random variable X_t that takes values from a state space $\mathcal{S} = \mathbb{N}$. Let us assume birth events occur at rate λ_n when the system is in state n, and death events at rate μ_n when in state n. The associated generator matrix then has as the following non-zero entries:

$$q_{n,n+1} = \lambda_n, \quad q_{n,n-1} = \mu_n, \quad \text{and} \quad q_{nn} = -(\lambda_n + \mu_n), \tag{2.15}$$

which translates into the following matrix

$$\underline{\underline{Q}} = \begin{pmatrix} -\lambda_0 & \lambda_0 & 0 & \dots & \dots \\ \mu_1 & -(\lambda_1+\mu_1) & \lambda_1 & 0 & \dots \\ 0 & \mu_2 & -(\lambda_2+\mu_2) & \lambda_2 & \ddots \\ \vdots & 0 & \ddots & \ddots & \ddots \\ \vdots & \vdots & \ddots & \ddots & \ddots \end{pmatrix}. \tag{2.16}$$

Since the number of individuals cannot be negative, it is necessary to set $\mu_n = 0$ for $n \leq 0$, i.e., the system cannot cross $n = 0$. State $n = 0$ is said to be a *reflecting state*. Naturally, we also need to set $\lambda_n = 0$ for $n < 0$. If $\lambda_0 = 0$, state $n = 0$ becomes an *absorbing state*. A schematic representation of a general birth-death process is presented in Figure 1.1.

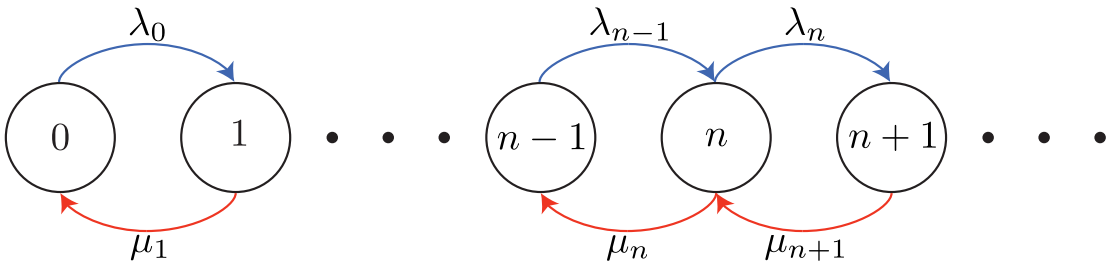

Figure 2.1: Schematic representation of a general birth-death process with birth rates λ_n and death rates μ_n. The states n represent the number of individuals. State $n = 0$ is reflecting (i.e., $\mu_n = 0$ for $n \leq 0$).

Kolmogorov equations of birth-death events

Inserting the generator matrix from Eq. (1.16) in Eq. (1.4), one obtains the respective Kolmogorov equations

$$\frac{\mathrm{d}P_n}{\mathrm{d}t}(t) = \lambda_{n-1}P_{n-1}(t) + \mu_{n+1}P_{n+1}(t) - (\lambda_n + \mu_n)P_n(t) \quad \text{for} \quad n \geq 0, \tag{2.17}$$

where $P_n = 0$ for $n < 0$. Depending on how the rates λ_n and μ_n vary with respect to n, the solution of this equation may vary. However, we can still say some properties that apply for any rates chosen. We present below a few of them.

Rate equations for first moments

Using the Kolmogorov equations one can easily construct the rate equations for the mean values of the number of individuals. Multiplying Eq. (1.17) by n and summing

both sides over n, one obtains

$$\frac{\mathrm{d}\langle n\rangle}{\mathrm{d}t} = \langle\lambda_n\rangle - \langle\mu_n\rangle\,, \tag{2.18}$$

where we write $\langle n\rangle \equiv \langle X_t\rangle$, $\langle\lambda_n\rangle = \sum_n \lambda_n P_n(t)$, and $\langle\mu_n\rangle = \sum_n \mu_n P_n(t)$. For example, for $\lambda_n = \lambda n$ and $\mu = \mu n$, we have $\langle\lambda_n\rangle = \lambda\langle n\rangle$ and $\langle\mu_n\rangle = \mu\langle n\rangle$, so that $\mathrm{d}\langle n\rangle/\mathrm{d}t = (\lambda-\mu)\langle n\rangle$.

Ergodicity condition

Given λ_n and μ_n, a birth-death process is said to be *ergodic* if satisfies the following properties [2]

$$\sum_{m=1}^{\infty}\prod_{n=1}^{m}\frac{\mu_n}{\lambda_n} \to \infty \quad \text{and} \quad \sum_{m=1}^{\infty}\prod_{n=1}^{m}\frac{\lambda_{n-1}}{\mu_n} < \infty. \tag{2.19}$$

The ergodic property indicates that the process is *irreducible* and *positive recurrent*. The former indicates that all the states communicate, i.e., there is a non-zero probability to transit between any pair of states in a finite number of steps; the latter means that there exists a finite expected time to return to any state.

Stationary distribution

If a birth-death process is ergodic, then it admits a unique stationary distribution $\underline{P}^{\mathrm{st}}$ given by the solution of Eq. (1.7). This is [3]

$$P_n^{\mathrm{st}} = P_0^{\mathrm{st}}\prod_{m=1}^{n}\frac{\lambda_{m-1}}{\mu_m}, \tag{2.20}$$

where

$$P_0^{\mathrm{st}} = \left(1+\sum_{k=1}^{\infty}\prod_{m=1}^{k}\frac{\lambda_{m-1}}{\mu_m}\right)^{-1}. \tag{2.21}$$

This distribution is a limiting distribution, i.e., $\lim_{t\to\infty}\underline{P}(t) = \underline{P}^{\mathrm{st}}$, which is independent of the initial condition $\underline{P}(0)$.

We describe below some processes given by different dependences on the rates λ_n and μ_n with respect to n that will be later explored in the following chapters. For further examples, see e.g. [1, 4].

2.2.2 Poisson process

The *Poisson process*, also called *Poisson point process*, is a very simple type of continuous-time Markov process. This will play an important role in the Gillespie algorithm described later in Section 1.5.1. In this process, we assume that new individuals are added at constant rate λ, i.e.,

$$\lambda_n = \lambda \quad \text{and} \quad \mu_n = 0, \tag{2.22}$$

so the master equation becomes

$$\frac{\mathrm{d}P_n}{\mathrm{d}t}(t) = \lambda P_{n-1}(t) - \lambda P_n(t). \tag{2.23}$$

An easy way to solve this equation is by calculating first the corresponding generating function. For that, we first note that the only transition probability permitted is

$$\mathbb{P}(X_{t+\Delta t} = n+1 | X_t = n) = \lambda \Delta t. \tag{2.24}$$

Then, according to Eq. (1.9), $f_1 = \lambda$, while $f_l = 0$ for $l \neq 1$. Using Eq. (1.10), one finds

$$\frac{\partial F(z,t)}{\partial t} = \lambda(z-1)F(z,t), \tag{2.25}$$

Setting an initial condition of zero individuals at time $t = 0$, i.e., $P_n(0) = \delta_{n,0}$, so that $F(z,0) = 1$, we get

$$F(z,t) = e^{\lambda t(z-1)}. \tag{2.26}$$

Expressing this as

$$F(z,t) = \sum_{n=0}^{\infty} z^n e^{-\lambda t} \frac{(\lambda t)^n}{n!}, \tag{2.27}$$

and comparing it against Eq. (1.8), it is direct that

$$P_n(t) = e^{-\lambda t} \frac{(\lambda t)^n}{n!}. \tag{2.28}$$

By virtue of equations (1.13) and (1.14), the mean value and variance become

$$\langle n \rangle = \lambda t, \tag{2.29}$$

and

$$\left\langle n^2 \right\rangle - \langle n \rangle^2 = \lambda t. \tag{2.30}$$

This process does not admit a stationary distribution as the conditions in Eq. (1.19) are not fulfilled. In fact, we have $\sum_{m=1}^{\infty} \prod_{n=1}^{m} (\mu_n/\lambda_n) = 0$ and $\sum_{m=1}^{\infty} \prod_{n=1}^{m} (\lambda_{n-1}/\mu_n) \to \infty$.

2.2.3 Pure birth process (Yule–Furry process)

This process[2] will be later used in Chapter 3 as basis to develop a growth model of multi-drug resistance whose growth rate will be determined from experimental data. In this model, we consider a population in which each individual reproduces at a constant rate λ, i.e.,

$$n \xrightarrow{\lambda} n+1. \tag{2.31}$$

There is no death process, so we set

$$\lambda_n = \lambda n \quad \text{and} \quad \mu_n = 0. \tag{2.32}$$

The master equation then becomes

$$\frac{\mathrm{d}P_n}{\mathrm{d}t}(t) = \lambda(n-1)P_{n-1}(t) - \lambda n P_n(t). \tag{2.33}$$

To solve this, we first calculate the generating function. Since the non-zero infinitesimal transition probabilities are

$$\mathbb{P}(X_{t+\Delta t} = n+1 | X_t = n) = \lambda n \Delta t, \tag{2.34}$$

we have $f_1(X_t) = \lambda X_t$, while $f_l = 0$ for $l \neq 1$. From Eq. (1.10) then, we find

$$\frac{\partial F(z,t)}{\partial t} = \lambda z(z-1)\frac{\partial F(z,t)}{\partial z}. \tag{2.35}$$

Assuming an initial condition of n_0 particles at $t = 0$, i.e., $P_n(0) = \delta_{n,n_0}$, so that $F(z,0) = z^{n_0}$, the solution becomes

$$F(z,t) = \left(\frac{1}{1 - e^{\lambda t}\,(1 - 1/z)}\right)^{n_0}. \tag{2.36}$$

Expanding in series of z, picking out the coefficient multiplying z^n, and comparing it against Eq. (1.8), one finds

$$P_n(t) = \binom{n+n_0-1}{n_0-1} e^{-\lambda n_0 t}(1 - e^{-\lambda t})^n, \tag{2.37}$$

which is a *negative binomial* distribution describing the probability of having n failures and n_0 successes, out of $n + n_0$ independent and identically distributed *Bernoulli trials* with probability of success $e^{-\lambda t}$.

[2] Yule [5] first studied this process in the context of evolution of species in 1924. A similar process was later studied in 1937 by Furry [6] focused on cosmic ray phenomena.

Finally, from equations (1.13) and (1.14), we have

$$\langle n \rangle = n_0 e^{\lambda t}, \tag{2.38}$$

and

$$\left\langle n^2 \right\rangle - \langle n \rangle^2 = n_0 e^{\lambda t}(e^{\lambda t} - 1). \tag{2.39}$$

As with the Poisson process, the Yule–Furry process does not admit a stationary distribution as the conditions in Eq. (1.19) are not fulfilled.

2.2.4 Simple birth-death process

In this process, we add the possibility to the Yule–Furry process that each individual within a population dies at a constant rate μ. This model will be later explored in Chapter 4 to construct a growth model of multi-drug resistance under constant drug concentrations. Using the same notation as before, we have

$$n \xrightarrow{\lambda} n+1, \quad \text{and} \quad n \xrightarrow{\mu} n-1, \tag{2.40}$$

so the rates become

$$\lambda_n = \lambda n, \quad \text{and} \quad \mu_n = \mu n. \tag{2.41}$$

The master equation takes the following form

$$\frac{\mathrm{d}P_n}{\mathrm{d}t}(t) = \lambda(n-1)P_{n-1}(t) + \mu(n+1)P_{n+1}(t) - (\lambda+\mu)nP_n(t), \tag{2.42}$$

where we set $P_n = 0$ for $n < 0$. The non-zero infinitesimal transition probabilities are

$$\mathbb{P}(X_{t+\Delta t} = n+1 | X_t = n) = \lambda n \Delta t \tag{2.43}$$

and

$$\mathbb{P}(X_{t+\Delta t} = n-1 | X_t = n) = \mu n \Delta t, \tag{2.44}$$

so that the non-zero coefficients f_l become $f_1(X_t) = \lambda X_t$ and $f_{-1}(X_t) = \mu X_t$. From Eq. (1.10) then,

$$\frac{\partial F(z,t)}{\partial t} = z\left[\lambda(z-1) + \mu(1/z - 1)\right] \frac{\partial F(z,t)}{\partial z}. \tag{2.45}$$

Assuming an initial condition of n_0 particles at $t = 0$, i.e., $P_n(0) = \delta_{n,n_0}$, so that $F(z,0) = z^{n_0}$, the solution becomes [1]

$$F(z,t) = \begin{cases} \left(\dfrac{\mu(z-1)e^{(\lambda-\mu)t} - (\lambda z - \mu)}{\lambda(z-1)e^{(\lambda-\mu)t} - (\lambda z - \mu)}\right)^{n_0} & \text{if } \lambda \neq \mu \quad (2.46a) \\ \left(\dfrac{1-(\lambda t-1)(z-1)}{1-\lambda t(z-1)}\right)^{n_0} & \text{if } \lambda = \mu. \quad (2.46b) \end{cases}$$

Expanding in z and picking out the coefficient multiplying z^n, one finds [1, 7]

$$P_n(t) = \sum_{m=0}^{\min(n_0,n)} \binom{n_0}{m} \binom{n_0+n-m-1}{n_0-1} p(t)^{n_0-m} q(t)^{n-m} (1-p(t)-q(t))^m, \quad (2.47)$$

where

$$p(t) = \begin{cases} \dfrac{\mu(e^{(\lambda-\mu)t}-1)}{\lambda e^{(\lambda-\mu)t} - \mu} & \text{if } \lambda \neq \mu \quad (2.48a) \\ \dfrac{\lambda t}{1+\lambda t} & \text{if } \lambda = \mu, \quad (2.48b) \end{cases}$$

and

$$q(t) = \begin{cases} \dfrac{\lambda(e^{(\lambda-\mu)t}-1)}{\lambda e^{(\lambda-\mu)t} - \mu} & \text{if } \lambda \neq \mu \quad (2.49a) \\ \dfrac{\lambda t}{1+\lambda t} & \text{if } \lambda = \mu. \quad (2.49b) \end{cases}$$

Finally, from equations (1.13) and (1.14), we have

$$\langle n \rangle = n_0 e^{(\lambda-\mu)t}, \quad (2.50)$$

and

$$\left\langle n^2 \right\rangle - \langle n \rangle^2 = \begin{cases} n_0 \left(\dfrac{\lambda+\mu}{\lambda-\mu}\right) e^{(\lambda-\mu)t}(e^{(\lambda-\mu)t}-1) & \text{if } \lambda \neq \mu \quad (2.51a) \\ 2\lambda t & \text{if } \lambda = \mu. \quad (2.51b) \end{cases}$$

Extinction probability

Unlike the Yule–Furry process (see Section 1.2.3), in this case the population may get extinct due to the death process involved. The *probability of extinction*, i.e., the probability that there are zero individuals at time t, is given by $P_0(t)$ from Eq. (1.47). We have

$$P_{\text{ext}}(t) \equiv P_0(t) = \begin{cases} \left(\dfrac{\mu(e^{(\lambda-\mu)t}-1)}{\lambda e^{(\lambda-\mu)t} - \mu}\right)^{n_0} & \text{if } \lambda \neq \mu \quad (2.52a) \\ \left(\dfrac{\lambda t}{1+\lambda t}\right)^{n_0} & \text{if } \lambda = \mu. \quad (2.52b) \end{cases}$$

From this we deduce that

$$\lim_{t\to\infty} P_{\text{ext}}(t) = \begin{cases} \left(\frac{\mu}{\lambda}\right)^{n_0} & \text{if } \lambda \geq \mu \quad (2.53a) \\ 1 & \text{if } \lambda < \mu, \quad (2.53b) \end{cases}$$

implying that extinction is certain only if $\mu \geq \lambda$.

Stationary distribution

To determine whether a simple birth-death process admits a stationary distribution, we look at the ergodicity conditions from Eq. (1.19). It is easy to see that these are fulfilled only when $\mu \geq \lambda$, in which case we have

$$\sum_{m=1}^{\infty} \prod_{n=1}^{m} \frac{\mu_n}{\lambda_n} = \sum_{m=1}^{\infty} \left(\frac{\mu}{\lambda}\right)^m \to \infty, \tag{2.54}$$

and

$$\sum_{m=1}^{\infty} \prod_{n=1}^{m} \frac{\lambda_{n-1}}{\mu_n} = \sum_{m=1}^{\infty} \left(\frac{\mu}{\lambda}\right)^m \underbrace{\left(\prod_{n=1}^{m} \frac{n-1}{n}\right)}_{=0} = 0 < \infty. \tag{2.55}$$

As seen above, when $\mu \geq \lambda$, the population dies out. We conclude then that

$$P_n^{\text{st}} = \begin{cases} \text{undefined} & \text{if } \lambda > \mu \quad (2.56a) \\ \delta_{n,0} & \text{if } \lambda \leq \mu, \quad (2.56b) \end{cases}$$

i.e., for $\lambda > \mu$ the population grows indefinitely (on average) and does not reach stationarity, while for $\lambda \leq \mu$ the population eventually gets extinct.

2.2.5 Birth-death process with non-linear growth rates

In many biological systems, we may encounter birth-death processes with non-linear growth rates. These are, in general, difficult to handle analytically, and may not admit closed-form expressions for relevant quantities (such as probability distributions). We present below briefly two models that will be later explored in this thesis.

Logistic growth rates

The previous examples of birth-death processes do not consider limitations of resources within a population. In more realistic cases, individuals may compete for a common

resource and some non-linear effects may take place on the population growth. A simple model that accounts for limiting resources is the so-called Verhulst[3] model [8]

$$\frac{\mathrm{d}\langle n\rangle}{\mathrm{d}t} = r\langle n\rangle\left(1-\frac{\langle n\rangle}{k}\right), \tag{2.57}$$

where r denotes the intrinsic growth rate and k is the carrying capacity of the population. The angular bracket represents the average over different realisations. The solution of this equation is an S-shaped curve, with $\langle n\rangle$ approaching k as time grows (assuming $r > 0$). Figure 1.2 shows a typical profile of this curve.

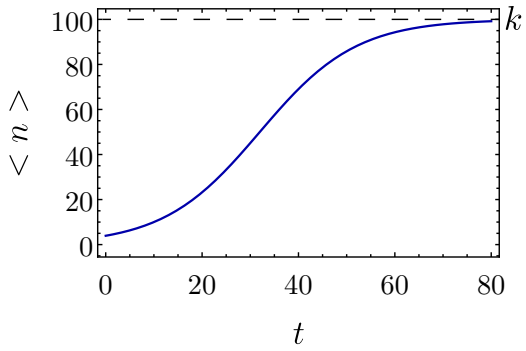

Figure 2.2: Mean logistic growth over time. The number of individuals grow following an exponential law at early stages, but approaches the carrying capacity k as time goes by. The profile shown is the solution of Eq. (1.57), i.e., $\langle n(t)\rangle = kn_0/\{n_0 + (k-n_0)\exp[-r(t-t_0)]\}$, with $k = 100, n_0 = 10, t_0 = 10$, and $r = 0.1$. Notice that $\langle n(t_0)\rangle = n_0$.

In order to model a birth-death process whose mean behaviour follows this equation, one needs to choose appropriately the birth and death rates depending on the requirements one desires from the model. A simple way is setting

$$\lambda_n = b(n)n, \quad \text{and,} \quad \mu_n = d(n)n, \tag{2.58}$$

with $b(n)$ and $d(n)$ the per capita birth and death rates, respectively. Using the approximation $\langle n^2\rangle = \langle n\rangle^2$ (which holds for large populations as fluctuations are lower than the number of individuals), and following Eq. (1.18), one requires then

$$b(n) - d(n) = r\left(1-\frac{n}{k}\right). \tag{2.59}$$

[3]The Verhulst or logistic growth model was introduced by the Belgian mathematician Pierre François Verhulst in 1838

In Chapter 3 we will study a model with logistic growth in which we will set the growth rates equal to zero for $n > k$ to stop the growth. In Chapter 4 we will consider $\lambda_n - \mu_n = 0$ for $n \geq k$, but keeping the rates as positive to keep fluctuations around $n = k$. For more examples see [4].

Moran model

This model[4] is used to describe the dynamics of populations with a fixed size N composed by two types of species that undergo birth and death events [10]. The states of this system are given by the number of individuals of one of the species. If the system is in state n, there will be n individuals of one type and $N - n$ of the other. The state space then is bounded by N, i.e., $\mathcal{S} = \{n | n \in \mathbb{N}, 0 \leq n \leq N\}$.

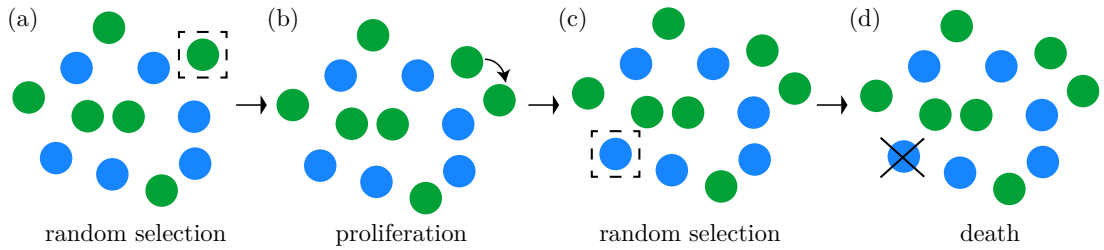

Figure 2.3: Schematic representation of a reproductive event of the Moran model: (a) An individual is chosen uniformly at random of either type. (b) That individual proliferates. (c) An individual of the other type is chosen uniformly at random. (d) That individual dies.

Let us denote the species by A and B. In order to keep the total size equal to N, the birth and death events must be coupled. Figure 1.3 shows a schematic representation of the events in a Moran model. Whenever a birth event occurs, let us say of species A, then one individual of species B, chosen uniformly at random, must die. The individual from species A is also chosen uniformly at random. The opposite event can also take place, i.e., one individual of species A dies and of B reproduces, with individuals chosen uniformly at random. This means the rate of increasing or decreasing n is the same. The situation in which the individuals chosen for birth and death are of the same type can also happen. This case does not have any effect in the system. The Moran model

[4]The Moran model was introduced by the Australian statistician P. A. P. Moran in 1958 as an alternative to the Wright-Fisher model [9].

then can be interpreted as a birth-death process with rates

$$\lambda_n = \mu_n = \frac{n}{N}\frac{(N-n)}{N}, \tag{2.60}$$

where the terms n/N and $(N-n)/N$ represent the probability of choosing randomly an individual of each species. Note that at $n = 0$ and $n = N$ both birth and death rates vanish, i.e., in those states the system cannot undergo any transition. States $n = 0$ and $n = N$ are said to be *absorbing* states. It is expected then that in the long time one of these states will be eventually reached.

Later in Chapter 3, we will use the Moran model to construct a model in which we will allow different types of species to either reproduce sexually or asexually.

2.3 Non-homogeneous birth-death process

Let us turn now to *non-homogeneous birth-death processes*, i.e., birth-death processes with time-dependent birth and death rates. These processes are suitable to model the effect of a time-varying external parameter, such as drug concentrations, that modules birth and death rates in time. A model of this type will be explored in Chapter 4 to describe the effect of oscillating drug concentrations on a multi-drug resistance model. Non-homogeneous processes can be simulated with the *Lewis' thinning algorithm* described below in Section 1.5.1.

We consider here a simple birth-death process with time-dependent rates of the form

$$\lambda_n = \lambda(t)n, \quad \text{and} \quad \mu_n = \mu(t)n, \tag{2.61}$$

where $\lambda(t)$ and $\mu(t)$ are the time-dependent per capita birth and death rates, respectively. These rates λ_n and μ_n leave unaltered the form of the master equation, with the only difference that now the right-hand side contains time-dependent functions. One obtains

$$\frac{\mathrm{d}P_n}{\mathrm{d}t}(t) = \lambda(t)(n-1)P_{n-1}(t) + \mu(t)(n+1)P_{n+1}(t) - [\lambda(t)+\mu(t)]nP_n(t). \tag{2.62}$$

Similarly, for the generating function we have

$$\frac{\partial F(z,t)}{\partial t} = z\left[\lambda(t)(z-1) + \mu(t)(1/z-1)\right]\frac{\partial F(z,t)}{\partial z}. \tag{2.63}$$

Setting an initial condition of n_0 individuals at time $t = t_0$, i.e., $F(z, t_0) = z^{n_0}$, the solution of this equation becomes

$$F(z,t) = \left(1 + \frac{1}{\dfrac{e^{-\beta(t)}}{(z-1)} - \displaystyle\int_{t_0}^{t} \lambda(t')e^{-\beta(t')}\mathrm{d}t'}\right)^{n_0}, \tag{2.64}$$

with

$$\beta(t) = \int_{t_0}^{t} [\lambda(t') - \mu(t')]\mathrm{d}t'. \tag{2.65}$$

As with the homogeneous case, by expanding $F(z, t)$ in series of z, and extracting the coefficient next to z^n, we construct the probability distribution. One finds

$$P_n(t) = \sum_{m=0}^{\min(n_0,n)} \binom{n_0}{m} \binom{n_0 + n - m - 1}{n_0 - 1} p(t)^{n_0-m} q(t)^{n-m} (1 - p(t) - q(t))^m, \tag{2.66}$$

with

$$p(t) = 1 - \frac{1}{e^{-\beta(t)} + \displaystyle\int_{t_0}^{t} \lambda(t')e^{-\beta(t')}\mathrm{d}t'}, \tag{2.67}$$

and

$$q(t) = 1 - \frac{e^{-\beta(t)}}{e^{-\beta(t)} + \displaystyle\int_{t_0}^{t} \lambda(t')e^{-\beta(t')}\mathrm{d}t'}. \tag{2.68}$$

All these previous expressions are valid whether $\lambda(t) \neq \mu(t)$ or $\lambda(t) = \mu(t)$.

The mean value and variance can again be obtained from equations (1.13) and (1.14). One finds

$$\langle n \rangle = n_0 e^{\beta(t)}, \tag{2.69}$$

and

$$\left\langle n^2 \right\rangle - \langle n \rangle^2 = n_0 e^{2\beta(t)} \int_{t_0}^{t} [\lambda(t') + \mu(t')]e^{-\beta(t')}\mathrm{d}t'. \tag{2.70}$$

Extinction probability

The probability distribution in Eq. (1.66) allows us to obtain the extinction probability of a population for given rates $\lambda(t)$ and $\mu(t)$, with an initial condition of n_0 individuals at $t = t_0$. This quantity takes the following form

$$P_{\text{ext}}(t) \equiv P_0(t) = \left(1 - \frac{1}{e^{-\beta(t)} + \displaystyle\int_{t_0}^{t} \lambda(t')e^{-\beta(t')}\mathrm{d}t'}\right)^{n_0}. \tag{2.71}$$

This has the form of tumour control probabilities calculated for temporal protocols of dose delivery [11, 12]. Using Eq. (1.65), we note that $\mathrm{d}e^{-\beta(t)}/\mathrm{d}t = [\mu(t) - \lambda(t)]e^{\beta(t)}$, so that $e^{-\beta(t)} = 1 + \int_{t_0}^{t} [\mu(t) - \lambda(t)]e^{\beta(t')}$. Using this, we can write

$$P_{\text{ext}}(t) = \left(\frac{\int_{t_0}^{t} \mu(t')e^{-\beta(t')}\mathrm{d}t'}{1 + \int_{t_0}^{t} \mu(t')e^{-\beta(t')}\mathrm{d}t'} \right)^{n_0}, \tag{2.72}$$

which shows more clearly the effect of the death rate $\mu(t)$ on the population extinction. This is useful as death events are what cause the extinction of the population. From here, one can conclude that the extinction probability tends to unity as $t \to \infty$ if and only if

$$\lim_{t\to\infty} \int_{t_0}^{t} \mu(t')e^{-\beta(t')}\mathrm{d}t' = \infty. \tag{2.73}$$

A clear example of this is the case $\mu(t) > \lambda(t)$ for any $t \geq t_0$.

2.4 Fluctuating environments

We turn now to another main aspect of this thesis: *fluctuating environments*. These describe the stochastic variation of external factors that alter the reaction parameters within a population. The cases that later will be explored are of fluctuating environments that alter the growth rates of biological populations following a birth-death process. In Chapters 3 and 4, we study a model of the evolution of multi-drug resistance which assumes an environment that changes deterministically, i.e., it varies over time following a given function of time. These cases fall into the category of non-homogeneous birth-death processes that were described in the previous section. In Chapters 5 and 6, we assume the environment behaves stochastically, and the previous framework cannot be applied. In such cases, one needs to treat the environment as a separate stochastic process, and study how its stochasticity affects the population. Depending on how the environment varies with the population state, or on how the typical timescale of the environment compares to the population timescale (i.e., if the environment is slow or fast compared to the population), one may be able to deduce analytical results of the environmental behaviour. Throughout this thesis, we assume the environmental process is Markovian. In this section, we describe the theoretical

framework of fluctuating environments using the tools presented above. We consider cases in which the environmental space is discrete and cases in which it is continuous. For the latter, we describe an environment that follows an Ornstein–Uhlenbeck process.

2.4.1 Discrete space: switching environments

When the environmental space is discrete, the environmental fluctuating process is usually referred to as a *switching environment* (see e.g. [13]). This case can describe, biological scenarios in which there is switching between a collection of discrete states such as phenotypical states in cell populations [14] or switching of resources consumed by bacteria [15].

Let us denote the environments by E_σ, with σ the environmental state. We assume the number of states the environment can take is bounded, i.e., the state space of the process is of the form $\mathcal{S} = \{\sigma | \sigma \in \mathbb{N}, \sigma_{\min} \leq \sigma \leq \sigma_{\max}\}$, for some $\sigma_{\min}$ and $\sigma_{\max}$. If the rates the environment switches are independent on the system state (e.g., the composition of the population), one can treat the environmental dynamics as a separate process from the population dynamics. In such cases, one can make use of the theoretical framework of homogeneous birth-death processes considering σ as the states and the switching rates as the birth and death rates.

Two environments

As an illustrative example, let us consider a simple case of two environmental states that do not depend on the system state. This case is often found in many biological systems for periodic or random switching environments (see e.g., [14, 16, 17]). Here we focus on the latter case. We assume the environment can be in states $\sigma = 0$ and $\sigma = 1$. We write k_+ for the rate of transitioning from $\sigma = 0$ to $\sigma = 1$, and k_- for the rate of transitioning from $\sigma = 1$ to $\sigma = 0$. This translates into the following environmental transitions

$$E_0 \xrightarrow{k_+} E_1 \quad \text{and} \quad E_1 \xrightarrow{k_-} E_0, \tag{2.74}$$

i.e., a telegraph process. This process is a birth-death process with rates $\lambda_0 = k_+$, $\mu_1 = k_-$, and $\lambda_1 = \mu_0 = 0$. It is easy to see that the ergodicity conditions from Eq. (1.19) are fulfilled for any $k_+, k_- > 0$, implying there exists a unique stationary

distribution. Inserting the rates λ_σ and μ_σ in Eqs. (1.20) and (1.21), and writing ρ^*_σ for the stationary distribution of finding the environment in state σ, we find

$$\rho^*_0 = \frac{k_-}{k_+ + k_-} \quad \text{and} \quad \rho^*_1 = \frac{k_+}{k_+ + k_-}. \tag{2.75}$$

Birth-death process in switching environments

To illustrate how to treat the effect of switching environments on population dynamics, let us consider a simple birth-death process subjected to population-independent switching environments. We use σ as before to represent the environmental states, and $\mathcal{S}$ to represent the space of environmental states. Writing λ^σ_n and μ^σ_n for the birth and death rates when in environment σ, we have

$$\lambda^\sigma_n = \lambda_\sigma n, \quad \text{and} \quad \mu^\sigma_n = \mu_\sigma n, \tag{2.76}$$

for $\sigma \in \mathcal{S}$, where λ_σ and μ_σ represent the per capita birth and death rates, respectively, when in environment σ.

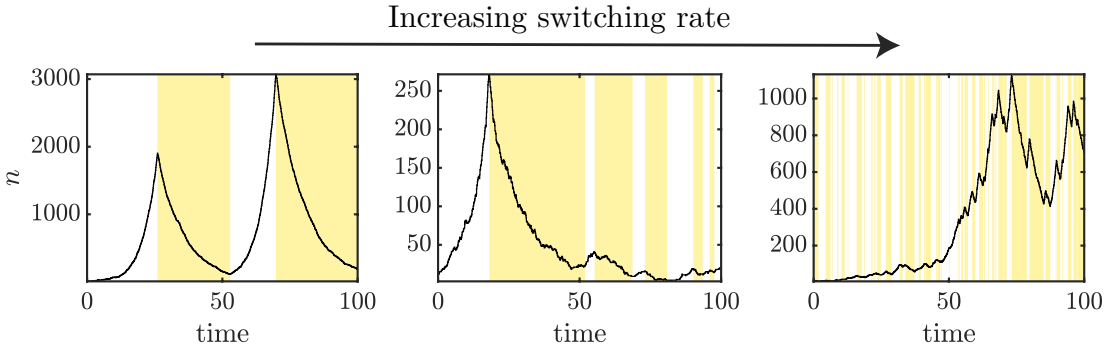

Figure 2.4: Sample paths of a two-environmental simple birth-death process showing different switching regimes. The colours represent the environmental states with $\sigma = 0$ as the white regions and $\sigma = 1$ as the yellow regions. The simulations were performed using the Gillespie algorithm. The rates are given by Eq. (1.76), with $\lambda_0 = 0.3, \mu_0 = 0.1, \lambda_1 = 0.1$, and $\mu_1 = 0.2$, i.e., on average the population increases in $\sigma = 0$ and decreases in $\sigma = 1$. The switching rates are the same in each environment, i.e., $k_0 = k_1$. From left to right panels we set them equal to $0.1, 0.01$, and 1.0.

The probability distribution $P_{n,\sigma}(t)$ of finding n individuals in the population and the environment in state σ at time t follows the master equation

$$\begin{aligned}\frac{\mathrm{d}P_{n,\sigma}}{\mathrm{d}t}(t) =& \lambda_\sigma(n-1)P_{n-1,\sigma}(t) + \mu_\sigma(n+1)P_{n+1,\sigma}(t) - (\lambda_\sigma + \mu_\sigma)nP_{n,\sigma}(t), \\ &+ \sum_{\substack{\sigma' \in \mathcal{S} \\ \sigma' \neq \sigma}} \left[k_{\sigma' \to \sigma} P_{n,\sigma} - k_{\sigma \to \sigma'} P_{n,\sigma'}\right],\end{aligned} \tag{2.77}$$

for $\sigma \in \mathcal{S}$, with $k_{\sigma\to\sigma'}$ the rate of switching from σ to σ'. This is the same master equation as in the simple birth-death process studied above (see Eq. (1.42)) but with additional terms that take into account the environmental dynamics. Figure 1.4 shows sample paths of this process in different switching regimes.

Slow and fast switching regimes

The inclusion of switching environments to a birth-death process (or to any branching process, in general) brings considerable difficulty to the analysis. In general, it is not possible to deduce analytical results. Depending on how fast the environment switches, however, one may resort to useful approximations. In particular, in the limits of *slow* and *fast switching environments*, it is possible to deduce closed-form solutions for the stationary distribution $P^{\mathrm{st}}_{n,\sigma}$.

We say the environment is slow when it switches slower than the typical population timescale. In this case, the environment spends enough time in each state that it reaches its stationary state in each of them. The stationary distribution of having n individuals can be obtained then as the weighted average of the distributions in each environmental state, with the weights determined by the stationary distribution of the environmental states [18]. More precisely, we have

$$P_n^{\mathrm{st(slow)}} = \sum_{\sigma\in\mathcal{S}} \rho^*_\sigma P_{n|\sigma}, \tag{2.78}$$

with $P_{n|\sigma}$ the stationary probability of having n individuals assuming a fixed environment σ. The distribution $P_{n|\sigma}$ is the stationary distribution of a simple birth-death process presented in Eq. (1.56).

If the environmental switching is fast compared to the population dynamics, we can treat the system as if it were in an effective fixed environment with growth rates λ_{eff} and μ_{eff}. These rates can be obtained as the weighted average of the rates in each environment, with the weights as the stationary distribution of the environmental states (i.e., the fraction of time spent in each environment) [18]. One finds then

$$\lambda_{\mathrm{eff}} = \sum_{\sigma\in\mathcal{S}} \rho^*_\sigma \lambda_\sigma \quad \text{and} \quad \mu_{\mathrm{eff}} = \sum_{\sigma\in\mathcal{S}} \rho^*_\sigma \mu_\sigma. \tag{2.79}$$

With these rates we can construct the stationary distribution of having n individuals using Eq. (1.47) for the distribution of simple birth-death process.

In Chapter 5 we will explore these approximations for both slow and fast regimes in a Moran-type model that switches between sexual and asexual reproduction.

2.4.2 Continuous space

In many biological scenarios the environment changes such that it takes values from a continuous range. This is the case of systems in which the environmental state σ models continuous parameters that fluctuates in time, such that temperature, concentration, density, etc. For some examples see [19–23].

In this thesis, continuous environments are only treated in Chapter 6 where we explore scenarios in which σ follows an Ornstein–Uhlenbeck process. We briefly present below the main properties of this process, and a simple case of a birth-death process whose rates depend on σ.

Ornstein–Uhlenbeck process

The Ornstein–Uhlenbeck process has been used in many biological areas [24], for example, to describe phenotypic evolution [25]. It was first introduced by Ornstein and Uhlenbeck in 1930 to model a frictional Brownian particle [26]. If σ follows this process, then its state space is $\mathcal{S} = \mathbb{R}$, and satisfies

$$\mathrm{d}\sigma = \theta(m - \sigma)\,\mathrm{d}t + s\,\mathrm{d}W, \tag{2.80}$$

with θ, m, and s constant parameters, and W a standard Wiener process. Since σ is unbounded, it can lead to unphysical situations depending on the system under study. This issue has to be dealt with care when modelling using an Ornstein–Uhlenbeck process. The previous equation can be written as a Langevin equation

$$\frac{\mathrm{d}\sigma}{\mathrm{d}t} = \theta(m - \sigma) + s\,\eta(t), \tag{2.81}$$

where $\eta(t)$ is zero-average Gaussian white noise. This equation can be integrated numerically using, for example, the Euler–Maruyama method that will later be explored (see Section 1.5.1). To ease the notation, we introduce the variables τ_c and v through the relations

$$\theta = 1/\tau_c \quad \text{and} \quad s = \sqrt{2v^2/\tau_c}, \tag{2.82}$$

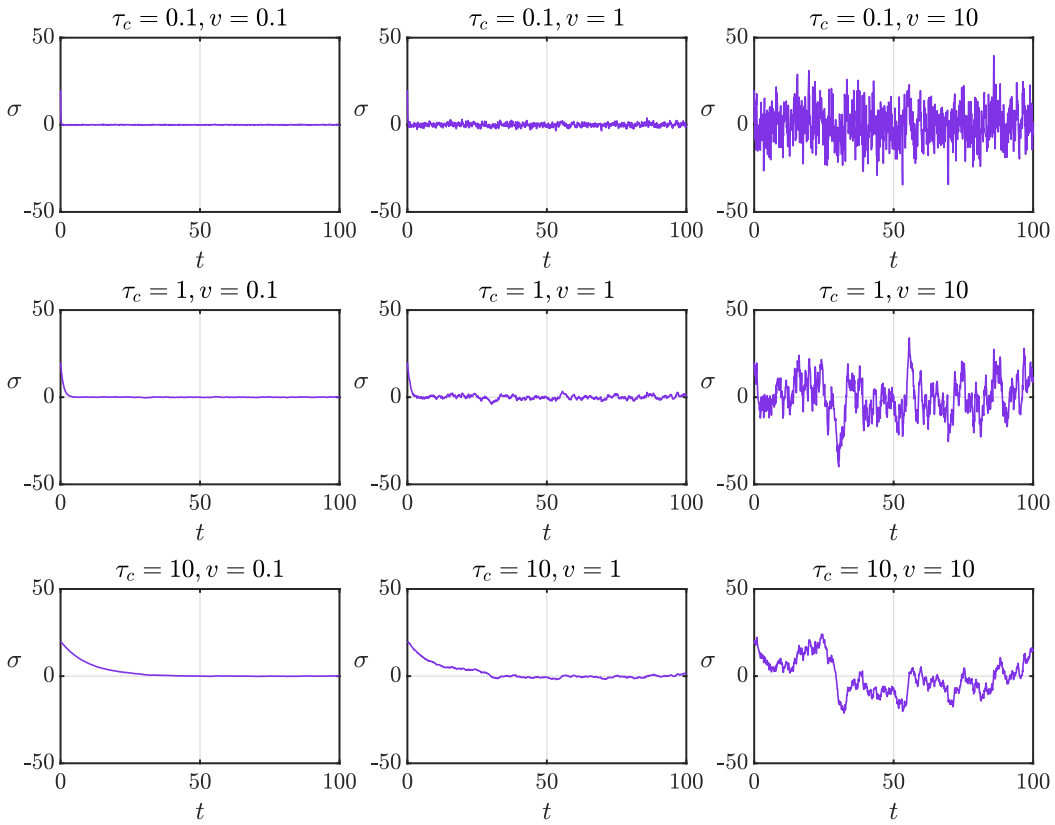

Figure 2.5: Sample paths of the Ornstein–Uhlenbeck process [see Eq. (6.26)] obtained by means of the Euler-Maruyama method (with time step $\mathrm{d}t = 0.01$) for different values of τ_c and v. Parameters used: $m = 0$, and $\sigma_{t=0} = 20$.

where τ_c controls the typical time to reach stationarity and v the fluctuations around the mean. Different sample paths obtained using the Euler–Maruyama method are presented in Figure 1.5.

The expected value of σ, with initial value σ_0 at t_0, takes the form

$$\langle \sigma \rangle \equiv E[\sigma] = \sigma_0 e^{-(t-t_0)/\tau_c} + m\left(1 - e^{-(t-t_0)/\tau_c}\right), \tag{2.83}$$

which shows that σ tends to m as t increases (assuming $\tau_c > 0$), i.e., m is the average in the long term. This means σ fluctuates, on average, approaching m as time goes by. This effect is called *mean reversion*, commonly used in finance [27]. Using the same initial condition for σ, the variance becomes

$$\mathrm{Var}[\sigma] \equiv \left\langle \sigma^2 \right\rangle - \langle \sigma \rangle^2 = v^2\left(1 - e^{-2(t-t_0)/\tau_c}\right), \tag{2.84}$$

and tends to v^2 as $t \to \infty$. The Fokker–Planck equation associated with the Ornstein–Uhlenbeck process is

$$\frac{\partial P}{\partial t} = \theta \frac{\partial}{\partial x}(x - m)P + \frac{D}{2}\frac{\partial^2 P}{\partial x^2}, \tag{2.85}$$

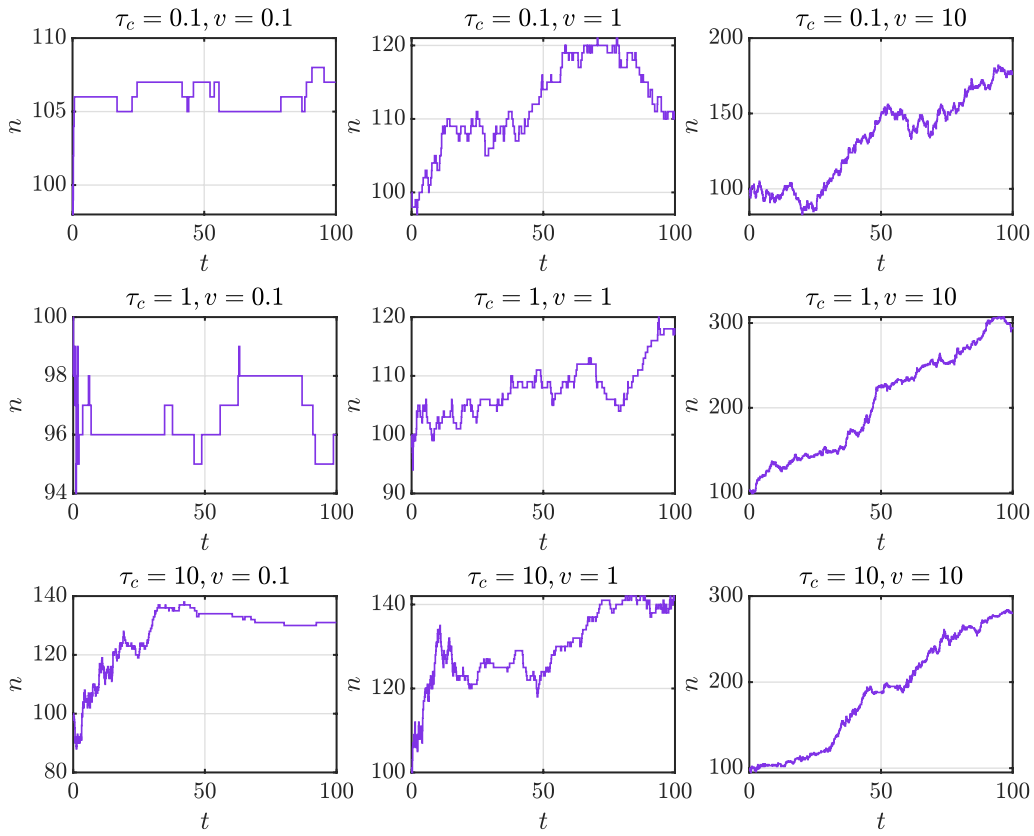

Figure 2.6: Samples paths of a birth-death process in a continuous environment with rates given as in Eq. (1.88) with $b = 1.1$ and $d = 1.0$. The environmental state σ is given by the sample paths from Figure 1.5.

with $D = s^2 = 2v^2/\tau_c$. The solution of this equation is

$$P_\sigma(t) = \frac{1}{\sqrt{2\pi \mathrm{Var}[\sigma]}} \exp\left[-\frac{1}{2}\frac{(\sigma - E[\sigma])^2}{\mathrm{Var}[\sigma]}\right], \tag{2.86}$$

with initial condition $P_\sigma(t - t_0) = \delta(\sigma - \sigma_0)$. The stationary distribution is obtained in the limit $t \to \infty$. This results in

$$\rho^*_\sigma \equiv \lim_{t\to\infty} P_\sigma(t) = \frac{1}{v\sqrt{2\pi}} \exp\left[-\frac{1}{2}\left(\frac{\sigma - m}{v}\right)^2\right]. \tag{2.87}$$

This is a normal distribution with mean m and variance v^2.

Simple birth-death process in continuous environments

Let us consider a simple birth-death process with growth rates depending on σ, which follows an Ornstein–Uhlenbeck process. The dependence on the rates λ^σ_n and μ^σ_n with

respect to σ is as in Eq. (1.76), i.e., $\lambda_n^\sigma = \lambda_\sigma n$ and $\mu_n^\sigma = \mu_\sigma n$, with

$$\lambda_\sigma = b|\sigma| \quad \text{and} \quad \mu_\sigma = d|\sigma|, \tag{2.88}$$

for $b, d > 0$. In Figure 1.6 we show sample paths of this process using the Gillespie algorithm approach as described in Chapter 6. We consider the sample paths of σ shown in Figure 1.5.

2.5 Further computational and mathematical tools

In this section, we present some numerical and mathematical tools that will be later used in the following chapters. We describe standard and well-known algorithms to simulate stochastic systems. These algorithms are suitable for systems under different conditions (e.g., if the rates depend on time or not) as we explain below. We also briefly present some properties of partitions of integer numbers that will be necessary in Chapter 5.

2.5.1 Numerical methods to simulate stochastic systems

Gillespie algorithm

The Gillespie algorithm [28, 29], often called stochastic simulation algorithm (SSA), is a standard method to simulate continuous-time Markov processes with constant per capita transition rates, e.g., homogeneous birth-death processes. This algorithm does not discretise time as other algorithms but it draws the time at which the next reaction occurs from an exponential distribution. The algorithm proceeds as follows:

Consider a system with reactions $i = 1, \ldots, M$ with transition rates W_i.

(i) Initialise the system at $t = 0$ in its initial state.

(ii) Compute W_i and $\lambda = \sum_{i=1}^{M} W_i$. Generate an uniformly distributed random number r between 0 and 1, and compute

$$\tau = -\frac{1}{\lambda} \ln r. \tag{2.89}$$

Update the time to $t + \tau$.

(iii) Generate an uniformly distributed random number p between 0 and 1, and execute one of the possible reactions. Reaction i occurs with probability W_i/λ, so if $0 \leq p < W_1/\lambda$ execute reaction 1, if $W_1/\lambda \leq p < (W_1 + W_2)/\lambda$ execute reaction 2, etc.

(iv) Update the state of the system accordingly and go to 2.

In the case of a birth-death process, the rates W_i are equal to λ_i and μ_i, i.e., the birth and death rates. If they depend on the population size (e.g., a simple birth-death process), one needs to update W_i in each iteration.

One disadvantage of the Gillespie algorithm is that it can become slow for large populations and/or when the transition rates are high, as more events occur per unit time. The Gillespie algorithm can be used as an approximation for systems with time-dependent rates as long as the rates do not exceedingly vary over time.

$\tau-$leaping algorithm

One alternative to deal with the ineffectiveness of the Gillespie algorithm in simulating systems with large populations or high transition rates is the so-called $\tau-$leaping algorithm [30]. Unlike the conventional Gillespie algorithm, this method uses a discretisation of time with time step τ. This step has to be small enough that the change of system state in the interval $[t, t+\tau]$ does not drastically change the transition rates. This condition is referred to as the *leap condition* [30]. The $\tau-$leaping algorithm then gives an approximation of the realisation of the system, but performs faster than the Gillespie algorithm which is an exact scheme. The algorithm proceeds as follows:

Consider a system with reactions $i = 1, \ldots, M$ and transition rates W_i. Let us denote the state of the system by $\mathbf{n}(t) = (n_1, \ldots, n_j, \ldots, n_N)$ and let $\nu_{i,j}$ be the change in n_j when reaction i occurs. Then,

(i) Initialise the system at $t = 0$ in its initial state.

(ii) Compute the W_i and update the time to $t + \tau$.

(iii) Generate independent Poissonian random numbers m_i with parameters τW_i. This is the number of times the event i occurs within the interval $[t, t+\tau)$.

(iv) Update the state of system $n_i(t+\tau) = n_i(t) + \sum_{j=1}^{M} \nu_{ij} m_j$ and go to 2.

In Chapter 6 we will describe an algorithm based on the $\tau-$leaping algorithm to simulate systems in fast fluctuating environments, both in discrete and continuous space.

Lewis' method (thinning algorithm)

The Lewis' method (often called the thinning algorithm) proposed by Lewis and Shedler in 1979 [31] is a useful exact method for simulating non-homogeneous Poison processes, i.e., processes with time-dependent transition rates. The algorithm proceeds as follows:

Consider a system with reactions $i = 1, \ldots, M$ with transition rates $W_i(t)$. To generate a sample path in the interval $[0, T]$,

(i) Initialise the system at $t = 0$ in its initial state.

(ii) Compute $\overline{W}_i = \sup_{0 \le t \le T} W_i(t)$ and $\overline{W} = \sum_{i=1}^{M} \overline{W}_i$. Generate an uniformly distributed random number r between 0 and 1, and compute the time when the next reaction occurs

$$\tau = -\frac{1}{\overline{W}} \ln r. \tag{2.90}$$

Update the time to $t + \tau$. If $t + \tau > T$, stop the simulation.

(iii) Generate an uniformly distributed random number p between 0 and 1. Reaction i occurs with probability $W_i/\overline{W}$, so if $0 \le p < W_1/\overline{W}$ execute reaction 1, if $W_1/\overline{W} \le p < (W_1 + W_2)/\overline{W}$ execute reaction 2, etc. If $\sum_{i=1}^{M} W_i/\overline{W} \le p \le 1$, do not execute any reaction.

(iv) Update the system state accordingly and go to 2.

For a simple birth-death process the rates W_i are equal to $\lambda_n = n\lambda(t)$ and $\mu = n\mu(t)$. In this case the maxima $\overline{W}_i$ are computed as $\overline{\lambda_n} = n \sup_{0 \le t \le T} \lambda(t)$ and $\overline{\mu_n} = n \sup_{0 \le t \le T} \mu(t)$.

Euler–Maruyama method

In cases in which one is interested in solving a stochastic differential equation, one can use the Euler–Maruyama method [32] which generates an approximate solution of equations of the form

$$\mathrm{d}X(t) = f(X(t))\,\mathrm{d}t + g(X(t))\,\mathrm{d}W(t), \tag{2.91}$$

where $\mathrm{d}W(t)$ represents a Wiener process. The method proceeds as follows:

Consider the stochastic differential equation in Eq. (1.91) for given functions $f(X)$ and $g(X)$. Set an interval $[0, T]$ and a time step $\Delta t = T/N$. The points generated will be at times $t_n = n\Delta t$ for $1 \leq n \leq N$.

(i) Initialise the system at $t = 0$ in its initial state $X(0)$.

(ii) Simulate the Wiener process as independent and identically distributed normal random variables $\Delta W(t_n)$ with mean 0 and variance Δt for $1 \leq n \leq N$.

(iii) Update the system state as

$$X(t_{n+1}) = X(t_n) + f(X(t_n))\Delta t + g(X(t_n))\Delta W(t_n). \tag{2.92}$$

Repeat it until $t_n = T$.

2.5.2 Partitions of integer numbers

In this section, we briefly present some properties of *partitions of integer numbers* that will be used in Chapter 5 to deduce stochastic quantities of a Moran-type model. We focus on a particular type of partitions called *compositions*.

A partition of a positive integer number N, or an *integer partition*, is any of the possible sets of positive integer numbers whose sum is equal to N [33, 34]. The elements of these sets are called *parts*, and the number of possible partitions of N is given by the so-called *partition function* $p(N)$ [35].

In a partition, the order of the parts in the partition is irrelevant. Thus, for example, the partitions of $N = 5$ are given by

$$\begin{aligned} 5 &= 5 \\ &= 4 + 1 \\ &= 3 + 2 \\ &= 3 + 1 + 1 \\ &= 2 + 2 + 1 \\ &= 2 + 1 + 1 + 1 \\ &= 1 + 1 + 1 + 1 + 1. \end{aligned}$$

These are seven as $p(5) = 7$. If we take into account the order of a partition, we call the partition a composition. A composition of M parts is usually referred to as a *M-composition* [33]. The number of M-compositions of N is given by $\binom{N-1}{M-1}$, so the total number of compositions of N becomes $\sum_{M=1}^{N} \binom{N-1}{M-1} = 2^{N-1}$. Taking the previous example, the 2-compositions of $N = 5$ are

$$\begin{aligned} 5 &= 4 + 1 \\ &= 1 + 4 \\ &= 3 + 2 \\ &= 2 + 3, \end{aligned}$$

which are 4 as $\binom{N-1}{M-1}$ takes this value for $N = 5$ and $M = 2$. The total number of compositions of $N = 5$ is $2^4 = 16$.

Notice the parts of a composition are strictly positive numbers. If the parts of a compositions are allowed to be equal to zero, we call them *weak compositions* [33]. We do not study these cases here.

Sum over compositions

A sum over M-compositions is usually denoted by

$$\sum_{\substack{n_1+\cdots+n_M=N \\ n_i\geq 1}} F(n_1,\ldots,n_M), \tag{2.93}$$

for given integers N and M. Depending on how the function F depends on the parts n_i of the M-compositions of N, it is possible to find closed-form solutions of sums of this type. We focus on the case

$$F(n_1,\ldots,n_M)=\prod_{k=1}^{M} f(n_k), \tag{2.94}$$

where $f:\mathbb{N}\to\mathbb{R}$ is an arbitrary function. For this case, the sum in Eq. (1.93) takes the form [36]

$$\sum_{\substack{n_1+\cdots+n_M=N \\ n_i\geq 1}} \prod_{k=1}^{M} f(n_k) = [x^N]\left(\sum_{i\geq 1} f(i)x^i\right)^M, \tag{2.95}$$

where we use the standard notation $[x^N]g(x)$ to denote the coefficient multiplying x^N in the polynomial $g(x)=\sum_i a_i x^i$, i.e., $[x^N]g(x)=a_N$. The sum in Eq. (1.95) then is equal to the coefficient multiplying x^N in the expansion of $\left(\sum_{i\geq 1} f(i)x^i\right)^M$. This coefficient is usually referred to as the *polynomial coefficient* or *extended binomial coefficient* [34, 36], and is denoted by $\binom{M}{N}_f$. By using the *Cauchy's integral formula* [37], the right-hand side of Eq. (1.95) can be expressed as

$$\frac{1}{N!}\frac{\partial^N f^M}{\partial x^N}(0)=\frac{1}{2\pi i}\oint_\gamma \frac{\Phi(z)^M}{z^{N+1}}\mathrm{d}z, \tag{2.96}$$

where γ is an appropriate rectifiable curve around the origin. We have defined the generating function $\Phi(x)=\sum_{i\geq 1} f(i)x^i$.

As an illustrative example, let us consider the case $f(n_i)=n_i$. Following Eq. (1.93), we have

$$\sum_{\substack{n_1+\cdots+n_M=N \\ n_i\geq 1}} \prod_{k=1}^{M} n_k. \tag{2.97}$$

The generating function then becomes

$$\Phi(x) = \sum_{i=1}^{\infty} i x^i = \frac{x}{(x-1)^2}. \tag{2.98}$$

Using the identity [38]

$$\binom{n}{k} = \frac{1}{2\pi i} \int_{|z|=\varepsilon} \frac{1}{(1-z)^{k+1} z^{n-k+1}}\, dz, \tag{2.99}$$

with $\varepsilon \ll 1$, we solve the integral in Eq. (1.96) and find

$$\sum_{\substack{n_1+\cdots+n_M=N \\ n_i \geq 1}} \prod_{k=1}^{M} n_k = \binom{N+M-1}{2M-1}. \tag{2.100}$$

In Chapter 5, we will explore cases with $f(n_i) = 1/n_i$ and $f(n_i) = 1/[n_i(N-n_i)!]$.

Bibliography

[1] N. T. Bailey, *The elements of stochastic processes with applications to the natural sciences*, Vol. 25 (John Wiley & Sons, New York, 1990).

[2] S. Karlin, and J. McGregor, "The classification of birth and death processes", Transactions of the American Mathematical Society **86**, 366–400 (1957).

[3] S. Karlin, and J. L. McGregor, "The differential equations of birth-and-death processes, and the Stieltjes moment problem", Transactions of the American Mathematical Society **85**, 489–546 (1957).

[4] N. S. Goel, and N. Richter-Dyn, *Stochastic models in biology* (Elsevier, New York, 2016).

[5] G. U. Yule, "A Mathematical Theory of Evolution, Based on the Conclusions of Dr. J. C. Willis, F.R.S.", Philosophical Transactions of the Royal Society of London. Series B, Containing Papers of a Biological Character **213**, 21–87 (1925).

[6] W. Furry, "On fluctuation phenomena in the passage of high energy electrons through lead", Physical Review **52**, 569 (1937).

[7] S. Tavaré, "The linear birth–death process: an inferential retrospective", Advances in Applied Probability **50**, 253–269 (2018).

[8] P.-F. Verhulst, "Notice sur la loi que la population suit dans son accroissement", Corresp. Math. Phys. **10**, 113–126 (1838).

[9] P. A. P. Moran, "Random processes in genetics", in Mathematical proceedings of the cambridge philosophical society, Vol. 54, 1 (Cambridge University Press, 1958), pp. 60–71.

[10] W. J. Ewens, *Mathematical Population Genetics* (Springer-Verlag, Berlin, 2004).

[11] M. Zaider, and G. Minerbo, "Tumour control probability: a formulation applicable to any temporal protocol of dose delivery", Physics in Medicine & Biology **45**, 279 (2000).

[12] B. Warkentin, P. Stavrev, N. Stavreva, C. Field, and B. G. Fallone, "A TCP-NTCP estimation module using DVHs and known radiobiological models and parameter sets", Journal of Applied Clinical Medical Physics **5**, 50–63 (2004).

[13] K. Wienand, E. Frey, and M. Mobilia, "Evolution of a Fluctuating Population in a Randomly Switching Environment", Physical Review Letters **119**, 158301 (2017).

[14] M. Acar, J. T. Mettetal, and A. Van Oudenaarden, "Stochastic switching as a survival strategy in fluctuating environments", Nature Genetics **40**, 471–475 (2008).

[15] G. Lambert, and E. Kussell, "Memory and fitness optimization of bacteria under fluctuating environments", PLoS Genetics **10** (2014).

[16] M. Thattai, and A. Van Oudenaarden, "Stochastic gene expression in fluctuating environments", Genetics **167**, 523–530 (2004).

[17] R. Lefever, and W. Horsthemke, "Bistability in fluctuating environments. Implications in tumor immunology", Bulletin of mathematical biology **41**, 469–490 (1979).

[18] P. Ashcroft, P. M. Altrock, and T. Galla, "Fixation in finite populations evolving in fluctuating environments", Journal Royal Society Interface **11**, 20140663 (2014).

[19] M. Assaf, M. Mobilia, and E. Roberts, "Cooperation dilemma in finite populations under fluctuating environments", Physical review letters **111**, 238101 (2013).

[20] M. Assaf, E. Roberts, and Z. Luthey-Schulten, "Determining the stability of genetic switches: explicitly accounting for mRNA noise", Physical Review Letters **106**, 248102 (2011).

[21] M. Assaf, E. Roberts, Z. Luthey-Schulten, and N. Goldenfeld, "Extrinsic Noise Driven Phenotype Switching in a Self-Regulating Gene", Physical Review Letters **111**, 058102 (2013).

[22] P. C. Bressloff, "Stochastic Fokker-Planck equation in random environments", Physical Review E **94**, 042129 (2016).

[23] E. Roberts, S. Be'er, C. Bohrer, R. Sharma, and M. Assaf, "Dynamics of simple gene-network motifs subject to extrinsic fluctuations", Physical Review E **92**, 062717 (2015).

[24] S. Ditlevsen, and A. Samson, "Introduction to stochastic models in biology", in *Stochastic biomathematical models* (Springer, Berlin, 2013), pp. 3–35.

[25] E. P. Martins, "Estimating the rate of phenotypic evolution from comparative data", The American Naturalist **144**, 193–209 (1994).

[26] G. E. Uhlenbeck, and L. S. Ornstein, "On the theory of the Brownian motion", Physical Review **36**, 823 (1930).

[27] R. Schöbel, and J. Zhu, "Stochastic volatility with an Ornstein–Uhlenbeck process: an extension", Review of Finance **3**, 23–46 (1999).

[28] D. T. Gillespie, "A general method for numerically simulating the stochastic time evolution of coupled chemical reactions", Journal of Computational Physics **22**, 403–434 (1976).

[29] D. T. Gillespie, "Exact stochastic simulation of coupled chemical reactions", Journal of Physical Chemistry **81**, 2340–2361 (1977).

[30] D. T. Gillespie, "Approximate accelerated stochastic simulation of chemically reacting systems", The Journal of Chemical Physics **115**, 1716–1733 (2001).

[31] P. W. Lewis, and G. S. Shedler, "Simulation of nonhomogeneous Poisson processes by thinning", Naval Research Logistics Quarterly **26**, 403–413 (1979).

[32] G. Maruyama, "Continuous Markov processes and stochastic equations", Rendiconti del Circolo Matematico di Palermo **4**, 48 (1955).

[33] S. Heubach, and T. Mansour, *Combinatorics of compositions and words* (CRC Press, Boca Raton, 2009).

[34] L. Comtet, *Advanced Combinatorics: The art of finite and infinite expansions* (Springer Science & Business Media, Dordrecht, 2012).

[35] M. B. Nathanson, *Elementary methods in number theory*, Vol. 195 (Springer Science & Business Media, New York, 2008).

[36] S. Eger, "Restricted weighted integer compositions and extended binomial coefficients", J. Integer Seq. **16**, 3 (2013).

[37] L. Hörmander, *An introduction to complex analysis in several variables* (Elsevier, Amsterdam, 1973).

[38] G. P. Egorychev, *Integral representation and the computation of combinatorial sums*, Vol. 59 (American Mathematical Soc., 1984).

Chapter 3

Mutators drive evolution of multi-resistance to antibiotics

Preface

The contents of this chapter constitutes a bioRxiv preprint[1] currently under review at Nature Ecology & Evolution. This work is co-authored with Tobias Galla[2,3], Danna R. Gifford[4], Christopher Knight[5], Marc Suñé[4,6], and Christine Joerres[4], where D.R.G. is the corresponding author.

E.B-C. contributed to the design of the stochastic model, performed analysis of experimental data, carried out stochastic simulations, and wrote parts of the manuscript. The data analysis consisted in extracting the growth parameters of the experimental data by performing curve fittings of growth curves of bacterial populations, then use these parameters to simulate the experiment through a stochastic model. E.B-C. was actively involved in producing the results presented in Secs. 3.2.4, 3.6.6, and 3.8, and also participated in discussions of the rest of the manuscript. For completeness, all

[1] D. R. Gifford, E. Berríos-Caro, C. Joerres, T. Galla, C. G. Knight, (2019), "Mutators drive evolution of multi-resistance to antibiotics", *bioRxiv preprint.* bioRxiv:643585.

[2] Theoretical Physics, Department of Physics and Astronomy, School of Natural Sciences, Faculty of Science and Engineering, The University of Manchester, Manchester M13 9PL, United Kingdom.

[3] Instituto de Física Interdisciplinar y Sistemas Complejos, IFISC (CSIC-UIB), Campus Universitat Illes Balears, E-07122 Palma de Mallorca, Spain.

[4] Division of Evolution and Genomic Sciences, School of Biological Sciences, Faculty of Biology, Medicine and Health, The University of Manchester, Manchester M13 9PT, United Kingdom.

[5] Department of Earth and Environmental Sciences, School of Natural Sciences, Faculty of Science and Engineering, The University of Manchester, Manchester M139PL, United Kingdom.

[6] Present address: Nordita, Royal Institute of Technology and Stockholm University, Roslagstullbacken 23, SE-106 91 Stockholm, Sweden.

the remaining sections are included. The reader not concerned in the details of the experimental setup can omit Secs. 3.6.1 to 3.6.5. Section 3.9 applies methods (Bayesian analysis) developed by D.R.G. These are not central to the thesis, and E.B-C. was not involved in developing or implementing these methods.

Abstract

Combination therapy is increasingly being used in an attempt to counter the evolution of drug-resistant infections. However, the success of this approach relies on its ability to prevent resistance to each component antibiotic from arising during treatment. Here we show that bacterial populations can evolve 'multi-resistance' by sequentially acquiring independent resistance mutations. We exposed experimental *Escherichia coli* populations to rising concentrations of single-drug and combination antibiotics. Introducing a 'mutator' strain at low-to-intermediate frequencies facilitated the evolution of multi-resistance. Crucially, mutators allowed multi-resistance to evolve during single-drug and combination treatments alike, meaning that direct selection for multi-resistance was not needed for it to occur. Eco-evolutionary simulations revealed that the sweep of mutator alleles in conjunction with single resistance alleles was key to multi-resistance evolution when it occurred, as the resulting increase in mutation supply allowed subsequent resistance mutations to arise in the same genetic background. Further simulations demonstrated that, while multi-resistance could also arise in large populations without mutators, the population size required was larger than typical of infections. Ultimately, our results suggest that the utility of combination therapy may be limited when mutators are present, and when achieving or maintaining therapeutic antibiotic concentrations is difficult—scenarios that both regularly occur in clinical settings.

3.1 Introduction

The global burden of antimicrobial resistance is spurring research into how existing drugs can be used more effectively to prevent resistance evolution. There has been sustained interest in using 'combination therapy' for preventing resistance in infections and cancer [1–4]. Where standard 'monotherapy' uses only one drug at a time, combination therapy uses multiple drugs concurrently. This approach has proved successful in clinical settings [5–7]. Combination therapy is currently used for some diseases caused by microbes (e.g. tuberculosis [8]), but there is growing interest in deploying it more broadly to combat antibiotic resistance [9–11]. Progress has been made in determining

how to best combine drugs to inhibit bacteria [12–14], especially through exploiting non-additive effects on growth (i.e. synergy and antagonism [4, 15]). Other strategies involving more than one drug, e.g. 'mixing' (assigning different antibiotics to different patients), and 'cycling', (using different antibiotics alternately), are also possible. Some models suggest an advantage of combination therapy over these other approaches [16] although this is not universal [17]. However, clinical evidence for the ability of combination therapy to prevent resistance evolution is mixed, with some combinations fairing no better than monotherapy for some types of infection [18]. Discovering what governs the ability of combinations to prevent resistance is therefore a critical area of research.

The idea that resistance to multiple antibiotics requires multiple independent resistance mutations is central to the rationale behind combination therapy. Although acquiring resistance to monotherapy ('single resistance') occurs regularly, acquiring resistance to combination therapy ('multi-resistance') is generally more difficult. The ability for combination therapy to prevent multi-resistance relies on two main assumptions. First, mutation rates to resistance are generally assumed to be small for bacteria, on the order of 10^{-7} to 10^{-10} per generation [19]. The probability of acquiring multiple independent resistance mutations during the same replication event is the product of their individual mutation rates [2, 20]. For two mutations, this is on the order of 10^{-14} to 10^{-20} per generation (discounting specific combinations where resistance occurs by 'multi-drug resistance' or 'cross-resistance' mechanisms [21]). The emergence of multi-resistance during a single replication event is therefore exceedingly rare. Second, inhibitory concentrations are assumed to occur rapidly after treatment. If growth of both sensitive and single-resistant organisms is inhibited, multi-resistance cannot be acquired over the course of several replications.

However, the assumptions of low mutation rates and rapid inhibition are capable of being violated in bacterial populations exposed to combination therapy. For instance, the presence of 'mutator' organisms (i.e. with higher mutation rates) may invalidate the assumption of low mutation rates. Mutators emerge spontaneously and persist at low-to-intermediate frequencies in host-associated bacterial populations [22] and infections [23–25]. Typical mutators have mutation rates 10- to 1000-fold higher than wild-type [26, 27]. Further, inhibitory concentrations may not be reached rapidly, or

may vary over time, due to antibiotic dosing regimens and drug pharmacokinetics. This can allow some degree of growth of sensitive and single-resistant strains, which can ultimately allow selection to act on resistant lineages [28–32]. Whether violating these assumptions can lead to multi-resistance warrants consideration. Mutators are a particular concern for the application of combination therapy, as multi-resistance is commonly observed in clinical mutator lineages [26, 33–36]. What direct evidence exists for the efficacy of combinations against mutators is mixed [37, 38]. Determining how frequently multi-resistance arises in populations where mutators are present, and what evolutionary mechanisms are responsible, is therefore important to predicting the success of combination therapy.

Here, we determined whether the presence of mutators could allow populations to overcome combination antibiotic treatment by evolving multi-resistance. We challenged mixed populations comprising wild-type (*Escherichia coli* K-12 BW25113) and mutator ($\Delta mutS$) organisms with rifampicin, nalidixic acid, and combination treatments that increased in concentration over time. Where mutators were present, multi-resistance evolved in both the single-drug and combination treatments. In contrast, where mutators were absent, only single-drug resistance was observed. We used stochastic simulations to directly test the evolutionary mechanisms leading to the evolution of resistance. This showed that differences in mutation rate were sufficient to explain multi-resistance evolution for typical bacterial population sizes. Mutator alleles swept from low to high frequency along with single-drug resistance, allowing resistance to a second drug to occur subsequently. Multi-resistance did not require spontaneous double mutants or multi-drug resistance mechanisms. Given the prevalence of mutators, multi-resistance may therefore complicate the wider use of combination therapy against bacterial infections.

3.2 Results

3.2.1 Mutators facilitate double resistance evolution by sequential acquisition of independent mutations

We subjected populations of bacteria with different initial mutator frequencies to antibiotic-free, single-drug or combination antibiotic treatment with rifampicin and/or nalidixic acid. Antibiotic concentrations were doubled daily over 6 days, starting at 0.625 mg/l and ending at 20 mg/l (where 10 mg/l of either drug is sufficient to inhibit the starting strain). Figure 3.1 shows the number of populations with detectable resistance under each treatment as detected by selective plating (with optical density of each population revealing a similar trend, Extended Data Figure 1). Several patterns emerge. In the absence of selection for resistance (i.e. left column of Figure 3.1), double resistance was not detected for any mutator frequency, although single resistance was observed. In the absence of mutators (i.e. top row of Figure 3.1), double resistance was not detected for any treatment, although single resistance was again observed. However, for populations where mutators were present and antibiotic selection was applied, both single and double resistance was observed. Strikingly, double resistance was observed for both the single-drug treatments and the combination treatment. In general, nalidixic acid treatment resulted in the fewest double-resistant populations, whereas rifampicin and combination treatment produced roughly similar numbers. The combination treatment resulted in the highest proportion of populations where no resistance was detected. In this sense, the combination treatment was more effective at suppressing resistance to the specific treatment applied, even in the presence of mutators. However, a considerable proportion of populations nevertheless exhibited double resistance when mutators were present.

The relationship between resistance at the final time point, mutator initial frequency and antibiotic treatment was determined using a Bayesian categorical mixed-effects model (Model M1 in the Supplementary Information). The fit of a full model incorporating both main effects and interactions was only marginally better than a main effects-only model, hence we present parameter estimates from the latter (given in full in Table 3.8 in the Supplementary Information). The main effect of mutators was positive for all resistance types, i.e. the posterior distributions of the estimates had

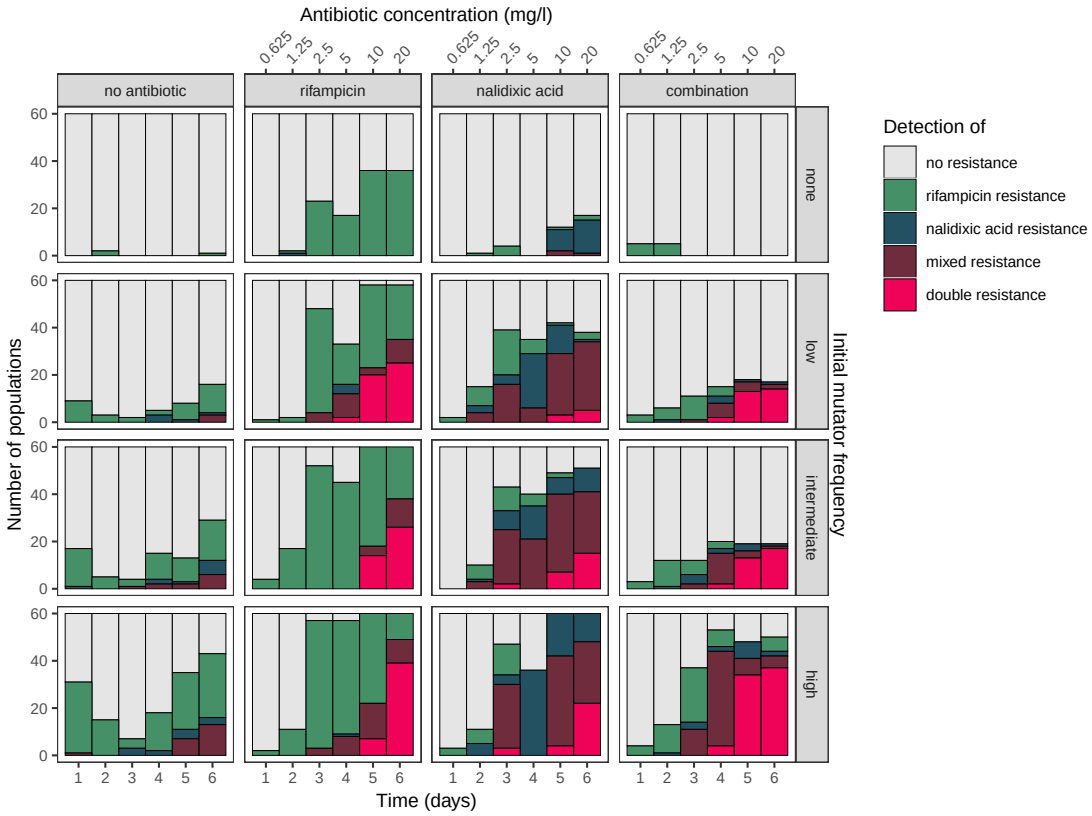

Figure 3.1: Emergence of antibiotic resistance in the presence and absence of selection for resistance in populations with and without mutators. Multi-resistance emerged when mutators were present (rows) under both mono- and combination antibiotic therapy (middle and right columns, respectively), but not in the absence of antibiotics (left column). Stacked bars show numbers of populations where each category of resistance was detected by selective plating. 'Rifampicin resistance' and 'nalidixic acid resistance' indicate growth on either rifampicin or nalidixic acid medium, respectively, but not on both nor in combination. 'Mixed resistance' indicates growth on both rifampicin and nalidixic acid medium separately but not in combination. 'Double resistance' indicates growth on both antibiotics separately and also in combination. For further details, see Model M1 in the Supplementary Information.

95% C.I. (confidence interval) greater than zero, with the exception of 'low' mutators and nalidixic acid resistance. While the mean effects of mutators increased with increasing mutator frequencies (low < intermediate < high, generally), the 95% C.I.s of their posteriors overlapped. Single antibiotic treatments had predictable effects on single-drug resistance, i.e. rifampicin resistance was more likely to occur under rifampicin treatment, but not nalidixic acid treatment, and vice versa. All antibiotic treatments increased the probability of double resistance evolving.

3.2.2 No evidence for a growth advantage of double resistance in single-drug treatments

The occurrence of double-resistant strains in single-drug treatments is surprising. We therefore used growth assays to test whether there could be any positive selection for double resistant strains in the presence of single antibiotics. To determine which treatments should result in positive selection for resistance, we assayed growth of sensitive, single- and double-resistant clones under all conditions experienced during experimental evolution. Growth assays were conducted on clones derived from fluctuation tests (based on the Luria-Delbrück experiment [94]) using the non-mutator wild-type BW25113, to minimise confounding effects of other mutations arising during experimental evolution. For the combination treatment, there was a clear advantage of double resistance over single-drug resistance for concentrations of 1.25 mg/l and above (Figure 3.2). These concentrations correspond to time periods where double resistance begins to be detected in the experiments. In contrast, there was no benefit of double resistance over rifampicin resistance in the rifampicin treatment [difference in growth = -0.07, 95% C.I.: $(-0.38, 0.23)$], and a disadvantage over nalidixic acid resistance in the nalidixic acid treatment [difference in growth = -0.75, 95% C.I.: $(-1.05, -0.45)$]. This provides no evidence of a benefit to double resistance in single drug treatments, suggesting that double resistance did not spread due to positive selection.

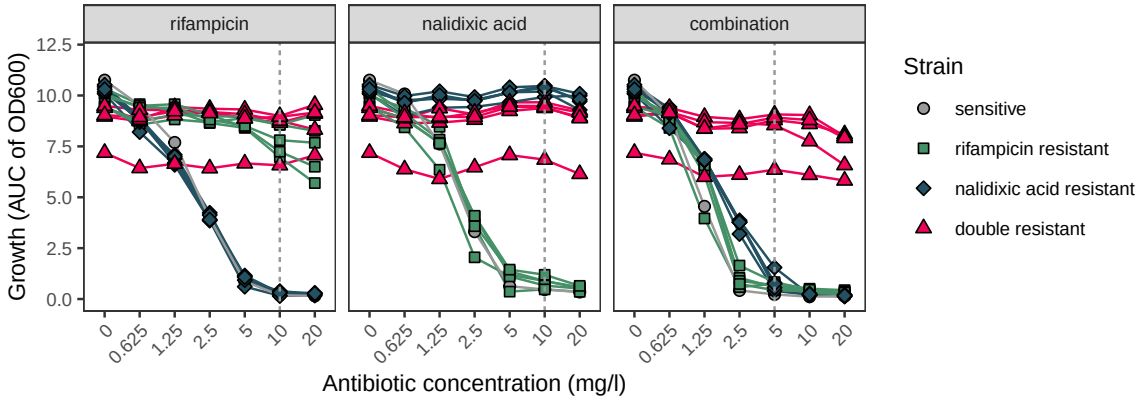

Figure 3.2: Growth of sensitive, single-, and double-drug resistant strains at antibiotic concentrations experienced during the resistance selection regime (AUC of OD600: area under curve of growth curves measuring optical density at 600 nm over time). Resistant strains (5 per type) were isolated in the wild-type *E. coli* K-12 BW25113 genetic background by fluctuation test(s). Vertical line indicates minimum inhibitory concentration of the wild-type. For all points, error bars ±SE (Standard Error) are smaller than plotting symbols. See Model M2 in the Supplementary Information.

3.2.3 Effect of mutator frequency on growth

In addition to altering the probability of observing multi-resistance, different initial mutator frequencies may also influence how well the resulting multi-resistant lineages grow. A higher mutator frequency may be a benefit to populations, through increase clonal interference between competing resistant lineages. It may also be detrimental, due to the accumulation of of deleterious mutations [39, 40]. To assess the effect of mutator frequency on growth, we compared the growth curves of multi-resistant clones that arose from populations with different initial mutator frequencies. We analysed the data using a Bayesian multivariate regression model (Figure 3.3, Table 3.9 and Model M3 in the Supplementary Information). From each growth curve, we calculated the area under the curve (AUC), and averaged over three replicate growth curves. Accounting for initial mutator frequency provided a worse fit than a model with only a global intercept (i.e. a flat line intersecting the horizontal axis at the overall average AUC), suggesting that initial mutator frequency did not have a considerable effect on growth overall. Thus, mutators did not seem to unduly suffer, or majorly benefit, from secondary mutations in our selection experiment. There was nevertheless a slight tendency toward higher AUC for intermediate and high mutator frequencies, both under antibiotic-free conditions and at maximum selection experiment concentration (i.e. 20 mg/l). The fitness of double-resistant clones was generally positively correlated between environments ($r = 0.69$, similar to single-resistant strains in single-drug environments [41]). However, there was some variation among the evolved clones. Notably, several clones demonstrated relatively higher growth under antibiotic-free conditions (compared to others with the same growth at 20 mg/l). One possible explanation for this is the acquisition of secondary mutations that are more beneficial in the antibiotic-free environment. However, there was similar variation among double mutants arising in the non-mutator genetic background selected via successive fluctuation tests, where secondary mutations are much less likely to have occurred. Hence, the variation cannot be decisively attributed to secondary beneficial mutations, and may instead reflect variation among the resistance alleles themselves.

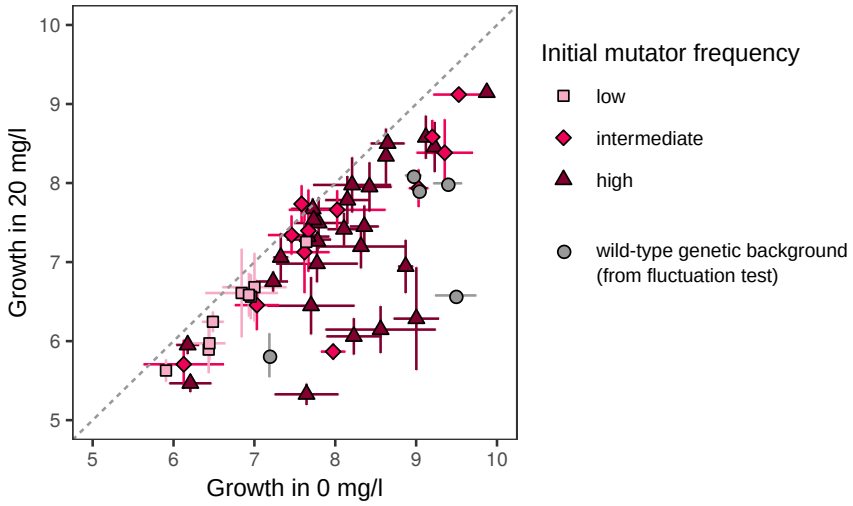

Figure 3.3: Effect of mutator frequency on growth of double-resistant mutants evolved during resistance selection. Growth under antibiotic-free conditions and the maximum combination concentration (20 mg/l) was positively correlated [residual $r = 0.69$, 95% C.I.: $(0.56, 0.79)$]. Each point represents mean±SE of area under the curve from three replicate growth curves obtained via optical density at 600 nm. See Model M3 in the Supplementary Information.

3.2.4 Stochastic simulations reveal evolutionary mechanisms of multi-resistance evolution

To gain insight into the drivers of resistance evolution, we used a stochastic population-dynamic simulation model. Specifically, we tested hypotheses regarding the roles of selection and mutation supply on the emergence of double resistance in single-drug and combination treated populations. Further, we tested the hypothesis that multi-resistance can arise sequentially, by disallowing the possibility of multi-drug resistance mutations. Using models is advantageous because it allows control over confounding factors that may also cause mutators to increase in frequency, such other beneficial variation that does not confer resistance. Stochastic approaches have been used by others to study resistance evolution where resistant variants have a possibility of going extinct while rare [42–44]. Our model captured the major features of the wet-lab experiments: mixed wild-type/mutator populations, increasing antibiotic concentrations, and periodic bottlenecks (i.e. periodic reductions of population). Consider a sensitive wild-type S. During growth, single mutations can occur, giving rise to rifampicin-resistant type R and nalidixic acid resistant type N. Subsequently, R and N can each give rise to double-resistant type D (Figure 3.4). Mutations may occur in either the wild-type or mutator genetic background, resulting in a total of eight possible genotypes, i.e. strains

S, R, N, and D of both wild and mutator types. Wild-type and mutator differ only in mutation rate. Model parameters were estimated experimentally from bacterial growth curves (see subsection 3.8.5), and from mutation rates assays performed with these strains previously by this group [19, 45].

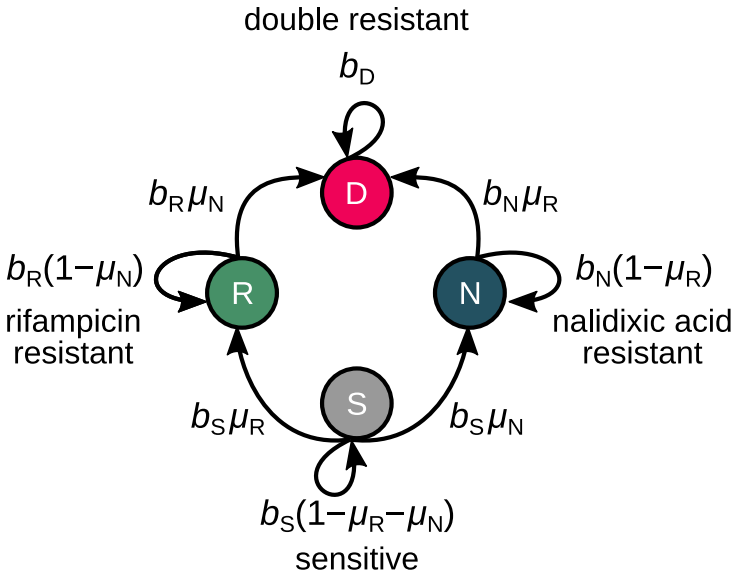

Figure 3.4: Population dynamics model of multi-resistance evolution. The model describes individuals of strains $i \in \{S, R, N, D\}$ (sensitive, rifampicin resistant, nalidixic acid resistant, double resistant). Each individual of type i produces an offspring with probability b_i in each time step. A mutation to rifampicin resistance occurs with probability μ_R, or nalidixic acid resistance with probability μ_N. Simultaneous acquisition of both mutations in one reproduction event is not allowed in the model (i.e. S cannot give rise to D, refer to Methods and Supplementary Information for further details).

Figure 3.5 shows the proportions of populations evolving resistance for 1000 replicate simulations (analogous to the experimental results shown in Figure 3.1). A Bayesian categorical model fitted to simulations produced parameter estimates that closely matched those from the experimental data, demonstrating that the simulations quantitatively recapitulate the experiments (Figure 3.12 and Model M4). In particular, we reproduce the main experimental findings that double resistance was constrained to populations treated with antibiotics, and that the presence of mutators facilitated double resistance evolution. We found that a small fraction of purely wild-type populations evolved double resistance (between 0/1000 and 15/1000 depending on treatment); this is consistent with our experimental results ($\leq 1/60$ per treatment). As the model excludes the possibility of double resistance emerging through a single reproductive event, this suggests that double resistance can emerge without invoking multi-drug resistance mechanisms (e.g. efflux pumps), simultaneous acquisition of two resistance

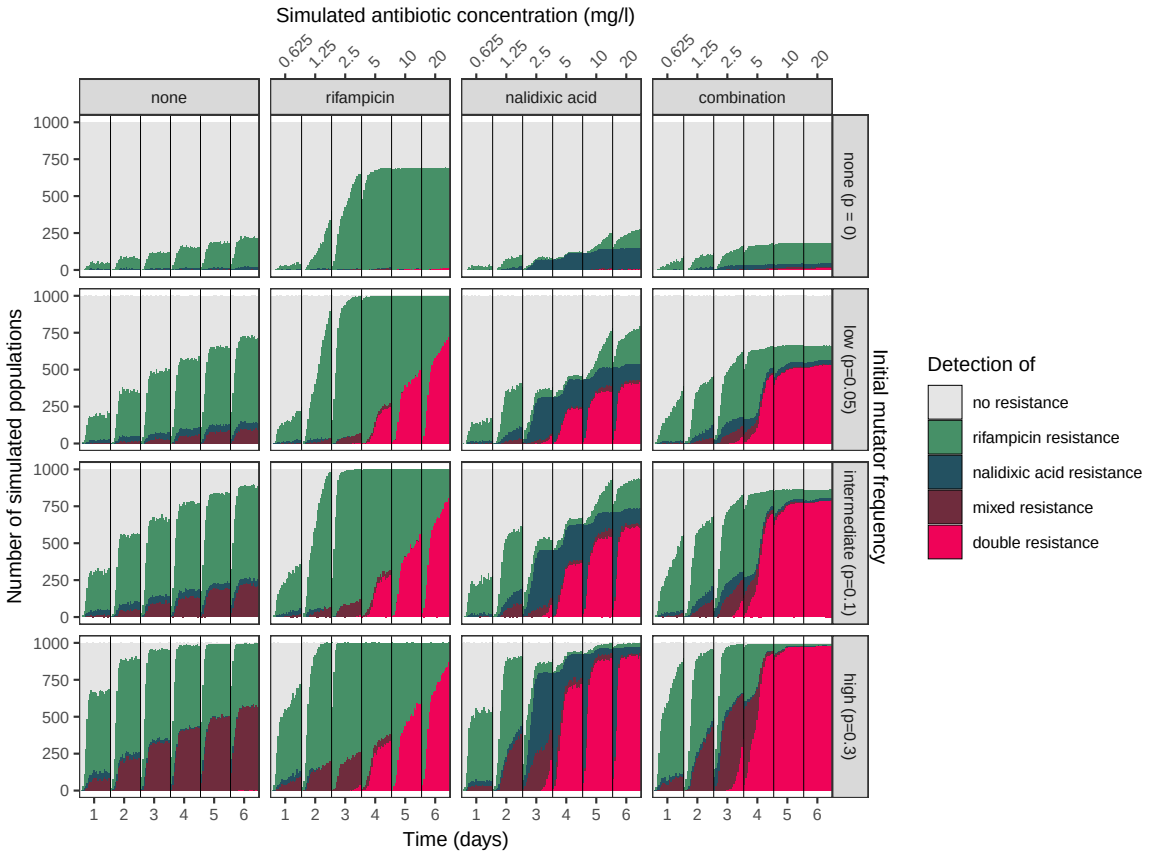

Figure 3.5: Emergence of antibiotic resistance in stochastic simulations of resistance evolution. Stacked bars show the number of populations with individuals of the types shown in Figure 3.4. 'Detection of' refers to the types of individuals present in a random sample of 1/200 of the population (simulating selective plating, see Methods), during each time step of the simulation. 'No resistance' indicates only type S was sampled (no R, N, or D). 'Rifampicin resistance' indicates at least one R (no N or D, any S), and 'nalidixic acid resistance' at least one N (no R or D, any S). 'Mixed resistance' indicates at least one each of R and N (no D, any S). 'Double resistance' indicates sampling at least one D (any S, R, or N). For further information, see Model M4 in the Supplementary Information.

mutations, or recombination.

There are two differences between the results of the experiment and the simulation, which may have arisen from allowing only eight possible genotypes in the simulations, compared to a vast number of possible genotypes that could have arisen during the experiment. First, in the 'no antibiotic' treatment, the number of populations with resistance was initially higher on day 1 than on days 2 or 3, but in the simulation it increased monotonically (compare leftmost columns of Figures 3.1 and 3.5). In the experiment, selective sweeps of adaptive mutations may have replaced rifampicin resistance mutations, which are generally costly for *E. coli* K-12 in rich medium [46]. Second, a higher proportion of mixed resistance was seen in the experiment, primarily

in the nalidixic acid treatment (third columns of Figures 3.1 and 3.5, compared directly in Figure 3.12). The simulation could have overestimated transitions from mixed resistance to double resistance if there were additional costs of double resistance that were not captured by our model (e.g. differences in lag time).

The simulation allows a closer look at the population dynamics of resistance evolution. Figure 3.6 shows the interquartile range (25% and 75% quantiles) of the number of bacteria of each resistance type for simulated population dynamics for the 'intermediate' ($q = 0.1$) initial mutator frequency. Examples of individual populations are shown in Figure 3.9, and the interquartile range for other initial frequencies is shown in Figure 3.2. In single-drug treated populations, mutators swept to high frequency due to genetic linkage with single-drug resistance (i.e. in the same genome). Multi-resistance then arose subsequently in a population now comprising mostly single-resistant mutators, although reached only low relative frequency due to the absence of selection for multi-resistance. In contrast, in combination-treated populations, multi-resistance swept toward fixation due to direct selection for multi-resistance. Increasing the frequency of mutators decreased variability in the number of multi-resistant bacteria present at the end of the simulation (Figure 3.2). This reveals different evolutionary mechanisms responsible for multi-resistance in single-drug and combination treatments: genetic hitch-hiking of mutator alleles under single-drug treatments, and direct selection for sequentially-evolved multi-resistance under combination treatment.

Multi-resistance evolution without mutators requires populations larger than typical infections

In addition to the presence of mutators, other characteristics of bacterial populations can influence their ability to acquire resistance. Along with mutation rate, population size is the other primary contributor to mutational supply. Sufficiently large populations may therefore evolve multi-resistance without the presence of mutators. To determine how large such populations would need be, we simulated resistance evolution using the same estimated parameters, except now considering a range of maximum population sizes from 5.71×10^7 to 5.71×10^{13}, i.e. 0.1 to 10^5 times the population size of our experimental conditions. Figure 3.7 shows the relationship between average proportion of each strain under different maximum population sizes after six days of simulated

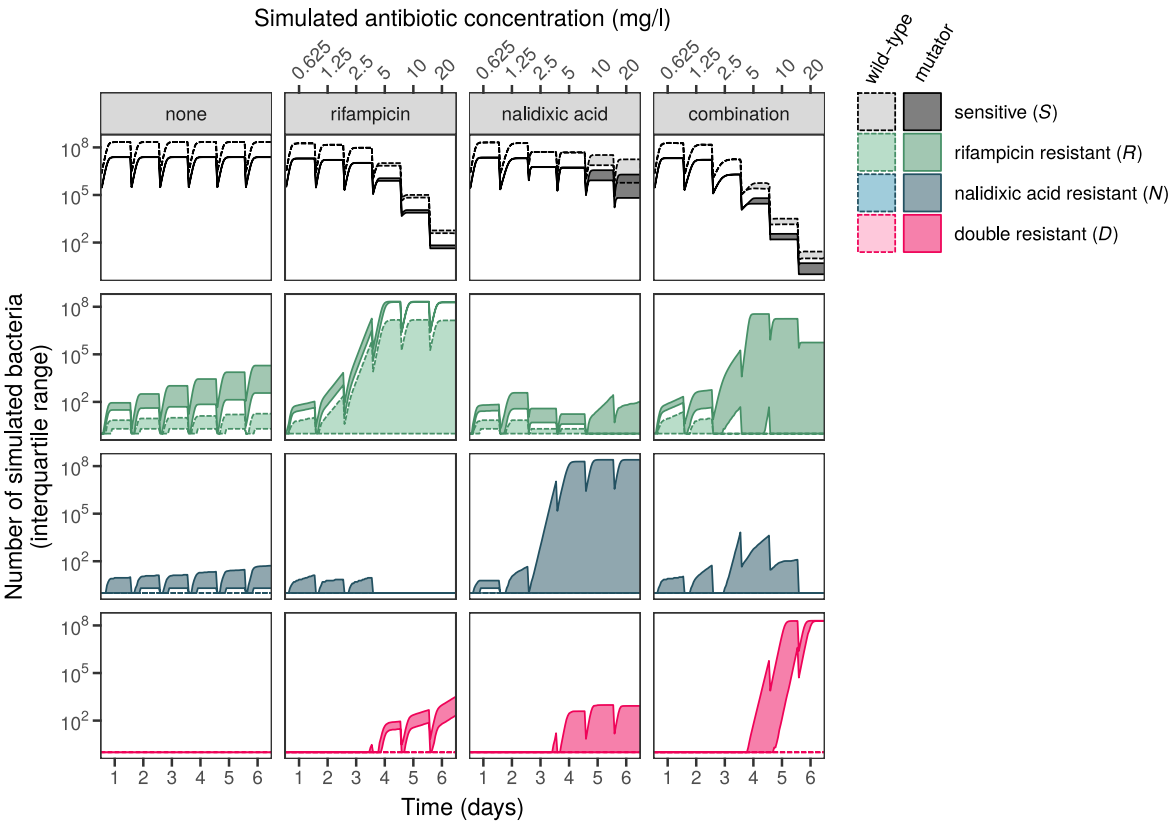

Figure 3.6: Population dynamics of simulated resistance evolution. Panels show the interquartile range (25% and 75% quantiles) of the number of bacteria of each resistance type (colours) for four treatments (columns) from 1000 replicate stochastic simulations. Results from the 'intermediate' ($q = 0.1$) initial mutator frequency are shown (other frequencies are shown in Figure 3.2).

evolution. Multi-resistance reached appreciable frequencies for maximum population sizes between 5.71×10^{10} (combination treatment) and 5.71×10^{13} (no antibiotic treatment). To put these numbers into context, these populations are comparable in size to the entire human-associated microbiome (approximately 10^{13} bacteria for an adult human of 70 kg [47]). In contrast, population sizes of bacteria in infections tend to be orders of magnitude smaller, e.g. blood stream infections ($\sim 10^7$ in 5 l of blood [48]), urinary tract infections ($\sim 10^9$ in 600 ml of urine [49]). Simulated populations of these sizes did not evolve multi-resistance in the absence of mutators. Bacterial meningitis is a potential counter-example, which can reach population sizes comparable to the simulations that evolved multi-resistance in the absence of mutators under combination therapy ($\sim 10^{11}$ in 150 ml of cerebrospinal fluid [50]).

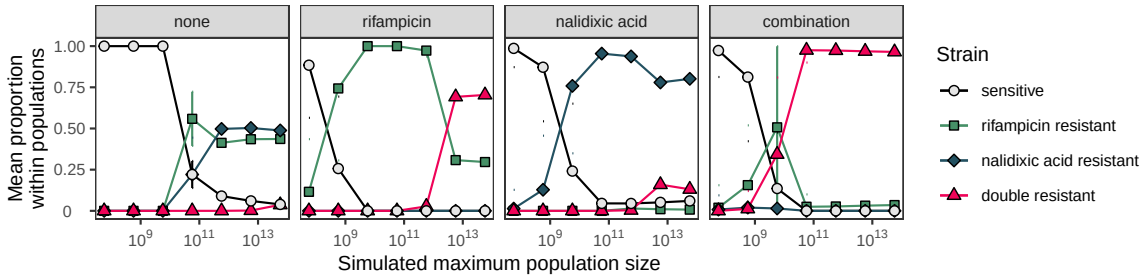

Figure 3.7: Proportion of each strain type (±Standard Deviation) found within simulated populations of different maximum size in the absence of mutators. Multi-resistance evolved in large simulated populations (5.71×10^{10}–5.71×10^{13}), which are comparable in size to the largest human-associated microbiome populations.

3.3 Discussion

Preventing resistance evolution is one of the key motivations behind the use of combination therapy [9]. However, our results demonstrate that the presence of mutators in bacterial populations can facilitate multi-resistance evolution, rendering the treatment ineffective. Mutators need only represent a fraction of the initial bacterial population for multi-resistance to evolve during antibiotic treatment. Crucially, in our work mutators allowed multi-resistance to evolve in both single-drug and combination treatments (Figure 3.1), in spite of providing no clear benefit in single-drug environments (Figure 3.2). Multi-resistant clones from populations with increased mutator frequencies did not appear to suffer growth defects in the presence or absence of the combination treatment (Figure 3.3). Our stochastic simulation model revealed that an increase in the probability of resistance mutation through the presence of mutators was sufficient to explain multi-resistance evolution (Figure 3.4 and Figure 3.5). Further, the simulations revealed that genetic hitch-hiking of mutator alleles with single-drug resistance lead mutator genotypes to sweep to high frequency whenever present (Figure 3.6). Multi-resistance evolution was also possible in very large populations, though the sizes required exceed those typically associated with human microbiomes (Figure 3.7). Our results uncover a pitfall of antibiotic combination therapy. Although combination treatment was more effective at preventing resistance overall, the populations that survived combination treatment almost entirely consisted of multi-resistant mutators. These populations are not only resistant to the antibiotics already seen, but also have increased potential for evolving resistance to other antibiotics. As mutators are abundant in patients [23–25, 33–36], particularly in chronic infections, these results suggest that combination

therapy may not prove entirely successful at preventing antibiotic resistance evolution.

Using stochastic simulations allowed us to test specific hypotheses about the mechanisms of multi-resistance evolution that we observed experimentally. We simulated evolution in mixed populations of wild-type and mutator individuals, which only differed in mutation rate to resistance. The simulations excluded multi-drug resistance mechanisms and spontaneous double mutants. Further, only a single allele for each resistance type was considered, and secondary mutations at other loci were excluded. Collectively, this demonstrated that a difference in mutation supply, which allows resistance mutations to be acquired sequentially, is sufficient to explain the observed multi-resistance evolution. While other mechanisms may influence resistance evolution, they need not be invoked here. These include, for example, differences in birth and death rate [51], the acquisition of fitter resistance alleles [52], and access to compensatory or otherwise beneficial mutations [53, 54]. Nevertheless, we do not eliminate the possibility that our evolved strains vary in ways not captured by this minimal model. Whole genome sequencing may illustrate such variation–indeed, populations with mutators are often rich in diversity that persists over prolonged periods [22, 55]. However, sequencing alone could not definitively determine whether any such variation was required for multi-resistance to evolve. Even with the simplifications made with respect to the underlying biology, the simulation results and experimental results were closely matched. This demonstrates that mechanistic insight into complex evolutionary processes can be gained even from relatively uncomplicated stochastic models.

What role mutators play in the failure of clinical combination therapy is an important area for future research. In addition to the pair studied here, resistance to a number of other antibiotics can be achieved through spontaneous mutation, e.g. streptomycin (in *rpsL*), fosfomycin (in *murA*, *glpT*, or *uhpT*), cycloserine (in *cycA*), trimethoprim (in *folA* and its promoter), nitrofurantoin (in *nfsA* or *nfsB*) and some beta-lactams (in penicillin binding proteins). Among clinical isolates, there is an established association between mutator phenotypes and multi-resistance [26]. A likely explanation for this existing association is successive rounds of monotherapy, rather than combination therapy. However, whether mutators can also allow multi-resistance to evolve during combination therapy needs to be established. Clinical trials of HIV combination therapy suggest the possibility [56], albeit with a much larger mutational supply than bacterial

populations (with or without mutators) [57]. Ultimately, however multi-resistance evolves, multi-resistant mutators may present a challenge for infection management. Mutators are better able to mitigate the fitness costs associated with antibiotic resistance by acquiring compensatory mutations [53]. Mutators may also more easily overcome other forms of bacterial control, such as vaccination [58] and phage therapy [59]. Unlike viruses, bacterial mutators are also unlikely to suffer from 'lethal mutagenesis' [60, 61] or 'mutational meltdown' [62] (i.e. the accumulation of deleterious mutations leading to extinction) due to having large population sizes and smaller mutation rates than the error threshold of these models [63]. Indeed, there is little evidence that mutators impair fitness over either short-term [64] or longer-term evolution [65] (except in the context of mutation accumulation experiments that keep population sizes artificially small [66]), and we found no evidence for it here (Figure 3.3). Together, this suggests that once multi-resistant mutator lineages become established, they will be difficult to eradicate, either through natural selection or through alternatives to antibiotics. This raises the possibility that screening for mutators, in addition to antibiotic susceptibility, could be valuable in clinical practice. bo Although here we have focused on a genetically-encoded mutator phenotype, other factors influencing mutational supply may also contribute to multi-resistance evolution. Mutation rate appears to be a phenotypically plastic trait across all domains of life [19], though the precise mechanisms through which this operates has yet to be established. Recent work has shown a link between mutation rate and efflux gene expression [67]. Environmental stress and mutagens can also transiently elevate mutation rates, e.g. via stress-induced mutagenesis [68], radical-induced DNA damage [69], or inhibition of DNA synthesis and activation of error-prone polymerases [70–72]. This may explain the high rate of multi-resistance in *Mycobacterium tuberculosis*, which is thought to have a relatively low mutation rate [73]. In addition to increasing the mean, increasing the variability of mutation rates has also been shown to increase the probability of multi-resistance [74]. Understanding the mechanistic underpinnings of mutation rates, and the relationship with resistance, allows for treatments that inhibit resistance evolution through decreasing the mutation rate [75]. Our work also highlights the need to consider the effects of possible treatments on mutation rate. Some antibiotics are themselves mutagenic [76] whereas antibiotic adjuvants that enhance antibiotic killing via SOS repression [77] potentially reduce

mutation rates [78]. Population size is the other major contributor to mutational supply [79] that can vary over orders of magnitude in different bacterial populations associated with infection [48–50]. Our simulations suggest multi-resistance can evolve without mutators, but the population size required largely exceeds those seen in infection.

3.4 Conclusion

A vast number of possible combination treatments can be generated from existing antibiotics [80]. However, our results suggest that the design of combination treatments should consider the potential for increasing resistance evolvability through indirectly selecting for high mutation rates. Recent work has demonstrated that treatments can indeed be optimised to prevent resistance evolution [37, 38]. However, testing all possible antibiotic combinations in this fashion is an insurmountable task [80]. A rational, high-throughput approach for designing combination therapies is needed. Our stochastic simulation model provides the basis for an *in silico* framework for predicting resistance evolution for any combination of antibiotics. Future work will identify ways of optimising combination therapies to prevent resistance evolution.

3.5 Data availability

Data, scripts and source code are available on GitHub:

https://github.com/dannagifford/multi-resistance/

3.6 Methods

3.6.1 Strains and media

Selection experiments involved 'wild-type' *E. coli* str. K-12 substr. BW25113 [F-, Δ(*araD-araB*)567, Δ*lacZ*4787(::*rrnB*-3), λ-, *rph*-1, Δ(*rhaD-rhaB*)568, *hsdR*514] [81], and a 'mutator' strain Δ*mutS* (as above, but with Δ*mutS*738::kan, indicating Δ*mutS* replacement with kanamycin resistance, which has not previously been observed affect resistance to the antibiotics we have studied here [19, 45]). Both strains were obtained from Dharmacon, Horizon Discovery Group, UK. Relative to the published reference

genome [82], whole genome resequencing of our isolates revealed no mutations in BW25113, and a single point mutation in Δ*mutS* (1,985,889 G>A, resulting in an amino acid substitution in *pgsA* A137V), which does not have a known association with resistance.

Routine culturing was performed in lysogeny broth [LB, 10 g/l tryptone (Fisher Scientific, UK), 5 g/l Bacto yeast extract (BD Biosciences, UK), 10 g/l NaCl (Fisher Scientific, UK)]. Selection experiments in the presence of antibiotic(s) were performed in Müller-Hinton broth (MH broth, 23 g/l, Sigma-Aldrich, UK). MH is a preferred medium for use with antibiotics [83]. Solid media were made by adding 12 g/l agar (BD Biosciences, UK) to either broth prior to autoclaving. Stock antibiotic solutions were prepared at 10 mg/ml. Rifampicin (Fisher Scientific, UK) was dissolved in methanol (Fisher Scientific, UK), and nalidixic acid (Fisher Scientific, UK) was dissolved in double distilled water, with 1N NaOH (Fisher Scientific, UK) added drop-wise until the antibiotic was solubilised. Strains were stored in LB with 40% glycerol at −80 °C.

3.6.2 Selection experiment under single-drug and combination treatments

We used experimental evolution to determine the effect of mutators on multi-resistance evolution under single and combination antibiotic treatments. Populations were founded from a mixture of mutator and wild-type individuals. Independent overnight cultures of wild-type and mutator were first grown separately in 5 ml MH broth. Volumetric mixtures of the cultures were made at ratios of 0%, 10%, 25%, and 50% mutator culture. The actual proportions of mutators were measured by plating serial dilutions of the populations on LB agar (total population count) and LB with 100 mg/l kanamycin agar (mutator count) on 90 mm round Petri dishes (to account for differences between volumetric and actual proportions arising from both variation in density and experimental error). The initial mixtures were assayed for resistance to rifampicin or nalidixic acid by plating on MH agar supplemented with rifampicin (50 mg/l) or nalidixic acid (30 mg/l) on 90 mm round Petri dishes. We discarded 5 cultures for having detectable rifampicin resistance at the beginning of the experiment. No cultures had detectable nalidixic acid resistance. This was undertaken to observe the evolution of multi-resistance from an

initially wild-type population (rather than single-drug resistance in an already resistant background). Resistance to these antibiotics arise due to mutations in their 'resistance determining regions', in *rpoB* for rifampicin [84], or in *gyrA* (Gram negative bacteria, such as *E. coli*) or *parC* (Gram positive bacteria) for nalidixic acid [85]. High-level resistance to either requires only a single base pair mutation in their target genes. Antibiotics in the parent classes of these antibiotics, rifamycins and fluoroquinolones, are often used in combination treatments (particularly against *M. tuberculosis*, where multi-resistance is rampant globally [86]).

We used a serial transfer protocol that exposed populations to increasing concentrations of antibiotics over a period of 6 days. The experiment was performed in 96-well microtitre plates (Nunc, Fisher Scientific, UK) in 200 μl volumes grown at 37 °C with 200 rpm shaking in an Innova 42R Incubator (Eppendorf, United Kingdom) for 22 h growth periods ('days'). Populations were initiated from the mixed cultures by diluting 1 μl of each into 200 μl of fresh culture using a 96-pin replicator (Boekel Scientific, Feasterville, PA, USA). At the end of each day, 1 μl of each population was pin replicated into 200 μl of fresh growth medium. If populations were to achieve the same size each day, a 1/200 dilution would imply $\log_2(200) \approx 7.64$ doublings per day. Four antibiotic treatment regimes were used: no antibiotic, rifampicin only, nalidixic acid only, or rifampicin and nalidixic acid combined. Antibiotic concentrations were doubled each day over the course of 6 days (0.625, 1.25, 2.5, 5, 10, 20 mg/l of each individual antibiotic). Population density was measured each day by optical density at 600 nm using a BMG POLARstar OPTIMA (BMG Labtech, Ortenberg, Germany). Protocols involving the increase of antibiotic concentrations over time and/or space has been used previously [4, 87, 88]. Under this approach, populations experience each concentration in sequence, hence resistance at higher concentrations is not independent from resistance at lower concentrations. This differs conceptually from experiments that use several different fixed antibiotic doses [89, 90], where resistance arising at each concentration is independent of the other concentrations.

3.6.3 Detection and analysis of resistance

Following each daily transfer, we assayed resistance by pin replicating 1 μl of overnight culture (equivalent to a random sample of 1/200th of the population) on MH agar

without antibiotic, or with rifampicin (50 mg/l), nalidixic acid (30 mg/l), or rifampicin and nalidixic acid combined (50 mg/l and 30 mg/l, respectively) in 120 mm square Petri dishes. These concentrations are above the MIC, and resistance is indicative of mutations in the typical resistance genes for these antibiotics in *E. coli*, *rpoB* and *gyrA*, respectively. Other selective concentrations may yield different mutants [90].

After overnight growth, populations were assigned one of five categories: 'sensitive' if they only grew on non-selective plates, 'rifampicin resistant' or 'nalidixic acid resistant', if they grew on one of the two single-drug plates, 'mixed resistant' if they grew on both single-drug selective plates but not combination selective plates, and 'double resistant' (i.e. multi-resistant to two antibiotics, the simplest form of multi-resistance) if they grew on combination selective plates. Note these outcomes refer to *establishment* of resistance, rather than *fixation*, i.e. the frequency of resistant individuals is > 0 and ≤ 1. Assaying resistance using this method shows good concordance with growth above MIC concentrations in broth (Figure 3.1). After the sixth day, evolved populations that grew on the combination plates were grown overnight in LB medium, and then stored at -80 °C.

We analysed resistance using a Bayesian categorical model, implemented in the `brms` package [91, 92] in R 3.5.3 [93]. Resistance was treated as a categorical response variable (categories defined as above), with antibiotic treatment ('no antibiotic', 'rifampicin', 'nalidixic acid', 'combination') and proportion of mutators ('none', 'low', 'medium', 'high') as categorical predictors. Row and column (i.e. position in the 96-well plate) were treated as random effects. We used Student's t priors, with location μ and scale σ estimated from a preliminary experiment, and degrees of freedom ν chosen to reflect uncertainty in the location, i.e. $t(\nu = 7, \mu = -5, \sigma = 2.5)$ for the intercept (i.e. the fitted value of the response when predictors take the reference level values 'no antibiotic' and 'zero' mutators). Priors for the parameters for the predictors were given as $t(\nu = 7, \mu = 0, \sigma = 2.5)$. We analysed both the 'main effects' of the predictors (i.e. the effect of a predictor on the response averaged across all levels of the other predictors), and their 'interaction effects' (i.e. the effect of a predictor being conditional on the value of another predictor). For an extended description of the analysis, see Model M1 in the Supplementary Information.

3.6.4 Growth parameters of single- and double-resistant clones

To determine the effects of single and double resistance on growth parameters, we selected five nalidixic acid resistant and five rifampicin resistant clones arising from the wild-type BW25113 genetic background via fluctuation tests [94], using an established protocol [95]. Briefly, 1 ml LB cultures of *E. coli* K-12 BW25113 were grown overnight in 96-well deep-well plates. The entire volume of each culture was plated on MH agar supplemented with rifampicin (50 mg/l) or nalidixic acid (30 mg/l) in the wells of a 6-well plate (each well approximately 35 mm in diameter). These 6-well plates were incubated for 48 h. To select double-resistant clones, we performed a second fluctuation test using resistant strains from the first, plating on the antibiotic to which they were not already resistant. Colonies were isolated from selective plates, grown overnight in LB medium, and then stored at −80 °C.

Growth curves of single- and double-resistant clones were generated by measuring optical density at 600 nm every 30 min for 45 h using a BMG FLUOstar OMEGA with Microplate Stacker (BMG Labtech, Ortenberg, Germany). Each clone was grown in duplicate at 37 °C under each of the antibiotic concentrations experienced during the selection experiments (i.e. 0.625, 1.25, 2.5, 5, 10, 20 mg/l each of rifampicin and/or nalidixic acid). Cultures were initiated by first growing clones overnight in 200 μl MH broth, then diluted 1/200 into a total volume of 200 μl MH broth containing one or both antibiotic(s). The growth curves were used to estimate parameters for the stochastic simulation model, described later (and in full in the Supplementary Information)). We used parameter estimates for resistant strains derived from the wild-type genetic background, as obtaining consistent estimates for mutators is difficult due to resistance occasionally emerging during the assay (a known problem [96]).

We also summarised these growth curves into a single metric, area under the curve (AUC), as the empirical growth curves did not follow a standard logistic shape (Figure 3.5, which we also account for in the simulations). We calculated AUC using the SummarizeGrowth function from the R package growthcurver [97]. AUC incorporates all of lag phase, growth rate, and density, and highly repeatable. To determine whether double resistance conferred a benefit under single-drug treatments, we fit a Bayesian multivariate linear regression model of AUC of different strains in the presence of each treatment over all concentrations. Student's t priors were used for the intercept

($\nu = 7, \mu = 10, \sigma = 2.5$) and the other effects ($\nu = 7, \mu = 0, \sigma = 2.5$) (see Figure 3.11 and Model M2 in the Supplementary Information). Effects of single-drug and double resistance were compared with point hypothesis tests on the population-level effects from this model using 95% credible intervals (C.I.s). For an extended description of the analysis, see Model M2 in the Supplementary Information.

Using the same protocol, growth curves for the double-resistant clones that evolved during the selection experiment (all in the mutator genetic background) were measured in antibiotic-free medium, and in 20 mg/l of the combination treatment. The association between AUC, initial mutator frequency and treatment was analysed using a Bayesian multivariate regression model. Student's t priors were used for the intercept ($\nu = 7, \mu = 10, \sigma = 2.5$) and the effect of mutator levels ($\nu = 7, \mu = 0, \sigma = 2.5$) for other estimated parameters (see Model M3 in the Supplementary Information).

3.6.5 Mutation rate estimates

Mutation rates to rifampicin resistance ($\mu_R = 6.7 \times 10^{-9}$ per cell division) and nalidixic acid resistance ($\mu_N = 7.4 \times 10^{-10}$ per cell division), were obtained for these strains in a previous publication [45], as was the mutator effect of $\Delta mutS$ (80-fold increase relative to wild type) [19]. Assuming mutations occur independently, we estimate the probability of both rifampicin and nalixidic acid resistance mutations occurring simultaneously during the same replication event (i.e. a 'spontaneous double mutant') for the wild-type as $\mu_R\mu_N = 5.0 \times 10^{-18}$, and for mutators as $\mu_R\mu_N \times 80^2 = 3.2 \times 10^{-14}$. We can use these probabilities to obtain a rough estimate for the probability of observing a simultaneous double mutant by simulating a fluctuation test using `rflan()` from the R package 'flan' [98]. We performed 10^6 simulations using the same parameters as the selection experiment (i.e. 60 independent populations, days 1–4 permitting wild-type growth, maximum population size of 5.71×10^8). For populations comprising only wild-type individuals, no spontaneous double mutants were observed in 10^6 simulations. For populations comprising solely mutators, a simultaneous double mutant was observed in 4210 out of 10^6 simulations. Hence, the probability that our selection experiment observed a spontaneous double mutant is very low.

3.6.6 Stochastic population dynamics model

We numerically simulated resistance evolution using a stochastic population dynamic model. The model is described in full in subsection 3.8.1. Briefly, the model describes four strains of types $i \in \{S, R, N, D\}$, where S is the sensitive ancestor, R is rifampicin resistant, N is nalidixic acid resistant, and D is double resistant (Figure 3.4). We denote the number of strain-i individuals in the population by n_i. Simulated populations were initiated with 5.71×10^6 individuals; this is our estimate of the starting population size in the experiments obtained by serial dilution plating. The initial population consisted of a fraction $1 - q$ of wild-type individuals, and a fraction q of mutators, for q taking a value of 0, 0.05, 0.1, or 0.3. Growth rates and carrying capacities for each strain i (Tables 3.2–3.3) were estimated empirically from growth curves, averaged over five independent clones of each type. We used clones derived from the wild-type BW25113 due to difficulty in getting consistent growth curves from the $\Delta mutS$ mutator strain due to adaptation occurring during the growth curve assay (a difficulty encountered when working with mutators [96]). Growth curves were fitted in MATLAB2016a, using a custom script (see Data availability statement for access). Mutation rates for strains used here were estimated by fluctuation test in a previous study using these specific strains [19]. Other parameter values were set to match the experimental procedure (initial frequency of mutators, dilution, duration of experiment).

Population growth is described as follows. Considering first population growth without mutation, for each time step, each of the n_i individuals of strain i produces one offspring with probability $b_i = \exp\{\Delta t\, r_i\,(1 - n_T/k_i)\} - 1$ for $n_T/k_i \leq 1$, where r_i is the net growth rate for strain i, and k_i is the carrying capacity. When $n_T/k_i \geq 1$, we set $b_i = 0$ to ensure that n_i remains constant. We have written $n_T = \sum_i n_i$ for the total number of individuals in the population. Time t is measured in units of hours. The quantity Δt is the time step of our simulations (we use $\Delta t = 0.01$ h, see subsection 3.8.2 for further discussion). In each time step, the number of offspring of strain i is binomially distributed, Binomial(n_i, b_i). The binomial distribution is a good approximation, for Δt small, of the less intuitive negative binomial function that accounts for the probability distribution of the offspring at each time step when a pure birth process is considered (see Supplementary Information subsection 3.8.2 for details). In subsection 3.8.3 we show that, for growth without mutations, the mean number of

individuals of each strain follows the deterministic Leslie-Gower competition model [99] (a discrete-time model conceptually similar to the Lotka-Volterra competition model in continuous time [100, 101]).

At the start of the simulation, there are no Type R, N, or D individuals. Type R and N individuals must initially arise by mutation in new Type S individuals that are produced, but afterward may produce new individuals of the same type, or produce Type D individuals by mutation. Once they have arisen, Type D individuals may also reproduce, but do not mutate. We write μ_R for the probability with which an offspring acquires resistance to rifampicin by mutation, and μ_N for the probability that the offspring acquires resistance to nalidixic acid. We exclude the possibility that both resistance mutations can be newly acquired in the same reproduction event (i.e. no double-mutation or multi-drug resistance mechanisms). The number of individuals of type i arising by mutation in any one time step is therefore Binomial$(n_S, b_S\mu_i)$ for $i \in \{R, N\}$. For $i = D$ the number of individuals generated through mutation is the sum of two binomial random numbers, Binomial$(n_R, b_R\mu_N)$ and Binomial$(n_N, b_N\mu_R)$. Population growth periods were 22 h, equivalent to 'days' of the selection experiment. At the end of each day, a dilution occurs in which the number of individuals of type i transferred to the next day is binomially distributed, Binomial$(n_i, 1/200)$. Simulations were written in C++ (source code available, see the 'Data Availability' statement). To compare simulations with the experimental results, we drew a random sample equivalent to 1/200th of all individuals from the simulated population whenever data was taken from the simulation. Detection of type i was recorded for a given population if a draw from Binomial$[n_T, n_i/(200 \cdot n_T)]$ was at least 1. This is equivalent to the resistance detection assay for the experimental results.

3.7 Extended data

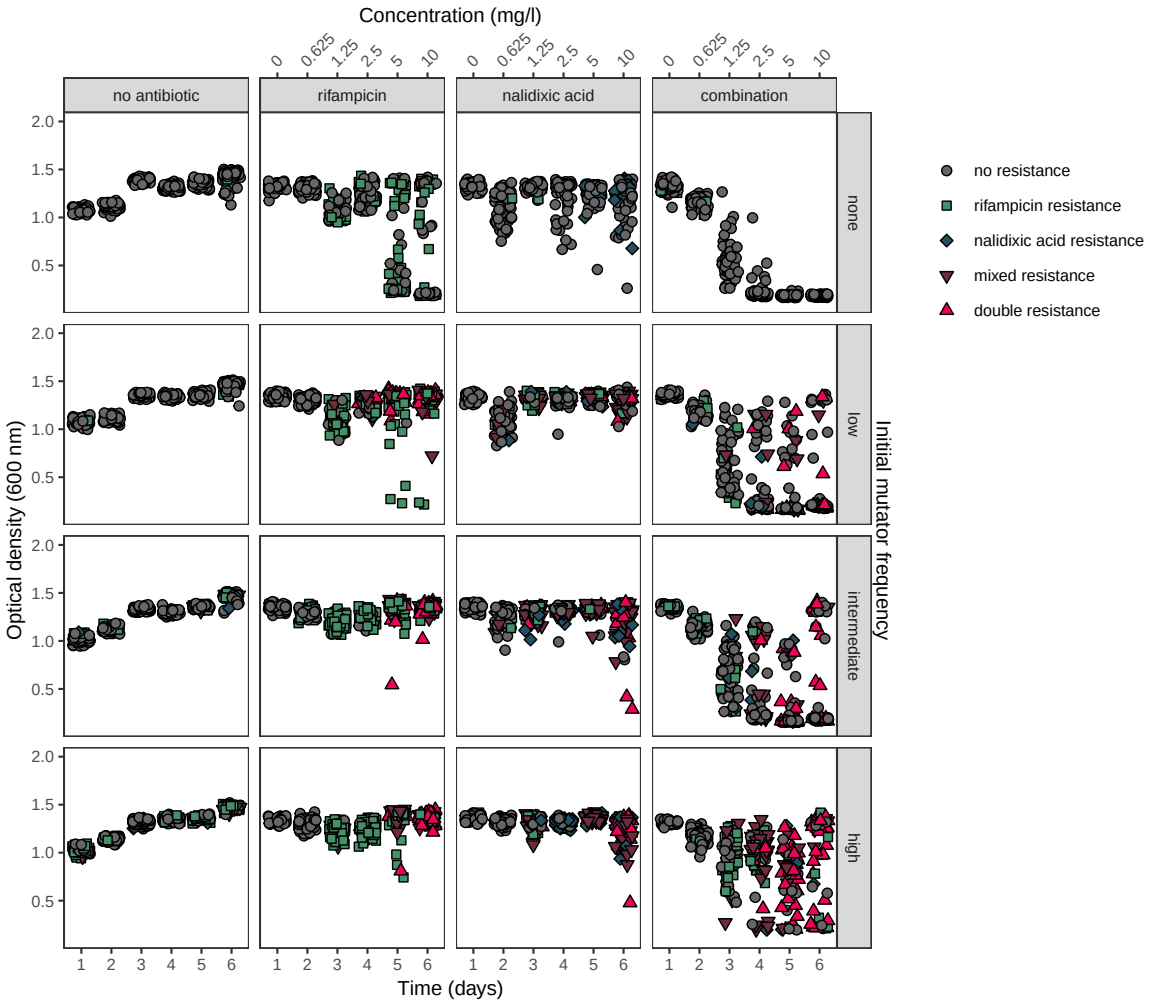

Extended Data Figure 3.1: Correspondence between optical density (OD) during selection experiment and detection of resistance. OD600 was measured each day at the end of the growth phase using a multi-mode microplate reader (BMG POLARstar OPTIMA, BMG Labtech, Ortenberg, Germany; note that this instrument gives higher values of OD than the BMG FLUOstar OMEGA used elsewhere to measure growth curves).

3.8 Appendix A: Stochastic population dynamics model of resistance evolution

3.8.1 Description of the model

As described in the main text, we numerically simulated resistance evolution using a stochastic population dynamic model. A conceptual diagram of the model can be

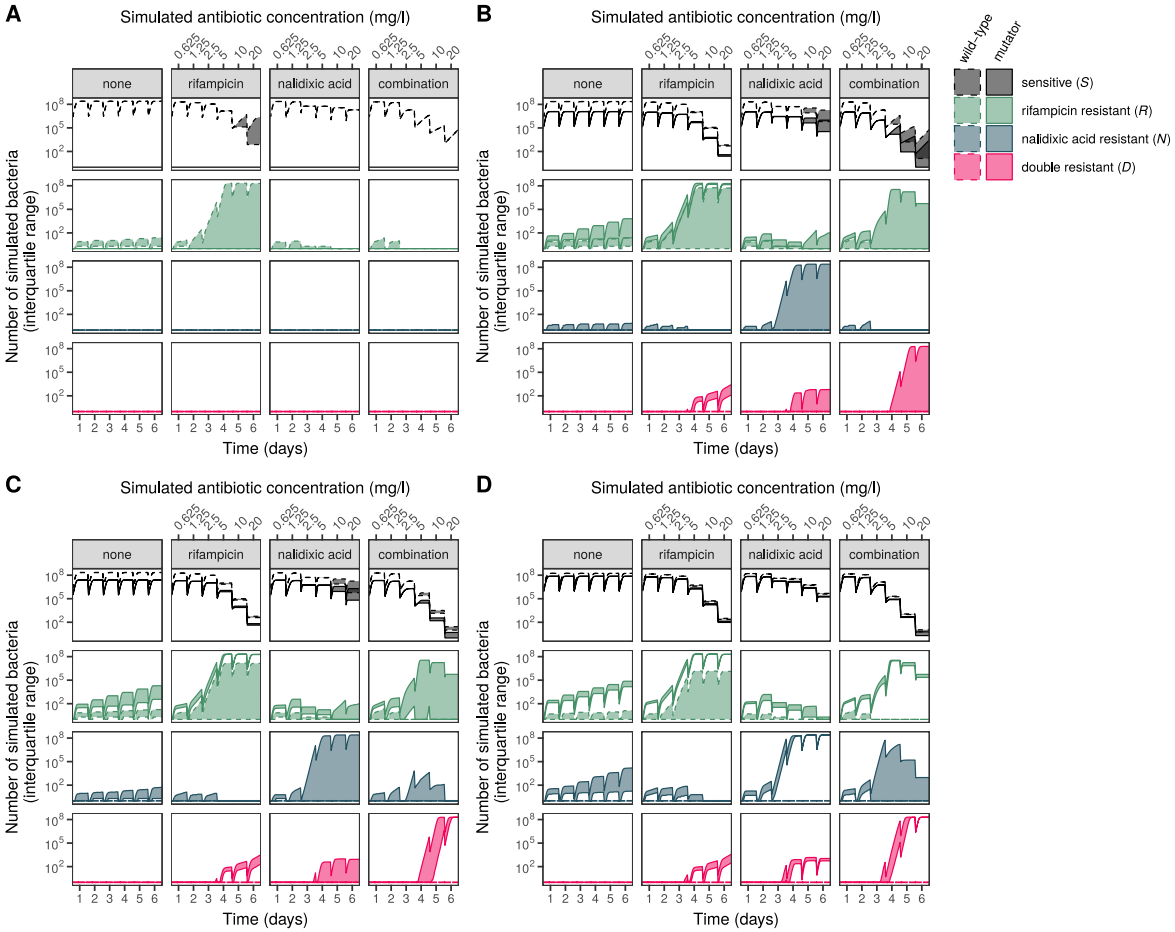

Extended Data Figure 3.2: Population dynamics of simulated resistance evolution. Areas indicate the interquartile range (25% and 75% quantiles) of the numbers of bacteria of each resistance type from 1000 replicate stochastic simulations. Panels A–D show different initial mutator frequencies: 'none', 'low' ($q = 0.05$), 'intermediate' ($q = 0.1$, as shown in Figure 3.6), 'high' ($q = 0.3$).

seen in main text Extended Data Figure 3.4. The model describes four strains of types $i \in \{S, R, N, D\}$, where S is the sensitive ancestor, R is rifampicin resistant, N is nalidixic acid resistant, and D is double resistant. Populations initially consist only of Type S, a fraction $1 - q$ of which are wild-type, and q of which are mutators. The conditions of the simulation are intended to replicate the selection experiment (see main text Methods for details). The simulated populations also experience increasing antibiotic concentrations, which double each day. As in the experiment, populations are allowed to grow for a fixed time period, during which mutations can arise, before being subjected to dilution. These processes are described in the following section.

3.8.2 Binomial approximation for stochastic growth processes

To simulate the growth of bacteria, we assume that each of the n_i individuals of strain i replicates at any time independently of the rest of the population, and regardless of its age, with a fixed replication rate λ_i. Setting mutations aside for the moment, this is described by the well-known Yule-Furry process whose master equation reads

$$\dot{p}_{n_i}(t) = -n_i\lambda_i p_{n_i}(t) + (n_i - 1)\lambda_i p_{n_i-1}(t), \tag{3.1}$$

where $p_{n_i}(t)$ is the probability that the number of bacteria of type i is n_i at time t. The first term on the right hand side of Eq. (3.1) accounts for the outflux of probability (per unit time) of state n_i, and the second for the influx into state n_i. We denote the solutions of Eq. (3.1) by $p_{n_i}(t; n_i^0)$ where n_i^0 indicates the number of bacteria at $t = 0$.

The master equation Eq. (3.1) admits an analytical solution; indeed, its solution with initial condition $p_{n_i}(0; n_i^0) = \delta_{n_i,n_i^0}$ (where δ_{n_i,n_i^0} is the Kronecker delta) is the negative binomial distribution function

$$p_{n_i}(t; n_i^0) = \binom{n_i - 1}{n_i - n_i^0} e^{-\lambda_i n_i^0 t} \left(1 - e^{-\lambda_i t}\right)^{(n_i - n_i^0)} = \binom{n_i - 1}{n_i - n_i^0} p_i^{n_i^0} q_i^{(n_i - n_i^0)}, \tag{3.2}$$

where $p_i = e^{-\lambda_i t}$and $q_i = 1 - p_i$. The expression in Eq. (3.2) is the probability that there are n_i individuals of strain i in the population at time t, given that there were n_i^0 such individuals at time $t = 0$. The pure-birth stochastic process described by Eq. (3.1) thus can be simulated by a discrete-time algorithm in which at every time step the number of bacteria is sampled from the negative binomial distribution Eq. (3.2). It is worth noting that this does not involve any approximation.

In order to incorporate mutations, it is necessary to know the number of offspring produced in one generation. Starting with n_i^0 cells, we denote the number of offspring by $n_{R,i}$. We then have $n_i = n_i^0 + n_{R,i}$ for the total number of individuals of type i.

Therefore, the probability $P_{n_{R,i}}(t; n_i^0)$ that $n_{R,i}$ offspring have been produced by time t is equal to the probability that there are $n_i = n_i^0 + n_{R,i}$ individuals in the population overall at t,

$$P_{n_{R,i}}(t; n_i^0) = p_{n_i^0 + n_{R,i}}(t; n_i^0). \tag{3.3}$$

This yields the following expression

$$P_{n_{R,i}}(t; n_i^0) = \binom{n_i^0 + n_{R,i} - 1}{n_{R,i}} p_i^{n_i^0} q_i^{n_{R,i}}. \tag{3.4}$$

In a discrete-time algorithm, the number of offspring $n_{R,i}$ at each time-step Δt is drawn from the probability distribution function $P_{n_{R,i}}(\Delta t; n_i^0)$ Eq. (3.4) with $p_i = e^{-\lambda_i \Delta t}$, $q_i = 1 - p_i$. While Eq. (3.4) describes the number of offspring, it is not easy to develop an intuitive interpretation of the expression on the right-hand side.

In search of a more transparent model, we explore the limit of a small time step Δt. Considering $\Delta t \ll 1/\lambda_i$ ($1/\lambda_i$ provides the time scale of the dynamical system), we can expand the probability of replication p_i in terms of $\lambda_i \Delta t$,

$$p_i = e^{-\lambda_i \Delta t} \approx 1 - \lambda_i \Delta t. \tag{3.5}$$

As the number of offspring produced in one generation is very small, in this limit of small $\lambda_i \Delta t$ we can also assume that n_i^0 is the dominant term in $n_i^0 + n_{R,i} - 1$ for large populations (as in our experiments where $n_i^0 \approx 10^9$). Thus

$$n_i^0 + n_{R,i} - 1 \approx n_i^0. \tag{3.6}$$

Accordingly, the PDF for the number of offspring Eq. (3.4) in the limit $\Delta t \ll 1/\lambda_i$ can be approximated as

$$P_{n_{R,i}}(t; n_i^0) \approx \binom{n_i^0}{n_{R,i}} (1 - \lambda_i \Delta t)^{n_i^0} (\lambda_i \Delta t)^{n_{R,i}}, \tag{3.7}$$

which we recognise as a binomial distribution with parameters n_i^0 and $\lambda_i \Delta t$. The convergence for $\Delta t \ll 1/\lambda_i$ of the binomial approximation Eq. (3.7) and the corresponding exact distribution for the number of offspring Eq. (3.4) for $\Delta t \ll 1/\lambda_i$ is displayed in Extended Data Figure 3.3.

The binomial distribution brings about a clear interpretation of the bacterial growth: at every time step we draw the number of offspring from a binomial distribution with number of trials equal to the number of individuals and the success probability of each trial determined by the replication rate. Another advantage of using a binomial distribution is that, as we will see below, it is appropriate for modelling the serial dilutions of cultures performed in the experiments. This means that a binomial model can conveniently account for all processes involved in the experiments.

Other techniques to simulate a continuous-time stochastic process, such as the Yule-Furry process described by Eq. (3.1), include the well-known Gillespie algorithm [102, 103]. However, this method can be time consuming when the simulation entails

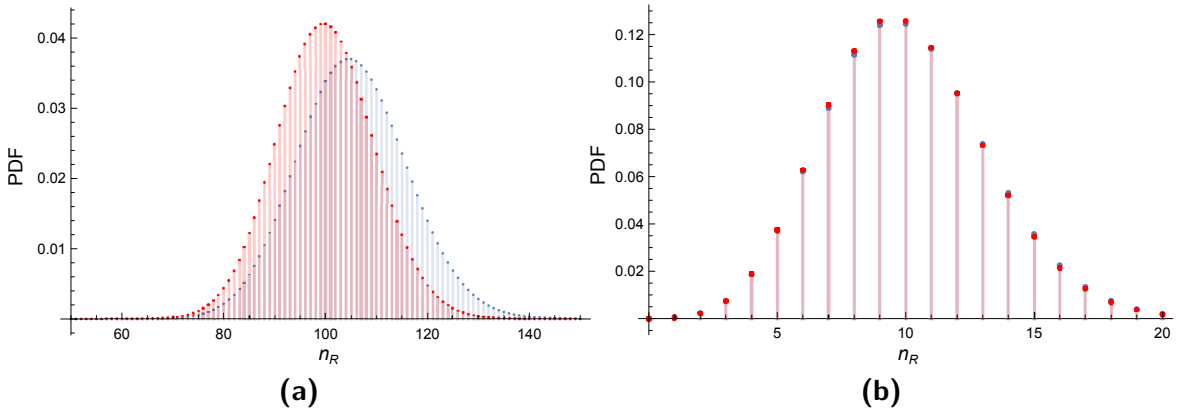

Extended Data Figure 3.3: Comparison between Eq. (3.4) (blue) and the binomial PDF approximation from Eq. (3.7) (red), for two values of Δt: A. $\Delta t = 0.1\,\mathrm{h}$, B. $\Delta t = 0.01\,\mathrm{h}$. Other parameter values used in both plots are $\lambda = 1\,\mathrm{h}^{-1}$, $n_i^0 = 1000$.

a large population, such as is the case of bacterial populations, which are often on the order of 10^9 individuals. Although there are approximations in discrete-time of the Gillespie algorithm to alleviate this issue, [e.g. tau-leaping, 104], we adopt instead the binomial approximation of the analytical solution of the master equation Eq. (3.1) because of its simple mathematical foundation and its clear interpretation. The binomial approximation is also useful for the implementation of mutation (see below).

We test the binomial approximation further in Extended Data Figure 3.4. In the figure we compare a realization of the continuous-time Yule-Furry process against the discrete-time analogues. The lines in both panels are obtained from simulations of the Yule-Furry process using the Gillespie algorithm. In panel A we compare this against samples from the solution for the Yule-Furry process in Eq. (3.4), drawn at discrete time points. Given that the solution is exact, we find very good agreement, remaining deviations are due to the stochastic nature of either trajectory but are small given the large size of the population. In panel B we compare against a trajectory constructed from the binomial approximation. This is obtained by sampling $n_{R,i}$ from the distribution in Eq. (3.7) at discrete points in time, the total population size is then $n_i^0 + n_{R,i}$. Deviations from the continuous-time trajectory can then be seen. This is due to the approximation leading to Eq. (3.7). However, the magnitude of these deviations reduces as the discretization step Δt becomes smaller, in-line with the fact that the binomial approximation is derived in the limit $\lambda_i \Delta t \ll 1$.

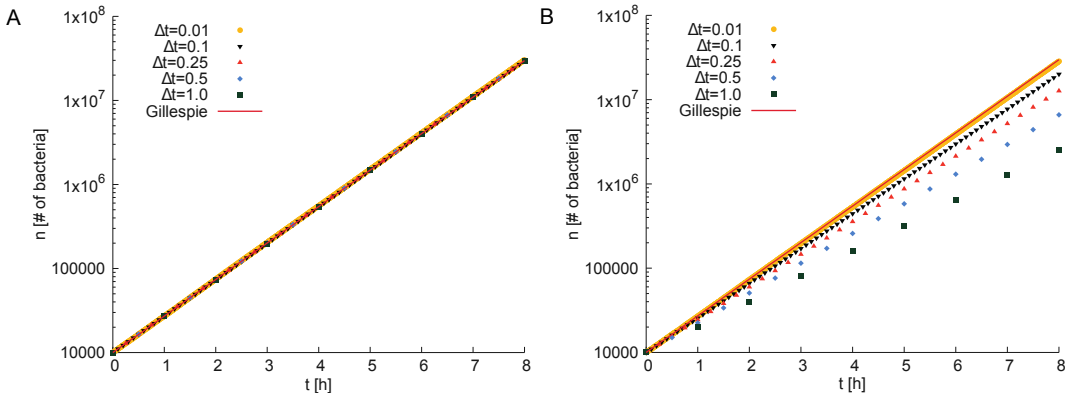

Extended Data Figure 3.4: Comparison between the continuous-time Yule-Furry process and discrete-time analogues. Both panels show the size of a bacterial population size as a function of time. The continuous line in either panel is from Gillespie simulations of the Yule-Furry process defined in Eq. (3.1). A. Comparison with a sample from the exact solution in Eq. (3.4), drawn at discrete time points (symbols). The agreement with the continuous trajectory is excellent irrespective of the choice of the time step Δt, as expected. B. Comparison with the binomial approximation (see text for details). In both panels we use $\lambda_i = 1h^{-1}$, and $n_i^0 = 10^4$.

Based on the results of Figures 3.3 and 3.4, and given that $\lambda_i \approx 1$ h^{-1} is a good benchmark for the replication rates that fit the experiments (see Table 3.2), we set $\Delta t = 0.01$ h for our simulations. This choice of Δt results in considerably lower simulation running times than using the Gillespie algorithm, providing thus an effective way for modelling the experiments.

3.8.3 Growth of bacteria

In order to capture the saturation of growth found in the experiment we use

$$b_i = \exp\left\{\Delta t\, r_i \left(1 - \frac{n_T}{k_i}\right)\right\} - 1, \tag{3.8}$$

where r_i is the growth rate per unit time of strain i. We interpret the reproduction probability b_i as an effective quantity, taking into account both birth and death processes of bacteria, i.e., a net growth rate; the quantity Δt denotes the length of time (in hours, h) of each time-step of the simulation. The parameter k_i is the carrying capacity for strain i, and represents the maximum value that n_i can take in absence of any other strain. The quantity $n_T = n_S + n_R + n_N + n_D$ is the total number of bacteria in the population. Given that n_T is time dependent, the reproduction rate b_i is time dependent as well. The term $r_i(1 - n_T/k_i)$ in the exponent in Eq. (3.8) resembles the Leslie-Gower competition model [99], a discrete-time version of the Lotka-Volterra competition model of [100, 101]. It takes into account the interaction between the

different strains. In the above model, we have assumed that the interaction is the same between each pair of strains (pure scramble competition, i.e. no direct interference, cross-feeding or similar).

Table 3.1: Definitions of model variables and parameters.

Parameter	Definition
t	time (hours)
i	strain $i \in \{S, R, N, D\}$
n_i	number of individuals (of strain i)
$\bar{n}_i$	mean number of n_i over different realisations of the experiment
r_i	growth rate of strain i
k_i	carrying capacity of strain i
μ_j	mutation rate to resist antibiotic, $j \in \{R, N\}$
n_T	total population size, $n_T = \sum_i n_i$
$\bar{n}_T$	mean of n_T over different realisations of the experiment
Δt	length of time per simulation time-step
t_i^c	time at regime switch of the diauxic growth of strain i
n_i^c	critical population size at growth regime switch of strain i, i.e. $n_i(t_i^c)$
q	initial frequency of mutators

To make the connection between Eq. (3.8) and the well-known Lotka-Volterra dynamics, we note that the expected value, $\bar{n}_i(t)$, of the number of individuals of type i in the population follows

$$\bar{n}_i(t + \Delta t) = \bar{n}_i(t) \times (1 + \bar{b}_i(t)), \tag{3.9}$$

where $\bar{b}_i(t)$ is the same as in Eq. (3.8), but using $\bar{n}_T$ (the expected value) instead of n_T. In writing the expression on the right of Eq. (3.9), we have factorized averages, i.e., $\overline{n_i(t)b_i(t)} = \overline{n}_i(t) \times \overline{b_i}(t)$. 3.9 indicates that each individual produces $\bar{b}_i$ offspring, on average, between t and $t + \Delta t$ ($0 \leq \bar{b}_i \leq 1$). The competitive Lotka-Volterra equations are obtained from Eqs. (3.8) and (3.9) in the limit $\Delta t \to 0$,

$$\frac{\mathrm{d}\bar{n}_i}{\mathrm{d}t} = r_i \bar{n}_i \left(1 - \frac{\bar{n}_T}{k_i}\right). \tag{3.10}$$

In performing the expansion in Δt, we have extrapolated the process to continuous time. In the presence of only a single strain, Eq. (3.10) reduces to the logistic dynamics

$$\frac{\mathrm{d}\bar{n}_i}{\mathrm{d}t} = r_i \bar{n}_i \left(1 - \frac{\bar{n}_i}{k_i}\right), \tag{3.11}$$

and has the analytical solution

$$\bar{n}_i(t) = \frac{k_i \bar{n}_i(t_0)}{\bar{n}_i(t_0) + [k_i - \bar{n}_i(t_0)]e^{-r_i(t-t_0)}}. \tag{3.12}$$

This describes a sigmoidal dynamic, starting from $\bar{n}_i(t_0)$ at time t_0, and approaching an asymptotic limit at the carrying capacity k_i at long times.

In our model, we set the growth rates, r_i, of strain i as zero when n_T crosses k_i. Hence, its population size remains constant when the total number of bacteria reaches or exceeds its carrying capacity. Our simulations operate in discrete time steps, but taking averages over multiple stochastic realisations we observe similar saturating behaviour for the expected number of individuals of the different strains.

3.8.4 Mutations

The simulation model also describes mutations. These can occur from sensitive bacteria S to either R or N, and, in turn, from R and N to D. The model excluded the possibility of direct mutations from S (sensitive) to D (double resistance). Following the same idea as before, we consider that any offspring of an individual of type S is of type R with probability μ_R, and of type N with probability μ_N. With the remaining probability $1 - \mu_R - \mu_N$ the offspring of a parent of type S is also of type S (no mutation). Similarly, an offspring of a parent of type R is of type D with probability μ_N, and an offspring of a parent of type N is of type D with probability μ_R.

The number of mutant offspring produced in this way will be binomially distributed. Specifically, we have

$$\begin{aligned}
n_S(t+\Delta t) &= n_S(t) + \text{Binomial}[n_S(t), (1-\mu_R-\mu_N)b_S], \\
n_R(t+\Delta t) &= n_R(t) + \text{Binomial}[n_R(t), (1-\mu_N)b_R] \; + \; \text{Binomial}[n_S(t), b_S\mu_R], \\
n_N(t+\Delta t) &= n_N(t) + \text{Binomial}[n_N(t), (1-\mu_R)b_N] \; + \; \text{Binomial}[n_S(t), b_S\mu_N], \\
n_D(t+\Delta t) &= n_D(t) + \text{Binomial}[n_D(t), b_D] \; + \; \text{Binomial}[n_R(t), b_R\mu_N] \\
&\qquad + \text{Binomial}[n_N(t), b_N\mu_R],
\end{aligned} \tag{3.13}$$

where we have written Binomial(n, p) for a binomial random number with parameters n and p; the probability that such a random number takes value j is $p_j = \frac{n!}{j!(n-j)!}p^j(1-p)^{n-j}$, for $j = 0, 1, \ldots, n$.

The parameters r_i and k_i for each strain are obtained by fitting the logistic model in Eq. (3.11) to growth curves resulting from experimental data, as we will describe next.

3.8.5 Estimating growth parameters from experimental data

To estimate growth rate and carrying capacity of strains S, R, N, and D, we carried out growth experiments of sensitive and resistant clones in pure culture. Growth curves were performed by measuring OD over time (Extended Data Figure 3.5), under conditions matching the selection experiment (see Methods in the main text). For each resistant strain (i.e. R, N, D), we isolated five independent mutant clones derived from the wild-type S type via fluctuation tests (see Methods in the main text).

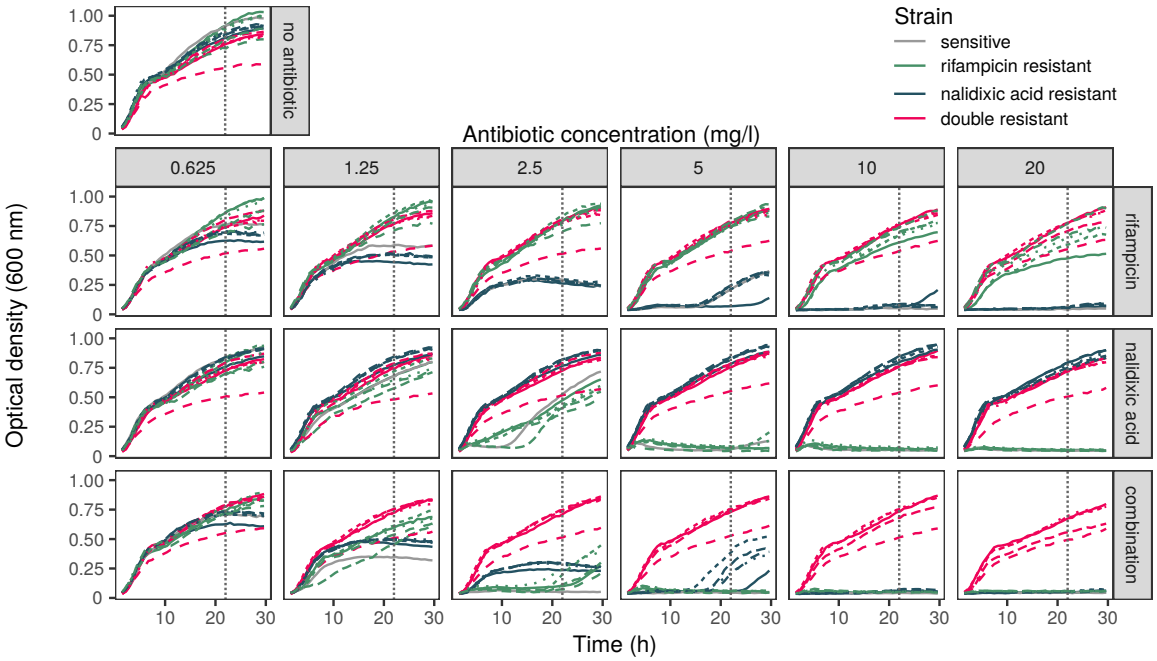

Extended Data Figure 3.5: Growth curves of sensitive, single-, and double-drug resistant strains in the absence of antibiotics, or in antibiotic concentrations experienced during the resistance selection regime. Curves shown here correspond to the areas under the curve shown in Extended Data Figure 3.2 of the main text. Note the shape of the curve is not a simple logistic shape in either the presence of absence of antibiotics, reminiscent of diauxic growth. This necessitated the curve fitting procedure outlined in Extended Data Figure 3.6 to give parameters detailed in Tables 3.2–3.4.

The growth curves deviate from a typical 'S'-shaped logistic curve, instead characterised by two 'plateaus', reminiscent of diauxic growth. Diauxic growth has been previously reported for MH media [105], as well as for other rich media [106, 107]. We account for this two-stage growth by fitting the data to growth curves of the form

$$n_i(t) = n_i^{(1)}(t)H(t_c - t) + n_i^{(2)}(t)H(t - t_c), \tag{3.14}$$

where

$$n_i^{(1)}(t) = \frac{k_i^{(1)} n_i^c}{n_i^c + [k_i^{(1)} - n_i^c] e^{-r_i^{(1)}(t-t_i^c)}}, \quad n_i^{(2)}(t) = \frac{k_i^{(2)} n_i^c}{n_i^c + [k_i^{(2)} - n_i^c] e^{-r_i^{(2)}(t-t_i^c)}}, \tag{3.15}$$

and where $H(t)$ is the Heaviside step function, $H(t) = 0$ for $t < 0$, $H(t = 0) = 1/2$ and $H(t) = 1$ for $t > 0$. $k_i^{(1)}$ and $k_i^{(2)}$ are the carrying capacities of strain i before and after the switch. The functions $n_i^{(1)}(t)$ and $n_i^{(2)}(t)$ are logistic growth curves that represent the two regimes of the diauxic growth. They are solutions of the one-strain logistic equation (3.11). They model the growth of bacteria when consuming one resource first, and then switch to another resource. The growth switches from $n_i^{(1)}$ to $n_i^{(2)}$ at time t_c, where $n_i^{(1)}(t)$ describes the growth for $t < t_i^c$ and $n_i^{(2)}(t)$ for $t > t_i^c$. Using the definition of the Heaviside function $H(t = 0) = 1/2$, one has $n_i(t) = n_i^c$ at $t = t_i^c$.

We illustrate the curve fitting using a single rifampicin resistant clone grown in the presence of the rifampicin, at the same concentrations used in the selection experiment (Extended Data Figure 3.6). For the purposes of the fit we only considered the first 25 h of the growth experiment, to eliminate potential experimental error introduced from evaporation of the growth medium. We measure time in units of hours, and the growth rates r_i are thus expressed in units of h^{-1}. The fits were performed using MATLAB 2016a, with Non-linear Least Squares as the fitting method. The code is available in the supplementary data. Parameters estimated in this way are given in Tables 3.2 and 3.3. Typically, these parameters explain a very large majority of the variation in OD (Table 3.4), except where there is effectively no growth (e.g. of S, R and N strains in high concentrations of the antibiotic combination).

The time point t_i^c and resulting population size n_i^c at which the growth switches from $n_i^{(1)}(t)$ to $n_i^{(2)}(t)$ is different for every strain, treatment, and drug concentration considered. Note that these parameters are obtained from growth experiments for single strains, whereas multiple strains are present in the simulation model.

In order to include the diauxic growth behaviour in the simulation model, we switch between the two growth regimes when the total population size $n_T(t)$ reaches a threshold n_T^c. This threshold is related to the n_i^c obtained from the fits of single-strain growth experiments to the diauxic behaviour in Eq. (3.14) as we will explain next.

Extended Data Figure 3.7 shows the distribution of n^c, the switching population values, obtained for the different treatments. Each graph shows a histogram of the

Table 3.2: Parameter estimates for $r_i^{(j)}$ from growth curve fitting used in simulations.

Treatment	Day(s)	Concentration (mg/l)	$r_R^{(1)}(h^{-1})$	$r_R^{(2)}(h^{-1})$	$r_N^{(1)}(h^{-1})$	$r_N^{(2)}(h^{-1})$	$r_D^{(1)}(h^{-1})$	$r_D^{(2)}(h^{-1})$	$r_S^{(1)}(h^{-1})$	$r_S^{(2)}(h^{-1})$
no antibiotic	1–6	–	1.173970	0.098993	1.151870	0.109296	0.958463	0.127234	0.947878	0.164112
rifampicin	1	0.625	1.043020	0.116856	0.970675	0.292025	0.902833	0.115857	1.093860	0.210714
rifampicin	2	1.250	1.056920	0.116220	1.093880	0.333938	0.865860	0.124027	1.105150	0.263604
rifampicin	3	2.5	0.982233	0.116832	1.063350	0.482605	0.900669	0.117007	0.948798	0.365733
rifampicin	4	5	0.937679	0.112200	0.807273	0.411240	0.921836	0.116490	0.840779	0.403584
rifampicin	5	10	0.921300	0.110723	0.083415	0.404481	0.937193	0.100619	0.192899	0.208367
rifampicin	6	20	0.923569	0.103764	0.213797	0.194690	0.950243	0.106703	0.373088	0.078366
nalidixic acid	1	0.625	1.020300	0.112120	1.063200	0.124669	0.958576	0.115087	1.044360	0.143468
nalidixic acid	2	1.250	0.925425	0.100114	1.072990	0.119817	0.990516	0.121795	0.691218	0.110424
nalidixic acid	3	2.5	1.722270	0.123658	1.053350	0.110569	0.909677	0.104766	2.209380	0.252918
nalidixic acid	4	5	1.590630	0.051378	1.026600	0.096470	1.035150	0.103146	1.918390	0.060882
nalidixic acid	5	10	1.512710	0.032302	1.014280	0.088789	1.043140	0.103496	1.401330	0.058245
nalidixic acid	6	20	1.219410	0.010868	1.075610	0.068764	0.972589	0.085056	1.525610	0.019976
combination	1	0.625	0.991571	0.110596	1.139640	0.189711	1.031820	0.123548	1.087100	0.199946
combination	2	1.250	0.758980	0.099015	1.061900	0.317303	0.981117	0.119622	0.701303	0.426269
combination	3	2.5	0.952536	0.231384	0.890059	0.208068	0.949267	0.103237	0.432370	0.133826
combination	4	5	1.501670	0.103079	0.306622	0.025243	0.917015	0.105881	0.199047	0.047624
combination	5	10	1.586230	0.052085	0.201779	0.037859	0.968774	0.101424	0.104680	0.041522
combination	6	20	1.291380	0.028238	0.082978	0.094658	0.950778	0.084560	0.203031	0.048298

Table 3.3: Parameter estimates for $k_i^{(j)}$ from growth curve fitting used in simulations.

Treatment	Day(s)	Concentration (mg/l)	$k_R^{(1)}$	$k_R^{(2)}$	$k_N^{(1)}$	$k_N^{(2)}$	$k_D^{(1)}$	$k_D^{(2)}$	$k_S^{(1)}$	$k_S^{(2)}$
no antibiotic	1–6	–	0.397273	1.157010	0.428896	1.028720	0.405555	0.833095	0.425338	1.000050
rifampicin	1	0.625	0.365385	1.022050	0.375063	0.640184	0.387929	0.842150	0.350036	0.763288
rifampicin	2	1.250	0.370709	1.025220	0.293331	0.453145	0.402572	0.847645	0.287164	0.568348
rifampicin	3	2.5	0.374061	1.000340	0.200545	0.255948	0.390664	0.880132	0.186229	0.261258
rifampicin	4	5	0.390581	0.990046	0.040360	0.249437	0.398351	0.884335	0.026746	0.277894
rifampicin	5	10	0.372689	0.848618	0.099165	0.045579	0.397357	0.922303	0.098903	0.011815
rifampicin	6	20	0.345292	0.787809	0.011372	0.229171	0.392850	0.886620	0.004270	0.012638
nalidixic acid	1	0.625	0.402715	0.959691	0.387546	0.973445	0.376097	0.829342	0.399527	0.937229
nalidixic acid	2	1.250	0.346634	0.852497	0.402417	0.983478	0.367056	0.831784	0.362044	0.894458
nalidixic acid	3	2.5	0.083131	0.778597	0.398977	0.992572	0.388202	0.870940	0.099981	0.041896
nalidixic acid	4	5	0.095932	0.030033	0.430679	1.071450	0.393713	0.896599	0.097372	0.012511
nalidixic acid	5	10	0.077944	0.016135	0.453037	1.114120	0.404768	0.878548	0.064421	0.011899
nalidixic acid	6	20	0.039098	0.005097	0.438773	1.188260	0.389642	0.919682	0.034497	0.005282
combination	1	0.625	0.399070	0.914482	0.374991	0.698327	0.378862	0.851363	0.364842	0.709612
combination	2	1.250	0.300167	0.791189	0.336533	0.456723	0.365759	0.819325	0.291848	0.313283
combination	3	2.5	0.050000	0.359507	0.203518	0.267444	0.381847	0.883465	0.034633	0.017086
combination	4	5	0.061611	0.019415	0.130177	0.012991	0.384839	0.875531	0.014570	0.005366
combination	5	10	0.030671	0.007802	0.052115	0.010491	0.365874	0.875381	0.003710	0.002113
combination	6	20	0.015235	0.012757	0.025458	0.026768	0.348358	0.842369	0.014907	0.001698

Table 3.4: R^2 values from growth curve fitting used in simulations for strains S, R, N, and D.

Treatment	Day(s)	Concentration (mg/l)	R^2_R	R^2_N	R^2_D	R^2_S
no antibiotic	1–6	0.31250	0.99957	0.99925	0.99907	0.99957
rifampicin	1	0.625	0.99960	0.99738	0.99966	0.99956
rifampicin	2	1.25	0.99964	0.99625	0.99958	0.99244
rifampicin	3	2.50	0.99958	0.98607	0.99946	0.99552
rifampicin	4	5	0.99956	0.99822	0.99967	0.99947
rifampicin	5	10	0.99966	0.99725	0.99969	0.94550
rifampicin	6	20	0.99933	0.99165	0.99974	0.37149
nalidixic acid	1	0.625	0.99959	0.99955	0.99953	0.99945
nalidixic acid	2	1.25	0.99974	0.99953	0.99964	0.99948
nalidixic acid	3	2.50	0.99763	0.99957	0.99944	0.99309
nalidixic acid	4	5	0.98397	0.99958	0.99970	0.98801
nalidixic acid	5	10	0.97461	0.99949	0.99970	0.96445
nalidixic acid	6	20	0.96781	0.99970	0.99932	0.95763
combination	1	0.625	0.99948	0.99940	0.99950	0.99913
combination	2	1.25	0.99962	0.99939	0.99964	0.99924
combination	3	2.50	0.97307	0.99931	0.99963	0.95726
combination	4	5	0.97735	0.98672	0.99960	0.88433
combination	5	10	0.93615	0.98740	0.99955	0.19791
combination	6	20	0.97295	0.97101	0.99955	0.35897

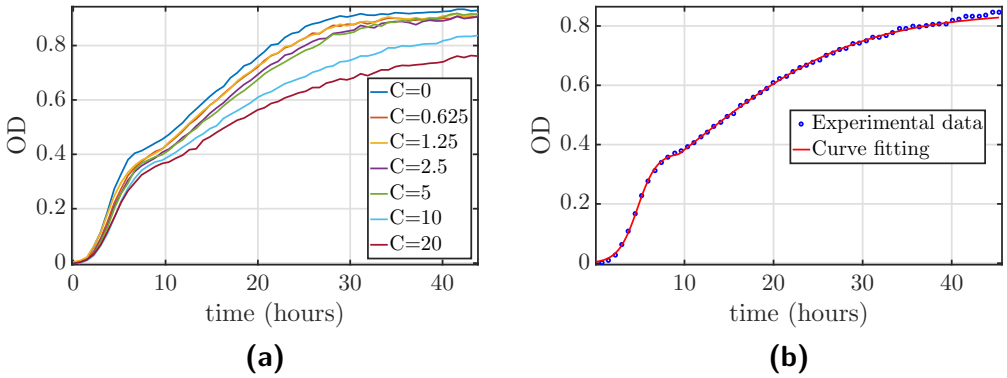

Extended Data Figure 3.6: A. Example growth curves of a rifampicin-resistant clone under rifampicin treatment, for several drug concentrations, C (mg/l). B. Curve fitting for $C = 10$ mg/l of the rifampicin treatment for the rifampicin-resistant strain, resulting in estimates $k_R^{(1)} = 0.372689$, $r_R^{(1)} = 0.921300$, $k_R^{(2)} = 0.848618$, $r_R^{(2)} = 0.110723$, $R_R^2 = 0.99966$ (other estimates and R^2 shown in Tables 3.2–3.4). OD–optical density.

values, n^c, obtained from the different drug concentrations and strains for the given treatment. Since there are 6 drug concentrations as each growth experiment proceeds, and 4 different strains, this results in 24 values for n^c per treatment. Evidently, for experiments in which no drug is given we only obtain four values of n^c (one for each strain). We do not show the corresponding histogram.

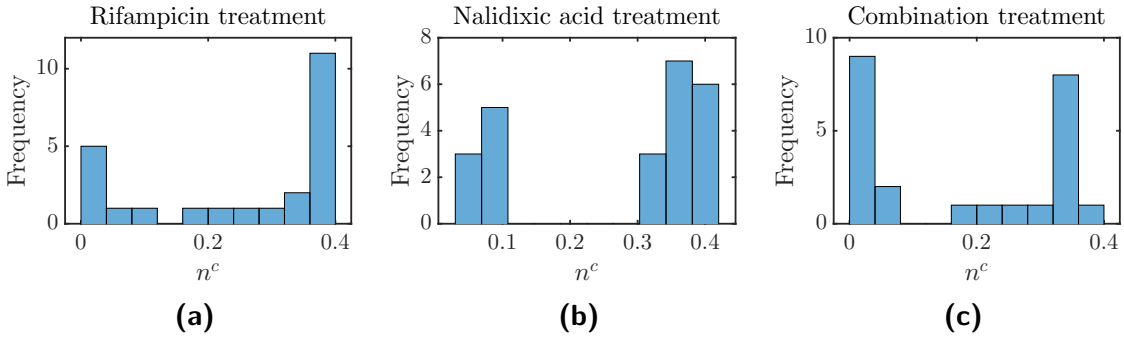

Extended Data Figure 3.7: Histograms of n^c obtained from fitting the diauxic growth curves in the text to experimental data; rifampicin, nalidixic acid, combination treatments in panels A, B and C, respectively. Each graph includes all the values (24 in total) of n_i^c obtained for each drug concentration and strain.

Each of the histograms is bimodal, with one peak close to $n^c = 0$, and the other at $n^c \approx 0.3$ on the optical-density scale . The left peak at $n^c \approx 0$ corresponds to strains incapable of growing in those environments (e.g. strain S for high values of antibiotic concentration, C). We estimate n_T^c as the mean value obtained from the peak on the right in each histogram, i.e. cases where strains were capable of growing. Results

are shown in Table 3.5. The value obtained in this way differs between the different treatments. For the case of no treatment we use the average over the four strains as threshold value n_T^c.

Table 3.5: Switching value, n_T^c, for the different treatments.

Treatment	Switching n_T^c
No antibiotic	0.4108
Rifampicin	0.3417
Nalidixic acid	0.3709
Combination	0.3154

As these parameters have been estimated from OD growth curves, they have so far been expressed in units of OD. In the next section, we will describe the relationship between OD and the number of bacteria.

3.8.6 Relationship between optical density and bacterial population size

To simulate population dynamics, the parameters we have estimated need to be expressed in terms of numbers of bacteria, rather than in units of OD. We therefore determined the relationship between OD and the number of bacteria present. Following growth in liquid MH (with and without antibiotics, as in the selection experiment), serial dilutions were plated on 90 mm Petri dishes containing LB agar (without antibiotics), and colony forming units (CFUs) were counted following overnight growth. To determine the best relationship between OD and number of bacteria, we performed stepwise model selection using the `step()` function in R. The best fitting model indicated a uniform slope across environments and strains (Extended Data Figure 3.8A, Table S4). We therefore converted OD into population size by multiplying OD by a constant (5.71×10^8 bacteria per unit OD). We also performed kill curves to quantify the extent of killing that occurs when populations first experience antibiotic treatment (Extended Data Figure 3.8B). To recapitulate the conditions experienced during the selection experiment, this was performed by pin replicating an overnight culture (1/200 dilution) into antibiotic containing medium (0.625, 1.25, 2.5, 5, 10, 20 mg/l of each

antibiotic treatment). Population sizes were estimated by plating dilutions on LB agar after 2, 4, 6, 8, and 24 h of exposure.

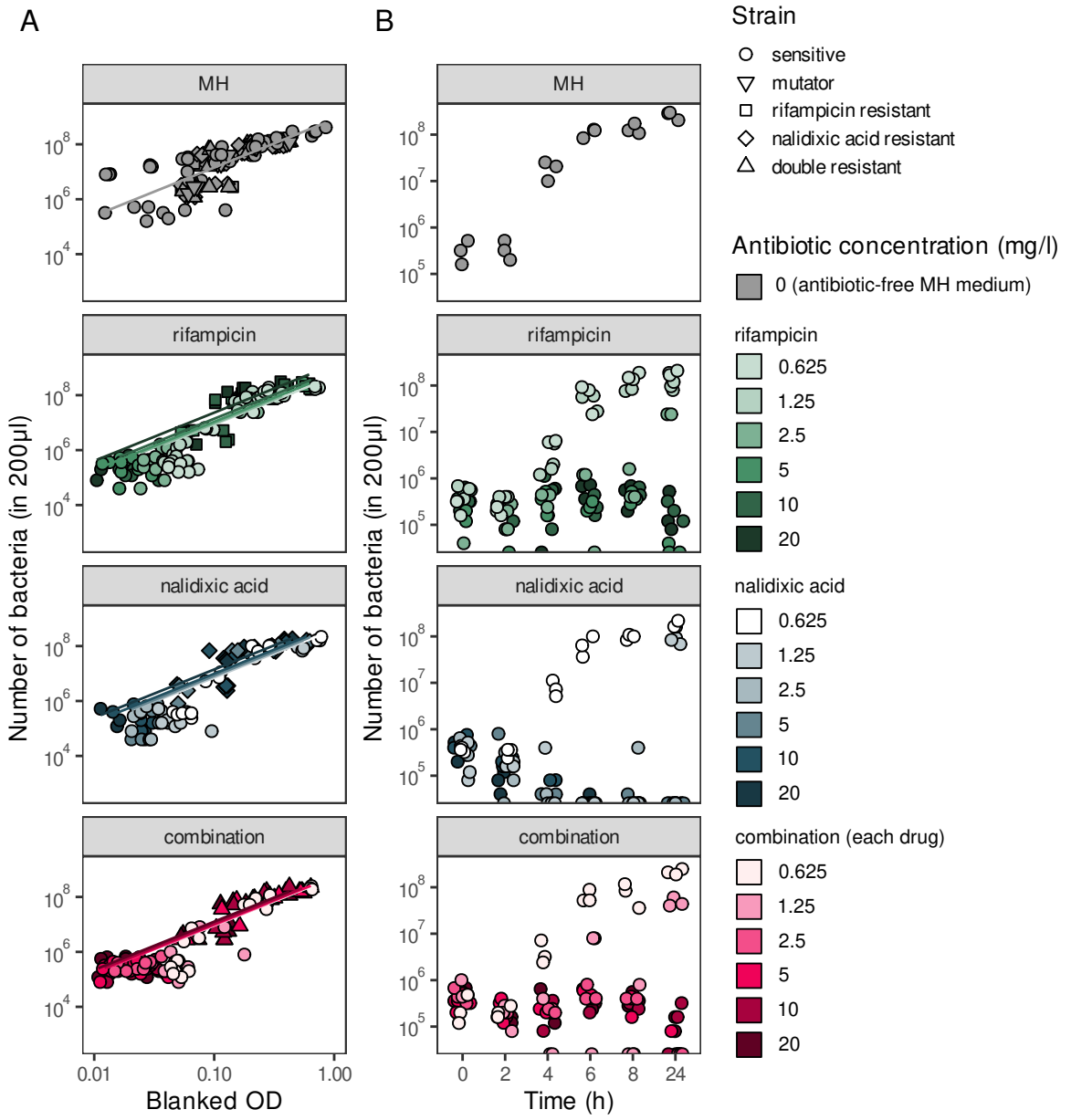

Extended Data Figure 3.8: A. Relationship between blank corrected optical density and number of bacteria in antibiotic concentrations experienced during the selection experiment. Regression lines are the best fitting linear model shown in Table 3.6. B. Time series of bacterial populations exposed to antibiotic concentrations experienced during the selection experiment. Blanked OD–blank corrected optical density.

Table 3.6: ANOVA for the full model and best model for predicting population size from optical density, chosen by stepwise model selection using AIC. N–population size, OD–blank corrected optical density (see Extended Data Figure 3.8)

Full model: $\log_{10}(\text{N}) \sim \log_{10}(\text{OD}) * (\text{antibiotic/concentration}) * \text{strain}$

Model term	*df*	Squared Error	F-statistic	p-value
$\log_{10}$(OD)	1	80.0	502	$< 10^{-16}$
antibiotic	3	0.95	1.99	0.12
strain	4	0.32	0.50	0.74
antibiotic:concentration	3	1.27	2.66	0.05
$\log_{10}$(OD):antibiotic	3	0.29	0.61	0.61
$\log_{10}$(OD):strain	4	0.88	1.38	0.24
antibiotic:strain	3	0.06	0.13	0.94
$\log_{10}$(OD):antibiotic:concentration	3	0.19	0.40	0.75
antibiotic:concentration:strain	3	0.10	0.22	0.88
$\log_{10}$(OD):antibiotic:strain	3	0.01	0.02	>0.99
$\log_{10}$(OD):antibiotic:concentration:strain	3	0.08	0.16	0.92
Residuals	228	36.4		

Overall model $F_{33,238} = 16.0$, p-value $< 10^{-16}$, adjusted $R^2 = 0.655$, AIC $= 296$

Best model: $\log_{10}(\text{N}) \sim \log_{10}(\text{OD}) + \text{antibiotic} + \text{antibiotic:concentration}$

Model term	*df*	Squared Error	F-statistic	p-value
$\log_{10}$(OD)	1	80.0	534	$< 10^{-16}$
antibiotic	3	0.95	2.12	0.10
antibiotic:concentration	3	1.53	3.40	0.02
residuals	254	38.1		

Overall model $F_{7,254} = 78.7$, p-value $< 10^{-16}$, adjusted $R^2 = 0.676$, AIC $= 256$

3.8.7 Simulating the experiments

Simulation conditions are given in Table 3.7. We use the values $k_i^{(1)}, r_i^{(1)}, k_i^{(2)}, r_i^{(2)}$ of each strain and treatment, and n_T^c obtained as defined above, for simulations of the stochastic model. Simulations are started from an initial population of 5.71×10^6 sensitive bacteria (type S); a frequency q of these are mutators and the remaining fraction $(1-q)$ consists of wild-type bacteria. In the simulations we use $\mu_R = 6.7 \times 10^{-9}$ and $\mu_N = 7.4 \times 10^{-10}$, as motivated in the main text. Mutators have a 80-fold increased mutation rates, μ_R and μ_N, compared to the wildtype.

The simulated experiment consists of six days of growth, where the concentration of antibiotic(s) is initially 0.625 on day 1, and doubled on each of the days 2 to 6.

Recall that the length of each time-step of the simulation, Δt, is expressed in units of hours (h). It has to be sufficiently small so that $0 \leq b_i \leq 1$ (b_i is a probability). This

Table 3.7: Simulation conditions.

Parameter	Value
Replicates	1000
Initial population size	5.71×10^6
Mean proportion transferred during dilution step	0.005
Duration between bottlenecks	22 h
Length of time per time-step (Δt)	0.01 h
Mutation rate to rifampicin resistance (μ_R)	6.7×10^{-9} mutations per replication
Mutation rate to nalidixic acid resistance (μ_N)	7.4×10^{-10} mutations per replication
Mutator effect	80-fold increase

means that we require

$$0 \leq \Delta t \leq \frac{\ln\ 2}{r_i(1 - n_T/k_i)}. \tag{3.16}$$

The upper bound on the right-hand side of the inequality takes its minimum value, $\ln\ 2/r_i$, when $n_T = 0$. From the fits of the experimentally obtained (single-strain) growth curves to solutions of the logistic dynamics, we find a maximum value of $r_i = 2.2h^{-1}$ for nalidixic acid treatment, strain S, drug concentration 0.25 mg/l. This in turn means that the simulations required $\Delta t \lesssim 0.3151$ h (similar to published estimates of *E. coli* minimum doubling time, e.g. [108]). For our simulations we have set $\Delta t = 0.01$ h as this case approximates the continuous-time approach well (see Figures 3.3 and 3.4). For higher values of Δt our approximation becomes less accurate, yet we can still obtain qualitatively equivalent results (we have choices of the time step tested up to $\Delta t = 0.25$).

An important aspect to take into account is the dilution carried out in the laboratory experiments at the end of each day, when 1/200 of the population is carried forward to the next day, and the rest discarded. In simulations we cycle through all members of the population at the end of each (simulated) day and retain each individual with probability 1/200; otherwise the individual is removed. This represents an independent Bernoulli event on the level of individual bacteria. The number of each type i carried forward follows a binomial distribution with mean $\mu = n_i/200$ and variance $\sigma^2 = n_i \times 1/200 \times 199/200 = n_i \times 4.975 \times 10^{-3}$, where n_i is the number of type i individuals. This allows the possibility that a strain type goes extinct if it arises too late into the growth cycle to achieve appreciable frequency.

An example of the growth obtained from the simulations is presented in Extended Data Figure 3.9.

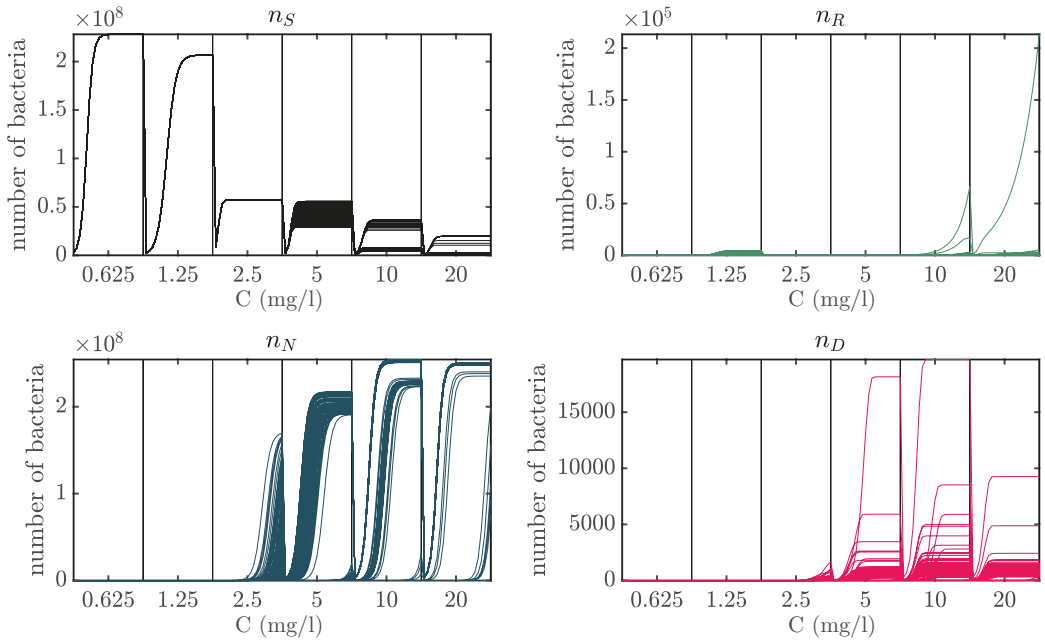

Extended Data Figure 3.9: Simulated growth curves for nalidixic acid treatment. Each panel shows 100 independent simulation runs. The data shown aggregates wildtype and mutant bacteria. C–antibiotic concentration (mg/l). Initial condition: 5.71×10^6 sensitive bacteria, with a frequency $q = 0.3$ of mutators. Curves for each value of C were simulated over 22 h. We have used $\Delta t = 0.01$ h. Compare to Extended Data Extended Data Figure 3.2D (nalidixic acid column).

3.9 Appendix B: Bayesian statistical analysis of experiments and simulations

3.9.1 Model M1: Detection of resistance arising during experimental evolution

Defining the model

Here we ask whether the initial mutator frequency and antibiotic treatments had an effect on resistance evolution, and whether these effects interacted. We fitted a categorical regression model (also called a 'multinomial logistic' model) to the data, to analyse how different initial mutator frequencies and antibiotic treatments affected which type of resistance was observed at the end of the experiment.

To make our analysis explicit, we will briefly describe the model here. We will refer to Y_i as the value of the ith observation, $x_{m,i}$ as the independent variables, and $\beta_{m,k}$ as the estimated model coefficients. It is the coefficients $\beta_{m,k}$ that are of interest as they relate how different experimental conditions influence the probability of observing any given outcome. Categorical regression can be formulated as an extension of logistic regression. Let Y_i be a categorical variable that takes a value k from $\{1, 2, ..., K\}$, and the probability that Y_i has outcome k be $\mathrm{P}(Y_i = k)$. We use a linear predictor function to compute $\mathrm{P}(Y_i = k)$. For a model considering M explanatory variables, this takes the form

$$f(k, i) = \beta_{0,k} + \beta_{1,k}x_{1,i} + \beta_{2,k}x_{2,i} + ... + \beta_{M,k}x_{M,i}, \tag{3.17}$$

where $\beta_{m,k}$ is the regression coefficient associated with the mth explanatory variable and the kth outcome, and $\beta_{0,k}$ is the intercept associated with the kth outcome. This function can be written more compactly using vector notation and taking the dot product, $f(k, i) = \vec{\beta}_k \cdot \vec{x}_i$, where $\vec{\beta}_k$ and $\vec{x}_i$ each have length $M + 1$, and $x_{0,i}$ is assigned a value of 1.

The reader may be familiar with binary logistic regression with $K = 2$ outcomes, usually with $k = 1$ defined as 'success' and $k = 0$ as 'failure'. The function $f(i, k)$ is linked to the probability of observing outcome k by taking the log of the odds-ratio of the two outcomes, i.e. the logit function.

If $p_i = \mathrm{P}(Y_i = 1)$,

$$\begin{aligned} \mathrm{logit}(p_i) &= \log\left(\frac{p_i}{1 - p_i}\right) = \vec{\beta}_1 \cdot \vec{X}_i \\ p_i &= \frac{e^{\vec{\beta}_1 \cdot \vec{X}_i}}{1 + e^{\vec{\beta}_1 \cdot \vec{X}_i}}, \end{aligned} \tag{3.18}$$

where $\vec{X}_i$ is the vector of values taken by the explanatory variables $\vec{x}_i$ for the observation Y_i.

For $K > 2$ outcomes, the multinomial logit can be thought of as computing $K - 1$ independent logistic regression models with respect to a consistent reference level [109]. If K is chosen as the reference level, $\beta_{0,K}$ is defined as the 'intercept' of the model and

all other elements of $\vec{\beta_K}$ are equal to zero. This results in

$$\begin{aligned} \log \frac{\mathrm{P}\left(Y_i = 1\right)}{\mathrm{P}\left(Y_i = K\right)} &= \vec{\beta}_1 \cdot \vec{X}_i \\ \log \frac{\mathrm{P}\left(Y_i = 2\right)}{\mathrm{P}\left(Y_i = K\right)} &= \vec{\beta}_2 \cdot \vec{X}_i \\ &\ldots \\ \log \frac{\mathrm{P}\left(Y_i = K-1\right)}{\mathrm{P}\left(Y_i = K\right)} &= \vec{\beta}_{K-1} \cdot \vec{X}_i \ . \end{aligned} \tag{3.19}$$

The fact that $\sum_{k=1}^{K} P(Y_i = k) = 1$ allows calculating $\mathrm{P}(Y_i = K) = 1/\Big(1 + \sum_{k=1}^{K-1} e^{\vec{\beta}_k \cdot \vec{X}_i}\Big)$, which can then be used to solve the other probabilities. For any outcome c, the general form of $\mathrm{P}\left(Y_i = c\right)$ is thus given as

$$\mathrm{P}\left(Y_i = c\right) = \frac{e^{\vec{\beta}_c \cdot \vec{X}_i}}{1 + \sum_{k=1}^{K-1} e^{\vec{\beta}_k \cdot \vec{X}_i}}, \tag{3.20}$$

which can then be used to estimate the coefficients $\vec{\beta}_k$ through various methods. The particular method we used, Bayesian categorical regression, is described in the next section.

Fitting the model and hypothesis testing using Bayesian categorical regression

In our particular analysis, Y_i represents the type of resistance observed, with five possible outcomes: 'no resistance', 'rifampicin resistance', 'nalidixic acid resistance', 'mixed resistance' and 'double resistance'. For 'mixed resistance', populations grew on selective plates containing either rifampicin or nalidixic acid, but *not* on plates containing both rifampicin and nalidixic acid, whereas 'double resistant' populations grew on plates containing both antibiotics. We note that these outcomes refer to *detection* of resistance, rather than *fixation*, i.e. the frequency of resistant individuals within each population has a value between > 0 and ≤ 1.

The independent variables, $\vec{x}_i$, were the initial mutator frequency, the antibiotic treatment applied, which microtitre plate the population inhabited, and position within each microtitre plate. Initial mutator frequency was treated as a categorical predictor (with levels 'zero', 'low', 'medium' or 'high', using 'zero' as the reference level), as we have no *a priori* expectation of a linear relationship between the proportion of mutators and the estimated coefficient. Antibiotic treatment was a categorical predictor (with

levels 'no antibiotic', 'rifampicin', 'nalidixic acid', or 'combination', using 'no antibiotic' as the reference level). Initial mutator frequency and antibiotic were each treated as a fixed effect (as variance estimates from random effects variables with fewer than five levels tends to be imprecise, see [110]). Plate number and position within each microtitre plate were treated as random effects.

Incorporating both fixed and random effects requires fitting a 'mixed-effects model' to the data. However, categorical mixed-effects models are not straightforward to fit using standard frequentist inference methods. While it is possible to fit such models in principle [111], there is not, to our knowledge, any readily-available software implementation. However, such models can be fit using recently-developed tools based on Bayesian inference methods [91, 92]. We provide an example below. Although software implementation initially motivated our choice of approach, there are additional benefits of Bayesian inference [112].

To estimate the coefficients, $\vec{\beta}_k$, we fit a mixed-effects categorical model using `brm()` from the `brms` package [91, 92] in R [93]. To fit a categorical model, 'family' was set to 'categorical' (with the default link 'logit'). To ensure convergence was achieved, we set `max_treedepth` = 15 and `adapt_delta` = 0.99. We ran four chains of 2000 iterations each, with 1000 burn-in iterations. To permit hypothesis testing on point estimates, samples from specified priors were drawn by setting `sample_prior="yes"`. The choice of priors was based on preliminary data, and is described in detail in a later section. Default values were used for other settings.

To evaluate whether the interaction between initial mutator frequency and antibiotic treatment was important, we compared the full model (i.e. main effects and interaction) to a model with a main-effects only using 'Pareto-smoothed importance sampling leave-one-out cross-validation' (PSIS-LOO [113]). Incorporating interactions effects into the model did not significantly improve fit (PSIS-LOO difference in fit: -2.6 ± 5.4 S.E.), hence we present estimates from the main effects model.

An example of the function call is shown below (full R scripts are also available, see 'Data Availability' statement in the main text).

```
# Control parameters and priors
priors = c(set_prior ("student_t(7, -5, 2.5)", class = "
    Intercept"),
```

```
        set_prior ("student_t(7, 0, 2.5)", class = "b"))
controls = list(adapt_delta = 0.99, max_treedepth = 15)
# Model calls
M1.full = state ~ (pmutS.text + antibiotic)^2 + (1|row) + (1|
    col)
M1.main = state ~ (pmutS.text + antibiotic)   + (1|row) + (1|
    col)
modelM1.full = brm(M1.full,
        family = categorical("logit"),
        chains = 4, cores = 4, iter = 2000, warmup = 1000,
        prior = priors, control = controls, sample_prior = "yes
            ",
        data = popnsday6)
modelM1.main = brm(M1.main,
        family = categorical("logit"),
        chains = 4, cores = 4, iter = 2000, warmup = 1000,
        prior = priors, control = controls, sample_prior = "yes
            ",
        data = popnsday6)
```

Establishing priors for the model

Priors were established through a preliminary experiment in which pure populations of either wild-type or mutator bacteria were subjected to increasing concentrations of single and combination antibiotic treatments, as in the experiment described in the main text (Extended Data Figure 3.10A). In contrast to the experiment presented in the main text, here only the optical density (OD) at 600 nm of each population was tracked (using a BMG POLARstar OPTIMA plate reader, BMG Labtech, Ortenberg, Germany) rather than its resistance state. A population was considered to be 'alive' with OD > 0.1, otherwise 'extinct'. Note that OD is a unitless quantity that is dependent on the equipment used to measure it. We observed that, in the absence antibiotic treatment, all populations survived. For single antibiotic treatments, all mutator populations survived, but some wild-type populations went extinct. For

the combination antibiotic treatment, 39/54 mutator populations survived, but all wild-type populations went extinct. First, we use this information to establish priors for the intercepts (Extended Data Figure 3.10B). Recall that 'zero' is the reference level for mutators, and 'no antibiotic' for antibiotics.

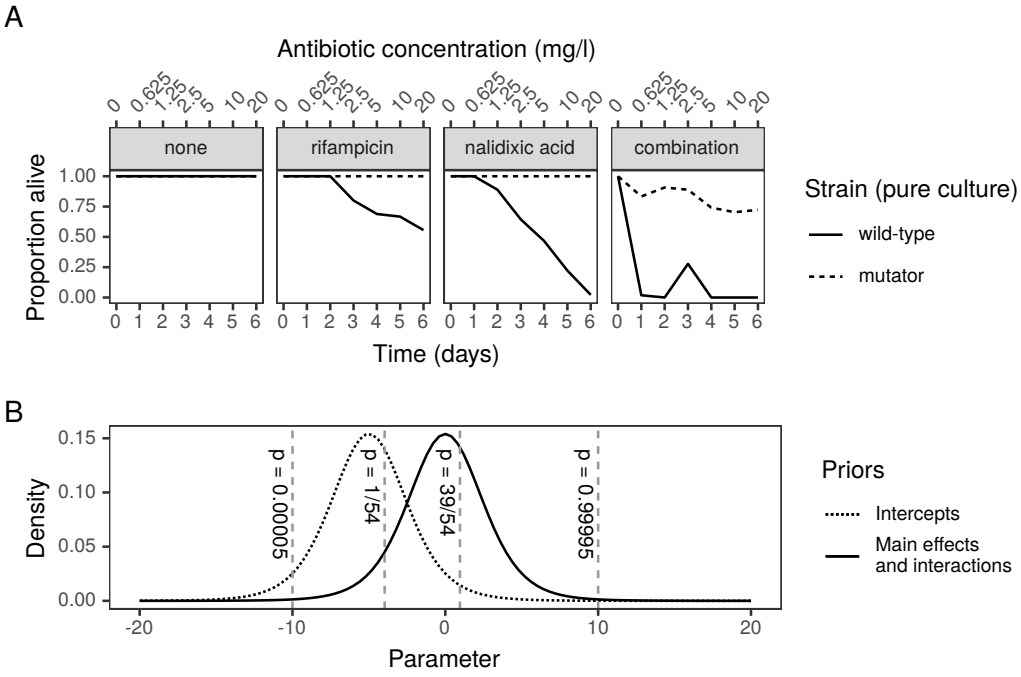

Extended Data Figure 3.10: A. Preliminary experiment tracking the proportion of populations 'alive' (i.e. with OD > 0.1) under experimental treatments. B. Illustration of priors used to conduct Bayesian categorical regression using information from preliminary experiment, indicated by vertical dashed lines. Curves show the probability density for a Student's t distribution with means $\mu = 0$ (solid) or $\mu = -5$ (dotted), standard deviation $\sigma = 2.5$ (both curves) and degrees of freedom $\nu = 7$ (both curves).

Out of 54 trials, we observed no alive populations in the wild-type populations. We have some confidence that the proportion of double resistant outcomes is then $p_{\text{double}} < 1/54$. Therefore, the intercept for double resistance should be less than $\text{logit}(1/54) \approx -3.97$. We therefore used a t-distribution with mean $\mu = -5$ and broad and heavy tails with standard deviation $\sigma = 2.5$, and degrees of freedom $\nu = 7$, to reflect uncertainty. This distribution covers both $p_{\text{double}} \approx 0$ in the left tail, and $p_{\text{double}} = 39/54$, i.e. the number of alive populations in pure mutator populations, in the right tail. Given that the probability of being single-drug resistant in the absence of antibiotic is likely greater than double resistant, intercepts for other resistance outcomes are likely covered by this distribution, and so we use the same prior for the other intercepts.

Next, we use this information to establish priors for the other coefficients. We observed that the presence of mutators increases survival in the presence of both single and combination antibiotics, hence the effect of mutators on *total* resistance (i.e. the sum of all resistance types observed) is likely to be positive. However, it is possible that different resistance types may have a negative relationship with the proportion of mutators, if for example, elevated mutation rates pushes double resistance to arise in the background of single-drug resistance, single-drug resistance may have a negative relationship with initial mutator frequency. Hence for the effects of initial proportion of mutators, we use a t-distribution centred at $\mu = 0$ with the same broad and heavy tails $\sigma = 2.5$, and $\nu = 7$ to reflect uncertainty. This covers the observed proportion of alive populations in a purely mutator population $p = 39/54$; we should however expect to observe fewer resistance events when the proportion of mutators is less than 1, as in the main text experiment. It also allows for the extreme possibilities of (nearly) zero or (nearly) all resistance, albeit with less weight given.

From this experiment, we have limited direct evidence for how the presence of antibiotics should affect the probability of observing resistance. On one hand, the presence of antibiotics decreased the number of alive populations (and an extinct population cannot be resistant). On the other, our growth measurements of resistant strains in the presence of antibiotics suggest a positive effect of being resistant in the presence of antibiotics, which would allow them to spread to high frequency and thus escape loss due to genetic drift. The effect of antibiotics is likely to be in the same range as for mutators (which includes 'no effect'), hence we use the same prior distribution (i.e. a t-distribution with $\mu = 0$, $\sigma = 2.5$, and $\nu = 7$).

Estimated model coefficients

Estimated model coefficients for the main-effects only model are shown in Table 3.8. These are reported as treatment contrasts (i.e. relative to the treatment of no antibiotics and no mutators). Bayesian hypothesis tests on fitted model coefficients were performed using `hypothesis()`, which calculates a Bayes factor using the Savage-Dickey density ratio method [114]. We used 95% credible intervals (95% C.I.s) for all hypotheses tested. Coefficients were estimated on the logit scale (i.e. log-odds, which can assume any value between $-\infty$ and ∞, corresponding to proportions of outcomes of $p_{\text{resistance type}} = 0$

and 1 respectively). A coefficient is estimated for each possible combination of response outcome (resistance type) and the predictors (initial mutator frequency and antibiotic), which indicates how a specific combination of predictor levels (e.g. 'low' mutator frequency and 'rifampicin' treatment) influences the probability that a given outcome is observed (e.g. 'rifampicin resistance').

Table 3.8: Effects of initial mutator frequency and antibiotic treatment on resistance type observed at the end of the experiment. Estimated model coefficients come from fitting a Bayesian categorical regression model to the data (see Model M1). Treatment contrasts on the logit scale are shown. (* denotes 95% credible intervals excluding zero).

Resistance type	Coefficient	Treatment contrast	95% credible interval	
rifampicin resistance	intercept	-2.83	(-3.58, -2.14)	*
	low	1.48	(0.78, 2.25)	*
	intermediate	1.98	(1.23, 2.74)	*
	high	3.36	(2.56, 4.17)	*
	rifampicin	3.29	(2.60, 4.02)	*
	nalidixic acid	-1.22	(-2.28, -0.29)	*
	combination	-2.22	(-3.16, -1.38)	*
nalidixic acid resistance	intercept	-4.00	(-5.06, -3.08)	*
	low	-0.88	(-2.30, 0.34)	
	intermediate	1.51	(0.65, 2.39)	*
	high	2.81	(1.90, 3.78)	*
	rifampicin	-2.41	(-7.70, 0.75)	
	nalidixic acid	2.67	(1.88, 3.54)	*
	combination	-0.88	(-2.11, 0.26)	
mixed resistance	intercept	-6.78	(-8.46, -5.37)	*
	low	4.27	(3.02, 5.81)	*
	intermediate	4.89	(3.60, 6.45)	*
	high	6.51	(5.20, 8.10)	*
	rifampicin	3.63	(2.77, 4.52)	*
	nalidixic acid	2.84	(2.18, 3.53)	*
	combination	-0.96	(-1.90, -0.10)	*
double resistance	intercept	-10.99	(-13.91, -8.71)	*
	low	5.14	(3.57, 7.39)	*
	intermediate	5.98	(4.36, 8.26)	*
	high	8.01	(6.35, 10.28)	*
	rifampicin	7.80	(6.21, 9.97)	*
	nalidixic acid	5.20	(3.71, 7.36)	*
	combination	4.22	(2.78, 6.33)	*

Checking robustness against choice of priors

A potential consequence of using informative priors in Bayesian inference is that they may influence the posterior distribution for estimated coefficients unduly if they are not chosen appropriately. However, the use of non-informative priors does not necessarily mitigate these problems (for an in-depth discussion, see [115]). To check the robustness of our model against the originally chosen priors, we refit the model using different priors. We set Student-t priors on the intercept with arbitrarily chosen μ of -10, -20, -30, -40, with (as before) $\sigma = 2.5$ and $\nu = 7$. The estimated coefficients resulting from using these priors are quantitatively similar to our original model. As a second approach to evaluating robustness, we also set strongly-informative priors on each coefficient of the model. We estimated means for each coefficient using a fixed-effects categorical model (i.e. without the random effects) by maximum likelihood using the `multinom()` function from the nnet package ([116], which refers to this type of model as 'multinomial logistic regression'). Note that assigning priors in this fashion is used here only as a diagnostic technique, and is not recommended as a basis for assigning priors more generally. For the model with these strong priors, the majority of coefficients were again similar to the original Model M1. The exception was for coefficients associated with the 'double resistance' outcome. Here, because there were zero double resistance events associated with the reference levels of the main effects of the model (i.e. no mutators, no antibiotics), the maximum likelihood estimated the intercept associated with this outcome to be very small (log-odds of -38.34, equivalent to an odds ratio of approximately 4.5×10^{-16}). The posterior distribution for the intercept was dominated by this strong prior. Consequently, the estimated coefficients for the coefficients associated with antibiotic treatment and the presence of mutators where there were double resistant outcomes observed were much larger than those estimated when using the original weakly-informative priors. However, we note that in all cases, the qualitative outcomes with respect to antibiotic treatment and the presence of mutators remain unchanged.

3.9.2 Model M2: Growth of strains derived from fluctuation tests

Defining the model

Here we determined under which conditions resistant strains achieved a growth advantage (see main text Extended Data Figure 3.2). Recall that growth was characterised using area under the curve (AUC) of growth curves from optical density measured at 600 nm. We compare the wild-type (*E. coli* K-12 BW25113) with single- and double-drug resistant mutants selected in the BW25113 genetic background through fluctuation tests (see Methods in main text). The model fitted to the data in Extended Data Figure 3.3 is a Bayesian two-way factorial model, with 'strain' and 'antibiotic' as predictor variables. We treated AUC measured in each antibiotic treatment as a multivariate response. This was on the basis that each strain was measured at several different concentrations, hence may be non-independent. We used Student's t priors, as opposed to a Gaussian priors, because doing so is more robust against extreme values (i.e. values that appear to be 'outliers', but where there is no evidence of error in data collection, [117]).

Establishing priors for the model

The intercept of this model is the mean AUC from the growth curves of OD, which is always greater than zero. To calculate empirical AUC, we used `SummariseGrowth()` from the `growthcurver`, which uses the trapezoidal rule to approximate the integral under the curve. OD values on this BMG FLUOstar OPTIMA plate reader are typically less than 1.2 for blank-corrected values. We used the trapezoidal rule to calculate extremes for the values of AUC, i.e.

$$\text{AUC} = \int_a^b f(x)dx \approx (b-a)\frac{f(a)+f(b)}{2}.$$

Since AUC was calculated over 25 h, the lower extreme is $(25-0)(0+0)/2 = 0$ (i.e. no growth) and the upper extreme is $(25-0)(1.2+1.2)/2 = 30$ (i.e. essentially instantaneous achievement of maximum density). However, previous experience from growing wild-type *E. coli* suggests they exit exponential growth in the region of 10 h

after inoculation after a 1/1000 dilution in MH broth, giving

$$\text{AUC} \approx \frac{(10-0)(0+1.2)}{2} + \frac{(25-10)(1.2+1.2)}{2} = 24$$

as a rough approximation of what would be expected under good growth conditions. Hence, the prior for the intercepts should give highest density between 0 and 24. This was specified as a t-distribution with mean $\mu = 10$ and broad and heavy tails with standard deviation $\sigma = 2.5$, and degrees of freedom $\nu = 7$. The presence of mutators could either increase or decrease evolved fitness relative to the intercept. To set the priors on the effect of mutators, we use a t-distribution centred on mean $\mu = 0$, with standard deviation $\sigma = 0.5$, and degrees of freedom $\nu = 7$. If the intercept takes a value in the region of the mean of its prior, this prior on the mutator effect allows for the extreme possibility that the presence of mutators results in an AUC of zero (if the coefficient takes value -10), or an AUC beyond the technical capabilities of the equipment (for values > 10), with low probability. This is illustrated in Extended Data Figure 3.11.

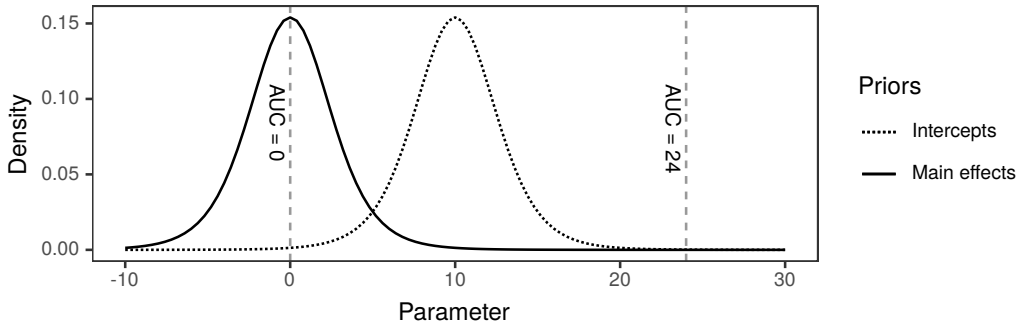

Extended Data Figure 3.11: Illustration of priors used to conduct Bayesian multivariate regression on the effect of mutators on growth. Curves show the probability density for a Student's t distribution with means $\mu = 0$ (solid) or $\mu = 10$ (dotted), standard deviation $\sigma = 2.5$ (both curves) and degrees of freedom $\nu = 7$ (both curves). Dashed vertical lines show prior information on technical upper and lower values for AUC, used to set a prior on the intercept.

Fitting the model and hypothesis testing

As previously, model fitting was performed using `brm()`. To use a Student's t model, 'family' was set to 'student' (with the default link 'identity'). To permit hypothesis testing on point estimates, samples from specified priors were drawn by setting `sample_prior="yes"`. To ensure convergence, we set `max_treedepth` = 15 and

`adapt_delta` = 0.99. Default values were used for other settings. As before, we used a 95% C.I. for hypotheses. As we are primarily interested in hypotheses on point estimates, we do not present the entire table of estimated effects here, though this can be generated with the R script provided (see the 'Data Availability' statement in the main text). We calculated the difference in AUC of the single-resistant and double-resistant strains in the two single-drug treatments. Estimated model coefficients are reported as treatment contrasts (i.e. relative to the wildtype and antibiotic-free treatment). For the rifampicin treatment, there was no benefit of double resistance over rifampicin resistance [95% C.I. of the difference = -0.07, 95% C.I.: $(-0.38, 0.23)$]. For the nalidixic acid treatment, there was a deleterious effect of double resistance over nalidixic acid resistance [95% C.I. of the difference = -0.75, 95% C.I.: $(-1.05, -0.45)$].

3.9.3 Model M3: Growth of double resistant strains from selection experiment

Defining the model

Here we determine whether initial mutator frequency had an effect on the growth of double resistant strains that evolved during selection. Decreased growth with a higher mutator frequency may occur if deleterious variation accumulated by the elevated mutation rate hitch-hikes to high frequency along with resistance. Alternatively, increased growth may be realised if the elevated mutation rate allowed the accumulation of beneficial mutations, or increased the clonal interference among resistance mutations. We fit a Bayesian multivariate Student's t mixed-effects model. We treated growth (measured by AUC) in the presence (20 mg/l) and absence (0 mg/) as a bivariate response variable, and initial mutator frequency as the sole population-level factor ('low', 'intermediate', 'high', with the growth of double resistant strains derived in the BW25113 wild-type background as the reference level). For the same reasons as in Model M2, we used a bivariate model to account for correlations arising from measuring the AUC of each strain multiple times in different environments. Also as in Model M2, we used a Student's t model to be robust to 'outliers' in the data. AUC at each concentration was measured over several 'replicate' experiments, which was treated as a varying factor common to both response variables.

Establishing priors for the bivariate linear model

The data collection for this analysis is the same as for the data analysed in Model M2, hence we use the same priors (Extended Data Figure 3.11).

Fitting the model and hypothesis testing

As previously, model fitting was performed using `brm()`. To use a Student's t model, 'family' was set to 'student' (with the default link 'identity'). To permit hypothesis testing on point estimates, samples from specified priors were drawn by setting `sample_prior="yes"`. To ensure convergence, we set `max_treedepth` = 15 and `adapt_delta` = 0.99. Default values were used for other settings. As before, we used 95% C.I.s for hypotheses. Estimated coefficients are given in Table 3.9, reported as treatment contrasts (i.e. relative to double resistance in the BW25113 strain). Growth measured by AUC in 0 mg/l and 20 mg/l of the combination antibiotic treatment was positively correlated [$r = 0.68$, 95% C.I.: $(0.56, 0.79)$]. The model incorporating initial mutator frequency was a worse fit than an intercept-only model (WAIC 564.6 ± 23.7 SE vs. 540.0 ± 25.2 SE), suggesting initial mutator frequency did not have a large influence on AUC of double resistant strains.

Table 3.9: Estimated coefficients for the population-level effect of mutators on growth (measured by AUC) of multi-resistant clones in 0 mg/l and 20 mg/l of the combination treatment, from the fit of a Bayesian bivariate regression model. Treatment contrasts are shown (* denotes 95% credible intervals excluding zero).

Concentration	Coefficient	Estimate	Error	95% credible interval	
AUC in 0 mg/l	intercept	8.77	0.47	(7.75, 9.65)	*
	low	-1.93	0.59	(-2.91, -0.47)	*
	intermediate	-0.65	0.58	(-1.59, 0.77)	
	high	-0.67	0.57	(-1.58, 0.74)	
AUC in 20 mg/l	intercept	7.37	0.54	(6.31, 8.51)	*
	low	-0.84	0.64	(-1.97, 0.62)	
	intermediate	0.17	0.64	(-1.02, 1.52)	
	high	-0.06	0.61	(-1.11, 1.36)	

3.9.4 Model M4: Detection of resistance arising during simulation

Defining the model

The model is defined as it is for Model M1, except without the random effects of position within the plate.

Establishing priors for the model

The same priors were used as for Model M1.

Fitting the model and comparing with Model M1

To determine concordance between simulations and experimental results, we fit a Bayesian categorical model to the simulation results and compared the estimated coefficients. We used the same approach and priors as in Model M1, with the exception of the absence of varying factors in the model fit to the simulations. As for Model M1, the full model did not provide a better fit than the main effects model (WAIC 1457.9 ± 50.0 SE vs. 1443.9 ± 50.7 SE). Estimated coefficient obtained from fitting the main-effects model to the output from the simulations are given in Table 3.10. Estimated coefficients from the simulation closely matched those from the experiment (Extended Data Figure 3.12).

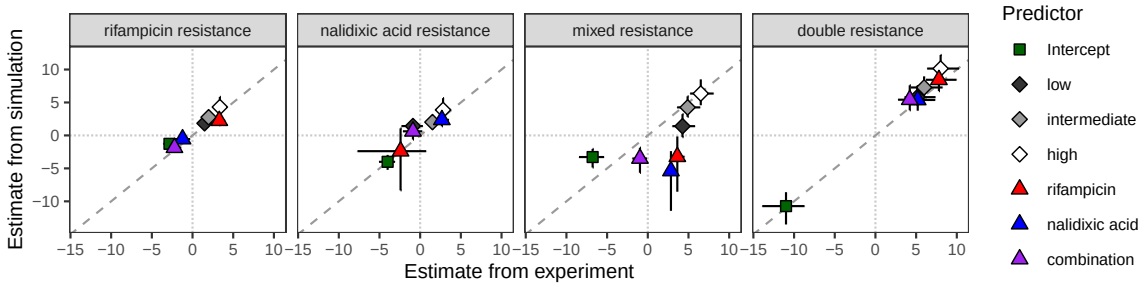

Extended Data Figure 3.12: Comparison of coefficients from Bayesian categorical models fitted to simulation and experimental data. Dashed diagonal line indicates 1:1 line; points falling on this line indicate coefficients are equal in both simulation and experiment.

Table 3.10: Effects of initial mutator frequency and antibiotic treatment on resistance type observed at the end of the simulations. Coefficients come from fitting a Bayesian categorical regression model to the simulations (see Model M4). Treatment contrasts on the logit scale are shown. (* denotes 95% credible intervals excluding zero).

Resistance type	Coefficient	Estimate	95% credible interval	
rifampicin resistance	intercept	-1.27	(-1.78, -0.79)	*
	low	1.84	(1.30, 2.42)	*
	intermediate	2.76	(2.10, 3.46)	*
	high	4.30	(3.10, 5.85)	*
	rifampicin	2.24	(1.55, 2.97)	*
	nalidixic acid	-0.55	(-1.14, 0.02)	
	combination	-1.86	(-2.58, -1.19)	*
nalidixic acid resistance	intercept	-4.00	(-5.22, -2.95)	*
	low	1.42	(0.60, 2.27)	*
	intermediate	2.02	(1.05, 2.99)	*
	high	3.87	(2.35, 5.65)	*
	rifampicin	-2.39	(-8.33, 1.07)	
	nalidixic acid	2.37	(1.39, 3.51)	*
	combination	0.63	(-0.62, 1.88)	
mixed resistance	intercept	-3.28	(-4.86, -2.05)	*
	low	1.40	(-0.26, 3.23)	
	intermediate	4.26	(2.81, 5.94)	*
	high	6.36	(4.58, 8.51)	*
	rifampicin	-3.23	(-8 .54, -0.16)	*
	nalidixic acid	-5.39	(-11.44, -2.38)	*
	combination	-3.50	(-5.66, -1.86)	*
double resistance	intercept	-10.72	(-13.51, -8.61)	*
	low	5.81	(4.55, 7.45)	*
	intermediate	7.28	(5.94, 8.97)	*
	high	10.15	(8.42, 12.21)	*
	rifampicin	8.44	(6.73, 10.75)	*
	nalidixic acid	5.38	(3.75, 7.61)	*

	combination	5.42	(3.81, 7.61) *

Bibliography

[1] V. T. Devita, R. C. Young, and G. P. Canellos, "Combination versus single agent chemotherapy: a review of the basis for selection of drug treatment of cancer", Cancer **35**, 98–110 (1975).

[2] S. Bonhoeffer, M. Lipsitch, and B. R. Levin, "Evaluating treatment protocols to prevent antibiotic resistance", Proceedings of the National Academy of Sciences **94**, 12106–12111 (1997).

[3] D. M. Livermore, "Minimising antibiotic resistance", The Lancet infectious diseases **5**, 450–459 (2005).

[4] M. Baym, L. K. Stone, and R. Kishony, "Multidrug evolutionary strategies to reverse antibiotic resistance", Science **351**, aad3292 (2016).

[5] J. S. Lopez, and U. Banerji, "Combine and conquer: challenges for targeted therapy combinations in early phase trials", Nature Reviews Clinical Oncology (2016).

[6] A. T. C. Collaboration, "Survival of HIV-positive patients starting antiretroviral therapy between 1996 and 2013: a collaborative analysis of cohort studies", The Lancet HIV (2017).

[7] R. B. Mokhtari, T. S. Homayouni, N. Baluch, E. Morgatskaya, S. Kumar, B. Das, and H. Yeger, "Combination therapy in combating cancer", Oncotarget **8**, 38022–38043 (2017).

[8] C. A. Kerantzas, and W. R. Jacobs, "Origins of combination therapy for tuberculosis: lessons for future antimicrobial development and application", MBio **8**, e01586–16 (2017).

[9] M. W. Pletz, S. Hagel, and C. Forstner, "Who benefits from antimicrobial combination therapy?", The Lancet Infectious Diseases **17**, 677–678 (2017).

[10] M. Tyers, and G. D. Wright, "Drug combinations: A strategy to extend the life of antibiotics in the 21st century", Nature Reviews Microbiology, 1 (2019).

[11] A. R. Coates, Y. Hu, J. Holt, and P. Yey, "Antibiotic combination therapy against resistant bacterial infections: synergy, rejuvenation and resistance reduction", Expert Review of Anti-infective Therapy (2020).

[12] M. Hegreness, N. Shoresh, D. Damian, D. Hartl, and R. Kishony, "Accelerated evolution of resistance in multidrug environments", Proceedings of the National Academy of Sciences **105**, 13977–13981 (2008).

[13] J. P. Torella, R. Chait, and R. Kishony, "Optimal drug synergy in antimicrobial treatments", PLoS computational biology **6**, e1000796 (2010).

[14] R. Peña-Miller, D. Läehnemann, G. Jansen, A. Fuentes-Hernandez, P. Rosenstiel, H. Schulenburg, and R. Beardmore, "When the most potent combination of antibiotics selects for the greatest bacterial load: the smile-frown transition", PLoS biology **11**, e1001540 (2013).

[15] C. Barbosa, R. Beardmore, H. Schulenburg, and G. Jansen, "Antibiotic combination efficacy (ACE) networks for a *Pseudomonas aeruginosa* model", PLoS biology **16**, e2004356 (2018).

[16] B. Tepekule, H. Uecker, I. Derungs, A. Frenoy, and S. Bonhoeffer, "Modeling antibiotic treatment in hospitals: A systematic approach shows benefits of combination therapy over cycling, mixing, and mono-drug therapies", PLoS Computational Biology **13**, e1005745 (2017).

[17] A. Ahmad, C. Zachariasen, L. E. Christiansen, K. Græsbøll, N. Toft, L. Matthews, J. E. Olsen, and S. S. Nielsen, "Multistrain models predict sequential multidrug treatment strategies to result in less antimicrobial resistance than combination treatment", BMC Microbiology **16**, 118 (2016).

[18] P. D. Tamma, S. E. Cosgrove, and L. L. Maragakis, "Combination therapy for treatment of infections with gram-negative bacteria", Clinical microbiology reviews **25**, 450–470 (2012).

[19] R. Krašovec, H. Richards, D. R. Gifford, C. Hatcher, K. J. Faulkner, R. V. Belavkin, A. Channon, E. Aston, A. J. McBain, and C. G. Knight, "Spontaneous mutation rate is a plastic trait associated with population density across domains of life", PLoS Biology **15**, e2002731 (2017).

[20] J. Maynard Smith, "Natural selection and the concept of a protein space", Nature **225**, 563–564 (1970).

[21] H. Nikaido, "Multidrug Resistance in Bacteria", Annu. Rev. Biochem. **78**, 119 (2009).

[22] R. S. Ramiro, P. Durão, C. Bank, and I. Gordo, "Low mutational load and high mutation rate variation in gut commensal bacteria", PLoS Biology **18**, e3000617 (2020).

[23] A. Oliver, R. Cantón, P. Campo, F. Baquero, and J. Blázquez, "High frequency of hypermutable *Pseudomonas aeruginosa* in cystic fibrosis lung infection", Science **288**, 1251–1253 (2000).

[24] M. D. Maciá, D. Blanquer, B. Togores, J. Sauleda, J. L. Pérez, and A. Oliver, "Hypermutation is a key factor in development of multiple-antimicrobial resistance in *Pseudomonas aeruginosa* strains causing chronic lung infections", Antimicrobial Agents and Chemotherapy **49**, 3382–3386 (2005).

[25] A. Couce, N. Alonso-Rodriguez, C. Costas, A. Oliver, and J. Blázquez, "Intrapopulation variability in mutator prevalence among urinary tract infection isolates of *Escherichia coli*", Clinical Microbiology and Infection **22**, 566–e1 (2016).

[26] I. Chopra, A. J. O'Neill, and K. Miller, "The role of mutators in the emergence of antibiotic-resistant bacteria", Drug Resistance Updates **6**, 137–145 (2003).

[27] M. Marinus, "DNA mismatch repair", EcoSal Plus **5** (2012).

[28] M. E. Levison, and J. H. Levison, "Pharmacokinetics and pharmacodynamics of antibacterial agents", Infectious Disease Clinics of North America **23**, 791–815 (2009).

[29] A. C. Palmer, and R. Kishony, "Understanding, predicting and manipulating the genotypic evolution of antibiotic resistance", Nature Reviews Genetics **14**, 243 (2013).

[30] T. Felton, J. Goodwin, L. O'Connor, A. Sharp, L. Gregson, J. Livermore, S. Howard, M. Neely, and W. Hope, "Impact of bolus dosing versus continuous infusion of piperacillin and tazobactam on the development of antimicrobial resistance in *Pseudomonas aeruginosa*", Antimicrobial Agents and Chemotherapy **57**, 5811–5819 (2013).

[31] A. Feder, K. Harper, and P. S. Pennings, "Challenging conventional wisdom on the evolution of resistance to multi-drug HIV treatment: Lessons from data and modeling", bioRxiv, 807560 (2019).

[32] E. Berríos-Caro, D. R. Gifford, and T. Galla, "Competition delays multi-drug resistance evolution during combination therapy", bioRxiv, 2020.05.27.119537 (2020).

[33] K. Miller, A. J. O'Neill, and I. Chopra, "*Escherichia coli* mutators present an enhanced risk for emergence of antibiotic resistance during urinary tract infections", Antimicrobial Agents and Chemotherapy **48**, 23–29 (2004).

[34] M.-R. Baquero, A. I. Nilsson, M. del Carmen Turrientes, D. Sandvang, J. C. Galán, J. L. Martínez, N. Frimodt-Møller, F. Baquero, and D. I. Andersson, "Polymorphic mutation frequencies in *Escherichia coli*: emergence of weak mutators in clinical isolates", Journal of Bacteriology **186**, 5538–5542 (2004).

[35] F. Labat, O. Pradillon, L. Garry, M. Peuchmaur, B. Fantin, and E. Denamur, "Mutator phenotype confers advantage in *Escherichia coli* chronic urinary tract infection pathogenesis", FEMS Immunology & Medical Microbiology **44**, 317–321 (2005).

[36] P. Komp Lindgren, P. G. Higgins, H. Seifert, and O. Cars, "Prevalence of hypermutators among clinical *Acinetobacter baumannii* isolates", Journal of Antimicrobial Chemotherapy **71**, 661–665 (2015).

[37] C. B. Landersdorfer, V. E. Rees, R. Yadav, K. E. Rogers, T. H. Kim, P. J. Bergen, S.-E. Cheah, J. D. Boyce, A. Y. Peleg, A. Oliver, N. R. L. Shin, Beom Soo, and B. J. B, "Optimization of a meropenem-tobramycin combination dosage regimen against hypermutable and nonhypermutable *Pseudomonas aeruginosa* via mechanism-based modeling and the hollow-fiber infection model", Antimicrobial Agents and Chemotherapy **62**, e02055–17 (2018).

[38] V. E. Rees, R. Yadav, K. E. Rogers, J. B. Bulitta, V. Wirth, A. Oliver, J. D. Boyce, A. Y. Peleg, R. L. Nation, and C. B. Landersdorfer, "Meropenem combined with ciprofloxacin combats hypermutable *Pseudomonas aeruginosa* from respiratory infections of cystic fibrosis patients", Antimicrobial Agents and Chemotherapy **62**, e01150–18 (2018).

[39] R. J. Söderberg, and O. G. Berg, "Kick-starting the ratchet: the fate of mutators in an asexual population", Genetics **187**, 1129–1137 (2011).

[40] B. H. Good, and M. M. Desai, "Evolution of Mutation Rates in Rapidly Adapting Asexual Populations", Genetics **204**, 1249–1266 (2016).

[41] D. Gifford, V. Furió, A. Papkou, T. Vogwill, A. Oliver, and R. MacLean, "Identifying and exploiting genes that potentiate the evolution of antibiotic resistance", Nature Ecology and Evolution **99**, 88 (2018).

[42] J. Foo, and F. Michor, "Evolution of resistance to targeted anti-cancer therapies during continuous and pulsed administration strategies", PLoS Computational Biology **5**, e1000557 (2009).

[43] M. G. De Jong, and K. B. Wood, "Tuning spatial profiles of selection pressure to modulate the evolution of drug resistance", Physical Review Letters **120**, 238102 (2018).

[44] H. K. Alexander, and R. C. MacLean, "Stochastic bacterial population dynamics restrict the establishment of antibiotic resistance from single cells", Proc. Natl. Acad. Sci. U.S.A., 201919672 (2020).

[45] R. Krašovec, H. Richards, D. Gifford, R. Belavkin, A. Channon, E. Aston, A. McBain, and C. Knight, "Opposing effects of final population density and stress on *Escherichia coli* mutation rate", ISME Journal (2018).

[46] M. G. Reynolds, "Compensatory evolution in rifampin-resistant *Escherichia coli*", Genetics **156**, 1471–1481 (2000).

[47] R. Sender, S. Fuchs, and R. Milo, "Revised estimates for the number of human and bacteria cells in the body", PLoS biology **14**, e1002533 (2016).

[48] O. Opota, A. Croxatto, G. Prod'hom, and G. Greub, "Blood culture-based diagnosis of bacteraemia: state of the art", Clinical Microbiology and Infection **21**, 313–322 (2015).

[49] R. Orenstein, and E. S. Wong, "Urinary tract infections in adults", American family physician **59**, 1225 (1999).

[50] E. Bingen, N. Lambert-Zechovsky, P. Mariani-Kurkdjian, C. Doit, Y. Aujard, F. Fournerie, and H. Mathieu, "Bacterial counts in cerebrospinal fluid of children with meningitis", European Journal of Clinical Microbiology and Infectious Diseases **9**, 278–281 (1990).

[51] A. Frenoy, and S. Bonhoeffer, "Death and population dynamics affect mutation rate estimates and evolvability under stress in bacteria", PLOS Biology **16**, e2005056 (2018).

[52] T. Vogwill, R. L. Phillips, D. R. Gifford, and R. C. MacLean, "Divergent evolution peaks under intermediate population bottlenecks during bacterial experimental evolution", Proceedings of the Royal Society B: Biological Sciences **283**, 20160749 (2016).

[53] G. G. Perron, A. R. Hall, and A. Buckling, "Hypermutability and compensatory adaptation in antibiotic-resistant bacteria", The American Naturalist **176**, 303–311 (2010).

[54] H. Jordt, T. Stalder, O. Kosterlitz, J. M. Ponciano, E. M. Top, and B. Kerr, "Coevolution of host-plasmid pairs facilitates the emergence of novel multidrug resistance", Nature Ecology and Evolution **4**, 863–869 (2020).

[55] B. H. Good, M. J. McDonald, J. E. Barrick, R. E. Lenski, and M. M. Desai, "The dynamics of molecular evolution over 60,000 generations", Nature **551**, 45 (2017).

[56] P. E. Sax, C. Tierney, A. C. Collier, E. S. Daar, K. Mollan, C. Budhathoki, C. Godfrey, N. C. Jahed, L. Myers, D. Katzenstein, et al., "Abacavir/lamivudine versus tenofovir DF/emtricitabine as part of combination regimens for initial treatment of HIV: final results", Journal of Infectious Diseases **204**, 1191–1201 (2011).

[57] J. M. Cuevas, R. Geller, R. Garijo, J. López-Aldeguer, and R. Sanjuán, "Extremely high mutation rate of HIV-1 *in vivo*", PLoS biology **13**, e1002251 (2015).

[58] C. D. Bayliss, J. C. Hoe, K. Makepeace, P. Martin, D. W. Hood, and E. R. Moxon, "*Neisseria meningitidis* escape from the bactericidal activity of a monoclonal antibody is mediated by phase variation of *lgtG* and enhanced by a mutator phenotype", Infection and immunity **76**, 5038–5048 (2008).

[59] C. Pal, M. D. Maciá, A. Oliver, I. Schachar, and A. Buckling, "Coevolution with viruses drives the evolution of bacterial mutation rates", Nature **450**, 1079 (2007).

[60] J. J. Bull, and C. O. Wilke, "Lethal mutagenesis of bacteria", Genetics **180**, 1061–1070 (2008).

[61] G. Martin, and S. Gandon, "Lethal mutagenesis and evolutionary epidemiology", Philosophical Transactions of the Royal Society B: Biological Sciences **365**, 1953–1963 (2010).

[62] S. Matuszewski, L. Ormond, C. Bank, and J. D. Jensen, "Two sides of the same coin: A population genetics perspective on lethal mutagenesis and mutational meltdown", Virus evolution **3**, vex004 (2017).

[63] E. Aston, A. Channon, R. V. Belavkin, D. R. Gifford, R. Krašovec, and C. G. Knight, "Critical Mutation Rate has an Exponential Dependence on Population Size for Eukaryotic-length Genomes with Crossover", Sci. Rep. **7**, 1–12 (2017).

[64] R. P. Maharjan, B. Liu, Y. Li, P. R. Reeves, L. Wang, and T. Ferenci, "Mutation accumulation and fitness in mutator subpopulations of *Escherichia coli*", Biology letters **9**, 20120961 (2013).

[65] A. Couce, L. V. Caudwell, C. Feinauer, T. Hindré, J.-P. Feugeas, M. Weigt, R. E. Lenski, D. Schneider, and O. Tenaillon, "Mutator genomes decay, despite sustained fitness gains,

in a long-term experiment with bacteria", Proceedings of the National Academy of Sciences **114**, E9026–E9035 (2017).

[66] K. Heilbron, M. Toll-Riera, M. Kojadinovic, and R. C. MacLean, "Fitness is strongly influenced by rare mutations of large effect in a microbial mutation accumulation experiment", Genetics **197**, 981–990 (2014).

[67] I. El Meouche, and M. J. Dunlop, "Heterogeneity in efflux pump expression predisposes antibiotic-resistant cells to mutation", Science **362**, 686–690 (2018).

[68] J. F. Petrosino, R. S. Galhardo, L. D. Morales, and S. M. Rosenberg, "Stress-induced β-lactam antibiotic resistance mutation and sequences of stationary-phase mutations in the *Escherichia coli* chromosome", Journal of Bacteriology **191**, 5881–5889 (2009).

[69] M. A. Kohanski, M. A. DePristo, and J. J. Collins, "Sublethal antibiotic treatment leads to multidrug resistance via radical-induced mutagenesis", Molecular Cell **37**, 311–320 (2010).

[70] S. H. Gillespie, S. Basu, A. L. Dickens, D. M. O'sullivan, and T. D. McHugh, "Effect of subinhibitory concentrations of ciprofloxacin on *Mycobacterium fortuitum* mutation rates", Journal of Antimicrobial Chemotherapy **56**, 344–348 (2005).

[71] S. K. Henderson-Begg, D. M. Livermore, and L. M. Hall, "Effect of subinhibitory concentrations of antibiotics on mutation frequency in *Streptococcus pneumoniae*", Journal of Antimicrobial Chemotherapy **57**, 849–854 (2006).

[72] T. D. Thi, E. López, A. Rodríguez-Rojas, J. Rodríguez-Beltrán, A. Couce, J. R. Guelfo, A. Castañeda-García, and J. Blázquez, "Effect of *recA* inactivation on mutagenesis of *Escherichia coli* exposed to sublethal concentrations of antimicrobials", Journal of Antimicrobial Chemotherapy **66**, 531–538 (2011).

[73] M. McGrath, N. Gey van Pittius, P. Van Helden, R. Warren, and D. Warner, "Mutation rate and the emergence of drug resistance in *Mycobacterium tuberculosis*", Journal of Antimicrobial Chemotherapy **69**, 292–302 (2013).

[74] H. K. Alexander, S. I. Mayer, and S. Bonhoeffer, "Population heterogeneity in mutation rate increases the frequency of higher-order mutants and reduces long-term mutational load", Molecular Biology and Evolution **34**, 419–436 (2017).

[75] M. N. Ragheb, M. K. Thomason, C. Hsu, P. Nugent, J. Gage, A. N. Samadpour, A. Kariisa, C. N. Merrikh, S. I. Miller, D. R. Sherman, and H. Merrikh, "Inhibiting the Evolution of Antibiotic Resistance", Mol. Cell **73**, 157–165.e5 (2019).

[76] H. Long, S. F. Miller, C. Strauss, C. Zhao, L. Cheng, Z. Ye, K. Griffin, R. Te, H. Lee, C.-C. Chen, and M. Lynch, "Antibiotic treatment enhances the genome-wide mutation rate of target cells", Proc. Natl. Acad. Sci. U.S.A. **113**, E2498–E2505 (2016).

[77] T. K. Lu, and J. J. Collins, "Engineered bacteriophage targeting gene networks as adjuvants for antibiotic therapy", Proc. Natl. Acad. Sci. U.S.A. **106**, 4629–4634 (2009).

[78] C. Y. Mo, S. A. Manning, M. Roggiani, M. J. Culyba, A. N. Samuels, P. D. Sniegowski, M. Goulian, and R. M. Kohli, "Systematically Altering Bacterial SOS Activity under Stress Reveals Therapeutic Strategies for Potentiating Antibiotics", mSphere **1** (2016).

[79] J. A. G. M. de Visser, and D. E. Rozen, "Clonal interference and the periodic selection of new beneficial mutations in *Escherichia coli*", Genetics **172**, 2093–2100 (2006).

[80] K. B. Wood, "Pairwise interactions and the battle against combinatorics in multidrug therapies", Proceedings of the National Academy of Sciences **113**, 10231–10233 (2016).

[81] K. A. Datsenko, and B. L. Wanner, "One-step inactivation of chromosomal genes in *Escherichia coli* K-12 using PCR products", Proceedings of the National Academy of Sciences **97**, 6640–6645 (2000).

[82] F. Grenier, D. Matteau, V. Baby, and S. Rodrigue, "Complete genome sequence of *Escherichia coli* BW25113", Genome Announcements **2**, e01038–14 (2014).

[83] J. Åhman, E. Matuschek, and G. Kahlmeter, "EUCAST evaluation of 21 brands of Mueller-Hinton dehydrated media for disk diffusion testing", Clinical Microbiology and Infection **S1198-743X(20)30043-4** (2020).

[84] B. P. Goldstein, "Resistance to rifampicin: a review", The Journal of antibiotics **67**, 625–630 (2014).

[85] L. S. Redgrave, S. B. Sutton, M. A. Webber, and L. J. Piddock, "Fluoroquinolone resistance: mechanisms, impact on bacteria, and role in evolutionary success", Trends in Microbiology **22**, 438–445 (2014).

[86] A. L. Manson, K. A. Cohen, T. Abeel, C. A. Desjardins, D. T. Armstrong, C. E. Barry III, J. Brand, P. Jureen, L. Malinga, D. Nordenberg, et al., "Genomic analysis of globally diverse *Mycobacterium tuberculosis* strains provides insights into the emergence and spread of multidrug resistance", Nature Genetics **49**, 395–402 (2017).

[87] G. Perron, A. Gonzalez, and A. Buckling, "The rate of environmental change drives adaptation to an antibiotic sink", Journal of Evolutionary Biology **21**, 1724–1731 (2008).

[88] H. A. Lindsey, J. Gallie, S. Taylor, and B. Kerr, "Evolutionary rescue from extinction is contingent on a lower rate of environmental change", Nature **494**, 463–467 (2013).

[89] J. Ramsayer, O. Kaltz, and M. E. Hochberg, "Evolutionary rescue in populations of *Pseudomonas fluorescens* across an antibiotic gradient", Evolutionary Applications **6**, 608–616 (2013).

[90] N. Harmand, R. Gallet, R. Jabbour-Zahab, G. Martin, and T. Lenormand, "Fisher's geometrical model and the mutational patterns of antibiotic resistance across dose gradients", Evolution **71**, 23–37 (2016).

[91] P.-C. Bürkner, "brms: An R Package for Bayesian Multilevel Models Using Stan", Journal of Statistical Software **80**, 1–28 (2017).

[92] P.-C. Bürkner, "Advanced Bayesian Multilevel Modeling with the R Package brms", The R Journal **10**, 395–411 (2018).

[93] R. C. Team, *R: A Language and Environment for Statistical Computing*, R Foundation for Statistical Computing (Vienna, Austria, 2019).

[94] S. E. Luria, and M. Delbrück, "Mutations of bacteria from virus sensitivity to virus resistance", Genetics **28**, 491 (1943).

[95] R. Krašovec, H. Richards, G. Gomez, D. Gifford, M. A, and C. Knight, "Measuring Microbial Mutation Rates with the Fluctuation Assay", Journal of Visualized Experiments **153**, e60406 (2019).

[96] A. Oliver, B. R. Levin, C. Juan, F. Baquero, and J. Blázquez, "Hypermutation and the preexistence of antibiotic-resistant *Pseudomonas aeruginosa* mutants: implications for susceptibility testing and treatment of chronic infections", Antimicrobial Agents and Chemotherapy **48**, 4226–4233 (2004).

[97] K. Sprouffske, and A. Wagner, "Growthcurver: an R package for obtaining interpretable metrics from microbial growth curves", BMC Bioinformatics **17**, 172 (2016).

[98] A. Mazoyer, R. Drouilhet, S. Despréaux, and B. Ycart, "flan: An R Package for Inference on Mutation Models", The R Journal **9**, 334–351 (2017).

[99] P. Leslie, and J. Gower, "The properties of a stochastic model for two competing species", Biometrika **45**, 316–330 (1958).

[100] V. Volterra, *Fluctuations in the abundance of a species considered mathematically*, 1926.

[101] A. J. Lotka, "The growth of mixed populations: two species competing for a common food supply", Journal of the Washington Academy of Sciences **22**, 461–469 (1932).

[102] D. T. Gillespie, "A general method for numerically simulating the stochastic time evolution of coupled chemical reactions", Journal of Computational Physics **22**, 403–434 (1976).

[103] D. T. Gillespie, "Exact stochastic simulation of coupled chemical reactions", Journal of Physical Chemistry **81**, 2340–2361 (1977).

[104] D. T. Gillespie, "Approximate accelerated stochastic simulation of chemically reacting systems", The Journal of Chemical Physics **115**, 1716–1733 (2001).

[105] A. Cavallero, C. Eftimiadi, L. Radin, and G. C. Schito, "Suppression of tricarboxylic acid cycle in *Escherichia coli* exposed to sub-MICs of aminoglycosides", Antimicrobial Agents and Chemotherapy **34**, 295–301 (1990).

[106] C. H. Wang, and A. L. Koch, "Constancy of growth on simple and complex media.", Journal of Bacteriology **136**, 969 (1978).

[107] G. Sezonov, D. Joseleau-Petit, and R. D'Ari, "*Escherichia coli* Physiology in Luria-Bertani Broth", Journal of Bacteriology **189**, 8746–8749 (2007).

[108] P. L. Irwin, L.-H. T. Nguyen, G. C. Paoli, and C.-Y. Chen, "Evidence for a bimodal distribution of *Escherichia coli* doubling times below a threshold initial cell concentration", BMC Microbiol. **10**, 207 (2010).

[109] C. B. Becg, and R. Gray, "Calculation of polychotomous logistic regression parameters using individualized regressions", Biometrika **71**, 11–18 (1984).

[110] X. A. Harrison, "A comparison of observation-level random effect and Beta-Binomial models for modelling overdispersion in Binomial data in ecology & evolution", PeerJ **3** (2015).

[111] D. Hedeker, "A mixed-effects multinomial logistic regression model", Statistics in medicine **22**, 1433–1446 (2003).

[112] C. J. J. Van Zyl, "Frequentist and Bayesian inference: A conceptual primer", New Ideas in Psychology **51**, 44–49 (2018).

[113] A. Vehtari, A. Gelman, and J. Gabry, "Practical Bayesian model evaluation using leave-one-out cross-validation and WAIC", Statistics and Computing **27**, 1413–1432 (2017).

[114] E.-J. Wagenmakers, T. Lodewyckx, H. Kuriyal, and R. Grasman, "Bayesian hypothesis testing for psychologists: A tutorial on the Savage–Dickey method", Cognitive Psychology **60**, 158–189 (2010).

[115] N. P. Lemoine, "Moving beyond noninformative priors: why and how to choose weakly informative priors in Bayesian analyses", Oikos **128**, 912–928 (2019).

[116] W. N. Venables, and B. D. Ripley, *Modern Applied Statistics with S*, Fourth, ISBN 0-387-95457-0 (Springer, New York, 2002).

[117] D. Feng, R. Baumgartner, and V. Svetnik, "A robust Bayesian estimate of the concordance correlation coefficient", Journal of biopharmaceutical statistics **25**, 490–507 (2015).

Chapter 4

Competition delays multi-drug resistance evolution during combination therapy

Preface

This chapter constitutes a manuscript[1] published by Journal of Theoretical Biology. This work is co-authored with Tobias Galla[2,3] and Danna R. Gifford[4].

E.B-C. conceived the initial conception of the study, performed the mathematical and numerical analysis of all the results presented, produced of all figures, and wrote the manuscript. T.G and D.R.G. contributed by designing the study, providing discussions guiding the work, analysis of results, and writing the manuscript.

[1] E. Berríos-Caro, D. R. Gifford, and T. Galla, "Competition delays multi-drug resistance evolution during combination therapy", Journal of Theoretical Biology 509, 110524 (2021). https://doi.org/10.1016/j.jtbi.2020.110524

[2] Theoretical Physics, Department of Physics and Astronomy, School of Natural Sciences, Faculty of Science and Engineering, The University of Manchester, Manchester M13 9PL, United Kingdom.

[3] Instituto de Física Interdisciplinar y Sistemas Complejos, IFISC (CSIC-UIB), Campus Universitat Illes Balears, E-07122 Palma de Mallorca, Spain.

[4] Division of Evolution and Genomic Sciences, School of Biological Sciences, Faculty of Biology, Medicine and Health, The University of Manchester, Manchester M13 9PT, United Kingdom.

Abstract

Combination therapies have shown remarkable success in preventing the evolution of resistance to multiple drugs, including HIV, tuberculosis, and cancer. Nevertheless, the rise in drug resistance still remains an important challenge. The capability to accurately predict the emergence of resistance, either to one or multiple drugs, may help to improve treatment options. Existing theoretical approaches often focus on exponential growth laws, which may not be realistic when scarce resources and competition limit growth. In this work, we study the emergence of single and double drug resistance in a model of combination therapy of two drugs. The model describes a sensitive strain, two types of single-resistant strains, and a double-resistant strain. We compare the probability that resistance emerges for three growth laws: exponential growth, logistic growth without competition between strains, and logistic growth with competition between strains. Using mathematical estimates and numerical simulations, we show that between-strain competition only affects the emergence of single resistance when resources are scarce. In contrast, the probability of double resistance is affected by between-strain competition over a wider space of resource availability. This indicates that competition between different resistant strains may be pertinent to identifying strategies for suppressing drug resistance, and that exponential models may overestimate the emergence of resistance to multiple drugs. A by-product of our work is an efficient strategy to evaluate probabilities of single and double resistance in models with multiple sequential mutations. This may be useful for a range of other problems in which the probability of resistance is of interest.

4.1 Introduction

The rise of drug resistance has triggered studies into different treatment regimes, aimed to prevent or delay the emergence of resistance. Combination therapies have attracted special attention, due to their effectiveness against viral, bacterial, and fungal infections, as well in the context of cancer (see e.g. [1–4]). Combination therapies have also shown success in managing HIV [5], malaria [6], and tuberculosis [7].

The ability of combination therapies to counteract antibiotic resistance relies on the idea that simultaneous acquisition of resistance to multiple antibiotics is extremely rare. For independent resistance mutations, this occurs with a rate equal to the product of mutation rates for resistance to each drug. For bacteria these are in the range of approximately 10^{-6} to 10^{-10} per genome replication (see [8]). Multi-resistance is therefore more likely to emerge via sequentially acquisition of resistance to each drug [2]. This is what combination therapies aim to prevent. These therapies can have limitations, however, for example due to differences between drugs in how quickly they are absorbed (i.e. pharmacokinetics, see [9, 10]).

Having the ability to predict the emergence of single or double resistance from mathematical or computational models may help to develop strategies to reduce resistance. Since mutations occur as random events, one of the main aims is to compute or estimate the probability that resistant cells are present in the population at a certain time after the drug treatment has started. Several theoretical approaches have been proposed, with a particular focus on drug treatments in cancer cells (see [11] for an overview). Other modelling work has focused on resistance in viral dynamics (see e.g. [12]). A systematic review of models of antimicrobial resistance can be found in [13].

Michor *et al.* [14] estimated the probability of extinction of a branching process with multiple types of mutations, for populations consisting entirely of sensitive cells at the start of the treatment. Their approach allows one to obtain the probability of successful therapy, that is, the therapy that kills both sensitive and mutant cancer strains at very long times after the treatment started. The calculations are based on the work of Iwasa and co-authors (see [15, 16]), where extinction probabilities were derived for an exponential growth model from a generating-function approach. Similarly, [17], estimated the probability of single resistance at the point in time at which the total cell population reaches a certain size. This was extended in [18] to a case with single and double resistants. This latter approach succeeded in obtaining the probability of having at least one double mutant before the total population has reached a particular size.

Later, [19] proposed a simpler approach, based on using the extinction probability of a single-type birth-death process, to estimate the emergence of single resistance in dosing schedules that affect both birth and death rates. Recently, the effects of

pharmacokinetics were studied by [20]. Related work can also be found in [21] for a process with multiple types of resistance, see also [22] for an experimental approach.

The work mentioned so far focuses largely on models with exponential growth, effectively ignoring interactions between cells. This is an approximation, but it works well for the early stages growth when non-linear interaction effects are not relevant (see e.g. [23]). In particular, this assumption is valid when the population size has not yet saturated at carrying capacity.

Although exponential growth can serve as a good approximation to study the emergence of single mutations, it may not be appropriate when multiple mutations take place in sequence. This is because the later mutations can occur during advanced phases of growth. At that stage interactions between cells may have become relevant, in particular when the population approaches its carrying capacity. In order to model such instances, one needs to go beyond simple unconstrained reproduction. The purpose of this work is to show how the choice of growth model affects predictions for the emergence of single and double resistance under combination therapy. We describe the evolution of resistance by means of three stochastic models: (i) A model with no interactions between cells, leading to exponential growth if growth rates are constant; (ii) A model in which each strain follows a logistic growth law, but where there are no interactions between the different strains; (iii) Logistic growth with competition between strains for a common resource. For each of the models we consider constant and time-dependent per capita birth and death rates. We derive analytical estimates for the probability of single and double resistance, and compare these with numerical simulations. The formalism to predict the emergence of resistance builds upon the work in [19].

Our results show that the prediction of single resistance in the logistic growth models is different from that for the model with exponential growth when the availability of resources is low. The probability of double resistance varies across the different growth models for a larger range of parameters (such as birth rates of sensitive or resistant strains, or the initial cell number). This difference to the exponential model is more pronounced in the model with competition between different strains. The growth of source strains for double mutants may then saturate before double mutants appear. This earlier saturation can alter the optimum treatment strategy, i.e., the therapy that

maximises the time at which first double mutants emerge.

The remainder of this paper is set out as follows. In Section 4.2 we provide the mathematical background definitions for our study. In particular, we describe the different growth models and we define the model we use for the effects of treatments on these growth laws. Section 4.3 contains our main analytical results. We derive approximations for the probability of single and double resistance, and describe how we evaluate the resulting numerical expressions efficiently. In Section 4.4 we then discuss these predictions for models with constant parameters. Time-dependent dosing protocols are studied in Section 4.5. In Section 4.6 we discuss limitations of our approach, before we conclude in Section 6.6. Further details of our calculations, and additional results can be found in the Supplementary Material.

4.2 Stochastic Model

4.2.1 General definitions

We focus on a cell population subjected to combination therapy of two different types of drugs labeled $\mathcal{A}$ and $\mathcal{B}$ respectively. The drugs may act concurrently, depending on the dosing schedule. Cells can develop resistance to one drug (single resistance) or to both drugs (double resistance) via independent mutations. Double resistance is acquired sequentially, that is, after acquiring first single resistance to either of the two drugs. We will not consider the possibility of acquiring resistance to both drugs through a single mutation, as this is sufficiently rare (see e.g. [2]). Our model excludes back mutations as these are also very unlikely (see e.g. [24]).

To model how the strains acquire resistance, we consider a multi-strain continuous-time birth-death process with mutations. The birth and death rates can vary over time, making the dynamics a so-called 'non-homogeneous' process [25]. There are four different strains in the population, labeled S, A, B, and D. Strain S denotes sensitive cells, i.e., this strain does not exhibit resistance to either drug. Cells of strain A are resistant to drug $\mathcal{A}$, but not to $\mathcal{B}$, and vice versa for B. Strain D consists of double-resistant cells.

The process is described by random variables $n_S(t)$, $n_A(t)$, $n_B(t)$, and $n_D(t)$, which represent the cell numbers (or number of individuals) for each strain at time t. We write

Table 4.1: Summary of the different birth and death events in the population, along with the associated rates per individual, and the total rate for any type of event in the population. The symbol $\emptyset$ represents removal of an individual from the population (i.e., death). The change of the state vector $\mathbf{n}(t) = (n_S(t), n_A(t), n_B(t), n_D(t))$ in each of the different possible events is shown in the last column. For completeness, we include here the exact rates of each reaction (e.g., we do not approximate $1 - \mu_A$ by 1 as we do below)

Transition	Rate per individual	Total event rate	Change of $\mathbf{n}(\mathbf{t})$
$S \to S + S$	$b_S(t)(1 - \mu_A - \mu_B)$	$n_S(t)b_S(t)(1 - \mu_A - \mu_B)$	$(1, 0, 0, 0)$
$S \to \emptyset$	$d_S(t)$	$n_S(t)d_S(t)$	$(-1, 0, 0, 0)$
$S \to S + A$	$b_S(t)\mu_A$	$n_S(t)b_S(t)\mu_A$	$(0, 1, 0, 0)$
$S \to S + B$	$b_S(t)\mu_B$	$n_S(t)b_S(t)\mu_B$	$(0, 0, 1, 0)$
$A \to A + A$	$b_A(t)(1 - \mu_B)$	$n_A(t)b_A(t)(1 - \mu_B)$	$(0, 1, 0, 0)$
$A \to \emptyset$	$d_A(t)$	$n_A(t)d_A(t)$	$(0, -1, 0, 0)$
$A \to A + D$	$b_A(t)\mu_B$	$n_A(t)b_A(t)\mu_B$	$(0, 0, 0, 1)$
$B \to B + B$	$b_B(t)(1 - \mu_A)$	$n_B(t)b_B(t)(1 - \mu_A)$	$(0, 0, 1, 0)$
$B \to \emptyset$	$d_B(t)$	$n_B(t)d_B(t)$	$(0, 0, -1, 0)$
$B \to B + D$	$b_B(t)\mu_A$	$n_B(t)b_B(t)\mu_A$	$(0, 0, 0, 1)$
$D \to D + D$	$b_D(t)$	$n_D(t)b_D(t)$	$(0, 0, 0, 1)$
$D \to \emptyset$	$d_D(t)$	$n_D(t)d_D(t)$	$(0, 0, 0, -1)$

$\mathbf{n} = (n_S, n_A, n_B, n_D)$. Members of different strains proliferate and die with rates $b_i(t)$ and $d_i(t)$ respectively, where $i \in \{S, A, B, D\}$. These rates can be explicit functions of time, reflecting time-dependent treatment strategies. In birth events a single individual of the population reproduces, and in death events a single individual is removed from the population.

In birth events, one of the two types of mutations can occur. For example, an offspring of strain S will be of type A with probability μ_A, and of type B with probability μ_B. This is described by the events $S \to S + A$ or $S \to S + B$, respectively. With the remaining probability, $1 - \mu_A - \mu_B$, the offspring is of type S ($S \to S + S$). Similarly, an offspring of a parent type A is of type D with probability μ_B ($A \to A + D$), and an offspring of an individual of type B is of type D with probability μ_A ($B \to B + D$). The per capita birth rate b_i has an explicit dependence on n_i in the model with logistic growth without competition between strains. Each b_i depends on all components of $\mathbf{n}$ in the model with competition between strains. This will be detailed further below. The rates associated with the possible events are summarised in Table 4.1. The last column of the table indicates how entries of the state vector (n_S, n_A, n_B, n_D) change in the different types of events.

4.2.2 Mean growth laws and production rates of mutants

The quantities $n_S(t)$, $n_A(t)$, $n_B(t)$, and $n_D(t)$ above are random variables, and differ from realisation to realisation of the stochastic birth-death dynamics. We write $\bar{n}_i(t)$, $i \in \{S, A, B, D\}$ for the average cell numbers at time t across realisations. In the limit of infinite populations these follow the ordinary differential equations

$$\begin{aligned}
\frac{\mathrm{d}\bar{n}_S}{\mathrm{d}t}(t) &= r_S(t)\bar{n}_S(t), \\
\frac{\mathrm{d}\bar{n}_A}{\mathrm{d}t}(t) &= b_S(t)\mu_A\bar{n}_S(t) + r_A(t)\bar{n}_A(t), \\
\frac{\mathrm{d}\bar{n}_B}{\mathrm{d}t}(t) &= b_S(t)\mu_B\bar{n}_S(t) + r_B(t)\bar{n}_B(t), \\
\frac{\mathrm{d}\bar{n}_D}{\mathrm{d}t}(t) &= b_A(t)\mu_B\bar{n}_A(t) + b_B(t)\mu_A\bar{n}_B(t) + r_D(t)\bar{n}_D(t).
\end{aligned} \tag{4.1}$$

The quantities

$$\begin{aligned}
r_S(t) &\equiv b_S\,(t)\,(1-\mu_A-\mu_B) - d_S\,(t)\,, \\
r_A(t) &\equiv b_A\,(t)\,(1-\mu_B) - d_A\,(t)\,, \\
r_B(t) &\equiv b_B\,(t)\,(1-\mu_A) - d_B\,(t)\,, \\
r_D(t) &\equiv b_D(t) - d_D(t)
\end{aligned} \tag{4.2}$$

represent the net growth rates for the different strains, and result from the balance of birth and death. In the exponential growth model the $b_i(t)$ do not depend on $\bar{\mathbf{n}}$. In the logistic model without competition between strains b_i is of the form $b_i = b_i(\bar{n}_i(t), t)$ in the deterministic limit. In the model with competition between strains, finally, we have $b_i = b_i(\bar{\mathbf{n}}(t), t)$. This is obtained from factorising averages in the deterministic limit, e.g. $\overline{b_i n_i} = \overline{b_i}\,\overline{n_i}$, and using $\overline{b_i(n_i, t)} = b_i(\overline{n}_i, t)$. In Eq. (4.2) we have simply written $b_i = b_i(t)$ to keep the notation compact.

To proceed we will assume that the probabilities μ_A and μ_B are small compared to one, values below 10^{-2} can serve as a reference for real-world biological systems, see e.g. [8]. We use this to approximate the terms $1-\mu_A$, $1-\mu_B$, and $1-\mu_A-\mu_B$ in Eq. (4.2) by a value of unity. This means that we overestimate the number of non-mutant offspring by a small fraction. In related models it has been shown that this simplification does not significantly alter the outcome [19]. With this simplification, the net growth rates in Eq. (4.2) become $r_i = b_i - d_i$. The mutation rates are still present in Eqs. (4.1), in the terms associated with mutations from source strains (the first term in each of the growth laws for strains A, B and D).

The rates with which single-resistants of type A or B are produced by mutations are given by the total rates of the events $S \to S+A$ and $S \to S+B$, respectively. In the fully stochastic model these are random quantities themselves, given by $W_A(t) = b_S(t)\mu_A n_S(t)$ and $W_B(t) = b_S(t)\mu_B n_S(t)$ (see Table 4.1). Within the deterministic approximation we can replace this by

$$\overline{W}_A(t) = \bar{b}_S(t)\mu_A \overline{n}_S(t) \tag{4.3}$$

and

$$\overline{W}_B(t) = \bar{b}_S(t)\mu_B \overline{n}_S(t). \tag{4.4}$$

The production rate of double mutants, resulting from mutations arising in the offspring of either A or B, is the sum of the rates for the two events $A \to A+D$ and $B \to B+D$. Focusing on mean values again, this becomes

$$\overline{W}_D(t) = \bar{b}_A(t)\mu_B \overline{n}_A(t) + \bar{b}_B(t)\mu_A \overline{n}_B(t). \tag{4.5}$$

The deterministic approximation we have made effectively amounts to writing $\overline{W}_i(\mathbf{n}(t)) \approx W_i(\bar{\mathbf{n}}(t))$. The resulting equations for the mean cell numbers are then closed in the $\{\bar{n}_i(t)\}$, with no dependence on higher-order moments of $n_i(t)$. This approximation is only necessary in the logistic growth models defined below. For the range of parameters we explore in this paper, theoretical predictions calculated based on this simplification are typically in good agreement with numerical simulations as we will see below. We discuss limitations below in Section 4.6, and we show instances in which the predictions of the theory deviate from numerical simulations in Section 4.13 of the Supplementary Material.

4.2.3 Specific growth laws

We will explore three different scenarios. The first is exponential growth, and describes, for example, bacterial populations with unlimited resources so that growth can continue indefinitely (e.g. as it is the case in so-called 'continuous' culture systems with constant growth rates, see [26]). The second scenario entails logistic growth for each strain, but with no competition between individuals of different strains. This describes situations where resources are limited, but each strain exploits a different resource (such as may occur if a resistance mutation allows a strain to occupy a new ecological or spatial niche,

[27, 28]). The growth of any one strain is then limited by the number of individuals of that strain, but not by individuals of other strains. The third scenario is logistic growth with competition within and between strains. The different strains compete for the same resources, such that the growth of any one strain is limited by the presence of all strains. This leads to competitive Lotka-Volterra equations [29]. This model represents a more realistic scenario as often resources are limited and organisms need to compete for them. We provide detailed mathematical definitions for each of the three scenarios below.

Throughout this paper and for every type of growth law, the initial population at time $t = 0$ is assumed to consist of n_0 sensitive cells and no resistant mutants, i.e., the initial condition is $\mathbf{n}(t = 0) = (n_0, 0, 0, 0)$.

Exponential growth model (EG)

In this model, the per capita birth and death rates do not depend on the cell number of any of the strains, i.e., the $b_i(t)$ and $d_i(t)$ may be time-dependent (reflecting time-varying drug concentrations), but they are not functions of $\mathbf{n}$. The differential equations for the $\overline{n}_i$ are then linear in $\bar{n}_i$. In the special case of constant per capita growth and death rates, the equations admit analytical solutions in the form of elementary exponential functions (see Section 4.9 of the Supplementary Material). When the rates are time-dependent, the solutions can be expressed as

$$\begin{aligned}
\bar{n}_S(t) &= n_0 \exp\left[\int_0^t r_S\,(t')\,\mathrm{d}t'\right], \\
\bar{n}_A(t) &= \int_0^t \overline{W}_A\,(t') \exp\left[\int_{t'}^t r_A\,(t'')\,\mathrm{d}t''\right]\mathrm{d}t', \\
\bar{n}_B(t) &= \int_0^t \overline{W}_B\,(t') \exp\left[\int_{t'}^t r_B\,(t'')\,\mathrm{d}t''\right]\mathrm{d}t', \\
\bar{n}_D(t) &= \int_0^t \overline{W}_D\,(t') \exp\left[\int_{t'}^t r_D\,(t'')\,\mathrm{d}t''\right]\mathrm{d}t'.
\end{aligned} \tag{4.6}$$

Even though these are not strictly exponential functions in the case of time-dependent rates we will nevertheless refer to this type of growth law as 'exponential growth', and use the shorthand 'EG'.

It is straightforward to interpret the first relation in Eq. (4.6). The growth of strain S is described by a single-strain birth-death process with initial condition n_0, and the net growth rate at time t' is $r_S(t')$ (this may be negative, in which case the number

of individuals of type S reduces with time). For the resistant strains (A, B and D) the term $\overline{W}_i(t')$ represents the (mean) rate with which individuals of this strain are produced in mutation events at time t'. The exponential term then accounts for their replication (or removal) between times t' and t through a birth-death process with net reproduction rate $r_i(t'')$ at time t''. Thus, the integral over t' counts all new mutations, and the offspring the mutant produces between the time of the mutant's appearance, t', and time t.

The n_i are not bounded in this model, implying that the cell numbers can grow to arbitrary values. This situation is not realistic as resources are limited in practice; in an infection for example, cell numbers are constrained by nutrients provided by the host [30, 31]. The two scenarios that we describe next hence account for limited growth.

Logistic growth model without competition between strains (LG)

In this scenario each strain follows a logistic growth law, that is to say, the cell number grows exponentially initially, but then approaches a carrying capacity at later times. We write k_i for the carrying capacity of strain i, and assume that the net growth rate r_i for strain i depends on n_i, but not on the cell numbers of the remaining strains. This describes for example microbial communities in which the different strains consume different resources. We will use the shorthand 'LG' to refer to this setup (logistic growth). In some circumstances the LG model can also approximate situations with overlap in the resources consumed by strains A and B on the one hand, and D on the other. For example, the resources for A and B might largely be depleted by the time double mutants emerge. Effectively, there is then no competition of D with either A or B.

There are several ways of choosing birth and death rates so that the resulting mean cell number follows a logistic growth law, see e.g. [32–34]. For example, the model could be such that the birth and death rates for strain i both become zero when the cell number n_i reaches the carrying capacity k_i. In a stochastic model this would mean that the birth-death dynamics comes to a complete halt when the carrying capacity is reached. As a consequence n_i will remain fixed at $n_i = k_i$, and no fluctuations around the carrying capacity are observed.

In our model, we make less restrictive assumptions. We only require that the cell number of a strain does not grow *on average* when it exceeds its carrying capacity (i.e. $r_i = b_i - d_i = 0$ when $n_i \geq k_i$ for $i \in \{S, A, B, D\}$). We make the choice $r_i = 0$ for $n_i > k_i$ for reasons of consistency with the logistic growth model with competition between strains. This will be explained in more detail below. In order to allow fluctuations of the cell numbers around the carrying capacity, we choose both birth and death rates to be non-zero at and above the carrying capacity.

To specify the birth and death rates, we start from a given per capita death rate $d_i(t)$, and assume that the per capita birth rate $b_i(t)$ equals $d_i(t)$ when $n_i(t) \geq k_i$. This implies $r_i(t) = b_i(t) - d_i(t) = 0$ for $n_i \geq k_i$, i.e. zero net growth. The net growth for strain i is chosen to be positive when $n_i < k_i$, with net growth rate $r_i(t) = \rho_i(t)[1 - n_i(t)/k_i]$. The factor in the square bracket ensures that the net growth rate reduces to zero as n_i approaches the carrying capacity k_i. The quantity $\rho_i(t)$ is the intrinsic growth rate of strain i, describing the per capita net growth rate of the strain in the limit of small cell numbers ($n_i \ll k_i$). A similar approach was used in [33] for a stochastic version of the Gompertz model. Other related works of similar models with coupled birth and death rates can be found in [35–37]. Summarising, we use

$$b_i(t) = \begin{cases} d_i(t) + \rho_i(t)\left(1 - \dfrac{n_i(t)}{k_i}\right) & \text{if} \quad n_i(t) \leq k_i \\ d_i(t) & \text{if} \quad n_i(t) > k_i. \end{cases} \tag{4.7}$$

The specifics of the external influence of drug therapy are reflected in the choice of the functions $d_i(t)$ and $\rho_i(t)$. This is discussed further in Sections 4.5.1 and 4.5.2.

The dynamics discussed above only describes changes in n_i due to reproduction and death of strain i, but it does not cover production of strains A, B and D due to mutations. For example, strain A may have reached carrying capacity and hence there is no intrinsic net growth of this strain ($r_A = 0$), but additional individuals of type A are still produced when mutations occur in reproduction events of strain S. This is reflected by the first term on the right-hand side of the growth laws for $\bar{n}_A, \bar{n}_B$ and $\bar{n}_D$ in Eq. (4.1). For example $b_S(t)\mu_A\bar{n}_S(t)$ will generally be positive, even when strain A has reached carrying capacity. In this situation, the cell number of strain A fluctuates stochastically, with a net increase over time due to mutations from strain S. The latter occurs with a rate proportional to μ_A, which is assumed to be much smaller than one.

As a consequence mutants will be generated at a rate which is slow compared to the reproduction rate of type-A individuals in the growth phase before saturation.

Logistic growth model with competition between strains (CLG)

This model is similar to the one in the previous section. Crucially though, the growth of any one strain can now be affected by the total cell number of all strains in the population. We write $n_T(t) = n_S(t) + n_A(t) + n_B(t) + n_D(t)$ for this total cell number. The model captures scenarios in which the different strains all compete for the same resource. We make the simplifying assumption that the interaction is the same between any pair of strains, such as for example pure scramble competition. There is no direct interference, cross-feeding or similar (see e.g. [38]). We will use 'CLG' to refer to this class of growth law ('competitive logistic growth').

Similar to the previous section, we use the per capita birth rate

$$b_i(t) = \begin{cases} d_i(t) + \rho_i(t)\left(1 - \dfrac{n_T(t)}{k_i}\right) & \text{if} \quad n_T(t) \leq k_i \\ d_i(t) & \text{if} \quad n_T(t) > k_i \end{cases} \tag{4.8}$$

for strain i. The net birth-death growth rates are $r_i = b_i - d_i$ as before. The term k_i is the carrying capacity of strain i in absence of its competitors.

This model describes a scenario in which all strains have the same interaction coefficients, but potentially different carrying capacities when grown in isolation. This could arise, for example, when strains uptake a common resource (or a set of common resources) at the same rate, but where the different strains convert these resources to offspring with different efficiencies.

This choice indicates that the growth rate for strain i will reduce to zero ($r_i = 0$) when the total cell number n_T exceeds k_i. In an alternative setup with $r_i < 0$ for $n_T > k_i$ only the strain with highest coefficient k_i would survive at long times. To see this, consider the case in which $n_T > k_i$ for species i, but $n_T < k_j$ for species j. The abundance of the first species would decline, that of the second species would continue to grow. Our approach ensures that the growth laws are such that the mean abundance $\bar{n}_i$ saturates when $\bar{n}_T \geq k_i$. The birth and death rates for strain i will nevertheless remain non-zero, and hence the number of cells of type i will keep fluctuating in the individual-based model.

This model is based on the competitive Lotka-Volterra equations [29]. In their general form (see e.g. [39]), these equations include an interaction matrix that accounts for the competition of any strain with any other; the interaction coefficients can – in principle – be different for different pairs of strains. We have here focused on the simple case, with all interaction coefficients set equal to unity. In previous work [40] we have used a similar setup to model growth curves obtained experimentally in populations of bacteria.

4.2.4 Effect of drug treatment on growth rates

What effects drugs have on the different strains may depend on factors such as environmental conditions, drug interactions, type of drugs used, etc. We assume synergistic effects of both drugs on the sensitive strain, i.e., the effect of the combination of both drugs on S is stronger than the effect of any one drug in isolation. We also assume that the growth of strain S will be suppressed by a larger amount in the presence of both drugs than that of any of the single-resistant strains. Growth of the double-resistant strain is not affected by any drugs in our model.

Net growth is described by the balance of birth and death rates. Depending on the type of drugs used, net growth can be affected in different ways. Bactericidal drugs (which kill bacteria) will primarily increase death rates even though birth rates may also be affected [41]. Bacteriostatic drugs (which do not necessarily kill bacteria but slow their reproduction) will mostly affect birth rates.

In practice, however, drugs will often affect birth and death rates simultaneously. In our model drug $\mathcal{A}$ reduces the birth rates of the sensitive strain S and of the single-mutant strain B (b_S and b_B, respectively). Strain A is resistant to drug $\mathcal{A}$. Similarly, drug $\mathcal{B}$ reduces b_S and b_A, but not b_B. At the same time drug $\mathcal{A}$ will also increase the death rate of strains S and B (d_S and d_B, respectively), and drug $\mathcal{B}$ increases d_S and d_A. The birth and death rates for the double-resistant strain (b_D and d_D) are not affected by either drug.

In order to capture this scenario, we write C_A and C_B for the (dimensionless) concentrations of the two drugs, and introduce

$$f_A(t) = 1 + C_A(t), \quad f_B(t) = 1 + C_B(t). \tag{4.9}$$

We allow drug concentrations to be a function of time to account for dosing schedules and drug pharmacokinetics. The quantities $f_A(t)$ and $f_A(t)$ describe the relative factors by which birth and death rates are reduced or enhanced, respectively. We note that $f_A = 1$ in the absence of drug $\mathcal{A}$, and similarly for f_B.

To model the effects of drugs in the exponential model we start from constant birth and death rates, labelled b_i^0, d_i^0. These coefficients describe the birth and death rates in the absence of any drugs ($C_A = C_B = 0$). The reduction of growth rates and increase of death rates is then captured as follows:

$$\begin{aligned} b_S(t) &= \frac{b_S^0}{f_A(t)f_B(t)}, & d_S(t) &= d_S^0 f_A(t) f_B(t), \\ b_A(t) &= \frac{b_A^0}{f_B(t)}, & d_A(t) &= d_A^0 f_B(t), \\ b_B(t) &= \frac{b_B^0}{f_A(t)}, & d_B(t) &= d_B^0 f_A(t), \\ b_D(t) &= b_D^0, & d_D(t) &= d_D^0. \end{aligned} \tag{4.10}$$

We will refer to this as an 'exponential growth model with time-dependent drug concentrations', even though the growth process is no longer strictly exponential when C_A and C_B are functions of time.

Equation (4.10) defines the $d_i(t)$ and $b_i(t)$ for the exponential model in the presence of drugs. For the logistic models with drug treatment, we use the same death rate $d_i(t)$ as in the exponential model. We then define the intrinsic growth rates $\rho_i(t) \equiv b_i(t) - d_i(t)$, with $b_i(t)$ and $d_i(t)$ as in Eq. (4.10). In this definition of $\rho_i(t)$ we use the birth rate $b_i(t)$ for the exponential model. The birth rates $b_i(t)$ for the logistic models are then constructed from $d_i(t)$ and $\rho_i(t)$ using Eqs. (4.7) and (4.8) respectively. This allows one to compare the outcome of the different growth models. When cell numbers are much smaller than the relevant carrying capacities the suppression of growth in the logistic models does not yet set in. The three models then exhibit similar behaviour.

The relations in the first line of Eq. (4.10) represent the reduction of the birth rate for strain S in the presence of any of the two drugs; similarly the death rate for strain S is increased. For simplicity we assume that the factors by which b_S is reduced are the same as the those by which d_S is increased. A similar approach is taken for the remaining strains. In principle, more general choices are possible, but in the spirit of constructing a stylised model capturing the essential effects, we proceed on the basis of

Eq. (4.10).

The multiplicative setup in Eq. (4.10) ensures that the birth and death rates remain non-negative, even for very high drug concentrations. This is harder to ensure in an additive model, for example of the form $b_A = b_A^0 - C_B$.

4.3 Probability of single and double resistance

In this section, we present analytical approximations for the probability that the population has developed resistance at a given time. More specifically, we calculate the probabilities that there is at least one individual of type A or of type B in the population at time t ($P[n_A(t) + n_B(t) > 0]$), and the probability that there is at least one double-resistant D in the population $P[n_D(t) > 0]$). The method to derive these probabilities is based on [19], where the probability of having at least one single-resistant was calculated for a linear model with exponential growth and only one type of single-resistant strain. Our contribution consists of extending this method to the non-linear growth models described in the previous section, and additionally, we also obtain the probability to find double resistance. We note that double mutants D can be generated from two parent sources (A and B) via mutations. We here only outline the main steps and results. Further details of the calculations can be found in the Supplementary Material (Section 4.8).

4.3.1 Extinction probability of single strains

The method of [19] makes use of the extinction probability in a single-species birth-death process with time-dependent birth and death rates. This is the probability that one single individual present at time t becomes extinct by time T, along with its lineage (i.e, the cell itself and all its descendants).

For strain i, and using the previous notation $b_i(t')$ and $d_i(t')$ for the per capita birth and death rates at time t', this probability is given by [25, 42]

$$P_{\text{ext},i}(t,T) = \frac{\int_t^T d_i\left(t'\right) e^{-\beta_i(t,t')}\mathrm{d}t'}{1+\int_t^T d_i\left(t'\right) e^{-\beta_i(t,t')}\mathrm{d}t'}, \tag{4.11}$$

with

$$\beta_i\left(t,t'\right) \equiv \int_t^{t'} r_i\left(t''\right) \mathrm{d}t'', \tag{4.12}$$

and $r_i(t) = b_i(t) - d_i(t)$ as before. This result is exact, provided the rates $b_i(t)$ and $d_i(t)$ are deterministic functions (for example externally determined birth and death rates). When one or both of these rates depend on the cell numbers $\mathbf{n}$ one can proceed based on an approximation in which one replaces $\mathbf{n}$ by the mean cell numbers $\bar{\mathbf{n}}$. We will make use of this approximation for the logistic growth models. If $d_i = 0$, the extinction probability is zero trivially, as there is no death process. The extinction probability in Eq. (4.23) tends to unity for $T \to \infty$ if and only if $\int_t^T d_i\left(t'\right) e^{-\beta_i(t,t')} \mathrm{d}t' \to \infty$. This can occur, for example, when the death rate is higher than the birth rate at all times, i.e., $r_i(t)$ is consistently negative and with it also $\beta_i(t,t')$.

In order to calculate the probabilities of single or double resistance one needs to evaluate $P_{\mathrm{ext},i}$ ($i \in \{A,B,D\}$) as defined above for each growth model, for both constant and time-dependent rates. Although this can be done numerically for cases which do not admit an analytical solution, the repeated evaluation of the integrals in Eqs. (4.23) and (4.24) can become very costly. One aspect of our work is the strategy developed to carry out these integrals efficiently. This is explained below in Section 4.3.4, after we first describe the main steps we follow to obtain the probabilities of single and double resistance.

4.3.2 Single resistance

As described in more detail in Section 4.8.2 of the Supplementary Material, the probability of having at least one single-resistant cell of either type A or B at time T after the treatment has started can be expressed in the form

$$P_R^{\mathrm{single}}(T) = 1 - \exp\left[-\int_0^T \left\{\Phi_A\left(t,T\right) + \Phi_B\left(t,T\right)\right\} \mathrm{d}t\right], \tag{4.13}$$

where

$$\Phi_A\left(t,T\right) = b_S(t)\bar{n}_S(t)\mu_A\left[1 - P_{\mathrm{ext},A}(t,T)\right], \tag{4.14}$$

and

$$\Phi_B\left(t,T\right) = b_S(t)\bar{n}_S(t)\mu_B\left[1 - P_{\mathrm{ext},B}(t,T)\right]. \tag{4.15}$$

The term $\Phi_i\left(t,T\right)$ represents the rate with which mutants of type $i \in \{A,B\}$ are produced at time t through mutations of strain S, requiring that the resulting mutant

lineage survives until the later time T. We will refer to the expression in Eq. (4.13) as the *probability of single resistance*.

Broadly speaking the above expressions indicate that the appearance of single mutants is guaranteed ($P_R^{\text{single}}(T) \to 1$ for $T \to \infty$) if mutation events from the sensitive strain continue indefinitely, and if mutants produced in this way do not all die out in the long run. We would expect the latter to be the case when the growth rate $r_i(t)$ remains positive throughout for either strain A or strain B (or both). Examples of such situations are shown in Figure 4.1. In the absence of mutation ($\mu_A = \mu_B = 0$) one has $\Phi_A = \Phi_B = 0$, and $P_R^{\text{single}}(T) = 0$ trivially as mutants never appear.

4.3.3 Double resistance

The procedure to obtain the probability of double resistance is analogous to that for single resistance. The main difference is now that there are two sources, strains A and B. The probability of having at least one double-resistant cell at time T becomes (see Section 4.8.2 of the Supplementary Material)

$$P_R^{\text{double}}(T) = 1 - \exp\left[-\int_0^T \left\{\Psi_A(t,T) + \Psi_B(t,T)\right\} \mathrm{d}t\right], \tag{4.16}$$

with

$$\Psi_A(t,T) = b_A(t)\mu_B \bar{n}_A(t)\left[1 - P_{\text{ext},D}(t,T)\right] \tag{4.17}$$

and

$$\Psi_B(t,T) = b_B(t)\mu_A \bar{n}_B(t)\left[1 - P_{\text{ext},D}(t,T)\right]. \tag{4.18}$$

The terms $\Psi_A(t,T)$ and $\Psi_B(t,T)$ represent the rates with which double-resistants are produced by mutation of strains A and B at time t, respectively, and requiring that their lineage survives until time T. We will refer to $P_R^{\text{double}}(T)$ in Eq. (4.34) as the *probability of double resistance*.

We stress again that we are using the mean numbers of source cells as an input for these expressions ($\bar{n}_A$ and $\bar{n}_B$). The limitations of this approach are discussed in Section 4.6.

4.3.4 Numerical integration of the probabilities of resistance

The previous expressions for the probabilities of resistance cannot always be reduced further. In addition, if the birth or death rates depend on the cell number of one or

more strains, it is necessary to make a deterministic approximation (involving the replacement of the rates by their mean values) in order to compute the integrals in Eqs. (4.23), (4.13), and (4.34). In many cases it is not possible to do this analytically, and one has to resort to evaluating the integrals numerically.

Evaluating the probabilities of single or double resistance at time T requires the calculation of the functions $\Phi_A(t,T)$, $\Phi_B(t,T)$ and $\Psi_A(t,T)$ and $\Psi_B(t,T)$ in Eqs. (4.13) and (4.34) for all times t up to T. These objects in turn involve $P_{\mathrm{ext},i}(t,T)$ for $i \in \{A,B,D\}$, and evaluating these would require access to the objects $\beta_i(t,t')$ for all combinations of times t,t' up to T [Eq. (4.23)]. We recall that $\beta_i\,(t,t') = \int_t^{t'} r_i(t'')dt''$ is the integrated net growth rate for strain i, see Eq. (4.24). As a consequence we would have to integrate the net growth rate r_i over the intervals $[t',t]$ for all combinations of $t' < t$ in the range up to T.

To make this process more efficient we first notice that – in absence of additional production of strain i through mutation – one has $\mathrm{d}\bar{n}_i(t)/\mathrm{d}t = r_i(t)\bar{n}_i(t)$. As a consequence $\bar{n}_i(t') = \bar{n}_i(t)\exp\left[\beta_i(t,t')\right]$. We note that the birth rate b_i for strain i depends on the number of cells n_i in the LG model [Eq. (4.7)], and on the total number of cells n_T in the CLG model [Eq. (4.8)]. The net growth rate r_i is then also dependent on n_i or n_T. For the purposes of the current analysis we replace n_i (or n_T) by their mean values $\bar{n}_i$ (or $\bar{n}_T$) in these expressions, where the mean cell numbers are obtained from the growth laws in Eq. (4.1). The quantity r_i can then be treated as a deterministic function of time. If we set $\bar{n}_i(t) = 1$, then the quantity $\beta_i(t,t')$ can directly be expressed in terms of $\bar{n}_i(t')$,

$$\beta_i\,(t,t') = \ln\ \bar{n}_i\,(t')\,. \tag{4.19}$$

Therefore, the calculation of $\beta_i\,(t,t')$ for a fixed combination of t and t' $(t' > t)$ reduces to the problem of finding $\bar{n}_i\,(t')$ for the initial condition $\bar{n}_i(t) = 1$. In principle this can be obtained from numerically integrating the growth law for strain i from the deterministic equations for $\bar{n}_i$, but it would imply separate integration runs for each initial time t due to the required initial condition $\bar{n}_i(t) = 1$. For the model with competition between strains, this also involves integrating the growth laws for all other strains.

In order to streamline this approach, our strategy consists of expressing the quantity $\bar{n}_i(t')$ (with initial condition $\bar{n}_i(t) = 1$) in terms of the solution $\bar{n}_i^0$ of the deterministic

mean growth law for strain i with initial condition $\bar{n}_i^0(0) = 1$ at time 0. The details of this are described in Section 4.10.2 of the Supplementary Material.

For the LG model we find ($t' > t$),

$$\bar{n}_i\left(t'\right) = \frac{k_i\left(\frac{k_i}{\bar{n}_i^0(t)} - 1\right)}{(k_i - 1)\left(\frac{k_i}{\bar{n}_i^0\left(t'\right)} - 1\right) + \left(\frac{k_i}{\bar{n}_i^0(t)} - 1\right)}. \tag{4.20}$$

We re-iterate that this is the solution of the growth law for strain i for times $t' > t$, subject to the initial condition $\bar{n}_i(t) = 1$. This initial condition can be verified directly from Eq. (4.20). We stress that $\overline{n}_i^0(t)$ and $\overline{n}_i^0(t')$ both feature on the right-hand side of Eq. (4.20).

Combining Eq. (4.20) with Eq. (4.19) we can find the integrated growth rate $\beta_i(t, t')$ for all combinations $t < t'$ in the range up to T, provided we know the solution $\bar{n}_i^0(t'')$ of the growth law for strain i with initial condition $\bar{n}_i^0(0) = 1$ ($t'' < T$). This trajectory can be obtained from one single numerical integration, significantly reducing the computational effort.

A similar approach can be taken for the model with competition between strains. This is discussed in more detail in Section 4.11 of the Supplementary Material.

In the next section we proceed to analyse the probabilities of single and double resistance for each growth model and compare the theoretical predictions with results from numerical simulations. For constant growth rates, the simulations are carried out using the Gillespie algorithm [43, 44], which generates a statistically faithful ensemble of sample paths. For explicitly time-dependent birth and death rates simulations are carried out using the so-called ‘ thinning algorithm’ by Lewis [45]; see also [46] for further discussion of this method. This scheme allows us to generate sample paths for time-dependent rates without losing precision as would happen with the Gillespie algorithm.

We focus on studying the probabilities of single and double resistance for the three growth models, and we study cases with constant drug and time dependent drug concentrations, respectively. We will concentrate on the effects the choice of the growth model has on these probabilities.

4.4 Probability of resistance for growth with constant coefficients

4.4.1 Setup, and comparison of theory and simulation

In the case of constant drug concentrations (approximating e.g. constant intravenous infusion, [47]) the birth and death rates for the exponential growth model [b_i and d_i in Eq. (4.10)] are time-independent. Similarly, the quantity ρ_i in the logistic growth models does not explicitly depend on time. Any dependence of b_i and d_i on time in the logistic models is through a functional dependence on $\bar{\mathbf{n}}(t)$ [c.f. Eqs. (4.7) and (4.8)]. To establish the baseline behaviour of the different growth models, we address this case of constant coefficients b_i and d_i in this section, that is coefficients without explicit dependence on time. Specifically, we will study how the probabilities of single and double resistance depend on the key model parameters for the three different types of growth.

The theoretical predictions of single and double resistance are obtained from Eqs. (4.23), (4.13) and (4.34). The extinction probability, the probability for single and double resistance can always be expressed in terms of the trajectories $\bar{n}_i(t)$, although the remaining integrals in the above equations may have to be carried out numerically.

For constant coefficients, closed-form solutions can be obtained for some of the quantities we are interested in, and in other cases we proceed numerically: (i) For the EG model, we can find a closed-form solution for the extinction probabilities $P_{\text{ext},i}(t,T)$, this is given in Eq. (4.37) in the Supplementary Material. Additionally, the mean cell numbers $\bar{n}_i(t)$ for each strain can be obtained in closed form from Eqs. (4.1), see Eq. (4.36). With these solutions in turn, one can then derive closed-form expressions for the functions Φ_A, Φ_B, Ψ_A and Ψ_B, and the probabilities of single and double resistance. This is explained further in Section 4.9 of the Supplementary Material. (ii) For the LG model, we can only find a closed-form solution for $\bar{n}_S(t)$, but not for the other strains. The probabilities of single and double resistance are calculated numerically using Eqs. (4.13) and (4.34). For further details see also Section 4.10 of the Supplementary Material. (iii) For the CLG model, we cannot express the mean cell number in closed form for any of the strains. This is due to the coupling and non-linearity of the

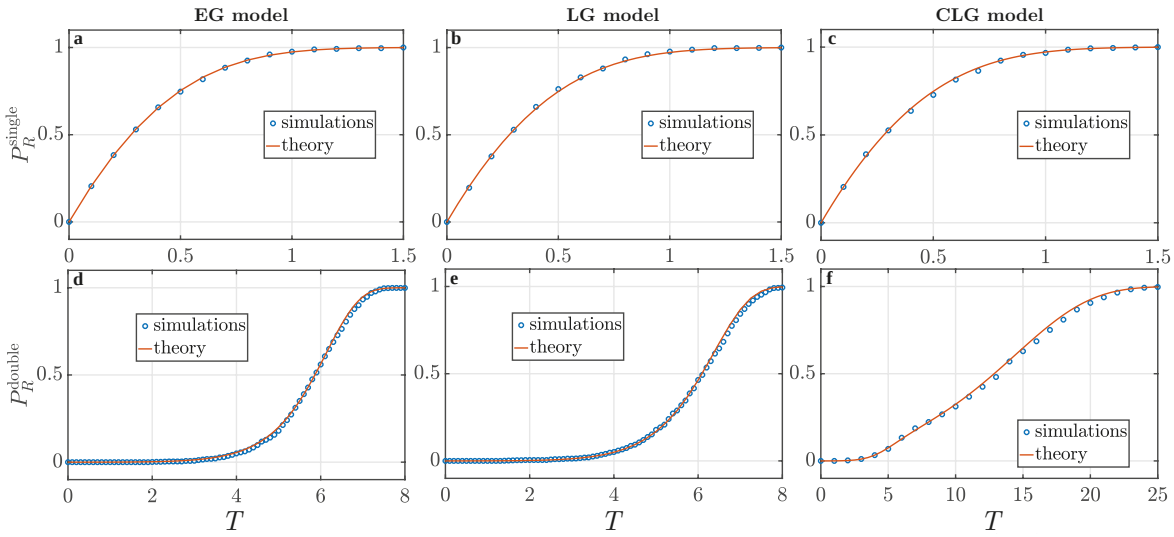

Figure 4.1: Single and double resistance probabilities for the three different growth models (EG exponential growth, LG logistic growth without competition between strains, CLG logistic growth with competition between strains). Theoretical predictions (solid lines) were obtained from equations (4.13) and (4.34), while numerical simulations (circles) were conducted using the Gillespie algorithm, results are averaged over 10000 runs. Parameters used: $b_S = 1.1, b_A = 1.2, b_B = 1.3, b_D = 1.4, d_S = d_A = d_B = d_D = 0.1, \mu_A = \mu_B = 10^{-4}, n_0 = 10^4$. For the logistic growth models, we have set $\rho_i = b_i - d_i$ for $i \in \{S, A, B, D\}$, and $k_S = 10^6, k_A = 1.1 \times 10^6, k_B = 1.2 \times 10^6, k_D = 1.3 \times 10^6$.

equations for the mean cell numbers. The probabilities of single and double resistance are again obtained numerically.

For the time-dependent dosing protocols considered in Section 4.5, we have not been able to find closed-form solutions of Eqs. (4.1) for any of the strains and in any of the growth models. As a consequence the extinction probabilities and probabilities of single or double resistance cannot be found in closed form either, and have to be evaluated numerically.

As mentioned above in Section 4.2.4, in order to be able to compare the outcome of the different growth models, we specify fixed death rates d_i for each strain, and then use these for all three types of growth. In the EG model also specify the birth rates b_i. In the two logistic growth models we then set $\rho_i \equiv b_i - d_i$, so that the behaviour of all three models is similar for very small cell numbers.

Figure 4.1 illustrates a typical profile of the probabilities of having at least one single-resistant individual (either of type A or B) or at least one double-resistant individual, respectively. In the figure we compare the theoretical predictions for the three growth models against results from numerical simulations of the stochastic dynamics. The

parameters used in the figure are for illustration, and do not necessarily represent a realistic situation. They describe a scenario in which the net birth-death rates, $r_i = b_i - d_i$, are positive for all strains. This ensures that cell numbers increase in time (on average), so that single and double mutants eventually emerge. As the graphs show, the profile of the emergence of single resistance is very similar for the three different growth models, while double resistance tends to emerge later in the model with competition than in the other two scenarios. Further illustrations comparing simulation and theory for different choices of the model parameters are shown in the Supplementary Material (Section 4.12.2).

In the following sections we discuss the behaviour of both single and double resistance when varying different model parameters. In particular, we consider the outcome as a function of the carrying capacities, k_i. In the limit of very high carrying capacities (very abundant resources), the logistic models reduce to the exponential model with unlimited growth. When the carrying capacities are finite, growth becomes restricted due to limited availability of resources.

4.4.2 Single resistance

Single resistance emerges through mutations during reproduction events of the sensitive strain S and is subsequently maintained provided the mutant strain does not become extinct. When the carrying capacity of sensitive cells k_S and single-resistant cells k_A and k_B are high compared to the initial number n_0 of sensitive cells, there is no noticeable difference between the predictions of single resistance in the three different growth models (all three models lead to largely exponential growth); an example is shown in the upper row of Figure 4.1. However, as we will discuss below, the relation between k_S on the one hand, and k_A and k_B on the other, can affect the timing of the emergence of single-resistants in the competitive model. This is the case when these coefficients are close to each other, and to the initial number of cells.

We show theoretical predictions for single resistance in Figure 4.2. In the figure we focus on the model with exponential growth, and we show the probability of finding at least one resistant cell as a function of time T, and varying a selection of model parameters. High probabilities of resistance are indicated by light colours. As one would expect, mutants tend to appear sooner as the birth rate b_S, the initial number

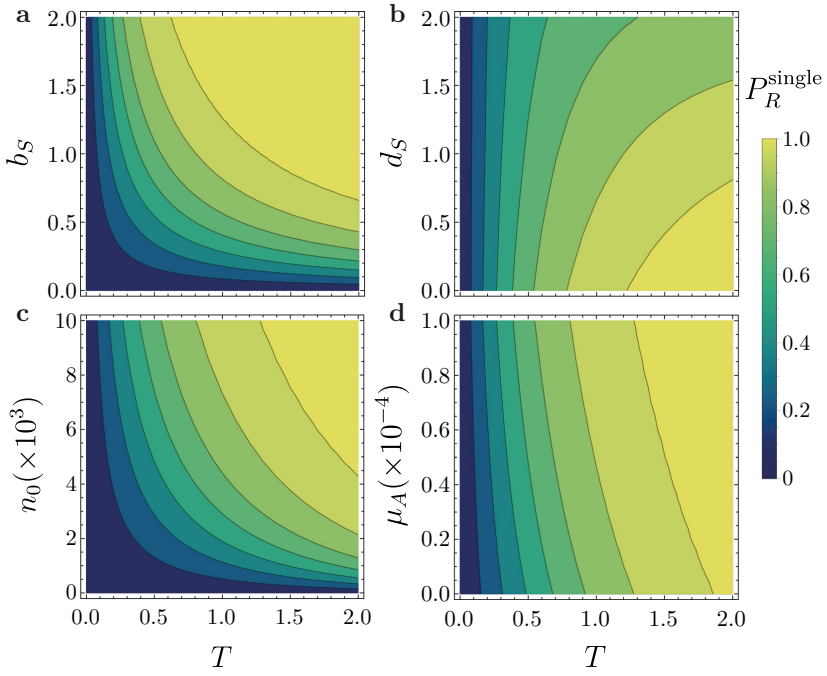

Figure 4.2: Theoretical prediction of the probability of single resistance obtained from Eq. (4.13) for the exponential growth model when varying only one parameter while keeping the others constant. When not varied, the parameters used are $b_S = 1.0, b_A = 1.1, b_B = 1.2, b_D = 1.3, d_S = d_A = d_B = d_D = 0.1, \mu_A = \mu_B = 10^{-4}$, and $n_0 = 10^4$.

of sensitive cells n_0 or the mutation rates μ_A, μ_B are increased. This can be seen by the increased amount of lighter colours as one moves up along the vertical axes of panels (a), (c) and (d) in Figure 4.2. Panel (b) shows that the probability of single resistances decreases for increasing death rates d_S of the sensitive strain. Figure 4.3 illustrates how the predictions for single resistance differs between the logistic models with and without competition between strains (LG and CLG respectively), and when the carrying capacity k_S is varied. In the LG model single mutants tend to appear sooner when the carrying capacity k_S is high, see Figure 4.3 (a). This is as expected, as for higher values of k_S the limitations of growth of the sensitive strain only set in at large cell numbers. The resulting higher number of sensitive individuals increases the chance of producing single mutants.

The dependence of the probability of single resistance on k_S is more intricate in the model with competition between strains (CLG). If the carrying capacity for strain S is close to the initial number of sensitive cells in the population, then the probability that single mutants emerge depends on how k_S compares to the carrying capacities k_A and k_B of the single mutant strain. We illustrate this Figure 4.3 (b) and (d) for a case with $\mu_A > \mu_B$ and $k_B > k_A$. The former of these conditions implies that the first

single mutants are likely to be of type A.

The curve in Figure 4.3 (d) shows interesting behaviour: We find that the probability of single resistance decreases with increasing k_S, provided k_S is sufficiently small. At an intermediate value of $k_S \approx k_A$ we observe a minimum. For higher values of k_S, the probability of single resistance then increases again with k_S. A small 'kink' is seen at $k_S \approx k_B$.

We attribute these features to a combination of several counteracting effects: (i) Generally, an increase in the carrying capacity k_S leads to a less restricted and therefore faster growth of the sensitive strain. A high carrying capacity also leads to higher numbers of sensitive cells in the long run. Both of these effects favour the emergence of single-resistant cells. (ii) If the carrying capacity k_S is lower than k_A and k_B, then the total cell number n_T is lower than k_A and k_B when strain S saturates. The population consists mostly of sensitive cells at this point. As first mutants emerge, they will be able to proliferate until the total size of the population reaches the carrying capacity of the relevant single-mutant strain. This is likely to be A because of the higher mutation rate $\mu_A > \mu_B$. The maximum number of single mutants A that can arise is broadly governed by the difference between k_A and the number of sensitive cells. The latter in turn is approximately given by k_S. Therefore, as k_S approaches k_A from below there is only little room for single-resistant cells to proliferate before saturation sets in. In some cases only a few single-resistant cells can be produced, and these may eventually die due to stochastic fluctuations. This effect acts to reduce the probability of single resistance as k_S approaches k_A from below.

In the example of Figure 4.3 (d), the second effect dominates over the first in the regime $k_S < k_A$, and the probability of single resistance is a decreasing function of k_S. When $k_A < k_S < k_B$, the suppression of growth of mutant strain A (effect (ii) above) is no longer relevant. Effect (i) now dominates, and the probability of single resistance becomes an increasing function of k_S. As a result a minimum is found for the probability of single resistance at $k_S = k_A$. When k_S hits k_B any suppression effect due to mutants of type B is also removed, and the probability of single resistance increases more sharply with k_S. This results in a 'kink' at $k_S = k_B$ in Figure 4.3 (d).

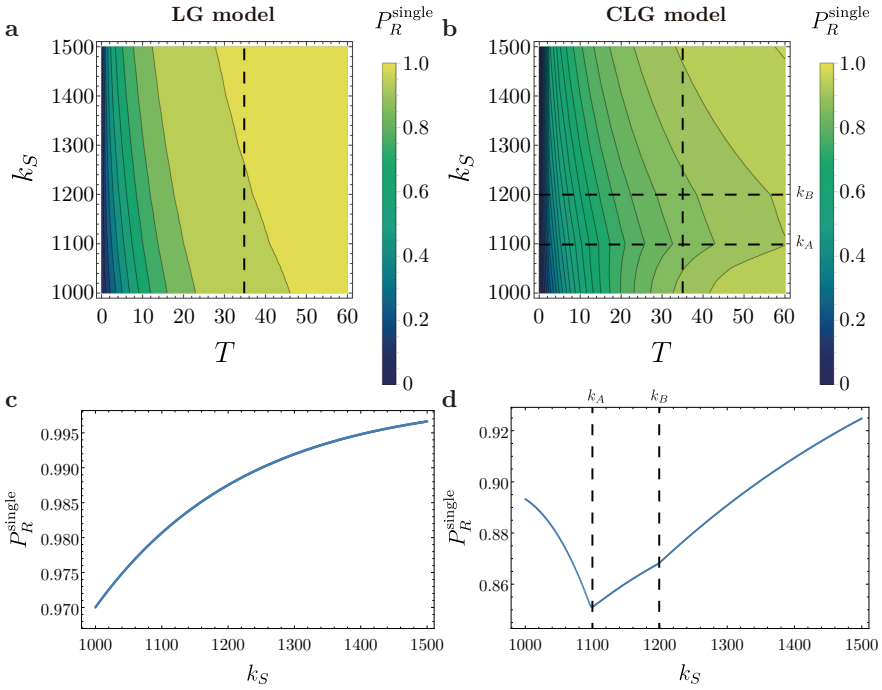

Figure 4.3: Theoretical prediction of the probability of single resistance for the logistic growth models without competition [LG, panels (a) and (c)], and with competition [CLG, panels (b) and (d)]. This is shown as a function of the carrying capacity k_S, for parameters $\rho_S = 0.9, \rho_A = 1.0, \rho_B = 1.1, \rho_D = 1.2, d_S = d_A = d_B = d_D = 0.1, \mu_A = 10^{-3}, \mu_B = 10^{-4}, n_0 = 10^3, k_A = 1.1 \times 10^3, k_B = 1.2 \times 10^3, k_D = 1.3 \times 10^3$. Panels (c) and (d) show vertical cuts in panels (a) and (b) respectively, indicated by the vertical dashed line in the upper graphs at $T = 35$.

4.4.3 Double resistance

We now compare the probability of double resistance in the three growth models. In Figure 4.4 we show the effects of varying b_S, d_S, b_A, and n_0 in turn; for other parameters see Section 4.12.1 of the Supplementary Material. In general, the logistic growth model without competition between strains (LG) seems to produce largely similar behaviour as the model with exponential growth (compare panels (a)–(d) with (e)–(h)). However, differences between the EG and LG models become apparent where the carrying capacities are varied. This will be discussed below in Fig. 4.5.

The logistic model with competition between strains, however, shows notably different behaviour from the other two models [see Figure 4.4(i)-(l)]. In particular we make the following observations:

(i) The time it takes for the probability of double resistance to reach a specified value near one in the CLG model is a non-monotonous function of the net growth rate r_S. This can be seen from the curved shape of the contour lines in Figure 4.4 (i). It becomes more likely to observe double resistance at a given time for

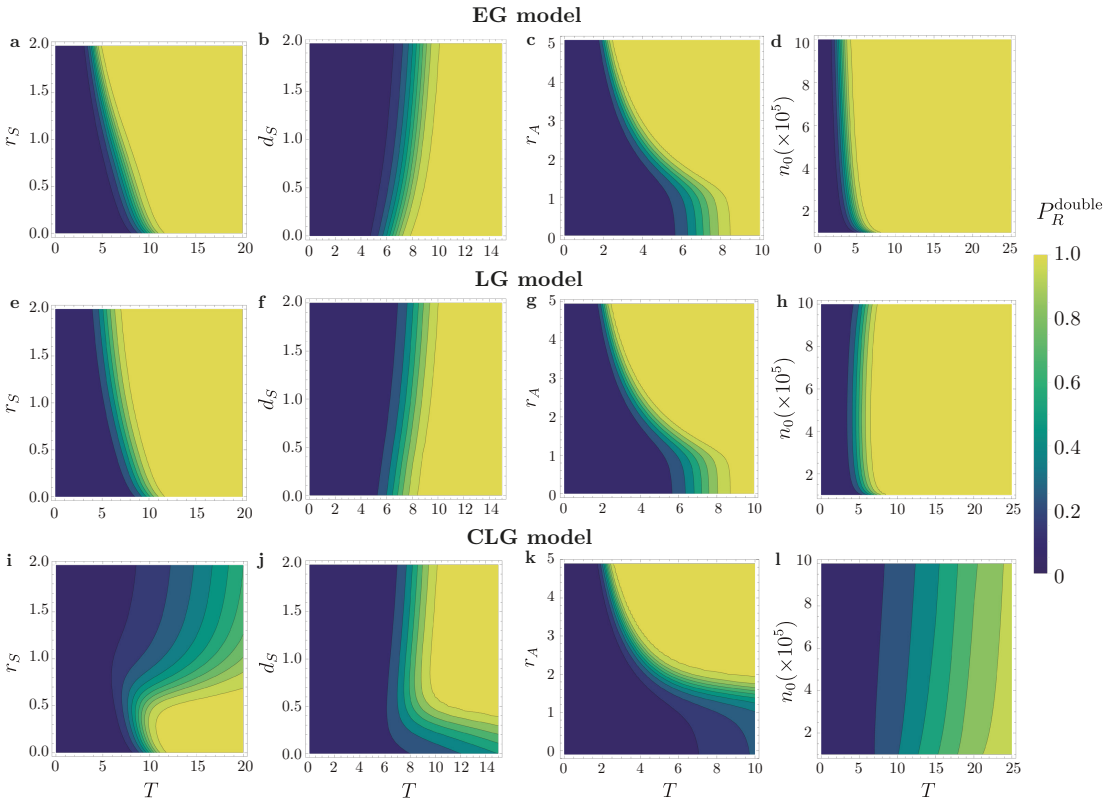

Figure 4.4: Theoretical prediction of the probability of double resistance for the three growth models when varying one parameter (EG exponential growth, LG logistic growth without competition between strains, CLG logistic growth with competition between strains). When not varied, the parameters used are $b_S = 1.0, b_A = 1.1, b_B = 1.2, b_D = 1.3, d_S = d_A = d_B = d_D = 0.1, \mu_A = \mu_B = 10^{-4}$, and $n_0 = 10^4$. When varying $r_S = b_S - d_S$ ($r_A = b_A - d_A$), only b_S (b_A) changes, keeping d_S (d_A) constant. As described in the main text, we have used $\rho_i = r_i$ for the logistic growth models. Carrying capacities used: $k_S = 10^6, k_A = 1.1{\times}10^6, k_B = 1.2{\times}10^6, k_D = 1.3{\times}10^6$. The lightest colour represents values of $P_R^{\text{double}} > 0.99$.

increasing r_S, provided r_S is sufficiently small. Once r_S has reached a certain point, however, increasing r_S further reduces the probability of finding double resistance at a fixed time. We first look at the regime of small r_S. The total cell number remains low enough to avoid saturating the growth of the emerging single mutants. Double-resistants then tend to appear sooner the larger the growth rate r_S of the sensitive strain. Hence, the probability of double resistance increases with r_S. As r_S is increased further, strain S grows fast enough for the total cell number to saturate the proliferation of emerging single-resistant strains (due to the competition between strains). This makes the emergence of double mutants less likely, hence the probability of double resistance decreases with r_S.

(ii) For low values of the death rate of strain S, d_S, double mutants tend to appear

later in the CLG model than in the other two growth models [compare the lower right of panel (j) in Figure 4.4 with the data in the lower right of panels (b) and (f)]. This effect is similar what was discussed in item 1. above. Lowering the death rate d_S while keeping the birth b_S fixed results in faster net growth of the sensitive strain. This means that the growth of the single-resistant strain saturates, thus reducing the chance of emergence of double mutants.

(iii) For low values of the net growth rate r_A of strain A (accounting for birth and death), double mutants tend to appear very late in the CLG model compared to the other growth models [compare the lower right of Figure 4.4 (k) with those in panels (c) and (g)]. A low value of r_A means that more time is required to generate a number of A individuals which is sufficiently large to make the appearance of double mutants likely. As the other present strains (S and B) have more time to grow, the total population size n_T becomes large enough to saturate the growth of strains A and B before the first double-resistants emerge. As a consequence, the chance of double mutants to emerge decreases.

(iv) For an increased number of initial cells n_0, it becomes less likely to observe double mutants at a given time [see Figure 4.4 (l)]. The delay in the emergence of double mutants is again explained by a saturation of the growth of sensitive and single-resistant strains. For higher initial number of sensitive cells, saturation occurs sooner, and double-resistant cells appear later.

These observations suggest that competition can affect the emergence of double resistance. The predictions shown in Figure 4.4 indicate that the typical time at which the first double-resistants appear can be notably different when competition is taken into account [compare e.g. Figure 4.4 panel (l) with panels (d) and (h)]. The difference between the competitive model and the other two models in producing double-resistants is mainly due the saturation of the sensitive and single-resistants before double mutants appear. This is an important factor to take into account for modelling resistance, in particular in situations where resources are limited. Moreover, our analysis indicates that the optimum treatment, i.e. the one that most delays the emergence of double-resistants, can also differ across the models. This can be illustrated using the behaviour of the probability of double resistance as d_S is varied,

see Figure 4.4 (b), (f) and (j). The model with competition between strains predicts that a low d_S would maximise the delay the emergence of double mutants, while the other models predict that a higher d_S would be best.

In addition, the carrying capacities can also affect the probability of double resistance in both logistic growth models. An example of this is displayed in Figure 4.5, where we vary the carrying capacity of strain S, or of only one of the single-resistant strains (strain A), or of both (strain A and B) at the same time.

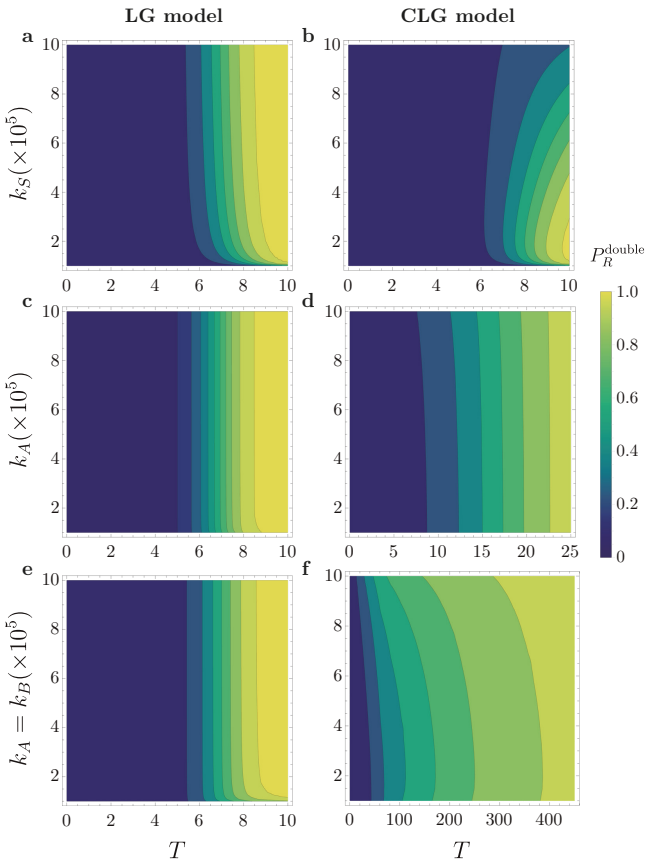

Figure 4.5: Theoretical prediction for the probability of double resistance for the logistic models without competition between strains (LG), and with between-strain competition (CLG) when varying the carrying capacities. When not varied, the parameters used are the same as in Figure 4.4. In panels (a) and (b) only k_S is varied; panels (c) and (d) show the probability of double resistance when k_A is varied. In panels (e) and (f), both k_A and k_B are varied at the same time. Notice the different range of times in panels (d) and (f) compared to the other panels.

The lower end of panels (a) and (b) show a situation in which the coefficient k_S is above the initial number of cells $n_0 = 10000$, but close to it. Double mutants tend to appear only after a relatively long time in this situation in both logistic models.

When k_S is sufficiently far above n_0, its precise value does not have a pronounced effect on double resistance in the LG model [see Figure 4.5(a)]. In the CLG model, however, an increase in the carrying capacity k_S of the sensitive strain results in a delayed emergence of double mutants [Figure 4.5(b)].

When varying only k_A [Figure 4.5 (c) and (d)], the probability of double resistance does not show a notable change in either of the logistic models. Independently of the dynamics of strain A, double mutants can still be produced from strain B. Notice, however, that double mutants tend to appear at later times in the CLG model than in the LG model. When both carrying capacities k_A and k_B are varied together [panels (e) and (f)], double resistance is significantly delayed in the CLG model in comparison to the LG model when k_A and k_B are high.

In summary we conclude that the carrying capacity of strain S has a stronger effect on the emergence of double resistance than each of the single-resistant carrying capacities.

4.5 Time-dependent drug concentrations

The analysis in the previous section focused on situations in which model parameters do not vary in time. In many instances however, drugs are administered using time-varying dosing schedules, giving rise to time-dependent death and growth rates. Most drug therapies use periodic dosing schedules, resulting in periodic time-dependences of drug concentrations (see e.g. [48, 49]). Modelling the the pharmacokinetics of different methods of repeat drug administration, we consider two different types of time-dependence for the drug concentrations. In the first scenario, drug concentrations are continuous in time and follow a sinusoidal profile. This approximates the pharmacokinetics for example of repeat antibiotic dosing via an extravascular route (e.g. oral administration). In the second scenario the drug concentration profiles consist of a periodic series of pulses, representing, for example, intermittent intravenous boluses [47, 50].

We note that the net growth rates of the strains affected by the drugs ($r_i = b_i - d_i$ for $i \in \{A, B, D\}$) in Eq. (4.10) can become negative when the concentration of the relevant drugs are sufficiently high. This leads to an effective reduction of the number of cells of the affected strains. Motivated by clinical treatment protocols, the drug

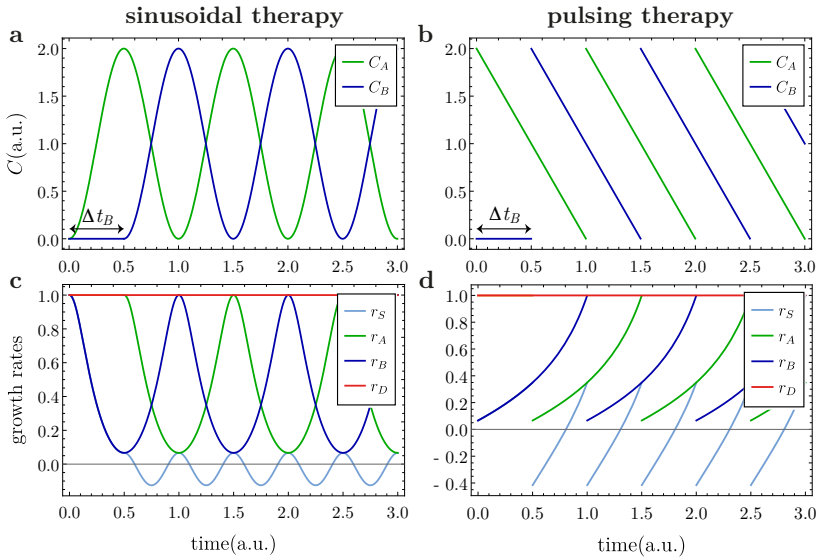

Figure 4.6: Drug concentrations $C_A(t)$ and $C_B(t)$ in the sinusoidal protocal (a) and for pulsing profiles (b) (period $P = 1$ and $\Delta t_B = 0.5$). Panels (c) and (d) show the respective growth rates ($r_i(t) = b_i(t) - d_i(t)$, with $i \in \{S, A, B, D\}$) affected by the drug effect described in equations (4.9)-(4.10). Parameters used: $b_S^0 = b_A^0 = b_B^0 = b_D^0 = 1.1, d_S^0 = d_A^0 = d_B^0 = d_D^0 = 0.1$.

therapies discussed below are designed such that the sensitive strain will eventually become extinct, which is the goal of treatment (see e.g. [51]). This is achieved if $\int_0^T d_S(t')\, e^{-\beta_S(0,t')} \mathrm{d}t' \to \infty$ as $T \to \infty$, with $\beta_S(0,t') \equiv \int_0^{t'} r_S(t'')\, \mathrm{d}t''$ as explained in Section 4.3.1. For oscillatory drug concentrations with period P it is sufficient that $\beta_S(0,P) < 0$, i.e., that the time-average of the net growth rate over one period is negative (assuming that $d(t')$ remains above a non-zero value for all t'). Our focus is on finding treatment protocols which minimise the probability of double resistance within the set of protocols which eliminate sensitive cells.

4.5.1 Sinusoidal drug concentrations

We first consider a sinusoidal drug profile, with period P. The drug concentrations take the form

$$C_A(t) = 1 - \cos\left[\frac{2\pi}{P} t\right],$$

$$C_B(t) = \begin{cases} 0 & \text{if} \quad t \leq \Delta t_B \\ 1 - \cos\left[\dfrac{2\pi}{P}\left(t - \Delta t_B\right)\right] & \text{if} \quad t > \Delta t_B. \end{cases}$$

Drug $\mathcal{A}$ is applied starting from time $t = 0$, initially with concentration zero ($C_A(t = 0) = 0$), and then following a periodic profile. The application of drug $\mathcal{B}$ starts at a

later time Δt_B ($C_B(t) = 0$ for $t \leq \Delta t_B$). The concentration of $\mathcal{B}$ then also follows a sinusoidal profile from time Δt_B onwards. The factors f_A and f_B range from 1 to 3 over each cycle. The drug profiles C_A and C_B are shifted by a time Δt_B [Δt_B mod P when $\Delta t_B > P$] and are out of phase by a fraction $\Delta t_B/P$ of a period [$(\Delta t_B \bmod P)/P$ when $\Delta t_B > P$].

A sample profile of the drug concentrations is shown in Figure 4.6 (a) for $P = 1$ and $\Delta t_B = 0.5$; the corresponding growth rates for the different strains are shown in Figure 4.6 (c).

4.5.2 Pulsing drug concentrations

In this protocol, the concentration of drug $\mathcal{A}$ is assumed to be of the form

$$C_A(t) = \frac{2}{P}\left[P - (t \bmod P)\right]. \tag{4.21}$$

This means that the profile $C_A(t)$ starts off at $C_A(t = 0) = 2$, and then falls linearly with slope $2P^{-1}$, so that the drug concentration becomes zero at $t = P$. Then the next pulse starts, i.e., C_A is re-set to its maximum value, and then falls off linearly again. Similar profiles have been used in [20, 48].

The concentration of drug $\mathcal{B}$ is assumed to be zero up to time Δt_B, and then follows a similar sequence of pulses. This is described by

$$C_B(t) = \begin{cases} 0 & \text{if } t \leq \Delta t_B \\ \\ \dfrac{2}{P}\left\{P - [(t - \Delta t_B) \bmod P]\right\} & \text{if } t > \Delta t_B. \end{cases} \tag{4.22}$$

The concentrations of both drugs are out phase as in the sinusoidal drug therapy, and attain their minima at the same times as in the sinusoidal protocol. Figure 4.6 (b) illustrates a sample profile for $P = 1$ and $\Delta t_B = 0.5$; we show the corresponding net growth rates for the different strains in panel (d).

We note that the total amount of drug given over time is identical in both treatment protocols. This can be seen for example by looking at the area under the curve $C_A(t)$ over one time period; we have $\int_{t'}^{t'+P} C_A(t)\,\mathrm{d}t = P$ for any $t' \geq 0$, both in sinusoidal and pulsing therapies (this also holds for $C_B(t)$ for any $t' \geq \Delta t_B$, i.e., when the treatment with drug $\mathcal{B}$ has started).

4.5.3 Probability of double resistance for time-dependent dosing schedules

In Figure 4.7 we show the probability of double resistance resulting from the periodic dosing protocols. Data is presented as a function of time, and for any pairing of the two therapy protocols and the three different growth models. We have considered the cases where drug $\mathcal{B}$ is administered from times $\Delta t_B = 0.0, 0.5\,P$ and $1.0\,P$, with $P = 1$. Predictions for other values of Δt_B, as well as the probability of single resistance, can be found in Section 4.12.3 in the Supplementary Material. We have chosen parameters such that the carrying capacities are not too far from the initial number of sensitive cells, allowing the limitations on growth in the logistic models to set in quickly. We observe that the double-resistant strain tends to appear later in the pulsing therapy than in the sinusoidal therapy (to see this compare the value of P_R^{double} for the two protocols at a given time). This is not surprising as, for equal parameters, the growth rate r_S spends more time taking negative values in the pulsing therapy than in the sinusoidal therapy [compare panels Figure 4.6 (c) and (d)].

In addition, we also note that, at equal times after the treatment has started, the probability of double resistance is considerably lower in the logistic model with competition between strains than in the other two growth models, independently of the treatment protocol. This is due to the early saturation of the growth of the single-resistant strains in the CLG model, inhibiting the emergence of double-resistants. We observe that the fraction of sensitive cells in the total population is small at the point where the growth of single-resistants saturates due to the effects of drugs. This is because the growth of sensitive cells is heavily suppressed by the treatment. As a consequence, the contribution of sensitive cells to the saturation of single-resistant strains is negligible in the CLG model.

Interestingly, the data in Figure 4.7 also shows that the optimum treatment within our model setting, i.e., the treatment with the lowest probability of double resistance at a given time, can be different for different growth models. We describe this in the context of the sinusoidal therapy: the optimum treatment in the exponential growth model is obtained when both drugs are administered at the same time, i.e. when $\Delta t_B = 0$ [see Figure 4.7 (a)]. This is not the case in the other two growth models [see

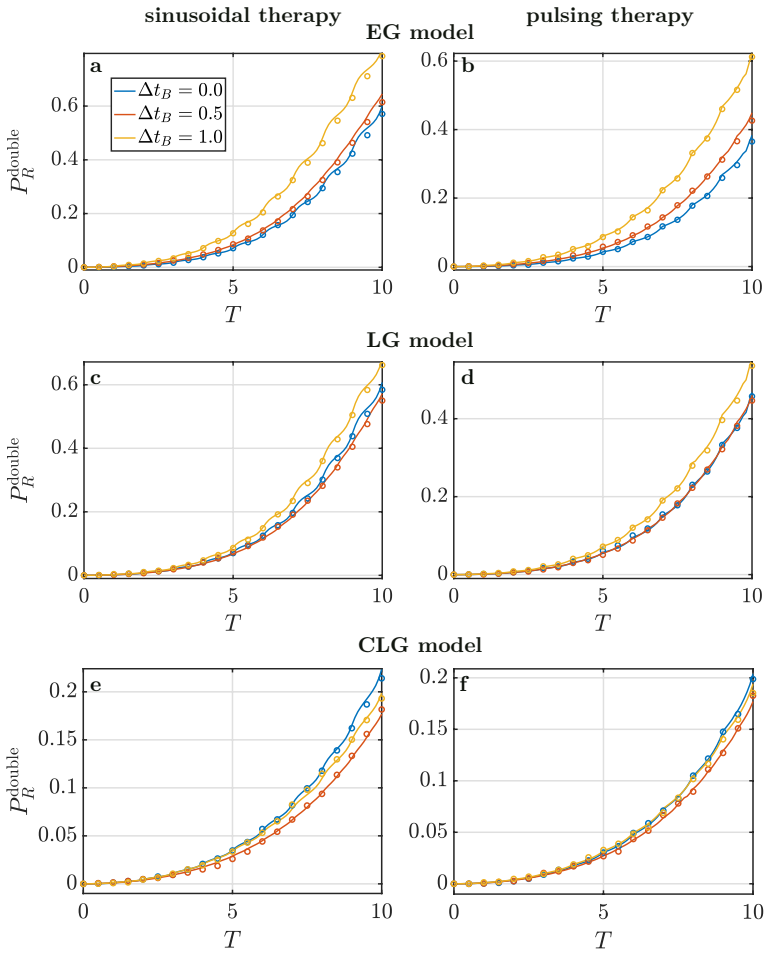

Figure 4.7: Probability of double resistance as function of time for each of the three growth models for different values of Δt_B for sinusoidal and pulsing therapies (EG exponential growth, LG logistic growth without competition between strains, CLG logistic growth with competition between strains). Solid lines represent the theoretical predictions, while open circles the numerical simulations. Parameters used: $b_S^0 = b_A^0 = b_B^0 = b_D^0 = 1.1, d_S^0 = d_A^0 = d_B^0 = d_D^0 = 0.1, \mu_A = \mu_B = 10^{-3}$, $n_0 = 5 \times 10^3$, $k_S = 10^4, k_A = 1.1 \times 10^4, k_B = 1.2 \times 10^4$, and $k_D = 1.3 \times 10^4$.

panels (c) and (e)]. In fact, for the logistic model with competition between strains [panel (e)], the case $\Delta t_B = 0$ turns out to be the worst treatment of the ones shown here, as double mutants would appear earliest. For the pulsing therapy, we observe similar behaviour. For both logistic growth models, the optimum treatment in each therapy is found when $\Delta t_B = 0.5$, i.e., when the drugs are applied alternately. This result is consistent with the findings from [52] for synergistic drug therapies.

In Figure 4.14 of the Supplementary Material we re-plot the data of Figure 4.7, but as function of Δt_B for a fixed time T. This further illustrates that the optimum treatment is achieved for different choices of the time lag Δt_B in the different growth models. Another example showing that the optimum treatment varies across the growth models is presented in Figure 4.15 in the Supplementary Material for a scenario with

higher carrying capacities.

4.6 Limitations of deterministic approximation and possible extensions of the model

The method we have presented to estimate the probabilities of single and double resistance can be used for constant and time-dependent drug concentrations in exponential and logistic growth models. However, our approach relies on an approximation. While we treat the emergence of single and double mutants and the persistence or extinction of their lineages as stochastic processes, we disregard fluctuations in the rates with which mutants first appear. To illustrate this, we focus on mutants of type A. They are arise from mutations in reproduction events of sensitive cells S. The rate with which individuals of type A emerge therefore depends on the number of sensitive cells in the population. As a consequence, the production of A in mutation events is a stochastic process with two levels of randomness. First, the number of sensitive cells is a random quantity. Second, each of the sensitive cells can produce mutants of type A with a certain probability upon reproduction, and the subsequent birth-death dynamics of the single-mutant cells is also stochastic. Our approach consists of neglecting the first type of randomness for the purposes of studying mutants of type A. In the production rate of A we replace the actual stochastic number of sensitive cells by its mean (over realisations). We do however retain the second type of randomness, and treat the subsequent extinction or persistence of the mutants as a stochastic process. This is captured by the extinction probabilities $P_{\text{ext},i}(t,T)$ in Eq. (4.23). In very much the same way we treat the number of A and B cells as deterministic for the purposes of calculating probability of double resistance, but retain the stochasticity of the production of double mutants, and the subsequent evolution of their lineages.

This approximation works well for the estimation of the probability of single resistance. Single-resistant cells are produced from sensitive cells in mutation events, and the number of sensitive cells is large from enough from the beginning to neglect fluctuations.

Double resistance on the other hand is produced from single-resistant cells. Single-resistant cells are not present in the population at the beginning, and their numbers

will initially be small. One would therefore expect that fluctuations of the number of cells of single resistants A and B will be more pronounced than those of the number sensitive cells. This may make the predictions for double resistance inaccurate. In simulations we find that this tends to be the case mostly when the first double mutant appears at long times after the start of the dynamics. This can occur for example when the initial number of sensitive cells, the mutation rates, or the birth rates are small. This comes from the fact that our theoretical approach takes into account the trajectory of single resistant strains from the start of treatment. If the time spent in phases in which fluctuations are relevant is considerably high, then the deterministic approximation employed becomes significantly inaccurate. We compare the predictions of our calculations against simulations for such cases in Section 4.13 of the Supplementary Material.

Simulations confirm that the number of the single-resistant cells can be subject to significant fluctuations under these circumstances. As a consequence, the deterministic approximation in the production rates of double mutants becomes inaccurate, and with it the approximation for the probability of double resistance in Eq. (4.34). Joint effects of the random occurrence of single-mutants, and their subsequent growth are a possible explanation for the fluctuations of the number of single-resistants. Typical cases in which the prediction for the presence single mutants appears to be affected less by these effects. We attribute this to the fact that single mutants arise from the sensitive strain, which is present from the start and not generated by random mutation events.

The analytical expressions for the probabilities of single and double resistance [Eqs. (4.13) and (4.34) respectively] are, valid for any type of growth law and type of interaction between different strains. In order to illustrate the behaviour of the model we have made several assumptions, which can, in principle, be relaxed. For example, birth and death rates need not be affected symmetrically by a common factor as in Eq. (4.10). We note that death rates mostly affect the extinction probability [Eq. (4.23)]. We would therefore expect birth rates to have a stronger quantitative effect on the probabilities of single and double resistance as they appear in the extinction probabilities [Eq. (4.23)], and in the functions $\Phi_{A,B}$ and $\Psi_{A,B}$ [Eqs. (4.14,4.15) and (4.17, 4.18) respectively]. Extending the model accordingly could establish how strong such an effect is. We note that [53] find that in experiments that it seems to make

relatively little difference for resistance selection whether a drug acts as a bacteriostatic or bactericidal agent.

When we evaluate probabilities for single and double resistance we assume that resistant strains are not affected by the relevant drug. One could make less stringent assumptions and require only partial resistance. For the double mutant this would mean a slower growth when either or both antibiotics are present than when they are absent, (i.e. change the scenario in Eq. (4.10) to one in which $b_D(t) < b_D^0$ and/or $d_D(t) > d_D^0$). Assuming that the residual net growth is still positive, we expect that the time to observe $P_R^{\text{double}} > 0$ would be increased.

The method and analysis can be extended to more complex situations, such as models with heterogeneous competition, and different forms of competitive or cooperative interactions. For example, cooperative interactions can allow sensitive bacteria to grow in the presence of antibiotics if a resistant strain is also present [54]. Conversely, cross-feeding has been observed to slow the emergence of resistance due to reduced effective growth rate [55]. Further, cell-cell interactions between different strains can influence the mutation rate itself [56]. Such complex interactions are therefore a natural topic for future work. The approach can also be generalised to combination therapies of more than two drugs, as well as to cases with more complex interactions between the drugs. It may also be interesting to account for heterogeneity of the mutation rate within the population, as this can affect resistance [57]. Given that the limitations of our approximation can be characterised, we think that the method we have developed can be useful for these questions, and for other biological problems in which multiple mutations occur sequentially.

4.7 Conclusions

Models for estimating the probability of drug resistance have previously been largely based on exponential growth (some exceptions are [58, 59]). The use of exponential growth models implies an assumption of infinite resources and the absence of competition between strains. Here, we have shown that the choice of growth model can affect the probability that resistant cells emerge in when resources are limited and when there is potential competition between strains.

To do this, we have investigated the evolution of single and double resistance by mutation in a stochastic multi-strain model. Our analysis focuses on three different growth laws: exponential growth, logistic growth without competition between strains and logistic growth with between-strain competition. We have examined cases in which the model parameters are not explicitly time-dependent, as well as simple time-dependent drug therapies. We have analytically estimated the probability of having at least one single or double-resistant cell in the population, and we have verified these predictions in numerical simulations. Our calculations require the evaluation of a large number of integral terms in the expressions for the probability of single and double resistance. As a by-product of our work we have provided strategies to reduce the number of integral terms to be evaluated, allowing us to make theoretical predictions more efficiently.

Our results show that the choice of growth model makes a difference for the probability of double resistance, both for abundant and limited resources—a distinction not seen for single drug resistance. Specifically, competition can considerably delay double resistance, both for constant model parameters and for time-dependent dosing schedules. This delay in double resistance occurs for a range of parameters for the sensitive and single-resistant strains. Consequently, modelling resistance with exponential growth laws may make combination treatments appear less effective than they are in the presence of between-strain competition. Further, careful attention needs to be paid to competition when planning treatments with time-dependent concentrations. Our results predict that the optimal dosing schedule for a combination treatment changes depending on the growth law used. An accurate representation of growth is therefore critical for infections where resource competition is strong. This is particularly relevant to long-term or chronic infections and cancer [60–64]. The exact way in which growth is modelled therefore requires careful consideration in the design of drug therapies. Our results are most applicable to combination therapies using drugs where multi-resistance is gained through spontaneous mutation. This is a common modality of evolution for many antibiotic combination therapies, particularly against *Mycobacterium tuberculosis* [65]. Nevertheless, future combination therapies may more commonly involve antibiotics where resistance is conferred by horizontal gene transfer, e.g. through the acquisition of conjugative plasmids [66]. Future work will

investigate how community-level interactions affect these other modalities for acquiring multi-resistance evolution.

Acknowledgements

We acknowledge support through a Presidential Doctoral Scholarship (The University of Manchester) to EBC, a Wellcome Trust Institutional Strategic Support Fund Award (204796/Z/16/Z) to DRG and TG. DRG is supported by a UKRI Innovation/Rutherford Fund Fellowship (MR/R024936/1). TG acknowledges financial support from the Maria de Maeztu Program for Units of Excellence in R&D, Spain (MDM-2017-0711).

Data archiving

Data, scripts and source code are available on GitHub:

https://github.com/ernestoberriosc/probabilities-resistance

Author contributions

All authors contributed to conceiving and designing the study. EBC carried out the mathematical analysis and numerical simulations. All authors contributed to analysing results and data, and to writing the paper.

4.8 Appendix A: Derivation of the probabilities of single and double resistance for general birth and death rates

In this section, we will give further details of the calculation of the probability of resistance, i.e., the probability of having at least one single resistant or double resistant individual at a certain time. We do this for general birth and death rates, assuming that these rates are given by deterministic functions. In other words, the birth and death rates may depend on the composition of the population, but if they do then

we ignore any stochasticity of the number of different cells in the population. The population starts from n_0 sensitive cells at time $t = 0$, and with no other cells.

The method we will use is based on [19], where the probability of having at least one single resistant was calculated for an exponential growth model. We extend this method to obtain the probability of double resistants for each of the three growth models defined in the main text.

4.8.1 Extinction probability for single cell and its lineage

We first consider the probability that one single individual of type i present at time t goes extinct by time T, along with its lineage. For strain i, this extinction probability is given by (see e.g. [25, 42]).

$$P_{\text{ext},i}(t,T) = \frac{\int_t^T d_i\left(t'\right) e^{-\beta_i(t,t')}\mathrm{d}t'}{1+\int_t^T d_i\left(t'\right) e^{-\beta_i(t,t')}\mathrm{d}t'}, \tag{4.23}$$

with

$$\beta_i\left(t,t'\right) \equiv \int_t^{t'} r_i\left(t''\right)\mathrm{d}t'', \tag{4.24}$$

where $b_i(t)$ and $d_i(t)$ are the birth and death rates for cells of type i, and $r_i(t) = b_i(t) - d_i(t)$. This is an exact result provided that the birth and death rates are both given by deterministic functions.

4.8.2 Probability of no resistance

The probability of having no resistant individuals of a given type $i \in \{A, B, D\}$ at time T is obtained by dividing the interval $[0, T]$ into a large number N of sub-intervals, each of length $\Delta t = T/N \ll 1$. One then requires that any resistant of type i which is produced in a given sub-interval $[t_k, t_k + \Delta t] \subseteq [0, T]$ ($t_k = (k-1)\Delta t$, $k \in \{1, 2, \ldots, N\}$) goes extinct by time T, along with its lineage.

For any sub-interval there are two possibilities:

(i) No relevant mutations occur, i.e. no resistant cells of type i are produced. The probability that this happens is

$$1 - \overline{W}_i(t_k)\Delta t, \tag{4.25}$$

as $\overline{W}_i(t_k)\Delta t$ is the probability that a relevant reproduction-mutation event occurs in this interval. The overbar indicates that we use a deterministic approximation for the rate $W_i(t_k)$.

(ii) A relevant mutation occurs (i.e., a resistant cell of type i is produced), but it goes extinct along with its lineage by time T. The probability for this event is

$$\overline{W}_i(t_k)\Delta t P_{\mathrm{ext},i}(t_k, T), \tag{4.26}$$

with $P_{\mathrm{ext},i}(t_k, T)$ as defined above.

Next, we will describe how to use this to estimate the probability of single and double resistance.

Single resistance

Following this idea, the probability that either no single resistant cell arises in $[t_k, t_k+\Delta t]$, or if one arises it goes extinct by time T along with its lineage becomes

$$\begin{aligned} P^{\mathrm{single}}_{0,t_k}(T) &= \left[1 - \left(\overline{W}_A(t_k) + \overline{W}_B(t_k)\right)\Delta t\right] \\ &\quad + \overline{W}_A(t_k)\Delta t P_{\mathrm{ext},A}(t_k, T) + \overline{W}_B(t_k)\Delta t P_{\mathrm{ext},B}(t_k, T) \\ &= 1 - \Delta t\Big\{ W_A(t_k)\left[1 - P_{\mathrm{ext},A}(t_k, T)\right] + W_B(t_k)\left[1 - P_{\mathrm{ext},B}(t_k, T)\right] \Big\}. \end{aligned} \tag{4.27}$$

This expression accounts for the fact that single resistants can be of type A or B, and that we are interested in situations where neither type is present. The terms $\overline{W}_A$ and $\overline{W}_B$ are the average production rates of mutants of type A and B from strain S, as defined in Eqs. (4.3) and (4.4) of the main text. To lowest order in Δt the above expression turns into

$$P^{\mathrm{single}}_{0,t_k}(T) \approx \exp\Big(- \Delta t\Big\{ W_A(t_k)\left[1 - P_{\mathrm{ext},A}(t_k, T)\right] + W_B(t_k)\left[1 - P_{\mathrm{ext},B}(t_k, T)\right] \Big\}\Big). \tag{4.28}$$

The probability that no single resistant cells (of either type A or type B) are present at time T in turn takes the form

$$P^{\mathrm{single}}_0(T) \equiv P\left(n_A(T) = n_B(T) = 0\right) = \prod_{k=1}^{N} P^{\mathrm{single}}_{0,t_k}(T), \tag{4.29}$$

since we require that single resistant cells produced in any interval $[t_k, t_k + \Delta t]$ get extinct along with their lineage. Inserting the expression from Eq. (6.38) and taking the limit $\Delta t \to 0$ (so that sums turn into integrals), we find

$$P_R^{\text{single}}(T) = 1 - P_0^{\text{single}}(T) = 1 - \exp\left[-\int_0^T \left\{\Phi_A(t,T) + \Phi_B(t,T)\right\} \mathrm{d}t\right], \tag{4.30}$$

with

$$\begin{aligned} \Phi_A(t,T) &= \overline{W}_A(t)\left[1 - P_{\text{ext},A}(t,T)\right], \\ \Phi_B(t,T) &= \overline{W}_B(t)\left[1 - P_{\text{ext},B}(t,T)\right]. \end{aligned} \tag{4.31}$$

The calculation can be extended to the case of several single resistant types, $i = 1, \ldots, M$. One would get

$$P_R^{\text{single}}(T) = 1 - \exp\left[-\int_0^T \left(\sum_{i=1}^{M} \Phi_i(t,T)\right) \mathrm{d}t\right], \tag{4.32}$$

with Φ_i analogous to Φ_A and Φ_B above.

Double resistance

The procedure to obtain the probability of double resistance is similar to the above line of reasoning. The main difference is that there are now two sources, the two single resistant strains A and B. As before, we start by writing down the probability that double resistant cells either do not arise in $[t_k, t_k + \Delta t]$, or, if they do, that they and their lineage goes extinct by time T. This probability is

$$P_{0,t_k}^{\text{double}}(T) = \left[1 - \overline{W}_D(t_k)\Delta t\right] + \overline{W}_D(t_k)\Delta t P_{\text{ext},D}(t_k, T), \tag{4.33}$$

where $\overline{W}_D$ is the average production rate of mutants type D (from strains A or B), given in Eq. (4.5) in the main text. Following the same steps as before, the probability of having at least one double resistant cell at time T becomes

$$P_R^{\text{double}}(T) = 1 - \exp\left[-\int_0^T \left\{\Psi_A(t,T) + \Psi_B(t,T)\right\} \mathrm{d}t\right], \tag{4.34}$$

with

$$\begin{aligned} \Psi_A(t,T) &= b_A(t)\mu_B \bar{n}_A(t)\left[1 - P_{\text{ext},D}(t,T)\right], \\ \Psi_B(t,T) &= b_B(t)\mu_A \bar{n}_B(t)\left[1 - P_{\text{ext},D}(t,T)\right]. \end{aligned} \tag{4.35}$$

We stress again that this approach is based on a deterministic approximation for the production rates W_A, W_B and W_D. More specifically, these rates can – in principle – depend on the composition of the population, $\mathbf{n}$, which is a stochastic variable. In our approximation the components n_i of $\mathbf{n}$ are replaced with their mean values $\bar{n}_i$, resulting for example in the appearance of $\bar{n}_A$ and $\bar{n}_B$ in Eq. (4.35). If such an approximation is not made, then W_A, W_B and W_D are stochastic variables.

4.9 Appendix B: Probabilities of resistance for the exponential growth model (EG) with constant growth coefficients

The differential equations for the mean values of cell numbers for the exponential growth model (abbreviated 'EG' in the main paper) are given in Eq. (4.6) in the main text. For constant coefficients b_i and d_i they have the following analytical solutions

$$\begin{aligned}
\bar{n}_S(t) &= n_0 e^{r_S t}, \\
\bar{n}_A(t) &= \frac{n_0 b_S \mu_A}{r_S - r_A}\left(e^{r_S t} - e^{r_A t}\right), \\
\bar{n}_B(t) &= \frac{n_0 b_S \mu_B}{r_S - r_B}\left(e^{r_S t} - e^{r_B t}\right), \\
\bar{n}_D(t) &= n_0 b_S \mu_A \mu_B \times \\
&\left[\frac{1}{r_S - r_D}\left(\frac{b_A}{r_S - r_A} + \frac{b_B}{r_S - r_B}\right)\left(e^{r_S t} - e^{r_D t}\right) + \frac{b_A}{(r_S - r_A)(r_D - r_A)}\left(e^{r_A t} - e^{r_D t}\right)\right. \\
&\left. + \frac{b_B}{(r_S - r_B)(r_D - r_B)}\left(e^{r_B t} - e^{r_D t}\right)\right].
\end{aligned} \tag{4.36}$$

If $b_A = b_B = 0$ (strains A and B do not replicate), then $\bar{n}_D(t) = 0$. Also, for $\mu_A = \mu_B = 0$ there are no single or double mutants as there are no mutations.

Moreover, for constant birth and death rates the expression in Eq. (4.23) reduces to

$$P_{\text{ext},i}(t,T) = 1 - \frac{r_i}{b_i - d_i e^{-r_i(T-t)}}. \tag{4.37}$$

If $d_i = 0$, then $P_{\text{ext},i}(t,T) = 0$. We also note that the expression for $P_{\text{ext},i}(t,T)$ shows that as T grows, two possible types of behaviour can occur at fixed t:

(i) If $b_i > d_i$ ($r_i > 0$), then $P_{\text{ext},i}(t,T)$ tends to its maximum value d_i/b_i. The probability of extinction at long times is then less than one.

(ii) If $b_i < d_i$ ($r_i < 0$), then $P_{\text{ext},i}(t,T)$ tends to one as $T \to \infty$, i.e. extinction is certain in the long run.

For the simple case of constant birth and death rates model, it is also possible to derive analytical solutions for the probabilities of single and double resistance. For the former we get

$$P_R^{\text{single}}(T) = 1 - e^{-[\phi_A(T)+\phi_B(T)]}, \tag{4.38}$$

with

$$\phi_A(T) = \frac{n_0 b_S \mu_A r_A}{r_S b_A}\left[e^{r_S T}\,{}_2F_1\left(1, \frac{r_S}{r_A}; \frac{r_A+r_S}{r_A}; \frac{d_A}{b_A}\right) - {}_2F_1\left(1, \frac{r_S}{r_A}; \frac{r_A+r_S}{r_A}; \frac{d_A e^{-r_A T}}{b_A}\right)\right], \tag{4.39}$$

and

$$\phi_B(T) = \frac{n_0 b_S \mu_B r_B}{r_S b_B}\left[e^{r_S T}\,{}_2F_1\left(1, \frac{r_S}{r_B}; \frac{r_B+r_S}{r_B}; \frac{d_B}{b_B}\right) - {}_2F_1\left(1, \frac{r_S}{r_B}; \frac{r_B+r_S}{r_B}; \frac{d_B e^{-r_B T}}{b_B}\right)\right], \tag{4.40}$$

where ${}_2F_1$ is the Gaussian hypergeometric function (also known as the ordinary hypergeometric function). The terms ϕ_A and ϕ_B capture mutations from strain S to A or B, respectively. If at least one of the functions ϕ_A and ϕ_B tends to infinity as $T \to \infty$, then $P_R^{\text{single}}(T) \to 1$. This can happen if at least one of r_A or r_B is positive.

We also note that $P_R^{\text{single}}(T)$ is trivially zero if n_0 or b_S vanish (no reproduction of sensitive cells), or if μ_A and μ_B are both zero (no mutations).

For constant birth and death rates b_i and d_i the probability of double resistance becomes

$$P_R^{\text{double}}(T) = 1 - e^{-[\psi_A(T)+\psi_B(T)]}, \tag{4.41}$$

where

$$\psi_A(T) = \frac{n_0 b_A \mu_B r_D b_S \mu_A}{b_D(r_S - r_A)}\left[\psi(r_S, r_D) - \psi(r_A, r_D)\right] \tag{4.42}$$

and

$$\psi_B(T) = \frac{n_0 b_B \mu_B r_D b_S \mu_A}{b_D(r_S - r_B)}\left[\psi(r_S, r_D) - \psi(r_B, r_D)\right]. \tag{4.43}$$

We have defined

$$\psi(r_l, r_D) = \frac{1}{r_\ell}\left[e^{r_\ell T}\,{}_2F_1\left(1, \frac{r_\ell}{r_D}; \frac{r_\ell+r_D}{r_D}; \frac{d_D}{b_D}\right) - {}_2F_1\left(1, \frac{r_\ell}{r_D}; \frac{r_\ell+r_D}{r_D}; \frac{d_D e^{-r_D T}}{b_D}\right)\right], \tag{4.44}$$

for $\ell = S, A, B$. The terms ψ_A and ψ_B take into account contributions from strains A and B that mutate into strain D, respectively. If n_0 or b_S vanish (no growth of sensitive cells), or μ_A and μ_B are zero (no mutations), or both b_A or b_B are zero (no growth of single resistant strains), then $P_R^{\text{double}}(T) = 0$, i.e., double resistance does not emerge.

4.10 Appendix C: Probabilities of resistance for the logistic growth model without competition between strains (LG)

4.10.1 Constant coefficients

Mean number of sensitive cells

For constant drug concentrations, the functions $d_i(t)$ (death rate) and $\rho_i(t)$ (intrinsic growth rate) are constant in time. The birth rate $b_i(t)$, however, depends on $n_i(t)$, so it is not constant [see Eq. (4.7) of the main paper].

For this model, there is no analytical solution to the differential equations for the mean cell numbers [Eqs. (4.1) in the main paper], except for strain S, for which one finds the logistic function

$$\bar{n}_S(t) = \frac{k_S}{1 + (k_S/n_0 - 1)\, e^{-\rho_S t}}. \tag{4.45}$$

For the other strains, it is necessary to integrate the equations for the mean cell numbers numerically.

Extinction probability for a single-species logistic birth-death process

In this section we derive a closed-form solution for the probability of extinction, $P_{\text{ext},i}$ of a single-species logistic birth-death process with time dependent rates. To do this, we follow a procedure similar to the one in [33] for the Gompertz model.

We focus on strain i, and start from the birth rate

$$b_i(t) = d_i + \rho_i \left(1 - \frac{\bar{n}_i(t)}{k_i}\right), \tag{4.46}$$

in which we have made the deterministic approximation, i.e., we have replaced the number of cells of type i by its mean value. This turns the birth rate into a time-dependent external function. The death rate d_i is constant, as is the rate ρ_i. However, the actual births and deaths are treated as stochastic events.

We label time by t' and assume that at a certain time $t' = t$ there is only one individual, $\bar{n}_i(t' = t) = 1$. The function $\bar{n}_i(t')$ follows the differential equation

$$\frac{\mathrm{d}\bar{n}_i}{\mathrm{d}t'}(t') = \rho_i \left(1 - \frac{\bar{n}_i(t')}{k_i}\right) \bar{n}_i(t'). \tag{4.47}$$

The solution of this equation, subject to the condition $\bar{n}_i(t' = t) = 1$, is

$$\bar{n}_i(t') = \frac{k_i}{1 + (k_i - 1)\, e^{-\rho_i (t' - t)}}. \tag{4.48}$$

Then, using Eq. (4.19), we write

$$\beta_i\,(t, t') = \log\, \bar{n}_i(t'), \tag{4.49}$$

so that,

$$\begin{aligned} \int_t^T d_i e^{-\beta_i(t,t')} \mathrm{d}t' &= d_i \int_t^T \frac{1}{\bar{n}_i(t')} \mathrm{d}t' \\ &= \frac{d_i}{k_i} \left[(T - t) - \frac{(k_i - 1)}{r_i} \left(e^{-\rho_i (T-t) - 1} \right) \right]. \end{aligned} \tag{4.50}$$

Finally, putting all together in Eq. (4.23), we obtain

$$P_{\mathrm{ext},i}(t, T) = \frac{\dfrac{d_i}{k_i} \left[(T - t) - \dfrac{(k_i - 1)}{\rho_i} \left(e^{-\rho_i (T-t)} - 1 \right) \right]}{\dfrac{d_i}{k_i} \left[(T - t) - \dfrac{(k_i - 1)}{\rho_i} \left(e^{-\rho_i (T-t)} - 1 \right) \right] + 1}. \tag{4.51}$$

This is the extinction probability for a single individual and its lineage in a single-species logistic growth model with constant coefficients ρ_i and d_i. Trivially, $P_{\mathrm{ext},i}(t, T) = 0$ for $d_i = 0$.

Single resistance

For the logistic model without competition between strains (LG), the average production rates of strains A and B are given by

$$\overline{W}_A(t) = \left[d_S + \rho_S \left(1 - \frac{\bar{n}_S(t)}{k_S} \right) \right] \mu_A \bar{n}_S(t) \tag{4.52}$$

$$\overline{W}_B(t) = \left[d_S + \rho_S\left(1 - \frac{\bar{n}_S(t)}{k_S}\right)\right]\mu_B\bar{n}_S(t). \tag{4.53}$$

We focus again on the case of constant coefficients d_i and ρ_i. Using the closed-form solution in Eq. (4.51) for the extinction probability, we use Eq. (4.31) to write

$$\Phi_A(t,T) = \frac{\left[d_S + \rho_S\left(1 - \frac{\bar{n}_S(t)}{k_S}\right)\right]\mu_A\bar{n}_S(t)}{\frac{d_A}{k_A}\left[(T-t) - \frac{(k_A-1)}{\rho_A}\left(e^{-\rho_A(T-t)} - 1\right)\right] + 1}, \tag{4.54}$$

and

$$\Phi_B(t,T) = \frac{\left[d_S + \rho_S\left(1 - \frac{\bar{n}_S(t)}{k_S}\right)\right]\mu_B\bar{n}_S(t)}{\frac{d_B}{k_B}\left[(T-t) - \frac{(k_B-1)}{\rho_B}\left(e^{-\rho_B(T-t)} - 1\right)\right] + 1}. \tag{4.55}$$

In these expressions, $\bar{n}_S$ is a logistic function with initial condition $\bar{n}_S(t=0) = n_0$ and growth rate ρ_S, i.e. $\bar{n}_S(t) = k_S/\left(1 + (k_S/n_0)e^{-\rho_S t}\right)$.

The expressions for Φ_A and Φ_B are integrated with respect to t in Eq. (4.30). Even though we can write down Φ_A and Φ_B in the above form, we have not been able to find an analytical solution for these integrals. The probability of single resistance is obtained by performing these integrals numerically.

Double resistance

For constant coefficients, the production rate of strain D in Eq. (4.5) of the main paper takes the form

$$\overline{W}_D(t) = \left[d_A + \rho_A\left(1 - \frac{\bar{n}_A(t)}{k_A}\right)\right]\mu_B\bar{n}_A(t) + \left[d_B + \rho_B\left(1 - \frac{\bar{n}_B(t)}{k_B}\right)\right]\mu_A\bar{n}_B(t), \tag{4.56}$$

for the logistic growth model with no competition between strains. Eqs. (4.17) and (4.18) become

$$\Psi_A(t,T) = \frac{\left[d_A + \rho_A\left(1 - \frac{\bar{n}_A(t)}{k_A}\right)\right]\mu_B\bar{n}_A(t)}{\frac{d_D}{k_D}\left[(T-t) - \frac{(k_D-1)}{\rho_D}\left(e^{-\rho_D(T-t)} - 1\right)\right] + 1}, \tag{4.57}$$

and

$$\Psi_B(t,T) = \frac{\left[d_B + \rho_B\left(1 - \frac{\bar{n}_B(t)}{k_B}\right)\right]\mu_A\bar{n}_B(t)}{\frac{d_D}{k_D}\left[(T-t) - \frac{(k_D-1)}{\rho_D}\left(e^{-\rho_D(T-t)} - 1\right)\right] + 1}. \tag{4.58}$$

While the function $\bar{n}_S(t)$ is available in closed form [see Eq. (4.45)], no analytical solutions were found for $\bar{n}_A(t)$ and $\bar{n}_B(t)$. This is because the single resistant types are produced from S, and $\bar{n}_S$ itself is a time-dependent quantity. The functions $\bar{n}_A(t)$ and $\bar{n}_B(t)$ are therefore obtained by numerical integration of the differential equations (4.1) in the main paper.

4.10.2 Time-dependent rates

We now assume that the rates $d_i(t)$ and $\rho_i(t)$ in Eq. (4.7) of the main text are functions of time. In order to obtain the extinction probability in an effective way, we use Eq. (4.49) to write Eq. (4.23) as

$$P_{\text{ext},i}(t,T) = \frac{\int_t^T \frac{d_i\,(t')}{\bar{n}_i\,(t')}\mathrm{d}t'}{1+\int_t^T \frac{d_i\,(t')}{\bar{n}_i\,(t')}\mathrm{d}t'}, \tag{4.59}$$

with $\bar{n}_i\,(t')$ as in Eq. (4.20), see also Sec. 4.3.4 of the main paper.

To derive Eq. (4.20), i.e. to express the solutions for $\bar{n}_i\,(t')$ (with initial condition $\bar{n}_i(t)=1$) in terms of solutions $\bar{n}_i^0\,(t')$ (with $\bar{n}_i^0(0)=0$), we integrate Eq. (4.47) to obtain

$$\bar{n}_i\,(t') = \frac{k_i}{(k_i-1)e^{-\int_t^{t'}\rho_i(t'')\mathrm{d}t''}+1}. \tag{4.60}$$

Similarly,

$$\bar{n}_i^0\,(t') = \frac{k_i}{(k_i-1)e^{-\int_0^{t'}\rho_i(t'')\mathrm{d}t''}+1}, \tag{4.61}$$

such that $\bar{n}_i^0(0)=1$. From this, we get

$$e^{-\int_0^{t'}\rho_i(t'')\mathrm{d}t''} = \frac{k_i/\bar{n}_i^0\,(t')-1}{k_i-1}, \tag{4.62}$$

and then

$$e^{-\int_t^{t'}\rho_i(t'')\mathrm{d}t''} = \frac{k_i/\bar{n}_i^0\,(t')-1}{k_i/\bar{n}_i^0(t)-1}. \tag{4.63}$$

Inserting this result into Eq. (4.60) gives Eq. (4.20) in the main text, i.e.,

$$\bar{n}_i\,(t'\geq t) = \frac{k_i\left(\frac{k_i}{\bar{n}_i^0(t)}-1\right)}{(k_i-1)\left(\frac{k_i}{\bar{n}_i^0\,(t')}-1\right)+\left(\frac{k_i}{\bar{n}_i^0(t)}-1\right)}. \tag{4.64}$$

The probabilities of resistance are then obtained by performing the integrals in Eqs. (4.30) and (4.34) numerically.

4.11 Appendix D: Probabilities of resistance for the logistic model with between-strain competition (CLG)

As explained in Section 4.4.1 of the main paper, we have not been able to derive analytical solutions of the mean cell numbers for the logistic growth model with competition between the strains. This is due to the coupling of the equations for the different $\bar{n}_i$, see Eq. (4.1) in the main paper, and the rates in Eq. (4.8). Because of the lack of closed form expressions for the $\bar{n}_i$ we cannot find an analytical solution for the extinction probability $P_{\text{ext},i}$ either, i.e., there is no closed-form equivalent of Eq. (4.51) in the CLG model, even when the coefficients d_i and ρ_i are constant.

As a consequence the $\bar{n}_i(t)$ are obtained from numerical integration of the differential equations for the mean cell numbers [Eq. (4.1)]. The extinction probabilities are then obtained from Eq. (4.59), where the required integral is again evaluated numerically. The integration is carried out by applying the strategy described in Section 4.3.4 of the main paper. We detail below how to apply it for the CLG model. This procedure is used both for constant and time-dependent coefficients d_i and ρ_i.

In order to calculate $P_{\text{ext},i}$, we focus on a single species following a birth-death process with birth rate

$$b_i(t) = \begin{cases} d_i(t) + \rho_i(t)\left(1 - \dfrac{\bar{n}_T(t)}{k_i}\right) & \text{if} \quad \bar{n}_T(t) \leq k_i \\ d_i(t) & \text{if} \quad \bar{n}_T(t) > k_i, \end{cases} \tag{4.65}$$

where $d_i(t)$ is a given death rate, and $\rho_i(t)$ the intrinsic birth rate of species i. As explained in Section 4.3.4, to obtain the extinction probability in an efficient manner we need to express solutions $\bar{n}_i\,(t')$ with initial condition $\bar{n}_i(t' = t) = 1$ in terms of solutions $\bar{n}_i^0(t')$ that satisfy $\bar{n}_i^0(t' = 0) = 1$. Notice that, although the focus is on species i, we cannot ignore the effect of the remaining species for the model with competition between strains: the function $\bar{n}_T(t')$ in Eq. (4.65) accounts for the mean value of the total number of cell across all species. The function $\bar{n}_i(t')$ follows

$$\frac{\mathrm{d}\bar{n}_i}{\mathrm{d}t'}(t') = \rho_i(t')\left(1 - \frac{\bar{n}_T(t')}{k_i}\right)\bar{n}_i(t'). \tag{4.66}$$

To proceed, we treat $\bar{n}_T(t')$ on the right hand-side of Eq. (4.66) as a given function.

Formally integrating we then obtain

$$\bar{n}_i(t') = \exp\left\{\int_t^{t'} \rho_i(t'') \left(1 - \frac{\bar{n}_T(t'')}{k_i}\right) \mathrm{d}t''\right\}, \tag{4.67}$$

where we note the initial condition $\bar{n}_i(t' = t) = 1$ The solution $\bar{n}_i^0(t')$ with condition $\bar{n}_i^0(0) = 0$ (see Section 4.3.4 of the main paper) is given by

$$\bar{n}_i^0(t') = \exp\left\{\int_0^{t'} \rho_i(t'') \left(1 - \frac{\bar{n}_T(t'')}{k_i}\right) \mathrm{d}t''\right\}. \tag{4.68}$$

Using these one obtains

$$\bar{n}_i(t' \geq t) = \frac{\bar{n}_i^0(t')}{\bar{n}_i^0(t)}, \tag{4.69}$$

with which $P_{\mathrm{ext},i}$ is obtained from Eq. (4.59) and from it, the probabilities of single and double resistance from Eqs. (4.30) and (4.34).

4.12 Appendix E: Further supplementary results

In this section, we present additional data from simulations and from the analytical approach. These complement the results in the main paper.

4.12.1 Probability of double resistance for constant growth rates

Figure 4.8 complements Fig. 4.4. It shows how the probability of double resistance, P_R^{double}, differs across the different growth models as a function of parameters not varied in Fig. 4.4. As in Fig. 4.4 parameters are varied in turn, i.e., all but the one shown on the vertical axis are kept fixed.

The data in the figure shows that varying d_A the emergence of double resistance shows a noticeable delay in the CLG model compared to the other two growth models. When only μ_A varies, however, all the models have similar probability of double resistance. This is because μ_B is high enough that double resistance does not get affected. This example shows that competition may not significantly affect the emergence of double resistance in some circumstances.

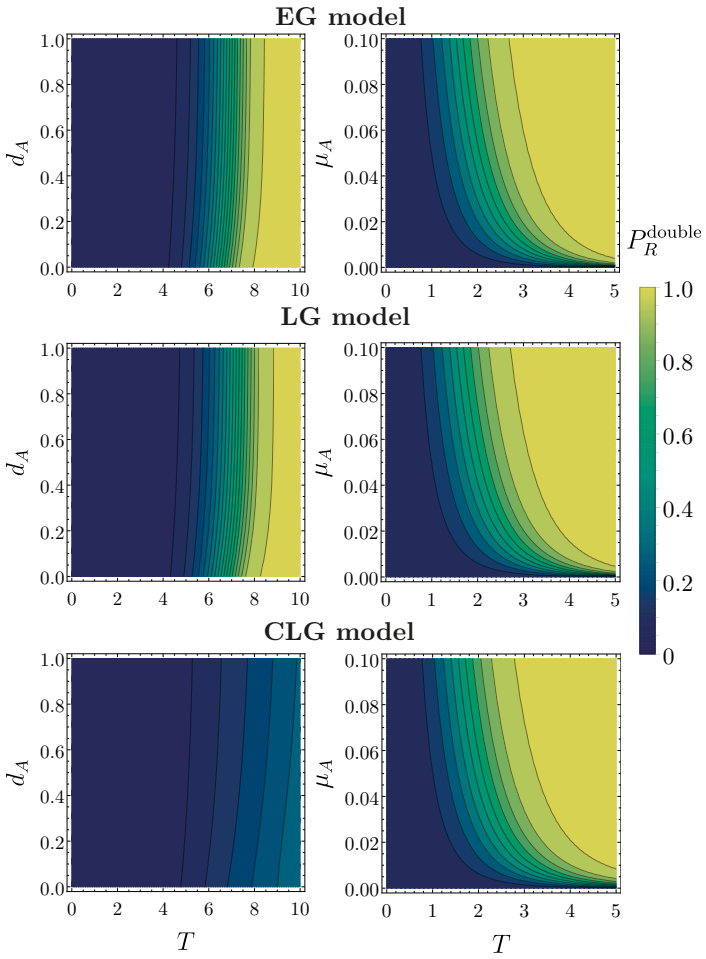

Figure 4.8: Theoretical prediction of the probability of double resistance for the three growth models when varying one parameter. When not varied, we use the same parameters as in Figure 4.4 of the main text, i.e. $b_S = 1.0, b_A = 1.1, b_B = 1.2, b_D = 1.3, d_S = d_A = d_B = d_D = 0.1, \mu_A = \mu_B = 10^{-4}$, $n_0 = 10^4$, $k_S = 10^6, k_A = 1.1 \times 10^6, k_B = 1.2 \times 10^6$, and $k_D = 1.3 \times 10^6$.

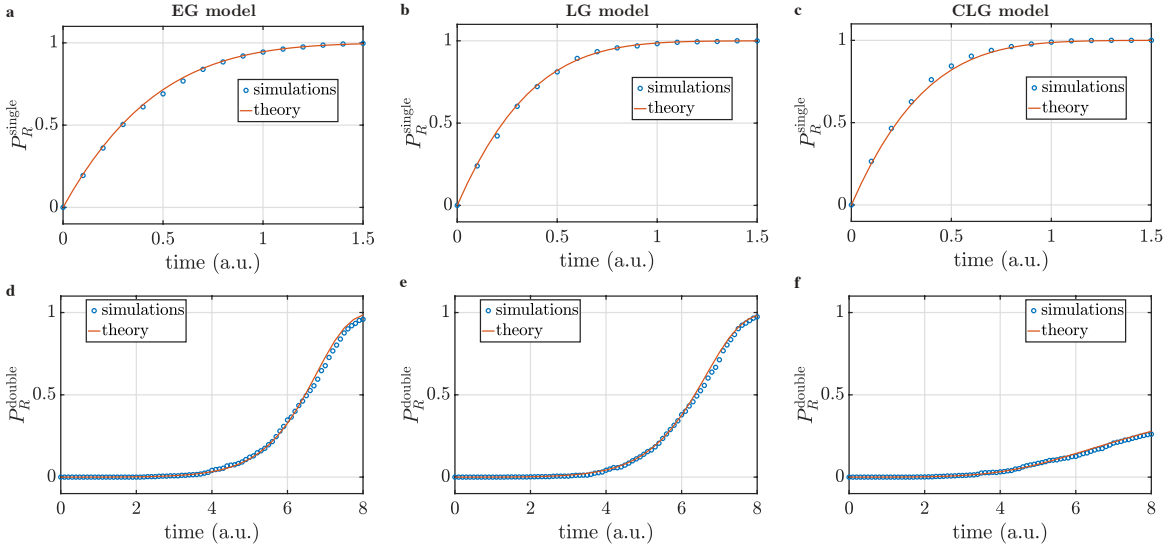

Figure 4.9: Probabilities of single and double resistance for the same parameters as in Figure 4.4 of the main text but with $d_S = 0.5$.

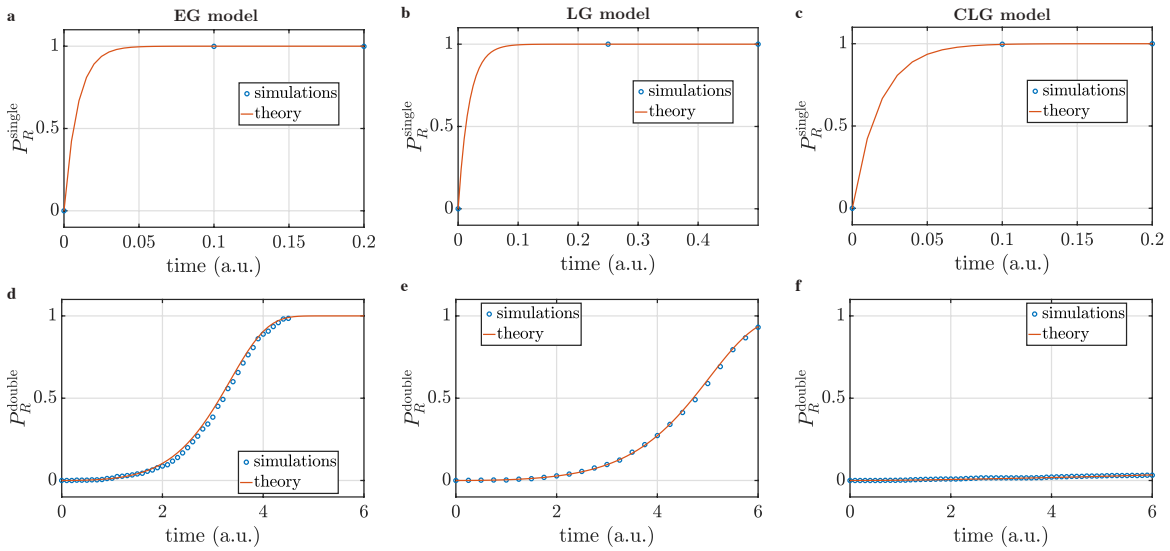

Figure 4.10: Probabilities of single and double resistance for the same parameters as in Figure 4.4 of the main text but with $n_0 = 5 \times 10^5$.

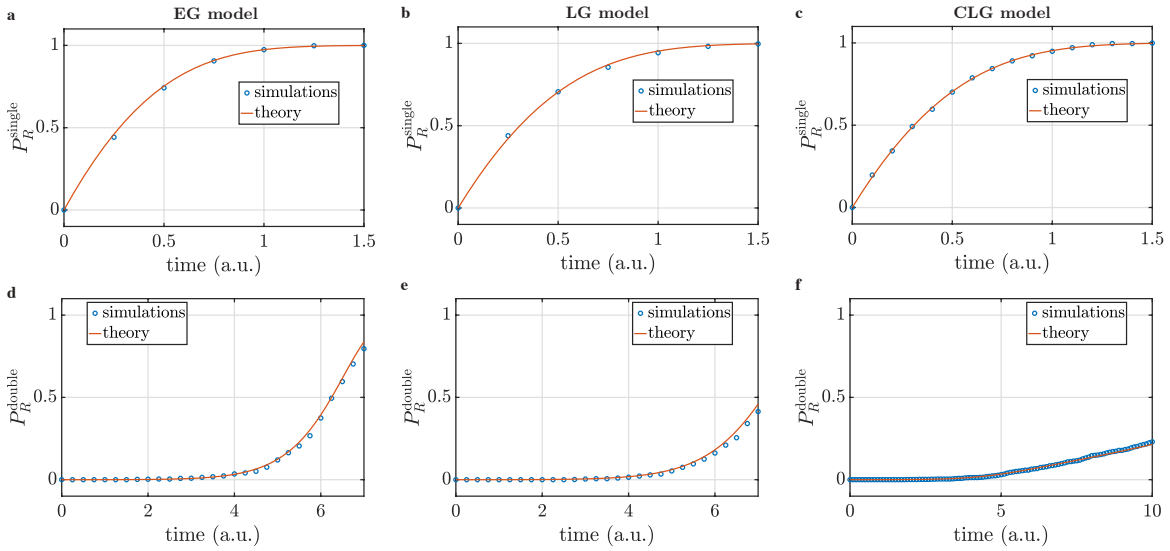

Figure 4.11: Probabilities of single and double resistance for same parameters as in Figure 4.4 of the main text but with $r_A = 0.1$.

4.12.2 Further tests of theoretical predictions for resistance against numerical simulations

In Figs. 4.9–4.11 we show data similar to that in Fig. 4.1 in the main paper, but for different choices of the model parameters. The figure shows the probabilities of single and double resistance as a function of time, both from simulations and as predicted

from the theory. The parameters in Figs. 4.9–4.11 are chosen such that they produce a noticeable difference in the prediction of double resistance relative to the results in Fig. 4.1, in particular for the model with competition between strains. We do this based on the results presented in Fig. 4.4 of the main paper, i.e., we select parameter values such that the delay in the emergence of double resistants is noticeably higher than with the parameters from Fig. 4.1.

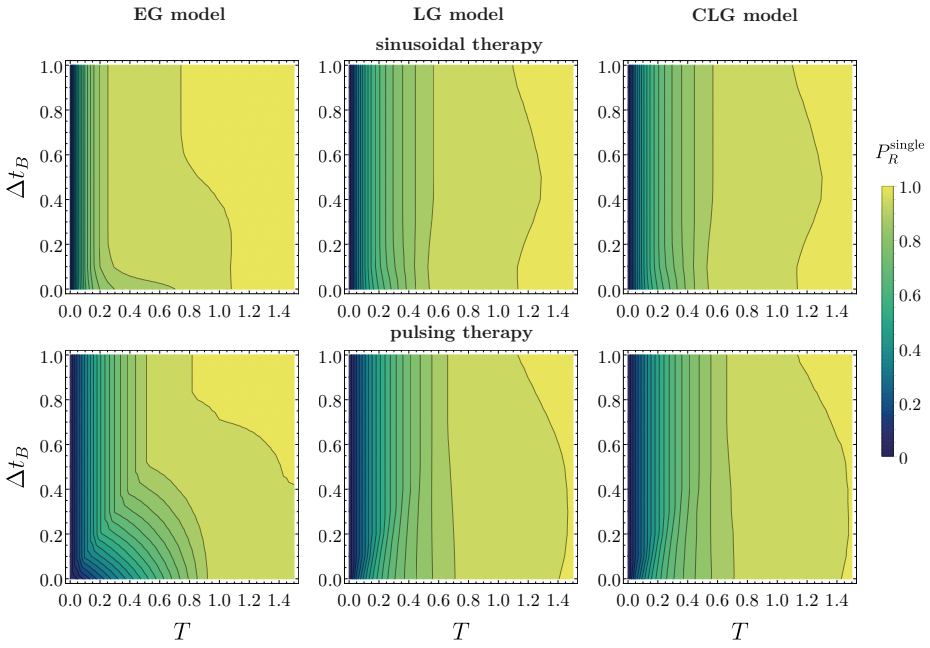

Figure 4.12: Theoretical prediction of single resistance for sinusoidal and pulsing drug therapies for parameters of Figure 4.7 from the main text: $b_S = b_A = b_B = b_D = 1.1, d_S = d_A = d_B = d_D = 0.1, \mu_A = \mu_B = 10^{-3}$, $n_0 = 5 \times 10^3$, $k_S = 10^4, k_A = 1.1 \times 10^4, k_B = 1.2 \times 10^4$, and $k_D = 1.3 \times 10^4$.

4.12.3 Probability of single and double resistance for time-dependent dosing schedules

In this section, we complement the results for the probabilities of single and double resistance shown in Section 4.7.

In Fig. 4.12, we show the theoretical prediction for the probability of single resistance using the same parameters and dosing schedules (sinusoidal and pulsing therapies) as in Fig. 4.7 of the main paper. As shown, the probability of single resistance is noticeably different in the exponential model than for the two models with logistic growth. Therefore it is important to consider carefully the choice of growth model

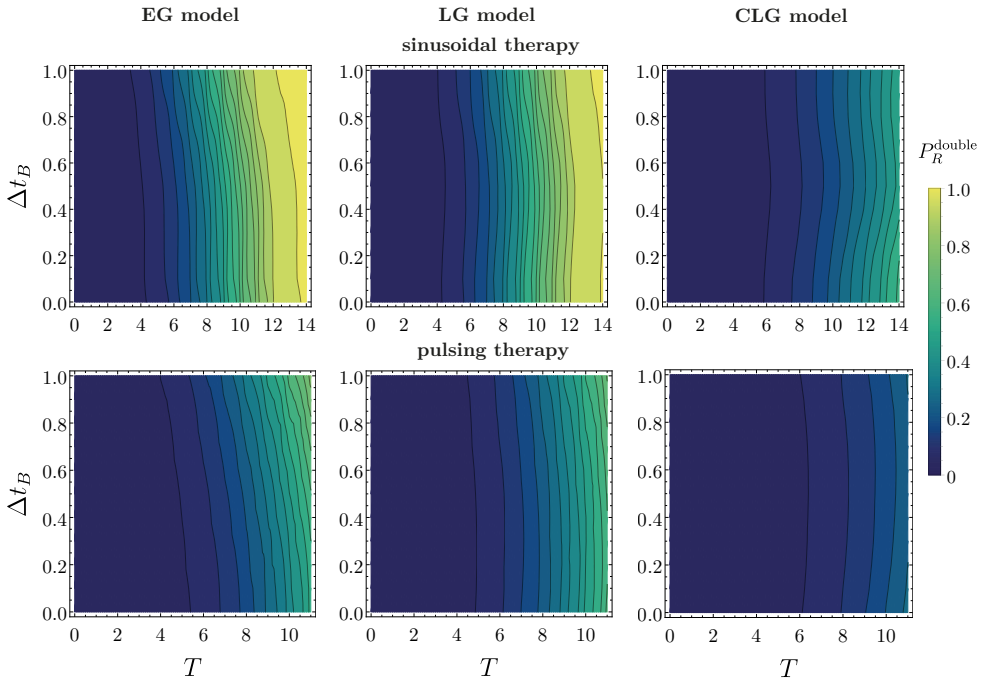

Figure 4.13: Theoretical prediction of the probability of double resistance for sinusoidal and pulsing drug therapies for parameters of Figure 4.7 from the main text: $b_S = b_A = b_B = b_D = 1.1, d_S = d_A = d_B = d_D = 0.1, \mu_A = \mu_B = 10^{-3}$, $n_0 = 5 \times 10^3$, $k_S = 10^4, k_A = 1.1 \times 10^4, k_B = 1.2 \times 10^4$, and $k_D = 1.3 \times 10^4$

to best describe a given biological system. If an exponential model is used, but the real-world system is subject to restricted growth then the prediction for example of the typical time at which first resistants emerge may not be accurate. Further, the value of Δt_B that optimises the treatment (most delays the emergence of single resistance) and the typical time at which the first single mutants emerge are both different in the exponential growth model than in the two logistic models.

In Figures 4.13 and 4.14, we re-plot data shown in Fig. 4.7 of the main paper. We now illustrate more clearly the effect of changing Δt_B in each growth model. Figure 4.13 demonstrates that the emergence of double resistance is considerably delayed by competition. In Fig. 4.14 we show the probability of double resistance, $P_R^{\text{double}}(T)$, as function of Δt_B for a given time T. This is shown for each of the three growth models, and for the sinusoidal and pulsing periodic treatments. The figure demonstrates that the optimum treatment is different for each of the three growth models.

In Fig. 4.15 finally we show the probability of double resistance with a higher initial sensitive cell number and higher carrying capacities values for each strain than in Fig. 4.7. For these parameters, the prediction of the competition model shows a more

pronounced difference than the prediction in Fig. 4.7 when varying Δt_B.

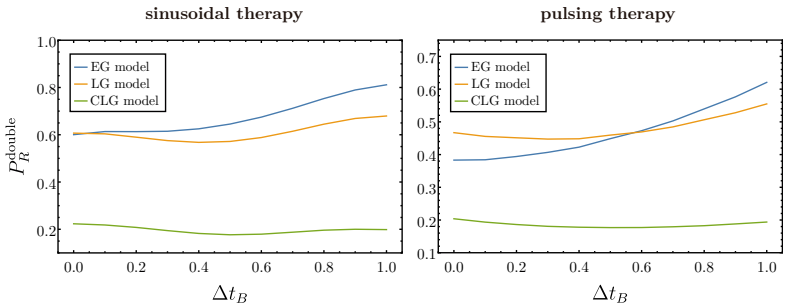

Figure 4.14: Theoretical prediction of the probability of double resistance for each growth model during sinusoidal (left panel) and pulsing therapy (right panel) as a function of Δt_B at time $T = 10$ after the treatment started. Parameters used are the same in Figure 4.7 from the main text: $b_S = b_A = b_B = b_D = 1.1, d_S = d_A = d_B = d_D = 0.1, \mu_A = \mu_B = 10^{-3}$, $n_0 = 5 \times 10^3$, $k_S = 10^4, k_A = 1.1 \times 10^4, k_B = 1.2 \times 10^4$, and $k_D = 1.3 \times 10^4$.

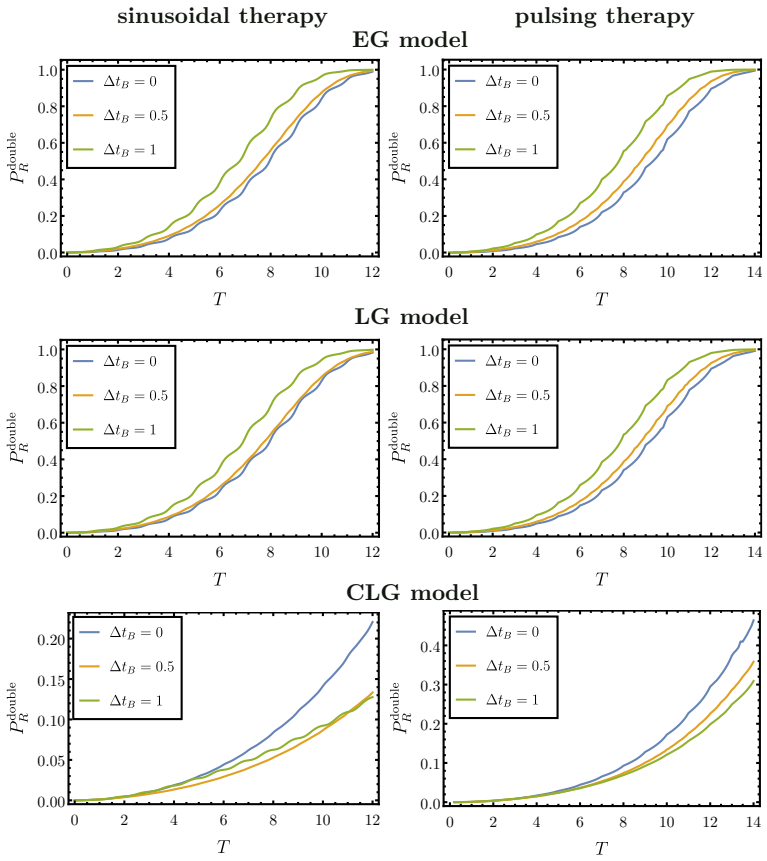

Figure 4.15: Theoretical prediction of the probability of double resistance for each growth model when varying Δt_B for sinusoidal and pulsing therapies. Parameters used: $b_S = b_A = b_B = b_D = 1.1, d_S = d_A = d_B = d_D = 0.1, \mu_A = \mu_B = 10^{-3}$, $n_0 = 10^4$, $k_S = 10^5, k_A = 1.1 \times 10^4, k_B = 1.2 \times 10^4$, and $k_D = 1.3 \times 10^4$.

4.13 Appendix F: Limitations of the analytical approach

In Fig. 4.16, we show an instance in which the theoretical predictions for the probability of double resistance deviate from results from simulations. Specifically, we have chosen smaller birth rates for each strain in panel (a), and smaller mutation rates in panels (b) and (c) than in Fig. 4.1 of the main paper. In either case, the overall effect is a delay in the emergence of double resistants. As explained in Section 4.6 the theoretical predictions then become less accurate.

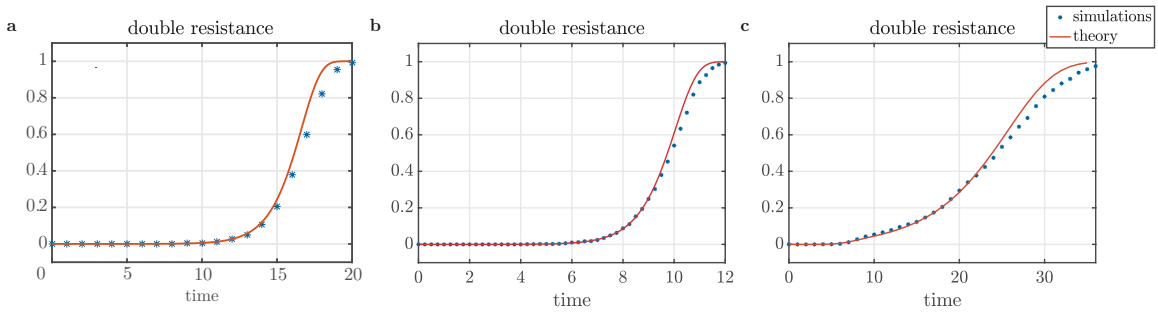

Figure 4.16: Theoretical prediction of double resistance for: (a) Exponential growth model for parameters: $b_S = 0.5, b_A = 0.8, b_B = 0.9, b_D = 1.0, d_S = d_A = d_B = d_D = 0.1, \mu_A = 10^{-6}, \mu_B = 10^{-4}$, $n_0 = 10^4$. (b) Non-competitive growth model for parameters: $b_S = 1.1, b_A = 1.2, b_B = 1.3, b_D = 1.4, d_S = d_A = d_B = d_D = 0.1, \mu_A = \mu_B = 10^{-5}, k_S = 10^7, k_A = 1.1 \times 10^7, k_B = 1.2 \times 10^7$, and $k_D = 1.3 \times 10^7$. (c) Competitive growth model for parameters: $b_S = 1.1, b_A = 1.2, b_B = 1.3, b_D = 1.4, d_S = d_A = d_B = d_D = 0.1, \mu_A = \mu_B = 10^{-5}, k_S = 10^7, k_A = 1.1 \times 10^7, k_B = 1.2 \times 10^7$, and $k_D = 1.3 \times 10^7$.

Bibliography

[1] V. T. Devita Jr, R. C. Young, and G. P. Canellos, "Combination versus single agent chemotherapy: a review of the basis for selection of drug treatment of cancer", Cancer **35**, 98–110 (1975).

[2] S. Bonhoeffer, M. Lipsitch, and B. R. Levin, "Evaluating treatment protocols to prevent antibiotic resistance", Proceedings of the National Academy of Sciences **94**, 12106–12111 (1997).

[3] D. M. Livermore, "Minimising antibiotic resistance", The Lancet Infectious Diseases **5**, 450–459 (2005).

[4] M. Baym, L. K. Stone, and R. Kishony, "Multidrug evolutionary strategies to reverse antibiotic resistance", Science **351**, aad3292 (2016).

[5] D. D. Richman, "HIV chemotherapy", Nature **410**, 995 (2001).

[6] F. Nosten, and N. J. White, "Artemisinin-based combination treatment of falciparum malaria", The American Journal of Tropical Medicine and Hygiene **77**, 181–192 (2007).

[7] D. Mitchison, and G. Davies, "The chemotherapy of tuberculosis: past, present and future", The International Journal of Tuberculosis and Lung Disease **16**, 724–732 (2012).

[8] R. Krašovec, H. Richards, D. R. Gifford, C. Hatcher, K. J. Faulkner, R. V. Belavkin, A. Channon, E. Aston, A. J. McBain, and C. G. Knight, "Spontaneous mutation rate is a plastic trait associated with population density across domains of life", PLoS Biology **15**, e2002731 (2017).

[9] P. Yeh, A. I. Tschumi, and R. Kishony, "Functional classification of drugs by properties of their pairwise interactions", Nature Genetics **38**, 489 (2006).

[10] R. Peña-Miller, D. Laehnemann, G. Jansen, A. Fuentes-Hernandez, P. Rosenstiel, H. Schulenburg, and R. Beardmore, "When the most potent combination of antibiotics selects for the greatest bacterial load: the smile-frown transition", PLoS Biology **11**, e1001540 (2013).

[11] P. M. Altrock, L. L. Liu, and F. Michor, "The mathematics of cancer: integrating quantitative models", Nature Reviews Cancer **15**, 730–745 (2015).

[12] H. K. Alexander, and S. Bonhoeffer, "Pre-existence and emergence of drug resistance in a generalized model of intra-host viral dynamics", Epidemics **4**, 187–202 (2012).

[13] A. M. Niewiadomska, B. Jayabalasingham, J. C. Seidman, L. Willem, B. Grenfell, D. Spiro, and C. Viboud, "Population-level mathematical modeling of antimicrobial resistance: a systematic review", BMC Medicine **17**, 81 (2019).

[14] F. Michor, M. A. Nowak, and Y. Iwasa, "Evolution of resistance to cancer therapy", Current Pharmaceutical Design **12**, 261–271 (2006).

[15] Y. Iwasa, F. Michor, and M. A. Nowak, "Evolutionary dynamics of escape from biomedical intervention", Proceedings of the Royal Society of London. Series B: Biological Sciences **270**, 2573–2578 (2003).

[16] Y. Iwasa, F. Michor, and M. A. Nowak, "Evolutionary dynamics of invasion and escape", Journal of Theoretical Biology **226**, 205–214 (2004).

[17] Y. Iwasa, M. A. Nowak, and F. Michor, "Evolution of resistance during clonal expansion", Genetics **172**, 2557–2566 (2006).

[18] H. Haeno, Y. Iwasa, and F. Michor, "The evolution of two mutations during clonal expansion", Genetics **177**, 2209–2221 (2007).

[19] J. Foo, and F. Michor, "Evolution of resistance to anti-cancer therapy during general dosing schedules", Journal of Theoretical Biology **263**, 179–188 (2010).

[20] S. Chakrabarti, and F. Michor, "Pharmacokinetics and drug interactions determine optimum combination strategies in computational models of cancer evolution", Cancer Research **77**, 3908–3921 (2017).

[21] I. Bozic, J. G. Reiter, B. Allen, T. Antal, K. Chatterjee, P. Shah, Y. S. Moon, A. Yaqubie, N. Kelly, D. T. Le, et al., "Evolutionary dynamics of cancer in response to targeted combination therapy", eLife **2**, e00747 (2013).

[22] H. K. Alexander, and C. MacLean, "Stochastic bacterial population dynamics prevent the emergence of antibiotic resistance within the mutant selection window", bioRxiv **458547** (2019).

[23] J. Monod, "The growth of bacterial cultures", Annual Review of Microbiology **3**, 371–394 (1949).

[24] R. C. Allen, J. Engelstädter, S. Bonhoeffer, B. A. McDonald, and A. R. Hall, "Reversing resistance: different routes and common themes across pathogens", Proceedings of the Royal Society B: Biological Sciences **284**, 20171619 (2017).

[25] N. T. Bailey, *The elements of stochastic processes with applications to the natural sciences*, Vol. 25 (John Wiley & Sons, New York, 1990).

[26] P. A. Hoskisson, and G. Hobbs, "Continuous culture–making a comeback?", Microbiology **151**, 3153–3159 (2005).

[27] S. Moreno-Gamez, A. L. Hill, D. I. S. Rosenbloom, D. A. Petrov, M. A. Nowak, and P. S. Pennings, "Imperfect drug penetration leads to spatial monotherapy and rapid evolution of multidrug resistance", Proceedings of the National Academy of Sciences of the United States of America **112**, E2874 (2015).

[28] A. Feder, K. Harper, and P. S. Pennings, "Challenging conventional wisdom on the evolution of resistance to multi-drug HIV treatment: Lessons from data and modeling", bioRxiv **807560** (2019).

[29] T. W. Schoener, "Alternatives to Lotka-Volterra competition: models of intermediate complexity", Theoretical Population Biology **10**, 309–333 (1976).

[30] V. H. Smith, and R. D. Holt, "Resource competition and within-host disease dynamics", Trends in Ecology & Evolution **11**, 386–389 (1996).

[31] V. Smith, "Host resource supplies influence the dynamics and outcome of infectious disease", Integrative and Comparative Biology **47**, 310–316 (2007).

[32] C. E. Smith, and H. Tuckwell, "Some stochastic growth processes", in *Mathematical Problems in Biology* (Springer, Heidelberg, 1974), pp. 211–225.

[33] P. Parthasarathy, and B. Krishna Kumar, "A birth and death process with logistic mean population", Communications in Statistics-Theory and Methods **20**, 621–629 (1991).

[34] N. S. Goel, and N. Richter-Dyn, *Stochastic models in biology* (Elsevier, New York, 2016).

[35] J. H. Matis, and T. R. Kiffe, "On approximating the moments of the equilibrium distribution of a stochastic logistic model", Biometrics **52**, 980–991 (1996).

[36] J. H. Matis, T. R. Kiffe, E. Renshaw, and J. Hassan, "A simple saddlepoint approximation for the equilibrium distribution of the stochastic logistic model of population growth", Ecological Modelling **161**, 239–248 (2003).

[37] J. H. Matis, T. R. Kiffe, and P. Parthasarathy, "On the cumulants of population size for the stochastic power law logistic model", Theoretical Population Biology **53**, 16–29 (1998).

[38] S. E. Jørgensen, and B. D. Fath, *Encyclopedia of Ecology* (Elsevier, Amsterdam, 2014).

[39] M. E. Gilpin, and F. J. Ayala, "Global models of growth and competition", Proceedings of the National Academy of Sciences **70**, 3590–3593 (1973).

[40] D. R. Gifford, E. Berríos-Caro, C. Joerres, T. Galla, and C. G. Knight, "Mutators drive evolution of multi-resistance to antibiotics", bioRxiv **643585** (2019).

[41] M. A. Kohanski, D. J. Dwyer, and J. J. Collins, "How antibiotics kill bacteria: from targets to networks", Nature Reviews Microbiology **8**, 423–435 (2010).

[42] E. Parzen, *Stochastic processes* (SIAM, San Francisco, 1999).

[43] D. T. Gillespie, "Exact stochastic simulation of coupled chemical reactions", The Journal of Physical Chemistry **81**, 2340–2361 (1977).

[44] D. T. Gillespie, "A general method for numerically simulating the stochastic time evolution of coupled chemical reactions", Journal of Computational Physics **22**, 403–434 (1976).

[45] P. W. Lewis, and G. S. Shedler, "Simulation of nonhomogeneous Poisson processes by thinning", Naval Research Logistics Quarterly **26**, 403–413 (1979).

[46] Y. Chen, *Thinning Algorithms for Simulating Point Processes*, 2016.

[47] L. Shargel, S. Wu-Pong, and A. B. C. Yu, *Applied Biopharmaceutics & Pharmacokinetics*, 5th ed. (Appleton & Lange Reviews/McGraw-Hill, Medical Pub. Division, New York, 2004).

[48] K. H. Ibrahim, B. W. Gunderson, E. D. Hermsen, L. B. Hovde, and J. C. Rotschafer, "Pharmacodynamics of Pulse Dosing versus Standard Dosing: In Vitro Metronidazole Activity against Bacteroides fragilis and Bacteroides thetaiotaomicron", Antimicrobial Agents and Chemotherapy **48**, 4195–4199 (2004).

[49] R. R. Burnette, "Fundamental pharmacokinetic limits on the utility of using a sinusoidal drug delivery system to enhance therapy", Journal of Pharmacokinetics and Biopharmaceutics **20**, 477–500 (1992).

[50] D. J. Chambers, "Principles of intravenous drug infusion", Anaesthesia & Intensive Care Medicine **20**, 61–64 (2019).

[51] J. Foo, and F. Michor, "Evolution of resistance to targeted anti-cancer therapies during continuous and pulsed administration strategies", PLoS Computational Biology **5**, e1000557 (2009).

[52] R. Peña-Miller, D. Lähnemann, H. Schulenburg, M. Ackermann, and R. Beardmore, "The optimal deployment of synergistic antibiotics: a control-theoretic approach", Journal of The Royal Society Interface **9**, 2488–2502 (2012).

[53] C. Hemez, F. Clarelli, A. C. Palmer, T. C. Chindelevitch, Leonid andd Cohen, and P. A. zur Wiesch, "Mechanisms of antibiotic action shape the fitness landscapes of resistance mutations", bioRxiv (2020).

[54] I. Frost, W. P. J. Smith, S. Mitri, A. S. Millan, Y. Davit, J. M. Osborne, J. M. Pitt-Francis, R. C. MacLean, and K. R. Foster, "Cooperation, competition and antibiotic resistance in bacterial colonies", The ISME Journal **12**, 1582–1593 (2018).

[55] E. M. Adamowicz, M. Muza, J. M. Chacón, and W. R. Harcombe, "Cross-feeding modulates the rate and mechanism of antibiotic resistance evolution in a model microbial community of Escherichia coli and Salmonella enterica", PLoS Pathogens **16**, e1008700 (2020).

[56] R. Krašovec, R. V. Belavkin, J. A. D. Aston, A. Channon, E. Aston, B. M. Rash, M. Kadirvel, S. Forbes, and C. G. Knight, "Mutation rate plasticity in rifampicin resistance depends on Escherichia coli cell–cell interactions", Nature Communications **5**, 1–8 (2014).

[57] H. K. Alexander, S. I. Mayer, and S. Bonhoeffer, "Population heterogeneity in mutation rate increases the frequency of higher-order mutants and reduces long-term mutational load", Molecular Biology and Evolution **34**, 419–436 (2017).

[58] D. Austin, and R. Anderson, "Studies of antibiotic resistance within the patient, hospitals and the community using simple mathematical models", Philosophical Transactions of the Royal Society of London. Series B: Biological Sciences **354**, 721–738 (1999).

[59] M. Baker, J. L. Hobman, C. E. Dodd, S. J. Ramsden, and D. J. Stekel, "Mathematical modelling of antimicrobial resistance in agricultural waste highlights importance of gene transfer rate", FEMS Microbiology Ecology **92**, fiw040 (2016).

[60] F. Wang, Z. Ma, and Y. Shag, "A competition model of HIV with recombination effect", Mathematical and Computer Modelling **38**, 1051–1065 (2003).

[61] A. L. Graham, "Ecological rules governing helminth–microparasite coinfection", Proceedings of the National Academy of Sciences **105**, 566–570 (2008).

[62] N. Mideo, "Parasite adaptations to within-host competition", Trends in Parasitology **25**, 261–268 (2009).

[63] M. E. Hibbing, C. Fuqua, M. R. Parsek, and S. B. Peterson, "Bacterial competition: surviving and thriving in the microbial jungle", Nature Reviews Microbiology **8**, 15 (2010).

[64] J. Baishya, and C. A. Wakeman, "Selective pressures during chronic infection drive microbial competition and cooperation", npj Biofilms Microbiomes **5**, 1–9 (2019).

[65] J. C. Palomino, and A. Martin, "Drug resistance mechanisms in Mycobacterium tuberculosis", Antibiotics **3**, 317–340 (2014).

[66] H. Jordt, T. Stalder, O. Kosterlitz, J. M. Ponciano, E. M. Top, and B. Kerr, "Coevolution of host–plasmid pairs facilitates the emergence of novel multidrug resistance", Nature Ecology & Evolution **4**, 863–869 (2020).

Chapter 5

Switching environments, synchronous sex, and the evolution of mating types

Preface

This chapter constitutes a bioRxiv preprint[1] currently under review at Theoretical Population Biology. This work is co-authored with Tobias Galla[2,3] and George W. A. Constable[4].

E.B-C. contributed to the design of the study and the construction of the mathematical methods developed here, performed the analysis of data and results, produced most of the figures, and wrote the manuscript. T.G. and G.W.A.C. contributed by providing discussions guiding the work, analysis of results, and writing the manuscript. G.W.A.C. conceived the initial idea of the study.

[1] E. Berríos-Caro, T. Galla, and G. W. A. Constable, "Switching environments, synchronous sex, and the evolution of mating types", *bioRxiv preprint*, bioRxiv 2020.07.31.230482 (2020). bioRxiv:230482.

[2] Theoretical Physics, Department of Physics and Astronomy, School of Natural Sciences, Faculty of Science and Engineering, The University of Manchester, Manchester M13 9PL, United Kingdom.

[3] Instituto de Física Interdisciplinar y Sistemas Complejos, IFISC (CSIC-UIB), Campus Universitat Illes Balears, E-07122 Palma de Mallorca, Spain.

[4] Department of Mathematics, University of York, York YO10 5DD, United Kingdom.

Abstract

While facultative sex is common in sexually reproducing species, for reasons of tractability most mathematical models assume that such sex is asynchronous in the population. In this paper, we develop a model of switching environments to instead capture the effect of an entire population transitioning synchronously between sexual and asexual modes of reproduction. We use this model to investigate the evolution of the number of self-incompatible mating types in finite populations, which empirically can range from two to thousands. When environmental switching is fast, we recover the results of earlier studies that implicitly assumed populations were engaged in asynchronous sexual reproduction. However when the environment switches slowly, we see deviations from previous asynchronous theory, including a lower number of mating types at equilibrium and bimodality in the stationary distribution of mating types. We provide analytic approximations for both the fast and slow switching regimes, as well as a numerical scheme based on the Kolmogorov equations for the system to quickly evaluate the model dynamics at intermediate parameters. Our approach exploits properties of integer partitions in number theory. We also demonstrate how additional biological processes such as selective sweeps can be accounted for in this switching environment framework, showing that beneficial mutations can further erode mating type diversity in synchronous facultatively sexual populations.

5.1 Introduction

Evolution is a fundamentally noisy affair [1]. It is therefore no surprise that over the last century theorists have increasingly sought to mathematically understand the effects of randomness on evolutionary models. Such noise has many distinct forms. The foundations of mathematical population genetics are rooted in models that capture how genetic drift (demographic noise), emerging from uncertainty in the order of birth and death events in finite populations, can drive population dynamics [2]. Meanwhile a more ecologically-oriented approach has been to consider the noise that might arise from uncertainty in environmental conditions [3, 4] (environmental noise), with a particular

emphasis in the evolutionary literature on transitions between discrete environmental states [5, 6] (capturing, for instance, an organism's switching behavioural responses to the fluctuating environment). However, in the last decade in particular, there has been an increasing interest in mathematically understanding the dynamics of populations subject to both demographic noise and environmental switching [7–10].

Beyond simply presenting a mathematical challenge, developing analytic techniques to attack such systems is important for understanding a host of problems in biology. One simple yet acute example is that of a population switching between environments in which selection is present in one environment and absent in the other [11]. Here one must understand the interplay of quasi-deterministic dynamics on the one hand (in the selective regime, where noise generates small fluctuations around average trajectories) and entirely noisy dynamics in the other (where genetic drift alone governs the population's behaviour). In this paper we will consider just such an evolutionary problem, demonstrating how it can be modelled and, more importantly analysed, quantitatively.

Mating types are self-incompatible gamete classes that can be understood as ancestral forms of the more familiar sperm-egg system [12, 13]. Unlike populations with true sexes however (which are defined by the size dimorphism between their gametes) the number of mating types (which are morphologically similar) is not restricted to two [14]. Instead, mating types are expected to experience negative frequency dependent selection, with rare types favoured due to their increased opportunities for finding a compatible mate of a distinct, non-self mating type. This has an important dynamical consequence; novel mutant mating types, which are initially rare, should nearly always successfully establish within a resident population, and therefore the number of mating types in a species is predicted to increase through time [15]. However, while species with many mating types are possible rising to many thousands in some fungi [16], species with more than 10 are rare and most have just two [17, 18]. This disagreement between simple evolutionary reasoning and empirical evidence sets the stage for what people call an evolutionary paradox [19].

Although many theories have been proposed to explain this discrepancy (reviewed in [19]), most rely on a deterministic selective advantage for two mating types, such as increased mating success between two types in pheromone signaling and receiving

roles [20], or decreased cytoplasmic conflict between two types in donor-receiver organelle inheritance roles [21]. In contrast, [15] demonstrated that under differing assumptions about the gamete encounter rate dynamics, the strength of selection for more than two types could be reduced. It was then verbally suggested that demographic stochasticity may play a role in further limiting the number of mating types. However without the analytic tools to quantify this effect, the hypothesis that genetic drift could govern mating type number through a balance between mutations and stochastic extinctions was somewhat neglected within the mating type literature, despite being well-established in the related but distinct system of self-incompatibility alleles in plants [22].

More recently, simulations were used to show that in a population that switched between sexual and asexual environments, mating type extinctions became more likely, with negative frequency dependent selection absent in the asexual regime, and the population dynamics entirely dominated by genetic drift [23]. Extending this logic, [24, 25] showed analytically that an increased rate of asexual to sexual reproduction would lower the number of mating types expected under a mutation extinction balance, and indeed that available empirical data showed a positive correlation between the rate of sexual reproduction and the number of mating types in these species.

For mathematical simplicity these latter models [24, 25] considered sexual reproduction to be occurring asynchronously, i.e., with each reproductive event having a fixed probability of sexual vs asexual reproduction. However this simplification fails to capture a biologically relevant aspect of reproduction in these species; sexual reproduction tends to be triggered by changing environmental conditions [26], such as falling nutrient levels [27] or other stress cues [28], and is thus synchronized in time across the entire population [29]. With such dynamics better captured by a switching environment model, it is interesting to ask what quantitative differences this increased level of biological realism might generate. More importantly, this shift in modelling framework also enables us to explore a richer array of biological questions.

In addition to demographic stochasticity, selective sweeps have been suggested as a mechanism that may increase mating type extinction rate and, therefore, further limit the number of mating types [30]. However the effect of these selective sweeps on mating type number can only be seen in asexual environments, where beneficial mutations are linked to the mating type background on which they arise [31]. In a sexual or even

partially sexual environment, genetic recombination breaks down associations between beneficial mutations and mating types, allowing the mutations to spread through the population without distorting mating type frequencies. Quantifying the effect of selective sweeps on these dynamics therefore requires a shift in modelling approach, away from simplified mathematical assumptions of asynchronisity and towards more biologically realistic switching environments [30]. In this paper we focus on this problem, describing a modelling framework and developing a mathematical analysis suitable for the task.

This article is organized as follows: in Section 5.2, we present the switching-environments model in which a population transition between entirely sexual and entirely asexual reproductive modes. Section 5.3 is dedicated to studying how the distribution of mating types changes as a function of the switching and mutation rates. We focus in particular on the regimes of fast, slow and intermediate environmental switching. In Section 5.4 we demonstrate how this new modelling framework allows us to address the issue of selective sweeps. Finally, we present the conclusions in Section 5.5.

5.2 Model definitions

5.2.1 Population dynamics

We consider a population genetics model similar to that proposed in [24]. The model describes a population of N individuals, who each are of a particular mating type. The different mating types are labelled by the index i. The population follows a dynamics similar to the Moran model (i.e., coupled birth-death events in continuous time) but now allowing three possible types of events: asexual reproduction, sexual reproduction, and mutation. Each reproduction event implies the removal of one individual so that the size of the population remains constant. Mutation events imply the introduction of a new mating type. We write n_i for the number of individuals of mating type i, and M for the total number of mating types in the population. These are time-dependent quantities. The number of mating types ranges from $M = 1$ (all individuals are of the same type) to $M = N$ (each individual is of a different mating type).

In the model by Constable and Kokko in [24] both sexual and asexual reproduction

were possible at any time, each occurring with a fixed rate. In this paper we instead consider the more biologically realistic scenario of a population that engages in sexual reproduction in response to changing environmental conditions. While the environment itself may be described by a continuous quantity (such as temperature) the population's response to the environment is binary (whether to engage in sexual reproduction or not). We therefore develop a model that switches stochastically between two different states, denoted S and A, respectively. We write $\sigma \in \{S, A\}$ for the environmental state. When the environment is in state S, only sexual reproduction is possible, and when it is in state A, only asexual reproduction is possible. We assume that the switching between these two environmental states occurs independently of the composition of the population, with rate $\lambda_{S\to A}$ from S to A, and $\lambda_{A\to S}$ for switches from state A to S. The switching processes can be written as

$$S \xrightarrow{\lambda_{S\to A}} A, \quad \text{and} \quad A \xrightarrow{\lambda_{A\to S}} S. \tag{5.1}$$

In the sexual environment S, we assume that any pair of individuals can reproduce, provided they belong to two different mating types. For example, one parent may be of mating type i, and the other parent of any other non-i mating type. The probability that this occurs for two individuals sampled at random from the population is $n_i(N - n_i)/N^2$. The offspring inherits the mating type of either parent with equal probability 1/2. To keep the population size fixed, another individual (type j) is simultaneously chosen uniformly at random to die. The rate for events in which an offspring of type i is generated and an individual of type j removed from the population is then

$$\mathcal{T}^S_{ij} = \frac{1}{2}\frac{n_i n_j}{N^2}\left(N - n_i\right). \tag{5.2}$$

We express time in units of generations, so that there are of the order of N events in the population per unit time. This means that rate in Eq. (5.2) has an extra factor N in comparison to the rate used in [24].

In the asexual environment A, reproduction follows the standard neutral Moran model. One individual is chosen uniformly at random to reproduce, and the offspring inherits the mating type of the parent. As above, another individual is simultaneously chosen at random to die. The rate for events in which an individual of type i reproduces

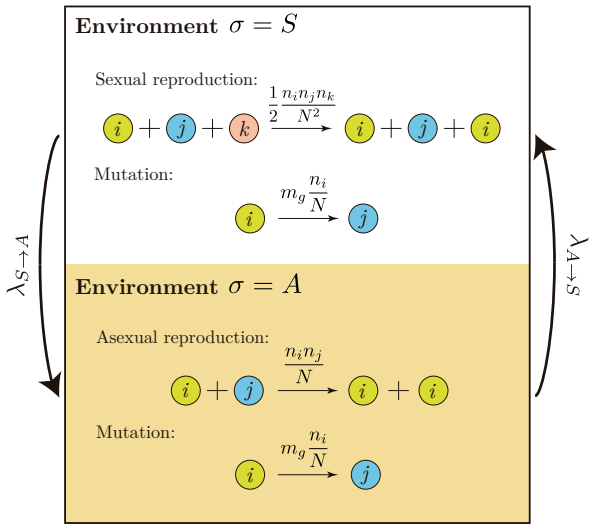

Figure 5.1: Illustration of the full model and the events occurring in the population: sexual reproduction, asexual reproduction, and mutation. In each of these events one individual is replaced by another of a different mating type. Transitions between environments occur independently of the state of the system at rate $\lambda_{S\to A}$ from $\sigma = S$ to $\sigma = A$, and $\lambda_{A\to S}$ from $\sigma = A$ to $\sigma = S$.

and an individual of type j is removed is then given by

$$\mathcal{T}_{ij}^{A} = \frac{n_i n_j}{N}. \tag{5.3}$$

Notice here we are ignoring any type of selection across mating types, so the dynamics is governed entirely by neutral genetic drift. If we considered selection, we would benefit the growth of certain mating types over the others, which can bring important consequences as we will see below when accounting for selective sweeps.

Following [24], we describe mutations as events in which one individual changes to a new mating type not currently present in the population. This leads to the rate

$$\mathcal{T}_{j}^{m} = m_g \frac{n_j}{N} \tag{5.4}$$

for mutation events from type j to a new type. The parameter m_g sets the typical number of mutations per generation in the population. The raw mutation rate is given by $m = m_g/N$. Defined in this way, Eq. (5.4) can also be interpreted biologically as capturing migration events from a highly diverse mating type pool.

The dynamics of the model above are summarised in Figure 5.1. We will refer to this as the 'full model' in the remainder of the paper. It describes a Markovian process. At each point in time its state is described by the state of the environment (S or A), and by the state vector of the population, $\mathbf{n} = (n_1, n_2, \dots)$. The i-th entry in this vector indicates how many individuals of mating type i are present in the population.

We have $\sum_i n_i = N$, and the number of non-zero entries in $\mathbf{n}$ indicates the number of mating types currently present in the population.

5.2.2 Environmental dynamics

Given that the environmental switching is independent of the composition of the population, the long-time probabilities to find either environmental state can be written down straight away,

$$\begin{aligned} P_A^{st} &= \frac{\lambda_{S\to A}}{\lambda_{S\to A}+\lambda_{A\to S}}, \\ P_S^{st} &= \frac{\lambda_{A\to S}}{\lambda_{S\to A}+\lambda_{A\to S}}. \end{aligned} \tag{5.5}$$

To ease the notation, we write $p_S = P_S^{st}$ for the probability to find the environment in state S. This indicates the rate of sexual reproduction.

The average time the environment spends in each of the two states between switches is given by

$$\tau_A = \frac{1}{\lambda_{A\to S}} \quad \text{and} \quad \tau_S = \frac{1}{\lambda_{S\to A}}. \tag{5.6}$$

The average time to switch from one state to the other and back, is then

$$\tau = \tau_A + \tau_S. \tag{5.7}$$

5.2.3 Reduced model

In order to analyse the dynamics of the population, we will focus on a *reduced model*, describing only the number of mating types M. This number changes over time through the birth-death and mutation events in the population. In a birth-death event the number of mating types can decrease by one (if the individual that dies is the last individual belonging to a particular mating type). When a mutation event occurs, the number of mating types in the population increases by one (unless the mutating individual is the last of its type). We are interested in the stochastic process for M, and will describe it with effective rates

$$M \xrightarrow{T^+_{M,\sigma}} M+1 \quad \text{and} \quad M \xrightarrow{T^-_{M,\sigma}} M-1. \tag{5.8}$$

For example, $T^-_{M,A}$ is the rate with which a mating type is driven to extinction when the environment is in state A, and when there are currently M mating types present

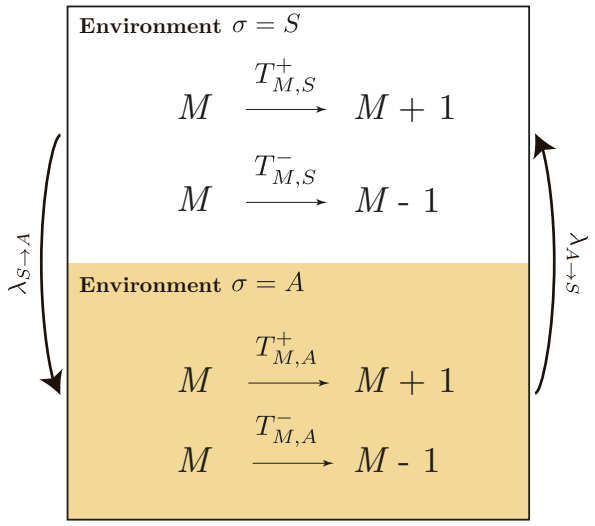

Figure 5.2: Schematic representation of the *reduced model*, where the focus is on the dynamics of the number of mating types M instead of the individuals. This model is described by effective birth and death rates $T^+_{M,\sigma}$ and $T^-_{M,\sigma}$, with $\sigma \in \{S, A\}$.

in the population. Figure 5.2 illustrates this approach. The reduced model focuses on the dynamics of the number of mating types M, without regard for the numbers n_i of individuals belonging to each mating type. The stochastic process for M is of course dependent on the composition of the vector state $\mathbf{n}$ in the full model, and as such, the reduced model constitutes an approximation of the dynamics in the full model.

The analytical challenge is to derive suitable expressions for the $T^{\pm}_{M,\sigma}$. While this is difficult for the case of switching environments, progress can be made by focusing on the case of a fixed environmental state, $\sigma = A$ or $\sigma = S$. In this case, the population will tend to a stationary state, described by the joint distribution of the number of mating types, M, and the vector of abundances $\mathbf{n}$. This distribution can be obtained analytically using an approach similar to that of [24].

We then proceed to use this distribution to calculate the rates $T^{\pm}_{M,\sigma}$ for the dynamics of M. To do this, we focus on marginals for specific values of M and use methods from number theory [32, 33] to sum over partitions $\mathbf{n}$ of the N individuals into mating types. Importantly, this approach accounts precisely for all possible transitions in which a change on state $\mathbf{n}$ leads to an increase or decrease in the number of mating types M. Our calculation of these rates relies on fixed environmental states A or S. To make this clear in the notation we write $T^{\pm}_{M|\sigma}$ for the rates computed in this way. Further details of the calculation can be found in Sections 5.6 and 5.7 of the Supplementary Material. The outcome of this approach is an analytical solution for the rates $T^{\pm}_{M|\sigma}$.

For environment $\sigma = A$, we find

$$T^{-}_{M|A} = (N-1)\frac{\begin{bmatrix} N-1 \\ M-1 \end{bmatrix}}{\begin{bmatrix} N \\ M \end{bmatrix}}, \tag{5.9}$$

and

$$T^{+}_{M|A} = m_g(N-1)\frac{\begin{bmatrix} N-1 \\ M \end{bmatrix}}{\begin{bmatrix} N \\ M \end{bmatrix}}, \tag{5.10}$$

where $\begin{bmatrix} N \\ M \end{bmatrix}$ is the unsigned Stirling number of the first kind [34]. For environment $\sigma = S$, the rates become

$$T^{-}_{M|S} = \frac{1}{2B_{N,M}}\left[(N-1)B_{N-1,M-1} - \frac{((N-1)!)^2}{N}\sum_{n_1=1}^{N-M+1}\frac{n_1}{(N-n_1)}\frac{B_{N-1-n_1,M-2}}{((N-1-n_1)!)^2}\right], \tag{5.11}$$

and

$$T^{+}_{M|S} = m_g\left(1 - \frac{B_{N-1,M-1}}{B_{N,M}}\right), \tag{5.12}$$

where $B_{k,\ell} = B_{k,\ell}(y_1, \ldots, y_{k-\ell+1})$ is the incomplete Bell polynomial [35]. The arguments y_i are the sequence $y_i = (i-1)!(N-1)_{i-1}$, with $(N-1)_{i-1}$ the falling factorial of $(N-1)$ with respect to $(i-1)$, given by $(N-1)_{i-1} = \prod_{j=0}^{i-2}(N-1-j)$. Further details can be found in Section 5.7.2 in the Supplementary Material. In Figure 5.3 we demonstrate the accuracy of the predictions for the rates $T^{\pm}_{M|\sigma}$ when compared against direct measurements of the rates from simulations of the full model with fixed environmental state.

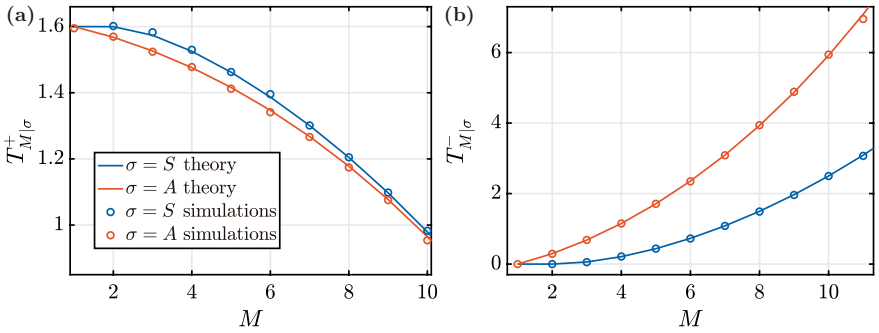

Figure 5.3: Theoretical predictions of rates $T^{+}_{M|\sigma}$ and $T^{-}_{M|\sigma}$ against numerical simulations of the full model with fixed environments, $\sigma = S$ and $\sigma = A$ respectively. Parameters are $N = 16$ and $m_g = 1.6$.

We now proceed to discuss the properties of these rates as a function of M. We first focus on the rates $T^{+}_{M|\sigma}$, i.e., events in which the number of mating types increases.

The introduction of new mating types occurs when one individual mutates from one mating type to another. In order for M to increase in this process, the mutating individual must not be the only representative of its type. As a consequence $T^+_{M|\sigma}$ tends to decrease with increasing M: if a large number of mating types is present in the population, then it is likely that some of these will only be represented by a small number of individuals, and possibly by a single member of the population. A mutation event involving this individual then does not lead to an increase of the number of mating types.

In birth-death events the number of mating types can decrease, irrespective of whether reproduction is sexual or asexual. A reduction of M occurs when the individual that dies in such an event is the only representative of its mating type. Given that the size of the population is fixed, this is more likely to be the case when the number of mating types is large, hence the rate $T^-_{M|\sigma}$ increases with M.

Using these rates we can obtain the stationary distribution for the number of mating types under fixed environmental conditions using standard results for continuous-time Markov chains [36]. We have

$$P^{st}_{M|\sigma} = \frac{T^+_{M-1|\sigma} \cdots T^+_{1|\sigma}}{T^-_{M|\sigma} \cdots T^-_{2|\sigma}} P^{st}_{1|\sigma}, \tag{5.13}$$

with

$$P^{st}_{1|\sigma} = \left[1 + \frac{T^+_{1|\sigma}}{T^-_{2|\sigma}} + \ldots + \frac{T^+_{N-1|\sigma} \cdots T^+_{1|\sigma}}{T^-_{N|\sigma} \cdots T^-_{2|\sigma}} \right]^{-1}. \tag{5.14}$$

Using this expression, we can write the stationary distribution in closed form for environment $\sigma = A$,

$$P^{st}_{M|A} = \frac{m_g^{M-1}}{(N-1)!} \frac{\begin{bmatrix} N \\ M \end{bmatrix}}{\binom{m_g+N-1}{m_g}}. \tag{5.15}$$

For environment $\sigma = S$, we use Eq. (5.13) with rates given by Eqs. (5.11) and (5.12). In Section 5.7.4 of the Supplementary Material we show that these predictions for $P^{st}_{M|S}$ and $P^{st}_{M|A}$ are in good agreement with numerical simulations.

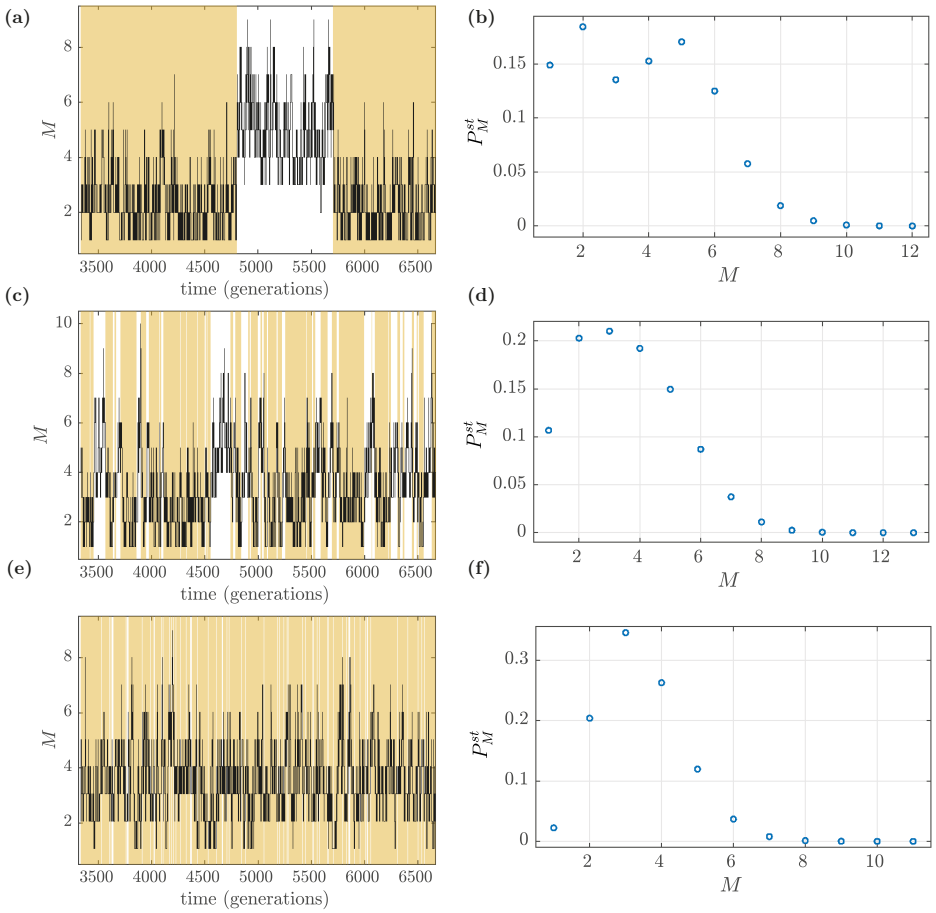

Figure 5.4: Sample path of the temporal evolution, and stationary distribution of the number of mating types M. The environment switches between $\sigma = S$ (entirely sexual reproduction) and $\sigma = A$ (entirely asexual reproduction). Coloured regions in (a), (c), and (e) represent the $\sigma = A$ environment. Data is shown for different switching regime. Panels (a) and (b) illustrate the case of slow switching ($\lambda_{A\to S} = \lambda_{S\to A} = 10^{-5}$), panels (c) and (d) of intermediate switching ($\lambda_{A\to S} = \lambda_{S\to A} = 10^{-3}$), and panels (e) and (f) of fast switching ($\lambda_{A\to S} = \lambda_{S\to A} = 10^{-1}$). Simulations have been carried out by using the Gillespie algorithm [37, 38] in the full model. The stationary distributions shown in panels (b), (d), and (f) have been obtained by time-averaging a long run until $t = 10^7$, with a time $t = 10^5$ left to equilibrate. Parameters used: $N = 30$ and $m_g = 0.3$.

5.3 Stationary distribution for the number of mating types under environmental switching

While in previous studies [24, 25, 30] the frequency of facultative sexual reproduction was measured by a single parameter (the probability of a reproduction event being

sexual), the switching environment model requires two parameters, $\lambda_{A\to S}$ and $\lambda_{S\to A}$. Importantly, while the probability of finding the population in a sexual state remains constant for a fixed ratio $\lambda_{A\to S}/\lambda_{S\to A}$ (see Eq. (5.5)), the population dynamics qualitatively changes as the values of these parameters are changed. This is illustrated in Figure 5.4, where typical time courses of the number of mating types present in the population are shown (left panels) along with the corresponding stationary distributions P_M^{st} (right panels). We next give a brief overview of the behaviour of the model.

In general we see in Figure 5.4 that while the number of mating types fluctuates, the number is typically higher when reproduction is sexual. In the sexual environment, rare mating types experience a reproductive advantage, with their per capita reproductive rate proportional to $(N - n_i)$ (see Eq. (5.2)). This means that novel mutants (or migrants) establish in the population with high probability [39]. In contrast, in the asexual environment mutants have no particular advantage as all mating types reproduce with the same per capita rate (see Eq. (5.3)). In this case, given sufficient time, mating types are driven to extinction as a result of neutral genetic drift.

Figure 5.4 shows three different regimes of environmental switching. In the upper panels the environment is slow compared to the typical time scales of the population dynamics. The stationary distribution of the number of mating types can then be bi-modal, as shown in panel (b). Here mating type numbers greater than $M = 1$ in the asexual regime are only maintained by mutation (or migration) providing a supply of new types. The distribution of M becomes unimodal when the typical time scale of environmental switching becomes comparable to the time scale of the evolutionary process in the population (panels (c) and (d)), and it remains unimodal when the environment is much faster than the population dynamics (panels (e) and (f)).

In the following sections we seek to quantify these dynamics mathematically. We begin by considering the limits of slow and fast environmental switching (Figure 5.4 (a,b) and (e,f), respectively), as these prove analytically tractable. We then go on to consider the range of intermediate switching. In order to illustrate the accuracy of our approximations as compared to simulations, we will use parameters compatible with manageable computing time (e.g. low population sizes and high mutation rates, for which the dynamics more rapidly approach a stationary distribution). In Section 5.3.3 we will explore more biologically reasonable parameter regimes that are prohibitively

expensive to investigate through simulation alone.

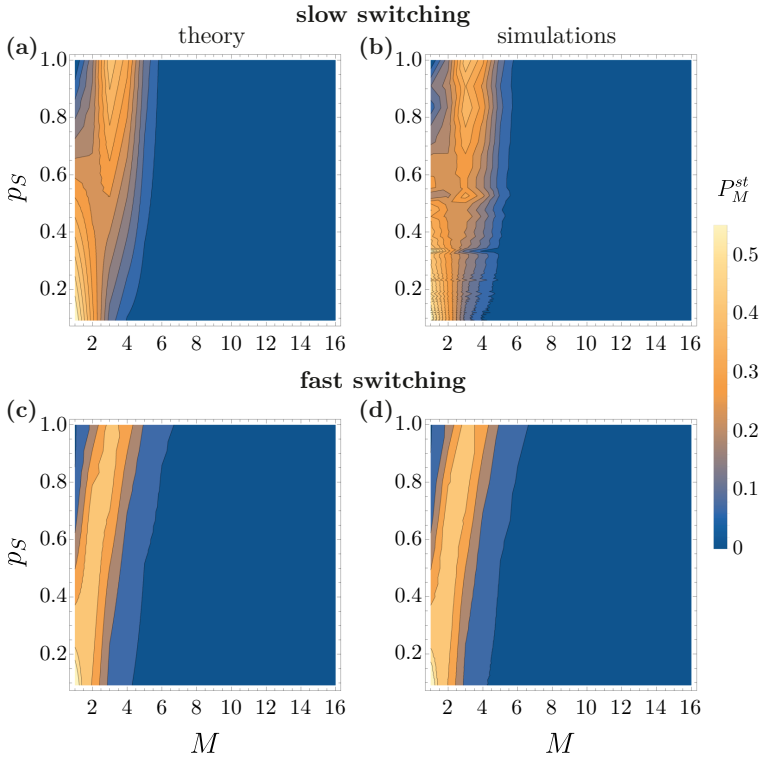

Figure 5.5: Stationary distribution P_M^{st} as function of M and p_S, for slow switching regimes (upper row) and fast switching regimes (lower row). Panels (a) and (c) show the result obtained from numerical simulations for parameters $N = 16$, $m_g = 0.16$ with $\lambda_{A\to S} = 10^{-6}$ (for (a)) and $\lambda_{A\to S} = 10^3$ (for (c)). Panels (b) and (d) show the corresponding theoretical predictions in Sections 5.3.1 and 5.3.2, respectively.

5.3.1 Slow environmental switching

When the environmental switching is slow (Figure 5.4 (a) and (b)) the system spends sufficient time in each environment for the number of mating types to reach stationarity. One then expects the overall distribution of the number of mating types P_M^{st} to be the weighted average of the stationary distributions from each environment. Mathematically, this means

$$P_M^{st} = (1 - p_S)P_{M|A}^{st} + p_S P_{M|S}^{st}. \tag{5.16}$$

This result can be obtained analytically from the master equation of the system (see below in Eq. (5.22)) in the limit of slowly switching environments, see Section 5.8.4 in the Supplementary Material. This approximation was also used in [7] for a game theory model with switching payoff matrices. The probability $p_S = P_S^{st}$ is given in Eq. (5.5), while the probability $P_{M|S}^{st}$ and $P_{M|A}^{st}$ are the stationary distributions for M

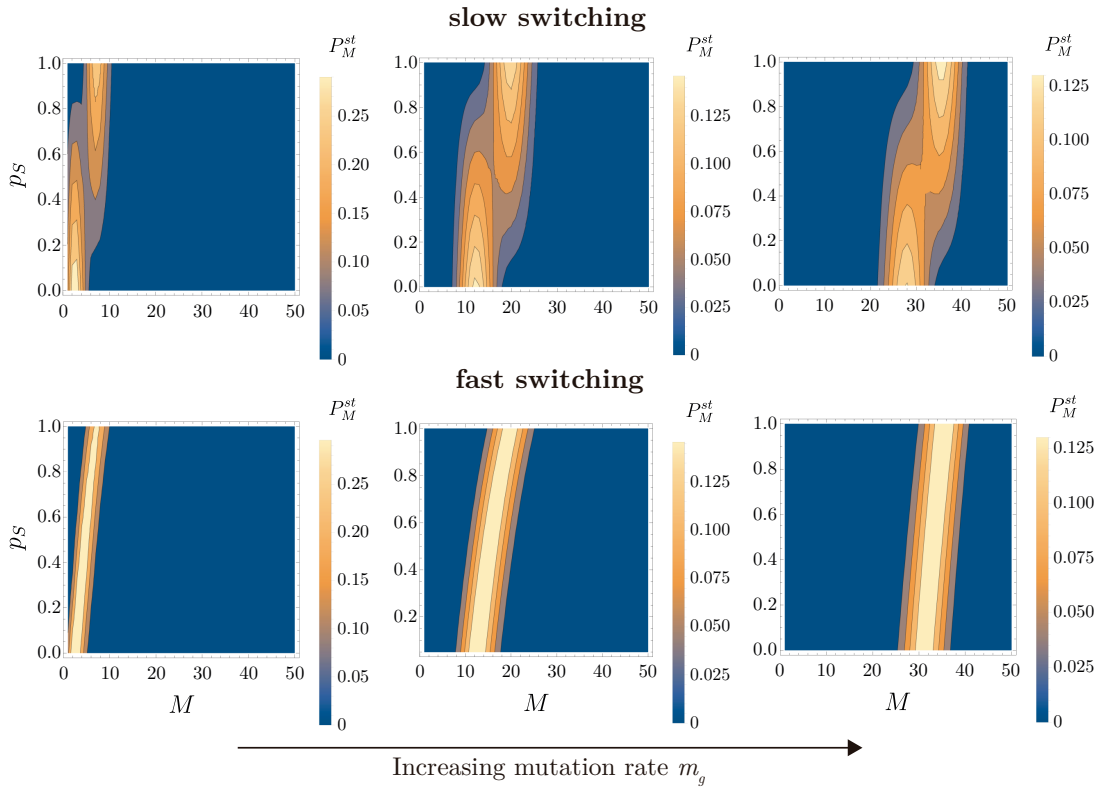

Figure 5.6: Theoretical prediction for stationary distribution P_M^{st}, for slow switching (upper row), and fast switching (lower row) as function of the number of mating types (M) and the average fraction of time spent in the sexual environment, p_S. The theoretical predictions for the two switching regimes are calculated from Eqs. (5.16) and (5.18), respectively. Panels (a) and (d) show the case of low mutation rate ($m_g = 0.5$), panels (b) and (e) are for intermediate mutation rate ($m_g = 5$), and panels (c) and (f) for high mutation rate ($m_g = 50$). Population size is $N = 50$.

assuming that the environmental state is fixed to S or A, respectively. These are given in Eqs. (5.13) and (5.14).

In Figure 5.5 (a) and (b), we compare this prediction for the limit of slow environmental change against numerical simulations. We show the distribution P_M^{st} as function of the fraction of time p_S spent in the sexual environment.

The upper panels in Figure 5.6 illustrate the behaviour of P_M^{st} in the regime of slowly varying environments. In particular we show how this stationary distribution changes with the rate p_S. We have now chosen a larger population than in Figure 5.5, and we show results for different mutation (or migration) rates m_g. As seen in the figure, the distribution is unimodal if the environment is predominantly in one of its two states (i.e., p_S is close to zero or one). The distribution is bimodal when the environment spends similar fractions of time in each state ($p_S \approx 1/2$), independent of the rate at which new mating types are added. We also see that the mode of the

distribution for P_M^{st} is lower if reproduction is always asexual ($p_S = 0$) than in the case of obligately sexual reproduction ($p_S = 1$). As m_g increases (new mating types arrive more frequently), the distribution gets wider around its peak, and the most probable number of mating types is shifted to higher values. Naturally, for very high (and biologically unrealistic) values of m_g the mode of P_M^{st} will be equal to the population size N.

5.3.2 Fast environmental switching

The simulation data in Figure 5.4 (e) and (f) illustrates the behaviour of the population in the limit of very fast environmental switching. Unlike in the regime of slow-switching environments, the stationary distribution P_M^{st} then only exhibits one peak.

To estimate the P_M^{st} in this regime, we follow the analytical approach developed in [7] for game theoretic models and calculate weighted averages of the transition rates $\mathcal{T}_{ij}^{\sigma}$ for all pairs i, j,

$$\mathcal{T}_{ij}^{\text{fast}} = (1 - p_S)\mathcal{T}_{ij}^{A} + p_S \mathcal{T}_{ij}^{S}. \tag{5.17}$$

This leads to

$$\mathcal{T}_{ij}^{\text{fast}} = \left[\overbrace{(1-p_S)n_i}^{\text{Asexual reproduction}} + \underbrace{\frac{p_S}{2}\frac{n_i}{N}(N - n_i)}_{\text{Sexual reproduction}} \right] \left[\underbrace{\frac{n_j}{N}}_{\text{Death}} \right], \tag{5.18}$$

and one recovers the limit studied in [24] for the case of asynchronous facultative sex. This is a model with a constant environment with an effective sex rate p_S. This sex rate determines the effective birth and death rates, $T_M^{+,\text{fast}}$ and $T_M^{-,\text{fast}}$. Further details of the derivation of these rates are given in Sections 5.7.2 of the Supplementary Material. We find

$$T_M^{-,\text{fast}} = \frac{1}{2B_{N,M}} \Bigg[(2 - p_S)(N-1)B_{N-1,M-1} - \frac{p_S}{N}(N-1)!(N_{p_S}-1)! \sum_{n_1=1}^{N-M+1} \frac{n_1}{(N_{p_S}-n_1)} \frac{B_{N-1-n_1,M-2}}{((N-1-n_1)!)^2} \Bigg], \tag{5.19}$$

and

$$T_M^{+,\text{fast}} = m_g \left(1 - \frac{B_{N-1,M-1}}{B_{N,M}} \right), \tag{5.20}$$

where the $B_{k,\ell} = B_{k,\ell}(y_1, \ldots, y_{k-\ell+1})$ are incomplete Bell polynomials as before. However, the y_i are now given by $y_i = (i-1)!(N_{p_S} - 1)_{i-1}$, where N_{p_S} is

$$N_{p_S} = \frac{2 - p_S}{p_S} N. \tag{5.21}$$

The stationary distribution for M is then obtained using Eqs. (5.13) and (5.14), with the replacement $T^{\pm}_{M|\sigma} \to T^{\pm,\text{fast}}_{M}$.

We test these theoretical predictions in Figure 5.5 (c) and (d), and find good agreement with simulations. The behaviour of the model is further explored in Figure 5.6 (d-f), where we show the stationary distribution for the number of mating types in the limit of fast environments, for varying values of the facultative sex rate and for different mutation rates. For the parameters in Figure 5.6 the distributions are not too dissimilar from the ones in the slow switching regime (panels (a-c)). However, one main difference is the absence of bi-modality when $p_S \approx 1/2$. Additionally, we find the distribution is wider around its peak.

5.3.3 Transition between slow and fast switching regimes

In the previous sections, we studied the stationary distribution of the number of mating types in the limits of slow and fast environmental dynamics. The differences between these limits are most pronounced at intermediate facultative sex rates ($p_S \approx 1/2$). We now focus on the regime of intermediate environmental switching. The time scale of the environmental dynamics is set by the cycle time τ, defined in Eq. (5.7), and we are therefore interested in situations where τ is comparable to the time scales of the evolutionary process in the population.

Stochastic simulations

Results from simulations are shown in Figure 5.7. We focus on the case $p_S = 1/2$. Cases with p_S close to zero and one are explored in Section 5.8.3 of the Supplementary Material. As shown in Figure 5.7, in the intermediate switching regime the stationary distribution P^{st}_{M} does not exhibit a clearly defined peak as in the fast switching regime, but rather it exhibits a wider distribution, with two peaks in some cases. When the population size is low (see first row of Figure 5.7), the distribution gets wider compared to the limiting cases (slow and fast switching regimes), and exhibits two peaks only

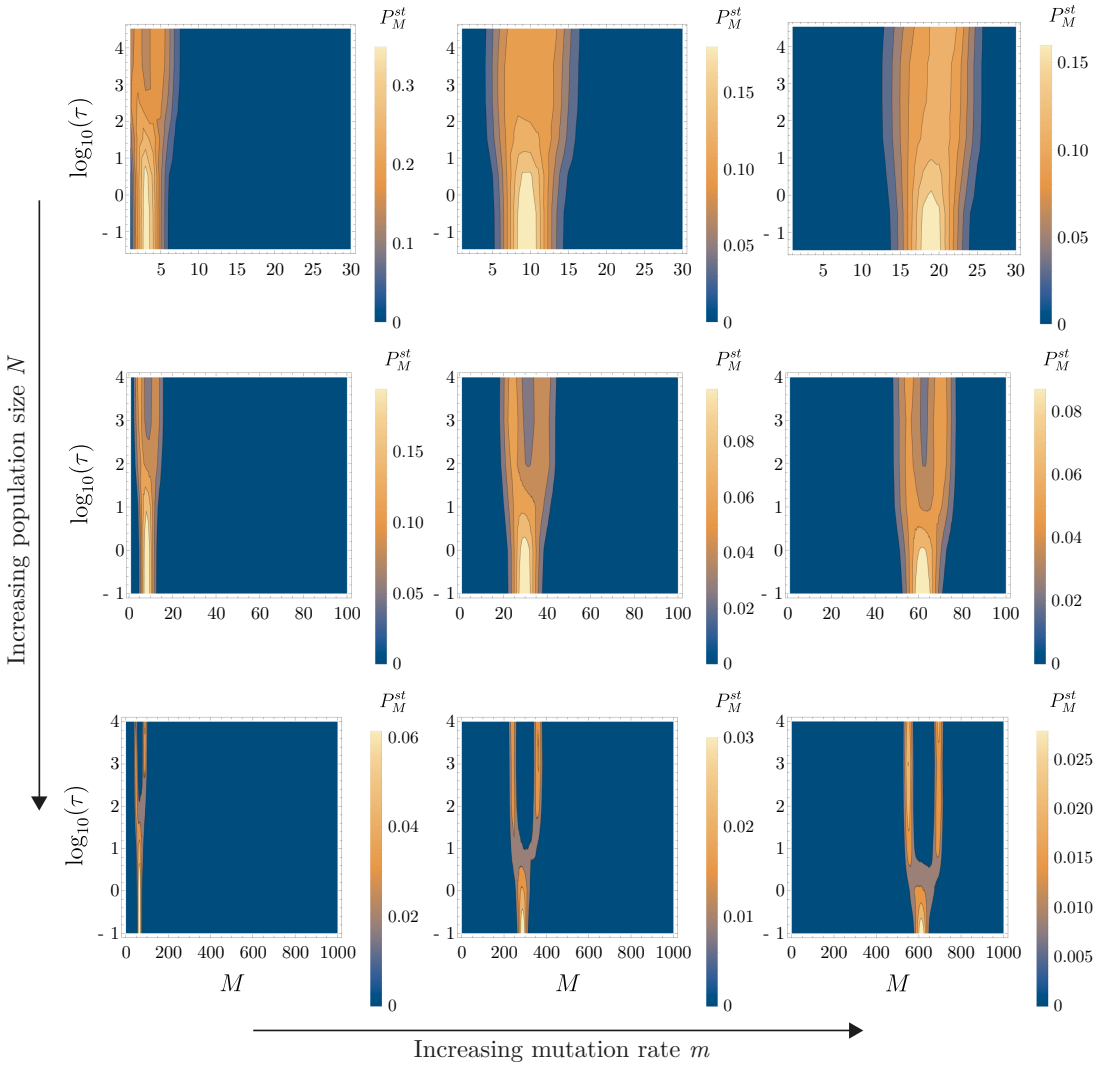

Figure 5.7: Simulation results of the stationary distribution P_M^{st} as function of M and τ, the average time of one switching period. Parameters used: upper row, $N = 30$; middle row, $N = 100$; lower row, $N = 1000$. Left column, $m = 0.01$; middle column $m = 0.1$; right column, $m = 0.5$. We set $\lambda_{S\to A} = \lambda_{A\to S}$ throughout. Numerical simulations were conducted by time-averaging a long run until time $t = 10^7$, with a time $t = 10^6$ left to equilibrate.

when the mutation rate is low (see Figure 5.7 (a) for high values of τ; this is the same distribution shown in Figure 5.4 (b)). For higher population sizes (see second row), the distribution makes a transition from a unimodal shape (fast switching regime) to bimodal (slow switching regime) for all values of the mutation rate used in the figure. In between (intermediate switching regime) the distribution is wider around its peak until it bifurcates in two. This situation is also observed for higher population sizes (see lower row), however, each of the two peaks become more narrow.

Generator-matrix approach

We have shown that in the single environment case, we are able to successfully reduce the combined dynamics of the number of mating types to an approximate one-step birth-death process for the number of mating types, M (see Section 5.2.3). We have further shown how this can be used to predict the population behaviour in the slow-switching limit (where the system takes on the average behaviour of the two independent environments, see Section 5.3.1), and in the fast-switching limit (where the system behaves as if it were in a single, effective environment, see Section 5.3.2). We now seek to extend this approach to the intermediate regime.

We begin by supposing that the dynamics of the full model (which involves transitions in the mating type abundances, $\mathbf{n}$) can be approximated as a coupled birth-death process in M and σ. The master equation for this process takes the general form

$$\frac{\mathrm{d}\underline{P}(t)}{\mathrm{d}t} = \underline{P}(t)\underline{\underline{Q}}, \tag{5.22}$$

where the entries of the row vector $\underline{P}(t)$ are the probabilities of finding the system at a certain state (M, σ) at time t. It is convenient to arrange the states such that this vector takes the form

$$\underline{P} = (\underbrace{P_{1,S}, \ldots, P_{M,S}, \ldots, P_{N,S}}_{\text{state } \sigma = S}, \underbrace{P_{1,A}, \ldots, P_{M,A}, \ldots, P_{N,A}}_{\text{state } \sigma = A}), \tag{5.23}$$

so the first half of entries correspond to states $(M, \sigma = S)$, and the second one to states $(M, \sigma = A)$. In both environments we have $1 \leq M \leq N$, with the bounds corresponding to the extreme cases of the whole population being of the same type $(M = 1)$, or each individual of a different type $(M = N)$. The matrix $\underline{\underline{Q}}$ is of size $2N \times 2N$, and it is convenient to write it in the following block structure,

$$\underline{\underline{Q}} = \begin{pmatrix} Q^{(S,S)} & Q^{(S,A)} \\ Q^{(A,S)} & Q^{(A,A)} \end{pmatrix}. \tag{5.24}$$

The $N \times N$ blocks $Q^{(S,A)}$ and $Q^{(A,S)}$ describe transitions between the environmental states. Given that the model does not include events in which both the environmental state and the number of mating types changes at the same time, these blocks are diagonal in M. We have $Q^{(S,A)}_{M,M'} = \lambda_{S\to A}\delta_{M,M'}$ and similarly $Q^{(A,S)}_{M,M'} = \lambda_{A\to S}\delta_{M,M'}$. We must now find an approximation for the transitions within each environment, $Q^{(S,S)}$

and $Q^{(A,A)}$. Ultimately there are no correct choices for these matrices as they are simply approximations of the full model. Below we follow one particular approach, while alternatives are discussed in Section 5.3.3.

We begin by assuming that on transitioning to the sexual environment, the system rapidly relaxes to quasi-stationary state in which the dynamics of mating-type number are well-approximated by the transition rates in the sexual environment at equilibrium (see Section 5.2.3). Thus $Q^{(S,S)}$ is tri-diagonal (only involving transitions that increase or decrease the number of mating types by one) with entries

$$\begin{aligned} Q^{(S,S)}_{M,M+1} &= T^{+}_{M|S}, \\ Q^{(S,S)}_{M,M} &= -T^{+}_{M|S} - T^{-}_{M|A} - \lambda_{S\to A}, \\ Q^{(S,S)}_{M,M-1} &= T^{-}_{M|S}. \end{aligned} \tag{5.25}$$

We can proceed analogously to construct the matrix $Q^{(A,A)}$ in the asexual environment.

Next, we calculate the stationary distribution $\underline{P}^{\mathrm{st}}$ for this approximate system, by setting the right hand side of Eq. (5.22) to zero,

$$\underline{P}^{\mathrm{st}}\underline{\underline{Q}} = 0. \tag{5.26}$$

The solution has to be normalised appropriately, i.e, we must impose $\sum_{M,\sigma} P^{\mathrm{st}}_{M,\sigma} = 1$. The marginal distribution for the number of mating types is obtained as $P^{\mathrm{st}}_{M} = \sum_{\sigma\in\{A,S\}} P^{\mathrm{st}}_{M,\sigma}$. The block structure of $\underline{\underline{Q}}$ reduces the complexity of the problem, and, as a consequence, the stationary state can be obtained numerically relatively easily.

Compared to numerical simulations, the theoretical approach presented here brings a considerable simplification for estimating the stationary distribution P^{st}_{M}. For the cases shown in Figure 5.7, simulations quickly become costly as both N and the switching rates increase, because more events occur per unit time. This is not a major obstacle, however, when solving Eq. (5.26). The matrix structure of $\underline{\underline{Q}}$ allows a fast numerical computation of $\underline{P}^{\mathrm{st}}$ even for large values of N. In cases in which the distributions $P^{\mathrm{st}}_{M,\sigma}$ fall off quickly with M one can truncate the range of M to values much smaller than N, additionally accelerating the analysis.

We now proceed to define more precisely when exactly we expect this approach to work. We know that the key assumption is that the system has sufficient time in each environment to relax to the quasi-stationary distribution obtained in that environment

when switching is absent. This assumption is required so that that we can approximate the rates $T^{\pm}_{M,\sigma}$ by $T^{\pm}_{M|\sigma}$ (a comparison to the case in which numerically-determined rates $T^{\pm}_{M,\sigma}$ are used in the generator matrix is presented in Section 5.7.5 of the Supplementary Material).

In the sexual environment, this assumption is valid across a large parameter range (strong selection for even mating type frequencies very rapidly brings the system to a quasi-stationary distribution around one of the system's fixed points). However in the asexual environment, relaxation to the stationary distribution takes far longer (this relaxation is driven entirely by genetic drift, which operates on a much slower timescale). Thus the requirement that this relaxation time is less than the typical time spent in the asexual environment provides the key restriction for the parameter range over which we expect the generator-matrix approximation to work. Assuming that the system in the sexual environment reaches $M_o^{(S)}$ mating types before transitioning to the asexual environment, we now calculate the mean time taken for the system to relax from $M_o^{(S)}$ to $M_o^{(A)}$ mating types in the asexual environment, where $M_o^{(S)}$ and $M_o^{(A)}$ are the mode number of mating types in the fixed sexual and asexual environments, respectively. Using the results of [40] for a neutral multi-allelic Moran model, we find that the condition that the system spends sufficient time in the asexual environment is given by

$$\tau_A \gg \tau_r \left(M_o^{(S)}, M_o^{(A)} \right), \tag{5.27}$$

where

$$\tau_r \left(M', M \right) = -N \sum_{s=M'-M}^{M'-1} (-1)^{s-M'+M} \binom{s-1}{M'-M-1} \binom{M'}{s} \frac{s}{M'} \log\left(\frac{s}{M'} \right) \tag{5.28}$$

is the mean time taken for the system to transition from a state with M' to M mating types in the asexual environment. Therefore, if the condition (5.27) is fulfilled, we expect that the system will have sufficient time to relax in the asexual environment to its quasi-stationary distribution for which $T^{\pm}_{M|A}$ are accurate approximations for $T^{\pm}_{M,A}$.

In Figure 5.8, we show the predictions obtained using this approach for the same parameters as in Figure 5.7 (middle row). The parameters used are within in the range in which the generator-matrix approach is in good agreement with numerical simulations (see Eq. (5.27)). We note that this does not require very slow environmental switching per se; if the modes $M_o^{(S)}$ and $M_o^{(A)}$ are sufficiently close, then intermediate

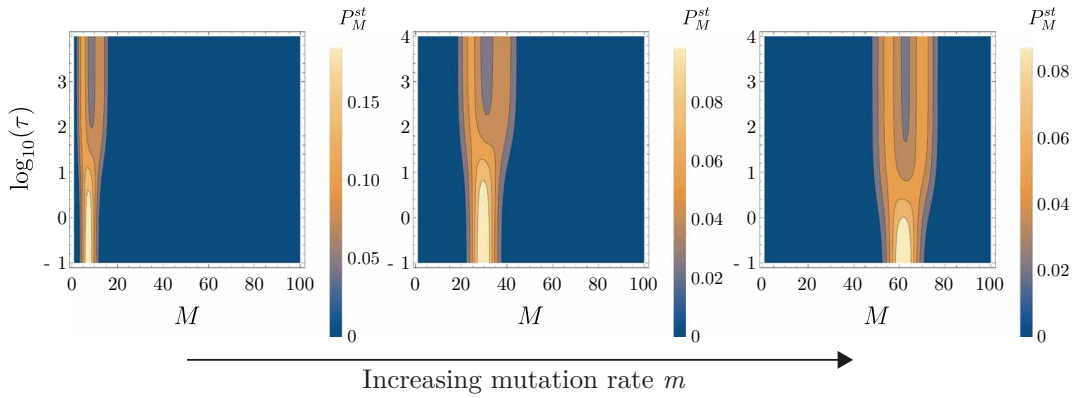

Figure 5.8: Theoretical prediction of P_M^{st} obtained as the solution of Eq. (5.26), i.e., the null space of matrix $\underline{\underline{Q}}^T$. Parameters used are the same as in the second row of Figure 5.7.

switching rates allow the system to relax to the quasi-stationary distribution in the asexual environment. In fact, for the parameters used in Figure 5.8 the mean time τ_r is about ten times lower than τ_A for intermediate switching regimes. Thus if m_g is large (such that $M_o^{(A)}$ is large) or N low (such that $M_o^{(S)}$ is low) we can still expect to see a good agreement between the generator-matrix approach and theory (see Figure 5.9). In biological terms we can therefore view the generator-matrix approach as being most useful when considering small populations, with migration (large m_g) taking place between spatially segregated patches.

In Section 5.8.1 of the Supplementary Material we show in more detail how the distribution P_M^{st} obtained from the generator-matrix approach compares against numerical simulations for different values of m_g and p_S. We illustrate in Section 5.8.2 how $P_{M,\sigma}^{st}$ obtained from this approach behaves as function of p_S for both $\sigma = S$ and $\sigma = A$. We also show that one can derive closed-form solutions of the stationary distributions $P_{M,\sigma}^{st}$ in terms of rates $T_{M|\sigma}^{\pm}$ in the limits of slow and fast environmental dynamics (Section 5.8.4). In the slow-switching limit we obtain the result presented in Eq. (5.16). In this limit the system spends a long time in each environmental state, and thus, using the rates $T_{M|\sigma}^{\pm}$ in the reduced model is a good approximation. For the fast-switching limit, however, this approximation is no longer valid; the system has insufficient time to relax to the quasi-stationary distribution in the asexual environment under which $T_{M|A}^{\pm}$ are accurate approximations for the transition rates, and so the theoretical prediction of P_M^{st} differs from the result presented in Section 5.3.2. Thus the generator-matrix approach can be understood as providing an approximation for

the regime of slow-to-intermediate switching that improves on the slow-switching limit in Section 5.3.1.

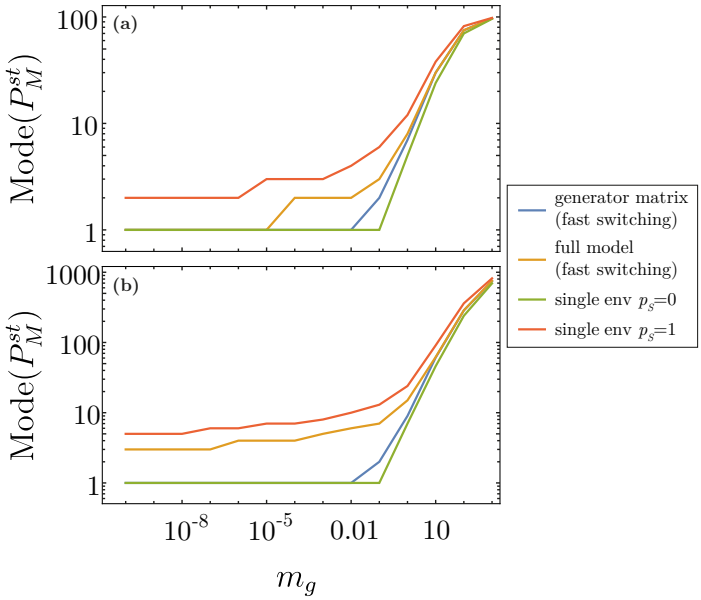

Figure 5.9: Mode of stationary distribution of the number of mating types, P_M^{st}, as function of m_g for $p_S = 0.5$ and population size: (a) $N = 100$ and (b) $N = 1000$. The prediction of the fast-switching limit in the full model is the approximation in Section 5.3.2, whilst the prediction of the generator-matrix approach in the fast-switching limit is described in Section 5.8.4 of the Supplementary Material. The predictions of single environments with $p_S = 0$ and $p_S = 1$ correspond to the non-switching cases in Section 5.7.

Alternatives to the generator-matrix approach

We have seen in Section 5.3.3 that while we can obtain a good approximation for the dynamics in the sexual environment in the environmental switching model, the approximation of the dynamics in the asexual environment is more challenging. This is perhaps surprising as in the asexual environment the dynamics of mating type frequencies are essentially given by a multi-allelic neutral Moran model, for which a wealth of well-established analytic results are available [40]. In this section we discuss two alternatives to the generator-matrix approach that leverage these results and demonstrate how, although initially plausible, each leads to their own set of issues.

First, we consider utilising standard results for the mean extinction time of a neutral allele. Assuming that on leaving the sexual environment with M' mating types the frequency of each mating type is evenly distributed as $n_i \approx N/M'$ (valid when N is large), the mean time to transition from M' to M mating types is given by Eq. (5.28) in

the absence of mutation. Given an initial number of mating types M', the mean time to subsequently transition from M to $M-1$ is then given by $\tau_r(M', M-1) - \tau_r(M', M)$. While this expression clearly features a dependence on the initial number of mating types in the asexual environment, M', we find that this dependence is weak and in fact drops out in the limit of large M'. Assuming then that m_g is small, such that the probability that the probability of transitioning from M to $M+1$ in the asexual environment is negligible, we can approximate the birth-death transitions in the asexual environment as

$$\begin{aligned} T^{+}_{M|A} &\approx 0, \\ T^{-}_{M|A} &\approx \left. \frac{1}{\tau_r(M', M-1) - \tau_r(M', M)} \right|_{M' \to \infty}. \end{aligned} \tag{5.29}$$

Here we have approximated the effective extinction rate of mating types, $T^{-}_{M|A}$, by inverse of the mean time to transition from M to $M-1$.

While this may at first seem entirely reasonable, we find in fact that this model largely underestimates the number of mating types seen in the full model. The central problem is that while the mean transition time implied by Eq. (5.29) does indeed approximate the mean transition time in the full model, the full distribution of transition times is poorly predicted. Equation (5.29) assumes that the waiting time for a transition from M to $M-1$ is exponentially distributed, with a non-zero probability of transitioning after a very small time in the asexual environment. However, the real distribution of transition times is peaked at a particular time, with transitions at very small times being impossible (it takes a minimum of N/M' reproductive events to drive a mating type extinct). In this way the approach suggested in Eq. (5.29) allows more frequent extinctions than actually observed, and thus a lower number of mating types in the stationary distribution than we see in simulations.

A second approach is to ignore the distinct asexual environment entirely, but to instead allow arbitrary transitions from a state M' to all states $M < M'$. Again, we assume that m_g is small, and ignore the possibility of an increase in the number of mating types in the asexual environment. In the sexual environment, we have contributions to the probability that the number of mating types increases or decreases by one, as in Section 5.3.3. When the system enters the asexual environment, we now ask what is the probability of transitioning from $M' \to M$ before the system reverts to

the sexual environment. In this way we can circumvent any direct modelling of the asexual environment while slightly increasing the complexity of the single-environment model by adding non-local transitions.

While the above approach may at first seem analytically challenging, progress is in fact possible. In [40], an expression was developed for the probability that exactly M alleles remain in a population at some time t. All we need to do is integrate this function over the probability of transitioning from the asexual to the sexual environment at time t (i.e., the exponential distribution with parameter $\lambda_{A\to S}$). We find then that accounting for the asexual environment yields the following contribution to the probability per unit time of transitioning from M to M':

$$\lambda_{S\to A}\Phi(M', M)\,, \tag{5.30}$$

with

$$\Phi(M', M) = \sum_{s=1}^{M'-M} (-1)^{M'-M-s} \binom{M'-s}{M'-M-s} \binom{M'}{s} F\left(\frac{s}{M'}\right)\,,$$

where

$$F\left(\frac{s}{M'}\right) = \frac{s}{M'} - \frac{1}{2}\sum_{l=0}^{\infty}\left\{(-1)^l\left[P_l\left(1-2\frac{s}{M'}\right) - P_{l+2}\left(1-2\frac{s}{M'}\right)\right]\frac{2N\lambda_{A\to S}}{2(1+N\lambda_{A\to S})+l(3+l)}\right\} \tag{5.31}$$

and $P_l(y)$ are Legendre polynomials.

The above technique provides an analytically elegant alternative to the generator-matrix approach. Unfortunately, it turns out to be numerically impractical. Equation (5.31) involves the infinite sum over Legendre polynomials, and the slow convergence of these terms is a known numerical issue [41]. Convergence is especially problematic when $N\lambda_{A\to S}$ is large, a range (large population size) that is particularly interesting biologically. Therefore while this second approach has the best potential for providing an analytic approximation to the number of mating types at intermediate regimes, its ultimate success relies on an improved analytic or numerical method for tackling Eq. (5.31), which lies outside the scope of this paper.

Since we are unable to fully analysing the intermediate switching regime, it is hard to exactly define when the system is found in this limit. We cannot determine, for example, for which parameters the mode bifurcates in two as observed in Fig. 5.7, or

which of both modes has a higher probability. The difficulty of analysing this regime in comparison to the slow and fast switching regimes relies on the absence of any approximation in which we can base our calculations. This means that in order to study the stationary distribution of the number of mating types we need to take into account every aspect of the system.

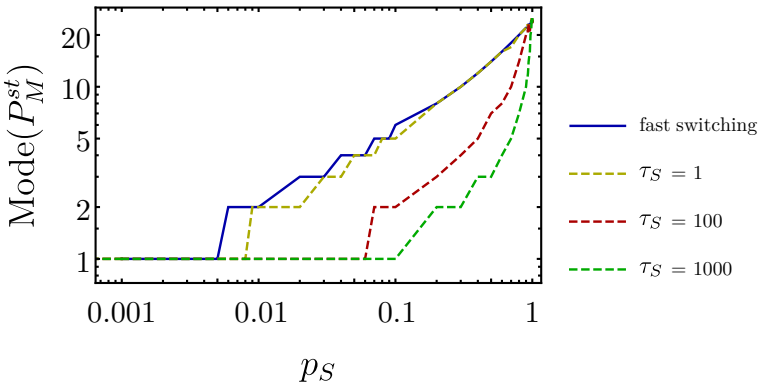

Figure 5.10: Mode of stationary distribution of the number of mating types, P_M^{st}, as function of the probability of being in a sexual environment, p_S, for parameters $N = 10^4$ and $m_g = 10^{-3}$. The prediction of the fast-switching regime is based upon the results studied in Section 5.3.2. For longer residency times in the sexual environment (i.e., longer τ_S), simulations of the full model (dashed lines) demonstrate a lower number of mating types, in qualitative agreement with the results of Section 5.3.3. Discrepancy between the fast-switching limit and the simulations increases as p_S increases, when the system enters the intermediate switching regime. As p_S approaches zero, the system enters the slow-intermediate regime described by the generator-matrix approach (see Eq. (5.27)), in which only one mating type can be maintained.

Regime of small m_g and large N

Having developed approximations for the intermediate regime when m_g is large and N is small, we here investigate the range and extent of the intermediate switching regime when m_g is small and N is large, reflecting a more panmictic population in which m_g can readily be interpreted as a mutation rate. In Figure 5.10 we plot the mode number of mating types in the stationary distribution as a function of the probability of being in a sexual environment, p_S, for varying mean residency times in the sexual state, τ_S. We see that for $p_S \approx 1$ (almost obligate sex) the number of mating types is well described by the fast-switching theory of Section 5.3.2. However as p_S is lowered, we begin to see departures from this theory, with the number of mating types consistently lower than that predicted by the fast-switching limit. These departures are ever more extreme as the time spent in the sexual environment (and consequently for fixed p_S,

also the time spent in the asexual environment) increases. We can therefore see that fast-switching theory very much represents an upper-bound on the mode number of mating types expected for a general set of parameters.

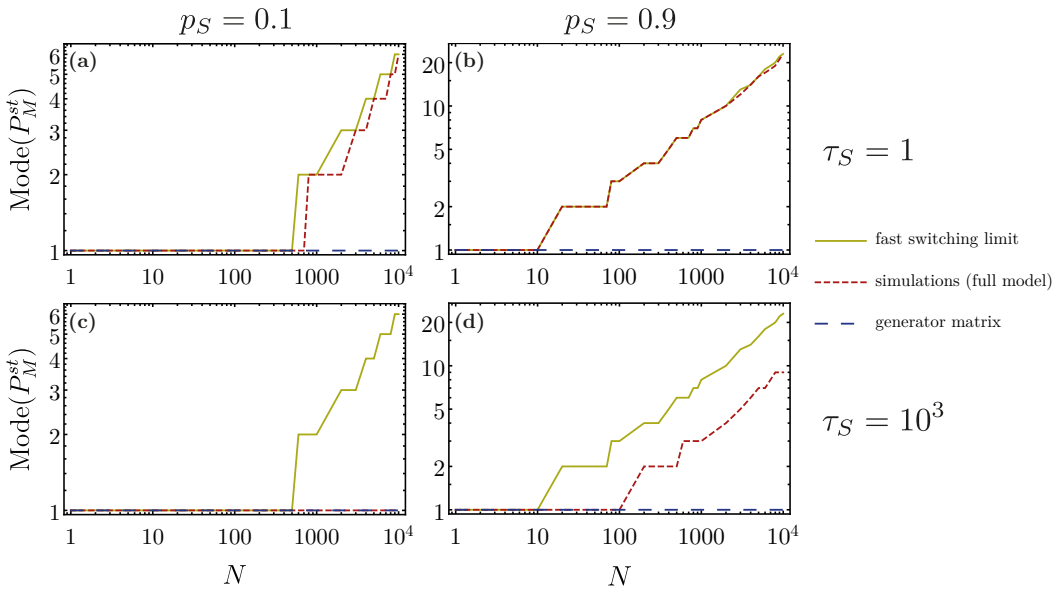

Figure 5.11: Mode of stationary distribution of the number of mating types, P_M^{st}, as function of the population size N for $m_g = 10^{-3}$ for different values of p_S and τ_S. The fast-switching prediction is based upon the results studied in Section 5.3.2, whilst the generator-matrix approach upon the prediction of the framework presented in Section 5.3.3. Simulations were run up to time $t = 10^8$, with measurements starting $t = 10^3$ to ensure stationarity.

While it is computationally impractical to investigate population sizes much larger than $N = 10^4$, or mutation rates much lower than 10^{-3} (as in Figure 5.10), we are nevertheless interested in what general patterns we might expect to see as we go beyond this regime. In Figure 5.11 we investigate how the mode number of mating types varies with population size. Broadly our results fit our intuition developed thus far; when the time spent in the asexual environment is very short (see panel (b)) the system is well-approximated by the fast switching theory, while when the time spent in the asexual environment is very long (see panel (c)) the generator-matrix approach works well (in fact, τ_r in Eq. (5.28) is less than one percent of τ_A for all the values of N shown in panel (c)). Meanwhile at intermediate switching regimes we see that the magnitude of departure from the fast-switching theory increases as time spent in the asexual environment increases (see panels (a) and (d)). However we also see now that as N increases, the simulation results for intermediate switching rates begin to approach the fast-switching limit. In the context of Eq. (5.28), this is perhaps unsurprising; the

timescale on which extinctions occur in the asexual environment is linearly dependent on N, and so, as this population size increases, the range of switching rates that can still be considered fast also increases.

5.4 Selective sweeps in the switching environmental model

In the previous section we demonstrated that explicitly accounting for switching environments led to both quantitative and qualitative changes in the model predictions. In this section we will show how this change in modelling formalism allows us to tackle a richer array of biological questions, without necessarily sacrificing tractability.

Suppose that mutations arise in the population at loci unlinked to the mating type locus at an average rate μ. We will further suppose that the mutant allele is under directional (frequency independent) selection, such that individuals carrying the mutation have a selective advantage s over individuals carrying the resident allele. If $s < 0$, the mutation will be selected against and will be rapidly lost from the population. If $s > 0$ the mutation will be selected for and (in the absence of stochastic extinction effects) will sweep to fixation. However the focus of interest for this study is the frequency of the mating type alleles. The impact of this selective sweep will have very different effects on the mating type frequencies depending on the environment, sexual or asexual, in which it occurs.

If this mutation arises while the system is in the sexual environment, it quickly spreads to all the present mating types via genetic recombination and has no effect on the number of mating types M. For instance, say that mutation occurs in an individual of mating type 1. While that individual experiences a selective advantage s, upon sexual reproduction with a non-self mating type (say of mating type 2) the beneficial mutation will have the opportunity to spread to another mating type class. Thus the beneficial mutation will rapidly spread through the mating type populations without appreciably distorting their frequencies.

Conversely, if this mutation arises while the system is in the asexual environment, it is confined to the mating type on which it occurs (genetic recombination is absent) and will cause large distortions in the mating type frequencies. Denoting by y the

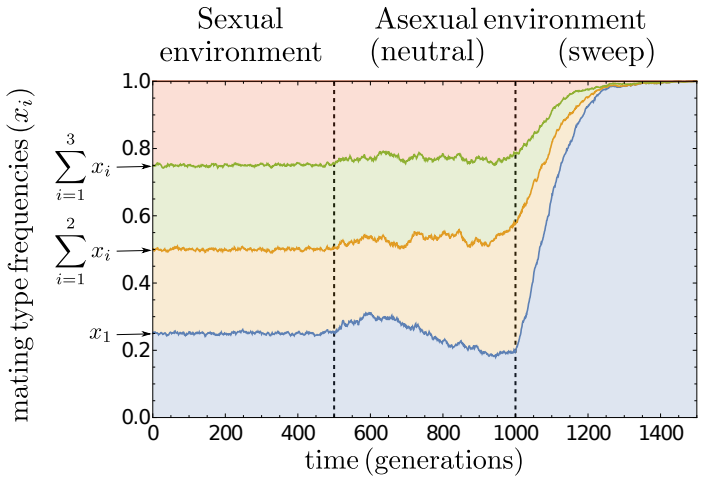

Figure 5.12: Illustration of the dynamics of mating type frequencies $x_i = n_i/N$ when selective sweeps are accounted for. In the sexual environment ($0 < t < 500$) mating type frequencies are held at approximately equal values by negative frequency dependent selection. Beneficial mutations at unlinked loci spread to each mating type subpopulation through recombination, and thus do not affect this even mating type distribution. In the asexual environment ($500 < t < 1500$), in the absence of beneficial mutations ($500 < t < 1000$) mating type frequencies fluctuate due to genetic drift alone. However when beneficial mutations occur ($t = 1000$), the mating type background on which they arise can hitchhike to fixation, reducing the number of mating types to one. Data is obtained from Gillespie simulation with $N = 5 \times 10^4$ and $s = 0.02$.

frequency of individuals carrying the beneficial mutation, their dynamics in the large N limit will be given by

$$\frac{\mathrm{d}y}{\mathrm{d}t} = sy(1-y) \implies y(t) = \frac{1}{1 + e^{-st}(N-1)} \,. \tag{5.32}$$

Let us suppose again that the beneficial mutation occurs in an individual of mating type 1. Then, assuming that initially the mating types were in approximately equal abundances, the dynamics for the mating type frequencies x_i is given by

$$x_1(t) = y(t) + \frac{1}{M}\left(1 - y(t)\right) \,, \tag{5.33}$$

$$x_i(t) = \frac{1}{M}\left(1 - y(t)\right) \,, \quad \forall\, i \geq 2 \,. \tag{5.34}$$

These dynamics are illustrated in Figure 5.12. We see that as the mutation sweeps through the population, the total number of individuals of mating types $i \geq 2$ decreases, and thus, stochastic extinctions of these mating type classes become more likely. Over only slightly longer timescales, fixation of a single mating type is all but guaranteed, with the mean time until the fixation of a single mutant given approximately by $2\log(N)/s$ in large populations. We now leverage the results of the previous section to provide a more simple approach using the reduced model. We explain this below.

In addition to the effective birth-death and switching environment processes previously present in the generator-matrix approach, we now consider the possibility that the system transitions to a state of one single mating type at constant rate ν when in the asexual environment. The rate ν can thus be understood as a compound parameter that captures the average rate at which a beneficial mutation occurs in an asexual environment $\mu(1-p_S)$ and has sufficient time to sweep a single mating type to fixation. this occurs with probability $\int_{t=2\log(N)/s}^{\infty}(1/\tau_A)\exp(-t/\tau_A)\,\mathrm{d}t$, and we therefore have

$$\nu = \mu(1-p_S)N^{-2/(s\tau_A)}\,, \tag{5.35}$$

where $2\log(N)/s$ is the conditional mean fixation time for a single mutant to fixate in large populations. We consider the rates $T^{\pm}_{M|\sigma}$ as before, first assuming a fixed environment. For environment $\sigma = A$ then, we have

$$M \xrightarrow{T^{+}_{M|A}} M+1, \quad M \xrightarrow{T^{-}_{M|A}} M-1 \quad \text{and} \quad M \xrightarrow{\nu} 1, \tag{5.36}$$

while for $\sigma = S$

$$M \xrightarrow{T^{+}_{M|S}} M+1, \quad \text{and} \quad M \xrightarrow{T^{-}_{M|S}} M-1.$$

The switching environment transitions are as in the previous sections (i.e., as in Eq. (5.1)). The stationary distribution P^{st}_M for this scenario can be estimated in a similar way to the method presented in Section 5.3.3, by constructing the corresponding generator matrix $\underline{\underline{Q}}$ in which the selective sweeps process $M \xrightarrow{\nu} 1$ is included (see Section 5.9.1 of the Supplementary Material for details). Figure 5.13 shows the theoretical prediction of P^{st}_M obtained from this approach for both switching environments, considering an equal fraction of time spent in each environment (i.e., $p_S = 1/2$).

The inclusion of selective sweeps brings interesting features in both switching regimes. For the slow-switching case (see upper row of Figure 5.13), we observe that the distribution still remains bimodal but with a considerably higher peak at $M = 1$. As ν increases, the distribution at both modes remains constant. On the other hand, for the fast-switching regime (see lower row of Figure 5.13), as ν increases the mode transitions from a value $M > 1$ to $M = 1$. In both regimes, the emergence of the peak at $M = 1$ occurs when ν crosses certain point determined by how high the mutation rate m_g is. As m_g increases, this point will naturally be higher.

The approach employed here to predict P^{st}_M is an approximation as it makes use of rates $T^{\pm}_{M|\sigma}$ that assume a fixed environment. We compare it against numerical

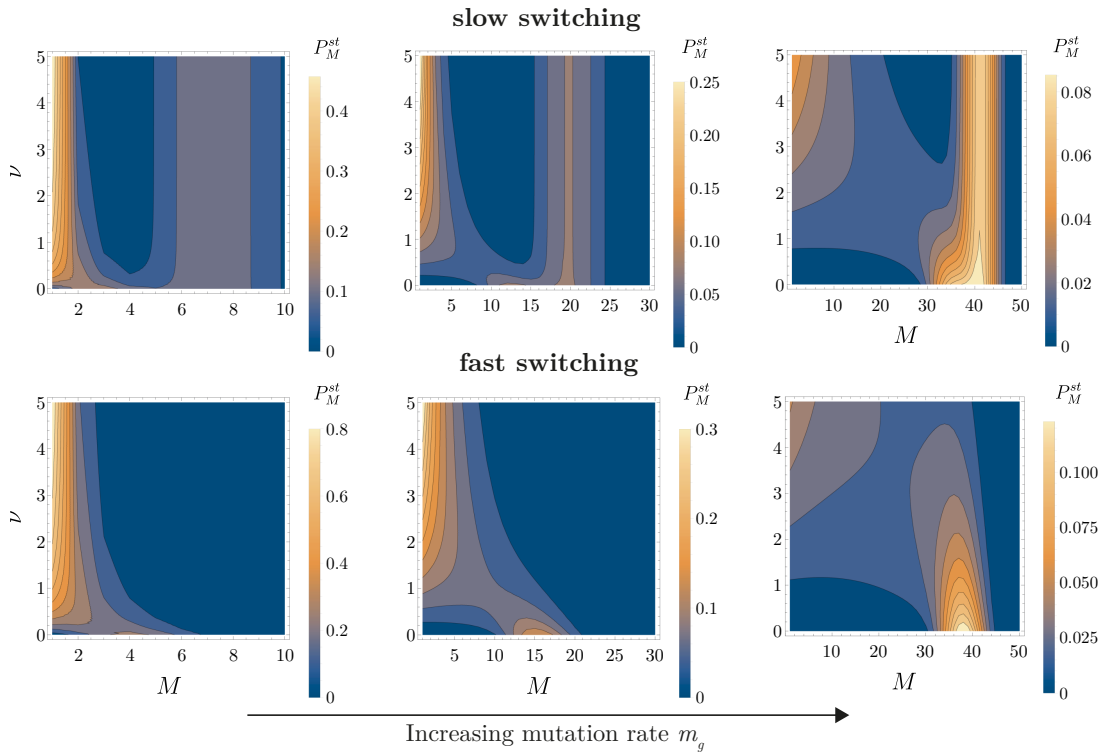

Figure 5.13: Theoretical prediction of P_M^{st} as function of M and ν for different values of m in slow and fast switching environments. Population size $N = 50$. From left to right panels: $m_g = 0.5, 5, 5$.

simulations in Section 5.9.1 in the Supplementary Material. We also explore the case of selective sweeps in a fixed asexual environment in Section 5.9.2. Our theoretical predictions capture the main effects on the distribution of the number of mating types when selective sweeps are included.

In the presence of selective sweeps we can then see the following biological picture emerge. In order for the populations to maintain more than a single (essentially non-functional) mating type, one of two scenarios must hold. In the first scenario we see $m_g \gg \nu$. In this case the rate of supply of new mating types (governed by m_g) far exceeds the extinction rate generated by selective sweeps (governed by ν). This would be appropriate if we were to consider m_g as representing a migration rate between geographically structured subpopulations. In the second scenario we see $s^{-1} > \tau_A$. In this case while selective sweeps can initiate in the asexual environment, switching is sufficiently fast that the sweeps cannot complete.

5.5 Conclusions

For reasons on tractability, most studies considering evolution in facultatively sexual populations focus on asynchronous sex, in which individuals probabilistically engage in sexual reproduction [29]. This is also true for models that have tried to capture the evolution of mating type number under demographic stochasticity [24, 25, 30]. In this paper we have released this restriction to consider the dynamics of the number of mating types under demographic stochasticity in populations that switch synchronously between asexual and sexual environments. In a course grained sense our model recapitulates previous theoretical and empirical observations that the number of mating types should be positively correlated with increasing amounts of sexual relative to asexual reproduction. However we have shown that the additional consideration of sexual synchrony generates both quantitative and qualitative differences from the asynchronous model, as well as offering scope for asking a richer array of biologically interesting questions.

With respect to quantitative differences between the asynchronous and synchronous models, we have shown the two models are only equivalent in the limit of fast switching between environments. However as switching becomes slower (and in particular as the amount of time in the asexual environment becomes longer) mating type extinctions become more likely in the synchronous model, lowering the expected number of mating types in the stationary distribution. For instance, in Figure 5.10 with a probability of $p_S = 1/2$ of being in the sexual environment, we see a reduction of more than 10 mating types when the time spent in the sexual environment is large ($\tau_S = 100$) relative to the asynchronous (fast-switching) theory. This reduction may explain previous overestimates in the expected number of mating types when compared with previous studies where asynchronous sexual reproduction was assumed [24, 25]. In fact the mode number of mating types can drop to just one type over a range of biologically relevant parameters.

Qualitative differences between the asynchronous and synchronous models are most apparent in small populations. In this scenario the parameter m_g can be interpreted as a per-generation migration rate (with mating types coming from a highly diverse pool), which we expect biologically to be much higher than a mutation rate. When

switching is fast, we see as before that the model tends to the limit of asynchronous switching. However, when switching is slow, a bimodal prediction for the number of mating types is possible. Here the population spends enough time in the asexual and sexual environments that the stationary distribution approaches a superposition of those in the fixed environments; just a single mating type is maintained in the sexual environment, while in the sexual environment ingressing mating types rapidly establish. We emphasise that this behaviour is not possible in the asynchronous model. While local absences of particular mating types are common in samples of fungi (e.g. *Coccidioides* [42]) and ciliates (e.g. *Tetrahymena pyriformis* [43]), obtaining empirical distributions of the number of mating types across geographic locations is hindered by low sample sizes. However our analysis agrees qualitatively with the observation that the presence of more than one mating type is indicative of more recent sexual activity [44]. Meanwhile observations of all mating types present across geographic regions (as for instance in *Dictyostelium discoideum* [45]) is consistent not only with the observation of relatively high rates of sexual reproduction, but also of a fast switching rate between asexual and sexual reproductive modes.

From a modelling perspective, by allowing for synchronous sexual reproduction we have also been able to tackle the issue of selective sweeps. In [30] it was shown that selective differences between mating types (induced, for instance, by non-neutral mutations at loci linked to the mating type locus) could rapidly reduce the number of types observed. As the model was deterministic and assumed asynchronous sexual reproduction, it could not quantify how selective sweeps (caused by beneficial mutations at loci unlinked to the mating type locus) might affect the number of types observed in isogamous species. Experimentally however, such sweeps have been shown to be strong drivers of mating type extinctions in facultatively sexual species such as *Chlamydomonas* [31] and *Tetrahymena* [46]. Accounting for this effect mathematically, we have been able to show that although this effect decreases rapidly with increasing population size, a substantial extinction risk is present when the product of the strength of beneficial mutations and the average time spent in the asexual environment is greater than one ($s\tau_A > 1$). We stress, however, that in dealing with selective sweeps we have made some approximations, such as including the effect of selective sweeps as an additional reaction to a switching environment scheme, with this latter employing

transition rates assuming a fixed environment. An exact approach would be to analyse a switching environment system with selective sweeps altogether. This brings, however, considerable difficulties for analytical study and is beyond the scope of this paper.

By accounting for demographic stochasticity, synchronous sex, and selective sweeps, our model suggests that the persistence of self-incompatible mating types in facultatively sexual populations may be even more precarious than previously believed [39]. In fact, a range of biologically plausible parameters suggest that just a single (functionally asexual) mating type is most probable at long times. Empirical phylogenies of isogamous species such as within fungi [47] and ciliates [48] show that such scenarios are relatively common. And yet despite this, species with distinct mating types have remained stable over long evolutionary periods, with highly conserved mating type loci [49]. In light of this it is possible to reframe the evolutionary question away from asking "*Why do most isogamous species have just two mating types?*" and towards "*How do so many facultatively sexual species maintain even two in the face of genetic drift and selective sweeps?*". Our bimodal results for small population sizes with an effective migration rate point to a possible solution, suggesting a role for spatial structure. If sex is not synchronised in time across a whole population, but rather synchronised across a finite set of spatial regions, mating type diversity may be maintained. However, further work, perhaps involving metapopulation models [50], would be needed to fully uncover how geographic population structure might affect the evolution of mating type number.

More broadly, our results also point to some important considerations in the general literature on the evolution of sexual reproduction. While the facultative nature of sexual reproduction in models that assume asynchronous sex is captured by just a single parameter (the probability of a sexual rather than asexual event), models of synchronous sex require the specification of two parameters (the mean time spent in sexual and asexual environments). For species in which sexual reproductive phases are induced in a seasonal or regular manner (such as *Tetrahymena* [51]), these parameters may be relatively straightforward to estimate. However for species in which sexual reproduction is irregular or very rare, such as (*Chlamydomonas* [52] or *Saccharomyces* [53]) estimating these parameters independently may pose a far greater challenge. Here 'rates of sexual reproduction' are often estimated using genomic methods that can be used to infer the long-time average number of sexual to asexual reproductive events (equivalent to

p_S in our model), but the of duration time spent in each state is left unspecified [53, 54]. While difficult to obtain, we suggest that obtaining estimates of these parameters is a worthwhile endeavour, as we have shown specifying their precise values can have important evolutionary consequences.

One example, with a direct relation to the current study, is the evolution of 'mating type switching', the ability of individuals to change their expressed mating type between asexual reproductive events. This has been previously explored using simulations of populations with synchronous sexual reproduction [23], with the number of asexual generations between single sexual generations varied. It was found that mating-type switching was more likely to evolve as the number of concurrent asexual generations increased (which distorted the relative frequencies of non-switching mating types through drift, and placed them at a selective disadvantage). While we also see strong distortions in mating type frequencies here when periods of asexual reproduction are long (large τ_A), it should be noted that we also observe distorted frequencies when the probability of being in the sexual environment is very small ($p_S = \tau_S/(\tau_S + \tau_A)$). Thus, long periods of asexual reproduction may not be needed for the evolution of mating type switching.

A second example is the enigma of the evolution of sexual reproduction and genetic recombination itself [55]. It has been suggested that facultative sex provides the best of both worlds [56], engendering species with the benefits of sexual reproduction (increased genetic diversity and evolvability [57]) while minimising the costs (for instance finding a suitable mate or the ubiquitous the costs of recombination [58]). In this sense it has been further suggested that in maximising the possibilities of finding a mate, synchronous sexual reproduction may be better still [29]. However, as we have shown, asynchronous sex can lead to its own costs at the population level in terms of an increased extinction probability of partners with which to mate. Thus, in the absence of a mechanism to provide assured sexual reproductive opportunities in later generations (such as mating type switching), some level of asynchronous sex may in fact be beneficial for maintaining the diversity of compatible partners at the population level.

In evolutionary modelling there is always a natural tension between analytic tractability and biological realism. The optimal point between these two extremes is ultimately subjective, however, an increased level of biological realism is arguably warranted if

it: (i) generates qualitative differences; (ii) generates quantitative differences or (iii) allows the exploration of more interesting biological questions. Under these metrics, we have shown that accounting for the synchrony of sex is an important modelling consideration for investigating the evolutionary dynamics of the number of mating types in finite populations. We have demonstrated that while analytic results can be derived in a relatively straightforward manner in the fast and slow switching regimes, intermediate switching rates pose more of an analytic challenge. While improvements on the slow-switching approximation through the generator-matrix approach are possible under certain conditions, a more generally applicable approximation is difficult to obtain. This is, as we have discussed, despite the relative simplicity of the neutral dynamics in the asexual environment. Developing further analytic methods for dealing with systems featuring both demographic stochasticity and switching environments presents an interesting mathematical challenge, but also one that is ultimately required for a full understanding evolution in facultatively sexual species. It is our hope that in the coming years this challenge will be taken up to yield new evolutionary insight on a host of problems involving facultative sex.

5.6 Appendix A: Effective rates $T^{-}_{M|\sigma}$ and $T^{+}_{M|\sigma}$ as function of $P^{\mathbf{st}}_{\mathbf{n}|\sigma}$

In this section, we provide details for the first step of the calculation of the rates $T^{-}_{M|\sigma}$ and $T^{-}_{M|\sigma}$ in the reduced model. These are defined in the main paper. Throughout the calculation we assume that the environmental state is fixed in time. This means that the birth and death rates in the full model do not vary with the environment. The result of this section is expressed in terms of the stationary distribution of states $\mathbf{n}$ of the full model, $P^{\mathrm{st}}_{\mathbf{n}|\sigma}$. Further evaluation then follows in the subsequent section of this Supplementary Material.

To derive results for the effective rates in the reduced model we start from the transition rates from the full model. The rates for birth-death events are given by

$$\begin{aligned} \mathcal{T}^{S}_{ij} &= \frac{1}{2}\frac{n_i n_j}{N^2}\left(N - n_i\right), \\ \mathcal{T}^{A}_{ij} &= \frac{n_i n_j}{N} \end{aligned} \tag{5.37}$$

in the two environmental states (S and A). This describes rate of events in which one individual of mating type i reproduces and an individual of type j is removed, i.e., events in which $n_i \to n_i + 1$ and $n_j \to n_j - 1$.

Mutation events occur with rates

$$\mathcal{T}^{m}_{j} = m_g \, \frac{n_j}{N}, \tag{5.38}$$

independent of the state of the environment.

We carry out the calculation at a more general level than needed for the system with two environmental states. Following [24], we allow for an arbitrary rate of sexual reproduction, $0 \leq p_S \leq 1$, and use

$$\mathcal{T}^{p_S}_{ij} = \left[(1 - p_S) \frac{n_i}{N} + \frac{p_S}{2} \frac{n_i}{N} \left(\frac{N - n_i}{N} \right) \right] n_j, \tag{5.39}$$

instead of the rates given in Eq. (5.37). We note that time is measured in units of generations in our model, so that the transition rates $\mathcal{T}^{p_S}_{ij}$ carry an extra factor N in comparison to [24].

The specific cases of fully sexual or fully asexual reproduction ($\sigma = S, A$) can be obtained by setting $p_S = 1$ or $p_S = 0$ respectively. We then recover the transition matrices defined in Eqs. (5.2) and (5.3) of the main paper as

$$\mathcal{T}^{p_S=1}_{ij} = \mathcal{T}^{S}_{ij} \quad \text{and} \quad \mathcal{T}^{p_S=0}_{ij} = \mathcal{T}^{A}_{ij}. \tag{5.40}$$

We write $T^{-}_{M|p_S}$ and $T^{+}_{M|p_S}$ for the effective rates of the reduced model, when the full model is such that birth-death events occur with the rates given in Eq. (5.37). Our aim is to calculate the $T^{\pm}_{M|p_S}$, when p_S is fixed in time in the full model.

5.6.1 Calculation of the effective rate $T^{-}_{M|p_S}$

For small Δt, the quantity $\Delta t \, T^{-}_{M|p_S}$ can be obtained from the probability that the number of mating types decreases by one in the next Δt units of time, given that there are currently M mating types. More precisely,

$$\begin{aligned} P^{-}_{M|p_S}(\Delta t) &\equiv P(\{M \to M-1\} | M \text{ mating types in the population }) \\ &= \Delta t \, T^{-}_{M|p_S} + \mathcal{O}(\Delta t^2). \end{aligned} \tag{5.41}$$

In this expression we have written $\{M \to M-1\}$ for the event in which the number of mating types reduces from M to $M-1$ in the next Δt units of time. We always assume a fixed value of p_S in the full model.

When M different mating types are present in the population, the system can be found in any state $\mathbf{n}$ that has M non-zero entries. We write $C_{\mathbf{n}}$ for the event that the population is in state $\mathbf{n}$. Since the population size is fixed at N, the sum of the entries of $\mathbf{n}$ is always N. The vectors $\mathbf{n}$ of this type are known 'compositions' (or '$M-$compositions') of the integer N [33]. We write $\mathcal{S}^M$ for the set of these compositions, i.e., $\mathcal{S}^M$ is the set of vectors $\mathbf{n}$ with precisely M non-zero entries, and with $\sum_i n_i = N$.

To ease the notation we introduce the following events (in the sense of probability theory):

$$\begin{aligned} A &= \text{the event in which the number of mating types reduces from } M \text{ to } M-1 \\ &\quad \text{in the next } \Delta t \text{ units of time.} \\ B_M &= \text{the event to find the population in a state with } M \text{ mating types} \\ C_{\mathbf{n}} &= \text{the event to find the population in state } \mathbf{n}. \end{aligned} \tag{5.42}$$

In this notation, $P^-_{M|p_S}(\Delta t) = P(A|B_M)$. We note that $B_M = \cup_{\mathbf{n}\in\mathcal{S}^M} C_{\mathbf{n}}$, and that the $C_{\mathbf{n}}$ are pairwise disjoint. The conditional probability in Eq. (5.41) can then be written as

$$\begin{aligned} P^-_{M|p_S}(\Delta t) &= \sum_{\mathbf{n}\in\mathcal{S}^M} P\left(A \cap C_{\mathbf{n}}|B_M\right) \\ &= \sum_{\mathbf{n}\in\mathcal{S}^M} \frac{P\left(A \cap C_{\mathbf{n}} \cap B_M\right)}{P(B_M)}. \end{aligned} \tag{5.43}$$

Noting that $C_{\mathbf{n}}$ is a subset of B_M for $\mathbf{n} \in \mathcal{S}^M$, we have $P\left(A \cap C_{\mathbf{n}} \cap B_M\right) = P\left(A \cap C_{\mathbf{n}}\right) = P(A|C_{\mathbf{n}})P(C_{\mathbf{n}})$. Using this, we find

$$P^-_{M|p_S}(\Delta t) = \sum_{\mathbf{n}\in\mathcal{S}^M} P\left(A|C_{\mathbf{n}}\right) \frac{P(C_{\mathbf{n}})}{P(B_M)}. \tag{5.44}$$

This formula has a straightforward interpretation. We are interested in the probability that the event A occurs (extinction of a mating type in the next Δt), given that there are currently M mating types in the population (condition B_M). If there are exactly M mating types in the population, then the population is in state $\mathbf{n} \in \mathcal{S}^M$ with probability $P(C_{\mathbf{n}}|B_M) = P(C_{\mathbf{n}})/P(B_M)$ (where we note $C_{\mathbf{n}} \subset B_M$). This is the second factor on

the right-hand side of Eq. (5.44). The first factor, $P(A|C_{\mathbf{n}})$, is the probability that A occurs given that the population is in state $\mathbf{n}$.

In the stationary state, the distribution $P(C_{\mathbf{n}})$ is then given by the stationary distribution of the full model for a fixed value of p_S. Results for this distribution were obtained by Constable and Kokko in [24] for general values of p_S (p_S maps to the parameter c in [24] via $c = 1 - p_S$). Using $P(C_{\mathbf{n}})$ we can express $P(B_M) = \sum_{n\in S^M} P(C_{\mathbf{n}})$.

The rate $T^-_{M|p_S}$ is obtained from $P^-_{M|p_S}(\Delta t)$ as

$$T^-_{M|p_S} = \lim_{\Delta t\to 0} \frac{P^-_{M|p_S}(\Delta t)}{\Delta t}. \tag{5.45}$$

The problem then reduces to calculating $P(A|C_{\mathbf{n}})$, for $\mathbf{n} \in \mathcal{S}^M$, i.e. the probability that a mating type becomes extinct in the next time interval Δt, if the composition of the population is currently $\mathbf{n}$.

As a first step, we find the overall rate with which $n_j \to n_j - 1$ for a fixed j (and always assuming fixed p_S). This takes the form

$$\sum_{i\neq j} \mathcal{T}^{p_S}_{ij} = \frac{n_j}{2N}\left[(2-p_S)(N-n_j) - \frac{p_S}{N}\left(\sum_{k=1}^{M} n_k^2 - n_j^2\right)\right]. \tag{5.46}$$

We write $\mathcal{F}^{p_S}_M(\mathbf{n})$ for overall rate of the event in which any entry $n_j = 1$ is reduced to zero. Summing over j in Eq. (5.46) and taking into account only contributions with $n_j = 1$, this is obtained as

$$\mathcal{F}^{p_S}_M(\mathbf{n}) = \frac{1}{2N}\left[(2-p_S)(N-1) + \frac{p_S}{N}\left(\sum_{k=1}^{M} n_k^2 - 1\right)\right]\left[\sum_{j=1}^{M} \delta_{n_j,1}\right]. \tag{5.47}$$

In this expression $\delta_{n_j,1}$ denotes the Kronecker delta, i.e. $\delta_{n,1} = 1$ if $n = 1$ and $\delta_{n,1} = 0$ otherwise. The sum $\sum_{j=1}^{M} \delta_{n_j,1}$ is therefore the number of entries of $\mathbf{n}$ that are equal to one. With this, we obtain

$$P(A|C_{\mathbf{n}}) = \mathcal{F}^{p_S}_M(\mathbf{n})\Delta t. \tag{5.48}$$

Putting everything together, we have

$$T^-_{M|p_S} = \frac{\sum_{\mathbf{n}\in\mathcal{S}^M} \mathcal{F}^{p_S}_M(\mathbf{n}) P^{\mathrm{st}}_{\mathbf{n}|p_S}}{\sum_{\mathbf{n}\in\mathcal{S}^M} P^{\mathrm{st}}_{\mathbf{n}|p_S}}. \tag{5.49}$$

We stress again that this is for a fixed sex rate p_S in the full model. The result is exact as long as we focus on long times (such that the population is in its stationary state).

The denominator on the right-hand-side in Eq. (5.49) is the stationary distribution of finding M mating types for a given p_S, $P^{\rm st}_{M|p_S}$.

The sums in Eq. (5.49) run over all $M-$compositions of N, $\mathbf{n} \in \mathcal{S}^M$. Using properties of sums over compositions it is possible to obtain a closed-form solution for $T^-_{M|p_S}$. We will describe this in detail below in Section 5.7.

5.6.2 Calculation of the effective rate $T^+_{M|p_S}$

To estimate $T^+_{M|p_S}$, we proceed in a similar way. We introduce

$$\begin{aligned} D \;\; = \;\; & \text{the event in which the number of mating types increases from } M \\ & \text{to } M+1 \text{ in the next } \Delta t, \end{aligned} \tag{5.50}$$

and obtain

$$P^+_{M|p_S}(\Delta t) = \sum_{\mathbf{n}\in\mathcal{S}^M} P\left(D|C_{\mathbf{n}}\right) \frac{P(C_{\mathbf{n}})}{P(B_M)}. \tag{5.51}$$

The probability $P(D|C_{\mathbf{n}})$ can be derived from the rate $\mathcal{T}^m_j$ in Eq. (5.38). Assuming a fixed value of p_S, one gets

$$\begin{aligned} P(D|C_{\mathbf{n}}) \;\; &= \;\; \Delta t \sum_{j:n_j>1} \mathcal{T}^m_j \\ &= \;\; \Delta t \, \frac{m_g}{N} \left(N - \sum_{i=1}^{M} \delta_{n_i,1} \right). \end{aligned} \tag{5.52}$$

The factor $N - \sum_{i=1}^{M} \delta_{n_i,1}$ on the right-hand side is the number of individuals in the population for which there is at least one other individual in the population with the same mating type (i.e, the sum excludes individuals who are 'singletons' in the population). Only mutation events of such individuals lead to an increase of the number of mating types. Introducing

$$\mathcal{G}_M(\mathbf{n}) = \frac{m_g}{N} \left(N - \sum_{i=1}^{M} \delta_{n_i,1} \right), \tag{5.53}$$

we obtain

$$T^+_{M|p_S} = \frac{\sum_{\mathbf{n}\in\mathcal{S}^M} \mathcal{G}_M(\mathbf{n}) P^{\rm st}_{\mathbf{n}|p_S}}{\sum_{\mathbf{n}\in\mathcal{S}^M} P^{\rm st}_{\mathbf{n}|p_S}}. \tag{5.54}$$

As for calculation of $T^-_{M|p_S}$, it is now necessary to carry out the sum over $M-$compositions of the integer N. We will describe in Section 5.7 how we do this.

5.7 Appendix B: Closed-form solutions of $T^{-}_{M|p_S}$, $T^{+}_{M|p_S}$, and $P^{st}_{M|p_S}$

In this section, we present closed-form solutions of rates $T^{-}_{M|p_S}$, $T^{+}_{M|p_S}$, and stationary distribution $P^{st}_{M|p_S}$ using the results derived in the previous section. The method we use is based on the number theory of partitions of integer numbers [32, 33].

As a first step we expand the terms inside the sums in Eqs. (5.49) and (5.54). We have

$$T^{-}_{M|p_S} = \frac{1}{2N}\left[(2-p_S)(N-1)+\frac{p_S}{N}\right]\frac{\sum_{\mathbf{n}\in\mathcal{S}^M}\left(\sum_{i=1}^{M}\delta_{n_i,1}\right)P^{\rm st}_{\mathbf{n}|\sigma}}{\sum_{\mathbf{n}\in\mathcal{S}^M}P^{\rm st}_{\mathbf{n}|\sigma}} - \frac{p_S}{2N^2}\frac{\sum_{\mathbf{n}\in\mathcal{S}^M}\left(\sum_{i=1}^{M}n_i^2\right)\left(\sum_{i=1}^{M}\delta_{n_i,1}\right)P^{\rm st}_{\mathbf{n}|p_S}}{\sum_{\mathbf{n}\in\mathcal{S}^M}P^{\rm st}_{\mathbf{n}|p_S}}, \tag{5.55}$$

and

$$T^{+}_{M|p_S} = \frac{m_g}{N}\left[N-\frac{\sum_{\mathbf{n}\in\mathcal{S}^M}\left(\sum_{i=1}^{M}\delta_{n_i,1}\right)P^{\rm st}_{\mathbf{n}|p_S}}{\sum_{\mathbf{n}\in\mathcal{S}^M}P^{\rm st}_{\mathbf{n}|\sigma}}\right]. \tag{5.56}$$

We notice that there are three sums involved:

$$\begin{aligned} S_1 &\equiv \sum_{\mathbf{n}\in\mathcal{S}^M}P^{\rm st}_{\mathbf{n}|p_S}, \\ S_2 &\equiv \sum_{\mathbf{n}\in\mathcal{S}^M}\left(\sum_{i=1}^{M}\delta_{n_i,1}\right)P^{\rm st}_{\mathbf{n}|p_S}, \\ S_3 &\equiv \sum_{\mathbf{n}\in\mathcal{S}^M}\left(\sum_{i=1}^{M}n_i^2\right)\left(\sum_{i=1}^{M}\delta_{n_i,1}\right)P^{\rm st}_{\mathbf{n}|p_S}. \end{aligned} \tag{5.57}$$

Each of these depends on the value of p_S. For $p_S = 0$, it is not necessary to calculate the last sum as the term including it in Eq. (5.55) vanishes. In what follows, we will analyse the relevant sums for general values of p_S. We do this first for the asexual environment ($p_S = 0$), and then for general $0 < p_S \leq 1$.

5.7.1 Asexual environment ($p_S = 0$)

The stationary distribution of the full model for $p_S = 0$ ($\sigma = A$) was obtained in [24] as

$$P^{\mathrm{st}}_{\mathbf{n}|A} = \alpha \times \prod_{k=1}^{M} \frac{1}{n_k}, \tag{5.58}$$

where α represents a suitable normalisation constant. We write $P^{\mathrm{st}}_{\mathbf{n}|A} = P^{\mathrm{st}}_{\mathbf{n}|p_S=0}$. This constant plays no role in the evaluation of the expressions on the right-hand sides of Eqs. (5.49) and (5.54), as $P^{\mathrm{st}}_{\mathbf{n}|A}$ appears in the numerator and in the denominator.

Calculation of $S_1 = \sum_{\mathbf{n}\in\mathcal{S}^M} P^{\mathbf{st}}_{\mathbf{n}|A}$

The sum $S_1 = \sum_{\mathbf{n}\in\mathcal{S}^M} P^{\mathrm{st}}_{\mathbf{n}|A}$ takes the following form as a sum over compositions

$$S_1 = \alpha \sum_{\substack{n_1+\cdots+n_M=N \\ n_i\geq 1}} \prod_{k=1}^{M} \frac{1}{n_k}. \tag{5.59}$$

This sum has the form $\sum_{n_1+\cdots+n_M=N,\, n_i\geq 1} \prod_{k=1}^{M} f(n_k)$, with $f(n_k) = 1/n_k$. For sums of this form there exists a closed-form solution. It is given by (see e.g. [59])

$$\sum_{\substack{n_1+\cdots+n_M=N \\ n_i\geq 1}} \prod_{k=1}^{M} f(n_k) = \frac{1}{N!}\frac{d^N}{dx^N}\bigg|_{x=0} \left(\sum_{i\geq 1} f(i)x^i\right)^M, \tag{5.60}$$

i.e., the sum is equal to the coefficient multiplying x^N in the power-series expansion of $\left(\sum_{i\geq 1} f(i)x^i\right)^M$.

To simplify matters we introduce the generating function $p(x) = \sum_{i\geq 1} f(i)x^i$, where the sum extends over all values of i for which the function $f(i)$ is defined. In the present case, $f(i) = 1/i$, and i can take arbitrarily large integer values. We find $p(x) = -\log(1-x)$.

Using Cauchy's integral formula [60] the coefficient multiplying x^N in the expression in Eq. (5.60) is given by

$$\frac{1}{N!}\frac{d^N}{dx^N}\bigg|_{x=0} p(x)^M = \frac{1}{2\pi i}\oint_\gamma \frac{p(z)^M}{z^{N+1}}\mathrm{d}z, \tag{5.61}$$

with γ an appropriate rectifiable curve around the origin. We find a solution to this integral by virtue of the integral representation of the Stirling numbers [61]. One obtains

$$\sum_{\substack{n_1+\cdots+n_M=N \\ n_i\geq 1}} \prod_{k=1}^{M} \frac{1}{n_k} = \frac{M!}{N!}\begin{bmatrix} N \\ M \end{bmatrix}, \tag{5.62}$$

where $\begin{bmatrix} N \\ M \end{bmatrix}$ is the unsigned Stirling number of the first kind [34].

Calculation of $S_2 = \sum_{\mathbf{n}\in\mathcal{S}^M}\left(\sum_{i=1}^{M}\delta_{n_i,1}\right)P^{\mathbf{st}}_{\mathbf{n}|A}$

The sum $\sum_{\mathbf{n}\in\mathcal{S}^M}\left(\sum_{i=1}^{M}\delta_{n_i,1}\right)P^{\mathrm{st}}_{\mathbf{n}|A}$ becomes

$$S_2 = \alpha \sum_{\substack{n_1+\cdots+n_M=N \\ n_i\geq 1}} \left(\sum_{i=1}^{M}\delta_{n_i,1}\right)\prod_{k=1}^{M}\frac{1}{n_k}. \tag{5.63}$$

Expanding the sum over the terms $\delta_{n_i,1}$, we find

$$\begin{aligned}
S_2 =& \alpha\left(\sum_{\substack{n_1+\cdots+n_M=N \\ n_i\geq 1}}\delta_{n_1,1}\prod_{k=1}^{M}\frac{1}{n_k} + \sum_{\substack{n_1+\cdots+n_M=N \\ n_i\geq 1}}\delta_{n_2,1}\prod_{k=1}^{M}\frac{1}{n_k}\right. \\
&\left. + \cdots + \sum_{\substack{n_1+\cdots+n_M=N \\ n_i\geq 1}}\delta_{n_M,1}\prod_{k=1}^{M}\frac{1}{n_k}\right) \\
=& \alpha\left(\sum_{\substack{n_2+\cdots+n_M=N-1 \\ n_i\geq 1}}\prod_{k=2}^{M}\frac{1}{n_k} + \sum_{\substack{n_1+n_3+\cdots+n_M=N-1 \\ n_i\geq 1}}\frac{1}{n_1}\prod_{k=3}^{M}\frac{1}{n_k}\right. \\
&\left. + \cdots + \sum_{\substack{n_1+\cdots+n_{M-1}=N-1 \\ n_i\geq 1}}\prod_{k=1}^{M-1}\frac{1}{n_k}\right) \\
=& \alpha M\left(\sum_{\substack{n_1+\cdots+n_{M-1}=N-1 \\ n_i\geq 1}}\prod_{k=1}^{M-1}\frac{1}{n_k}\right).
\end{aligned} \tag{5.64}$$

In the first line, we have applied the Kronecker delta functions $\delta_{n_i,1}$. In the second line, we have relabelled the n_i so that each term takes the same form.

The resulting sum over compositions in the last line of Eq. (5.64) is the same as the one in Eq. (5.62), but with N and M replaced by $N-1$ and $M-1$, respectively. Therefore,

$$\sum_{\substack{n_1+\cdots+n_M=N \\ n_i\geq 1}}\left(\sum_{i=1}^{M}\delta_{n_i,1}\right)\prod_{k=1}^{M}\frac{1}{n_k} = \frac{M!}{(N-1)!}\begin{bmatrix} N-1 \\ M-1 \end{bmatrix}. \tag{5.65}$$

Rates $T^{-}_{M|A}$ and $T^{+}_{M|A}$, and stationary distribution $P^{st}_{M|A}$

Substituting these results into Eqs. (5.55) and (5.56), we find

$$T^{-}_{M|A} = (N-1)\frac{\begin{bmatrix} N-1 \\ M-1 \end{bmatrix}}{\begin{bmatrix} N \\ M \end{bmatrix}}, \tag{5.66}$$

and

$$T^{+}_{M|A} = m_g(N-1)\frac{\begin{bmatrix} N-1 \\ M \end{bmatrix}}{\begin{bmatrix} N \\ M \end{bmatrix}}. \tag{5.67}$$

We stress again that $\begin{bmatrix} N-1 \\ M-1 \end{bmatrix}$ and $\begin{bmatrix} N \\ M \end{bmatrix}$ are not binomial coefficients, but instead unsigned Stirling numbers of the first kind.

Using the standard expression for the stationary distribution of two-species one-step birth-death processes (see Eq. (5.13) from the main text]), and after further algebra, we finally find

$$P^{\mathrm{st}}_{M|A} = \frac{m_g^{M-1}}{(N-1)!} \frac{\begin{bmatrix} N \\ M \end{bmatrix}}{\binom{m_g+N-1}{m_g}}. \tag{5.68}$$

5.7.2 Facultative sex ($0 < p_S < 1$) and sexual environment ($p_S = 1$)

We now consider values of $p_S > 0$. In this case the stationary distribution of the full model is given by (see [24] for details)

$$P^{\mathrm{st}}_{\mathbf{n}|p_S} = \alpha \prod_{k=1}^{M} \frac{1}{n_k\,(N_{p_S} - n_k)!}, \tag{5.69}$$

with

$$N_{p_S} = N\left(\frac{2-p_S}{p_S}\right). \tag{5.70}$$

In the case of purely sexual reproduction, N_{p_S} reduces to $N_{p_S=1} = N$.

The constant α in Eq. (5.69) again ensures normalisation, and is not important for the quantities we seek to calculate. The constant does not necessarily take the same value as the analogous constant in the previous section.

Calculation of $S_1 = \sum_{\mathbf{n}\in\mathcal{S}^M} P^{\mathbf{st}}_{\mathbf{n}|p_S}$

The sum $\sum_{\mathbf{n}\in\mathcal{S}^M} P^{\mathrm{st}}_{\mathbf{n}|p_S}$ can be written as sum over compositions

$$\sum_{\mathbf{n}\in\mathcal{S}^M} P^{\mathrm{st}}_{\mathbf{n}|p_S} = \alpha \sum_{\substack{n_1+\cdots+n_M=N \\ n_i\geq 1}} \prod_{k=1}^{M} \frac{1}{n_k(N_{p_S}-n_k)!}. \tag{5.71}$$

As with the asexual environment, this sum has the form $\sum_{n_1+\cdots+n_M=N,\, n_i\geq 1} \prod_{k=1}^{M} f(n_k)$, where we now have $f(n_k) = 1/[n_k(N_{p_S}-n_k)!]$. Therefore,

$$\sum_{\mathbf{n}\in\mathcal{S}^M} P^{\mathrm{st}}_{\mathbf{n}|p_S} = \alpha\, \frac{1}{N!} \frac{d^N}{dx^N}\bigg|_{x=0} p(x)^M \tag{5.72}$$

with $p(x) = \sum_{i\geq 1} f(i)x^i$. The index i in the sum in $p(x)$ extends up to the maximum integer number for which $f(i)$ is defined. In the present case this maximum value is

given by $\lfloor N_{p_S} \rfloor$ with $\lfloor \cdot \rfloor$ the floor function ($\lfloor x \rfloor$ is the largest integer lower than or equal to x). Thus $p(x)$ is a a finite sum. Defining $L = \lfloor N_{p_S} \rfloor$, we have

$$p(x)^M = \left(\sum_{i \geq 1}^{L} \frac{x^i}{i(N_{p_S} - i)!} \right)^M . \tag{5.73}$$

Applying the multinomial theorem, i.e.,

$$(x_1 + x_2 + \cdots + x_m)^n = \sum_{\substack{k_1 \geq 0, \ldots, k_m \geq 0 \\ k_1 + k_2 + \cdots + k_m = n}} \binom{n}{k_1, k_2, \ldots, k_m} \prod_{i=1}^{m} x_i^{k_i} , \tag{5.74}$$

the M-th power of the function $p(x)$ becomes

$$\begin{aligned} p(x)^M &= \sum_{\substack{k_1 \geq 0, \ldots, k_L \geq 0 \\ k_1 + k_2 + \cdots + k_L = M}} \binom{M}{k_1, k_2, \ldots, k_L} \prod_{i=1}^{L} \left(\frac{x}{i(N_{p_S} - i)!} \right)^{k_i} \\ &= \sum_{\substack{k_1 \geq 0, \ldots, k_L \geq 0 \\ k_1 + k_2 + \cdots + k_L = M}} \binom{M}{k_1, k_2, \ldots, k_L} \prod_{i=1}^{L} \left(\frac{1}{i(N_{p_S} - i)!} \right)^{k_i} x^{k_1 + 2k_2 + \cdots + Lk_L} , \end{aligned} \tag{5.75}$$

where the sum extends over all the partitions of M, i.e., to all the possible ways of expressing M as a sum of non-positive integers (i.e., we allow them also to take zero values). This means we allow the number of parts, i.e., the positive summands in a partition, to vary in the sum evaluation.

Based on Eq. (5.72), we now need to extract the coefficient multiplying x_N in the expression in Eq. (5.75). We therefore need to identify all terms $x^{k_1 + 2k_2 + \cdots + Lk_L}$ in Eq. (5.75) such that $k_i \geq 0$, $k_1 + 2k_2 + \cdots + Lk_L = N$ and $k_1 + \cdots + k_L = M$. The sequences $k_1, \ldots, k_L$ that satisfy these two conditions represent compositions of N into M positive parts (i.e., with a fixed number M of summands) [35]. For fixed M, there can be no parts greater than $N - M + 1$, so necessarily $k_{N-M+2} = \cdots = k_L = 0$. Therefore,

$$\begin{aligned} &\frac{1}{N!} \frac{d^N}{dx^N} \bigg|_{x=0} p(x)^M \\ &= \sum_{\substack{k_1 + k_2 + \cdots + k_{N-M+1} = M \\ k_1 + 2k_2 + \cdots + (N-M+1)k_{N-M+1} = N}} \binom{M}{k_1, k_2, \ldots, k_{N-M+1}} \prod_{i=1}^{N-M+1} \left(\frac{1}{i(N_{p_S} - i)!} \right)^{k_i} \\ &= \frac{M!}{N!} \sum_{\substack{k_1 + k_2 + \cdots + k_{N-M+1} = M \\ k_1 + 2k_2 + \cdots + (N-M+1)k_{N-M+1} = N}} \binom{N}{k_1, k_2, \ldots, k_{N-M+1}} \prod_{i=1}^{N-M+1} \left(\frac{1}{i(N_{p_S} - i)!} \right)^{k_i} \\ &= \frac{M!}{N!} B_{N,M}(x_1, \ldots, x_{N-M+1}), \end{aligned}$$

where $B_{k,\ell}(x_1,\ldots,x_{k-\ell+1})$ is the incomplete Bell polynomial [35] evaluated at $x_i = (i-1)!/(N_{p_S}-i)!$ for $i \in \{1,2,\ldots,k-\ell+1\}$. It is convenient to express x_i in the form

$$x_i = (i-1)!(N_{p_S}-1)_{i-1}x_1, \tag{5.76}$$

with $(N_{p_S}-1)_{i-1}$ the falling factorial of $(N_{p_S}-1)$ with respect to $(i-1)$. Next, we use the following relation [35]

$$B_{k,\ell}(ax_1,\ldots,ax_{k-\ell+1}) = a^\ell B_{k,\ell}(x_1,\ldots,x_{k-\ell+1}). \tag{5.77}$$

We arrive at

$$\sum_{\substack{n_1+\cdots+n_M=N\\ n_i\geq 1}} \prod_{k=1}^{M} \frac{1}{n_k(N_{p_S}-n_k)!} = \frac{M!}{N!(N_{p_S}-1)!^M} B_{N,M}(y_1,\ldots,y_{N-M+1}), \tag{5.78}$$

with $y_i = (i-1)!(N_{p_S}-1)_{i-1}$.

Calculation of $S_2 = \sum_{\mathbf{n}\in\mathcal{S}^M}\left(\sum_{i=1}^M \delta_{n_i,1}\right) P^{\mathbf{st}}_{\mathbf{n}|p_S}$

To calculate $\sum_{\mathbf{n}\in\mathcal{S}^M}\left(\sum_{i=1}^M \delta_{n_i,1}\right) P^{\mathrm{st}}_{\mathbf{n}|p_S}$, we proceed in the same way as we did for the asexual environment (see Section 5.7.1). This sum has the form

$$S_2 = \alpha \sum_{\substack{n_1+\cdots+n_M=N\\ n_i\geq 1}} \left(\sum_{i=1}^M \delta_{n_i,1}\right) \prod_{k=1}^{M} \frac{1}{n_k(N_{p_S}-n_k)!}. \tag{5.79}$$

Expanding the sum over i this yields

$$\begin{aligned}
&\sum_{\substack{n_1+\cdots+n_M=N\\ n_i\geq 1}} \delta_{n_1,1} \prod_{k=1}^{M} \frac{1}{n_k(N_{p_S}-n_k)!} + \cdots + \sum_{\substack{n_1+\cdots+n_M=N\\ n_i\geq 1}} \delta_{n_M,1} \prod_{k=1}^{M} \frac{1}{n_k(N_{p_S}-n_k)!} \\
&= \sum_{\substack{n_2+\cdots+n_M=N-1\\ n_i\geq 1}} \frac{1}{(N_{p_S}-1)!} \prod_{k=2}^{M} \frac{1}{n_k(N_{p_S}-n_k)!} \\
&\quad + \cdots + \sum_{\substack{n_1+\cdots+n_{M-1}=N-1\\ n_i\geq 1}} \frac{1}{(N_{p_S}-1)!} \prod_{k=1}^{M-1} \frac{1}{n_k(N_{p_S}-n_k)!} \\
&= \frac{M}{(N_{p_S}-1)!} \sum_{\substack{n_1+\cdots+n_{M-1}=N-1\\ n_i\geq 1}} \prod_{k=1}^{M-1} \frac{1}{n_k(N_{p_S}-n_k)!}.
\end{aligned} \tag{5.80}$$

As before, in the first equality we have applied the functions $\delta_{n_i,1}$, while in the second step, we have relabelled the terms n_i so that each sum takes the same form. The

resulting sum is nothing but Eq. (5.78) using $N-1$ and $M-1$ instead of N and M (without affecting N_{p_S}), respectively. Therefore,

$$\sum_{\substack{n_1+\cdots+n_M=N\\ n_i\geq 1}} \left(\sum_{i=1}^{M}\delta_{n_i,1}\right)\prod_{k=1}^{M}\frac{1}{n_k(N_{p_S}-n_k)!} = \frac{M!}{(N-1)!(N_{p_S}-1)!^M}B_{N-1,M-1}(y_1,\ldots,y_{N-M+1}), \tag{5.81}$$

with $y_i=(i-1)!(N_{p_S}-1)_{i-1}$.

Calculation of $S_3=\sum_{\mathbf{n}\in\mathcal{S}^M}\left(\sum_{i=1}^{M}n_i^2\right)\left(\sum_{i=1}^{M}\delta_{n_i,1}\right)P^{\mathbf{st}}_{\mathbf{n}|p_S}$

This sum takes the form

$$S_3=\sum_{\substack{n_1+\cdots+n_M=N\\ n_i\geq 1}}\left(\sum_{i=1}^{M}\delta_{n_i,1}\right)\frac{n_1^2+\cdots+n_M^2}{n_1(N_{p_S}-n_1)!\cdots n_M(N_{p_S}-n_M)!}. \tag{5.82}$$

Expanding the sum over index i, and relabelling n_i appropriately, yields

$$S_3=\frac{M}{(N_{p_S}-1)!}\left(\sum_{\substack{n_1+\cdots+n_{M-1}=N-1\\ n_i\geq 1}}\prod_{k=1}^{M-1}\frac{1}{n_k(N_{p_S}-n_k)!} + \sum_{\substack{n_1+\cdots+n_{M-1}=N-1\\ n_i\geq 1}}\frac{n_1^2+\cdots+n_{M-1}^2}{\prod_{k=1}^{M-1}n_k(N_{p_S}-n_k)!}\right). \tag{5.83}$$

The first sum inside the brackets is of the same form as the expression in Eq. (5.78), but with N and M replaced by $N-1$ and $M-1$, respectively, without affecting N_{p_S}. Therefore we have

$$\sum_{\substack{n_1+\cdots+n_{M-1}=N-1\\ n_i\geq 1}}\prod_{k=1}^{M-1}\frac{1}{n_k(N_{p_S}-n_k)!} = \frac{(M-1)!}{(N-1)!(N_{p_S}-1)!^{M-1}}B_{N-1,M-1}(y_1,\ldots,y_{N-M+1}). \tag{5.84}$$

To calculate the second sum inside the brackets on the right-hand side of Eq. (5.83), we note that by symmetry the $M-1$ terms resulting when expanding the numerator $n_1^2+\cdots+n_{M-1}^2$ are all equal after the sum over compositions is carried out. In other words

$$\sum_{\substack{n_1+\cdots+n_{M-1}=N-1\\ n_i\geq 1}}\frac{n_1^2+\cdots+n_{M-1}^2}{\prod_{k=1}^{M-1}n_k(N_{p_S}-n_k)!} = (M-1)\sum_{\substack{n_1+\cdots+n_{M-1}=N-1\\ n_i\geq 1}}\frac{n_1}{(N_{p_S}-n_1)!}\frac{1}{\prod_{k=2}^{M-1}n_k(N_{p_S}-n_k)!}. \tag{5.85}$$

This leads to

$$\sum_{\substack{n_1+\cdots+n_{M-1}=N-1\\ n_i\geq 1}} \frac{n_1^2+\cdots+n_{M-1}^2}{\prod_{k=1}^{M-1} n_k(N_{p_S}-n_k)!} =$$
$$(M-1)\sum_{n_1=1}^{N-M+1} \frac{n_1}{(N_{p_S}-n_1)!}\left(\sum_{\substack{n_2+\cdots+n_{M-1}=N-1-n_1\\ n_i\geq 1}} \frac{1}{\prod_{k=2}^{M-1} n_k(N_{p_S}-n_k)!}\right). \tag{5.86}$$

The sum over n_1 ranges from the minimum to the maximum value n_1 can take in the compositions. The sum inside the brackets is of the same form as the expression in Eq. (5.78) ,with N and M replaced by $N-1-n_1$ and $M-2$, respectively, without affecting N_{p_S}. We therefore have

$$\sum_{\substack{n_1+\cdots+n_{M-1}=N-1\\ n_i\geq 1}} \frac{n_1^2+\cdots+n_{M-1}^2}{\prod_{k=1}^{M-1} n_k(N_{p_S}-n_k)!} =$$
$$\sum_{n_1=1}^{N-M+1} \frac{n_1}{(N_{p_S}-n_1)!}\frac{(M-1)!}{(N-1-n_1)!(N_{p_S}-1)!^{M-2}} \times B_{N-1-n_1,M-2}(y_1,\ldots,y_{N-n_1-M+2}), \tag{5.87}$$

with $y_i=(i-1)!(N_{p_S}-1)_{i-1}$.

Putting everything together, we finally arrive at

$$\sum_{\substack{n_1+\cdots+n_M=N\\ n_i\geq 1}} \left(\sum_{i=1}^{M}\delta_{n_i,1}\right)\frac{n_1^2+\cdots+n_M^2}{n_1(N_{p_S}-n_1)!\cdots n_M(N_{p_S}-n_M)!} =$$
$$\frac{M!}{(N_{p_S}-1)!^{M-1}}\left(\frac{1}{(N-1)!(N_{p_S}-1)!}B_{N-1,M-1}(y_1,\ldots,y_{N-M+1})+\right.$$
$$\left.\sum_{n_1=1}^{N-M+1}\frac{n_1}{(N_{p_S}-n_1)!}\frac{1}{(N-1-n_1)!}B_{N-1-n_1,M-2}(y_1,\ldots,y_{N-n_1-M+2})\right), \tag{5.88}$$

with $y_i=(i-1)!(N_{p_S}-1)_{i-1}$.

Rates $T^-_{M|p_S}$ and $T^+_{M|p_S}$, and stationary distribution $P^{st}_{M|p_S}$

Putting the different results together, we find for fixed rate of sexual reproduction $p_S>0$:

$$T^-_{M|p_S} = \frac{1}{2}(2-p_S)(N-1)\frac{B_{N-1,M-1}(y_1,\ldots,y_{N-M+1})}{B_{N,M}(y_1,\ldots,y_{N-M+1})} - \frac{p_S}{2N}\frac{(N-1)!(N_{p_S}-1)!}{B_{N,M}(y_1,\ldots,y_{N-M+1})}$$
$$\times \sum_{n_1=1}^{N-M+1}\frac{n_1}{(N_{p_S}-n_1)!}\frac{B_{N-1-n_1,M-2}(y_1,\ldots,y_{N-n_1-M+2})}{(N-1-n_1)!}, \tag{5.89}$$

and

$$T^+_{M|p_S} = m_g \left(1 - \frac{B_{N-1,M-1}(y_1,\ldots,y_{N-M+1})}{B_{N,M}(y_1,\ldots,y_{N-M+1})}\right). \tag{5.90}$$

Recall we have $B_{k,\ell} = B_{k,\ell}(y_1,\ldots,y_{k-\ell+1})$ with $y_i = (i-1)!(N_{p_S}-1)_{i-1}$. From these rates we can construct the stationary distribution $P^{st}_{M|p_S}$ using the standard formula for birth-death processes (see Eq. (5.13)).

We recall from Section 5.3.2 in the main paper that the rates $T^-_{M|p_S}$ and $T^+_{M|p_S}$ from Eqs. (5.89) and (5.90) correspond to the rates in the fast switching limit, i.e., $T^{-,\text{fast}}_M$ and $T^{-,\text{slow}}_M$. As explained in there, in this limit the system behaves as if there was a fixed environment with sex rate p_S.

5.7.3 Alternative expressions of rates $T^-_{M|p_S}$ and $T^+_{M|p_S}$ for cases $0 < p_S \leq 1$

In Section 5.7.2 we derived analytical closed-form expressions of rates $T^-_{M|p_S}$ and $T^+_{M|p_S}$ for $0 < p_S \leq 1$. The results are exact in the stationary state, but the evaluation of these expressions may be computationally costly for large population sizes N. We therefore proceed to derive equivalent expressions which are easier to evaluate numerically.

For that, we start from Eqs. (5.55) and (5.56) and express the sums over compositions as standard non-partition sums, i.e., as sums of indexed numbers with defined lower and upper bounds of summation. Denoting by P the number of entries higher than 1 of a given state $\mathbf{n}$, we first express each sum over compositions in Eqs. (5.55) and (5.56) as sums over P. The sum S_1 (see Eq. (5.57)) can be written in the form

$$\sum_{\mathbf{n}\in\mathcal{S}^M} P^{\text{st}}_{\mathbf{n}|p_S} = \sum_{P=0}^{P_{\max}} S^P_{M,p_S}(N-M), \tag{5.91}$$

with a suitable $S^P_{M,p_S}(N-M)$ (see below), and where $P_{\max}$ is the maximum number of mating types with strictly more than one individual. For a given N and M this is

$$P_{\max} = \begin{cases} 0 & \text{if } N = M \\ N-M & \text{if } N/2 \leq M < N \\ M & \text{if } M < N/2. \end{cases} \tag{5.92}$$

Notice that when $N = M$ then there will necessarily be exactly one individual of each mating type, so $P_{\max} = 0$.

The term $S^P_{M,p_S}(N-M)$ in Eq. (6.67) represents the sum of $P^{\rm st}_{\mathbf{n}|p_S}$ over compositions with P elements higher than one for a given N and M, i.e.,

$$S^P_{M,p_S} \equiv \sum_{\substack{n_1+\cdots+n_M=N \\ |G|=P \\ G=\{n_i>1:1\leq i\leq M\}}} P^{\rm st}_{\mathbf{n}|p_S}, \tag{5.93}$$

This can be expressed as a recursive sum of the form

$$S^P_{M,p_S}(Q) = (N_{p_S}-1)!\left(\frac{M-P+1}{P}\right)\sum_{k_P=2}^{Q-P+2}\frac{1}{k_P(N_{p_S}-k_P)!}S^{P-1}_{M,p_S}(Q+1-k_P), \tag{5.94}$$

with base cases

$$S^1_{M,p_S}(Q) = \frac{M}{(N_{p_S}-1)!^{M-1}}\frac{1}{(Q+1)(N_{p_S}-Q-1)!}, \tag{5.95}$$

and

$$S^0_{M,p_S}(Q) = \frac{1}{(N_{p_S}-1)!^{M}}\delta_{Q,0}. \tag{5.96}$$

The procedure to derive the previous expressions is laborious but straightforward. The strategy for this is to sort the $M-$compositions $\mathbf{n}$ in $\sum_{\mathbf{n}\in\mathcal{S}^M} P^{\rm st}_{\mathbf{n}|p_S}$ such that we sum them starting from those compositions which contain entries with the lowest values to those with the highest values. Then we identify which compositions contain the same elements and regroup them.

Following with the rest of the sums over compositions in Eqs. (5.55) and (5.56), one finds hat the sum S_2 takes the form

$$\sum_{\mathbf{n}\in\mathcal{S}^M}\left(\sum_{i=1}^M \delta_{n_i,1}\right)P^{\rm st}_{\mathbf{n}|p_S} = \sum_{P=0}^{P_{\max}}(M-P)\times S^P_{M,p_S}(N-M), \tag{5.97}$$

as $M-P$ is the number of entries equal to one for state $\mathbf{n}$. Following the same logic as with S^P_{M,p_S}, the sum S_3 becomes

$$\sum_{\mathbf{n}\in\mathcal{S}^M}\left(\sum_{i=1}^M n_i^2\right)\left(\sum_{i=1}^M \delta_{n_i,1}\right)P^{\rm st}_{\mathbf{n}|p_S} = \sum_{P=0}^{P_{\max}}(M-P)\times \Gamma^P_{M,p_S}(N-M), \tag{5.98}$$

where the term $\Gamma^P_{M,p_S}(N-M)$ represents the sum of $\left(\sum_{i=1}^M n_i^2\right)P^{\rm st}_{\mathbf{n}|p_S}$ over compositions with P elements higher than one. This is

$$\begin{aligned}\Gamma^P_{M,p_S}(Q) =& \binom{M}{P}\frac{1}{(N_{p_S}-1)!^{M-P}} \\ &\times\sum_{k_P=2}^{Q-P+2}\frac{1}{k_P(N_{p_S}-k_P)!}\Lambda^{P-1}_{p_S}(M-1+k_P^2, N-M+1-k_P),\end{aligned} \tag{5.99}$$

with

$$\Lambda^{P}_{p_S}(L,Q) = \sum_{k_P=2}^{Q+2-P} \frac{1}{k_P(N_{p_S}-k_P)!}\Lambda^{P-1}_{p_S}(L-1+k_P^2, Q+1-k_P), \tag{5.100}$$

with base cases

$$\Gamma^{1}_{M,p_S}(Q) = \frac{M}{(N_{p_S}-1)!^{M-1}}\Lambda^{1}_{p_S}(M,Q), \quad \Lambda^{1}_{p_S}(L,Q) = \frac{L-1+(Q+1)^2}{(Q+1)(N_{p_S}-Q-1)!}, \tag{5.101}$$

and

$$\Gamma^{0}_{M,p_S}(Q) = \frac{M}{(N_{p_S}-1)!^{M}}\Lambda^{0}_{p_S}(M,Q), \quad \Lambda^{0}_{p_S}(L,Q) = \delta_{Q,0}. \tag{5.102}$$

Putting everything together in Eqs. (5.55) and (5.56), we finally find

$$\begin{aligned} T^{-}_{M|p_S} =& \frac{1}{2N}\left[(2-p_S)(N-1)+\frac{p_S}{N}\right]\frac{\sum_{P=0}^{P_{\max}}(M-P)\times S^{P}_{M,p_S}(N-M)}{\sum_{P=0}^{P_{\max}} S^{P}_{M,p_S}(N-M)} \\ &- \frac{p_S}{2N^2}\frac{\sum_{P=0}^{P_{\max}}(M-P)\times \Gamma^{P}_{M,p_S}(N-M)}{\sum_{P=0}^{P_{\max}} S^{P}_{M,p_S}(N-M)}, \end{aligned} \tag{5.103}$$

and

$$T^{+}_{M|p_S} = \frac{m_g}{N}\left(N - \frac{\sum_{P=0}^{P_{\max}}(M-P)\times S^{P}_{M,p_S}(N-M)}{\sum_{P=0}^{P_{\max}} S^{P}_{M,p_S}(N-M)}\right). \tag{5.104}$$

5.7.4 Comparison against numerical simulations with fixed environment

In Figure 5.14 we compare the predictions for the rates $T^{-}_{M|p_S}$ and $T^{+}_{M|p_S}$ in Eqs. (5.89) and (5.90) against numerical simulations for different values of p_S with $0 < p_S < 1$. Cases with $p_S = 0$ and $p_S = 1$ are displayed in Figure 5.3 in the main paper. A comparison of theory and numerical simulations for the stationary distribution at fixed p_S is shown in Figure 5.15.

5.7.5 Comparison against numerical simulations with switching environments

The previous results assume a fixed environment with sex rate p_S. When introducing switching between environments $\sigma = S$ and $\sigma = A$, our predictions then may differ

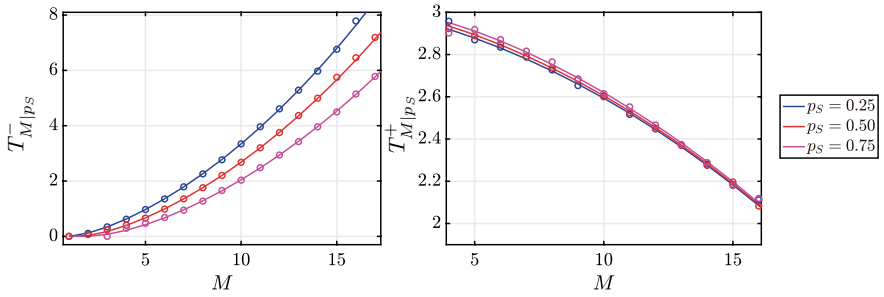

Figure 5.14: Rates $T^-_{M|p_S}$ and $T^+_{M|p_S}$ obtained from theory (solid lines) and numerical simulations of the full model (dotted lines) with fixed rate of sexual reproduction p_S. Parameters: $N = 30$, $m_g = 3.0$. Simulations were run up to time $t = 10^7$, with measurements starting $t = 10^6$ to ensure stationarity.

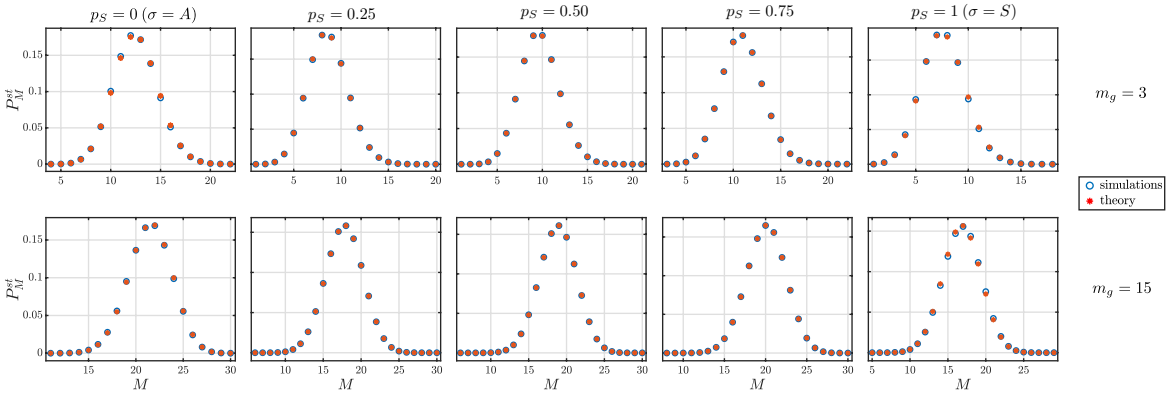

Figure 5.15: Stationary distribution $P^{\text{st}}_{M|p_S}$ for fixed rate of sexual reproduction p_S for population size $N = 30$ with $m_g = 3$ (upper row) and $m_g = 15$ (lower row). The theoretical predictions are given by the results presented in Sections 5.7.1 and 5.7.2. Numerical simulations are of the full model. Simulations were run up to time $t = 10^7$, with measurements starting $t = 10^6$ to ensure stationarity.

in certain circumstances. This discrepancy comes from the fact that rates $T^{\pm}_{M|\sigma}$ are calculated from the distribution of vector states $P^{st}_{\mathbf{n}|\sigma}$ from the full model for a fixed environment (as shown in Section 5.6). In the case of switching environments the effective birth and death rates become $T^{\pm}_{M,\sigma}$, which specify the rate of transitions $(M, \sigma) \to (M \pm 1, \sigma)$. In this case σ is not fixed as in rates $T^{\pm}_{M|\sigma}$. Following the same idea presented in Section 5.6, rates $T^{\pm}_{M,\sigma}$ would need to be obtained from $P^{st}_{\mathbf{n},\sigma}$, i.e., the stationary distribution of states (n, σ) in the full model with switching environments. Obtaining $P^{st}_{\mathbf{n},\sigma}$, however, is beyond the scope of the present work.

In this section we explore this difference when varying the fraction of time spent in the sexual environment, p_S. As explained in Section 5.3.3, the fact of using rates $T^{\pm}_{M|\sigma}$ in the generator-matrix approach has consequences in the prediction of the stationary distribution P^{st}_M when using this approach for intermediate and fast-switching regimes.

We provide more details of this in the next section.

In Figure 5.16, we illustrate a comparison of $T^{\pm}_{M,S}$ (obtained from simulations) against the theoretical prediction of $T^{\pm}_{M|S}$. As shown, the prediction gets better as the fraction time spent in environment $\sigma = S$ is higher (i.e., as p_S increases). Conversely, we compare $T^{\pm}_{M,A}$ and $T^{\pm}_{M|A}$ in Figure 5.17, showing that the prediction gets worse when increasing p_S.

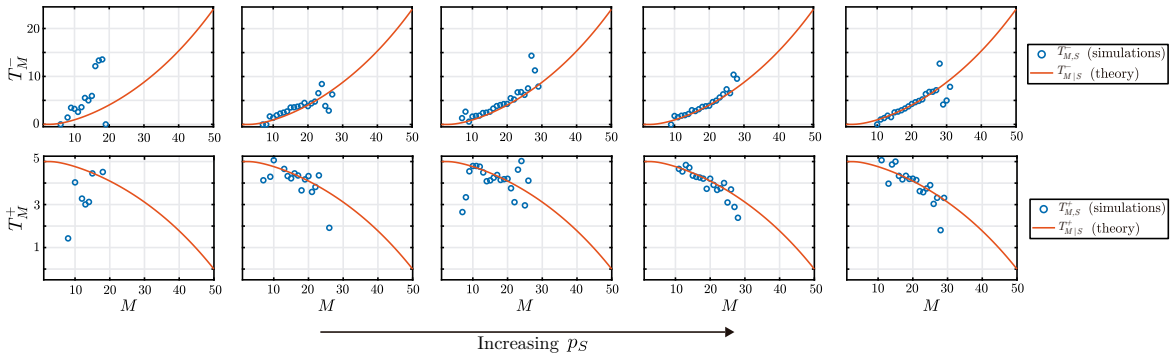

Figure 5.16: Comparison between $T^{\pm}_{M,S}$ (simulations) and $T^{\pm}_{M|S}$ (theory). We fix the average time cycle $\tau = 2$ generations throughout and vary the fraction of time spent in the sexual environment, p_S. From right to left panels, we set for each column $p_S = 0.01, 0.25, 0.50, 0.75, 0.99$. Remaining parameters: $N = 50$, $m_g = 5$.

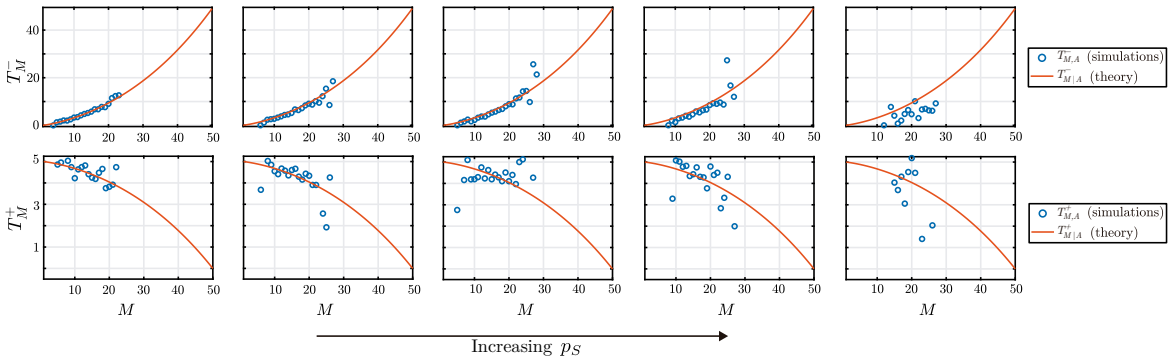

Figure 5.17: Comparison between $T^{\pm}_{M,A}$ (simulations) and $T^{\pm}_{M|A}$ (theory). We fix the average time cycle $\tau = 2$ generations throughout and vary the fraction of time spent in the sexual environment, p_S. From right to left panels, we set for each column $p_S = 0.01, 0.25, 0.50, 0.75, 0.99$. Remaining parameters: $N = 50$, $m_g = 5$.

5.8 Appendix C: Markov chain generator matrix approach

As explained in Section 5.3.3, the rates $T^{+}_{M,\sigma}$ and $T^{-}_{M,\sigma}$ used to construct the generator matrix $\underline{\underline{Q}}$ are those derived for situations in which the environment does not switch

between states. In other words, we use the rates $T^{+}_{M|\sigma}$ and $T^{-}_{M|\sigma}$ ($\sigma = A, S$) obtained in Sections 5.6.1 and 5.6.2 of this Supplement ($\sigma = A$ corresponds to setting $p_S = 0$, and $\sigma = S$ to $p_S = 1$). Assuming a fixed value of p_S is an approximation for the model in which the environment switches between the states with purely sexual and purely asexual reproduction. In this section, we explore the implications of this approximation.

5.8.1 Comparison against simulations

Figure 5.18 shows how the stationary distribution $P^{\rm st}_M$ obtained from the generator-matrix approach compares against numerical simulations. For the graphs shown, we have fixed the average period of one environmental switching cycle, τ, while varying the average fraction spent in each environment. We show how the distribution compares to simulations for different values of m_g for which, based on Figure 5.9, we expect to see a good or bad agreement. As shown, as m_g increases the prediction from the generator-matrix approach becomes better. In Section III C 2 we discuss the reasons of this.

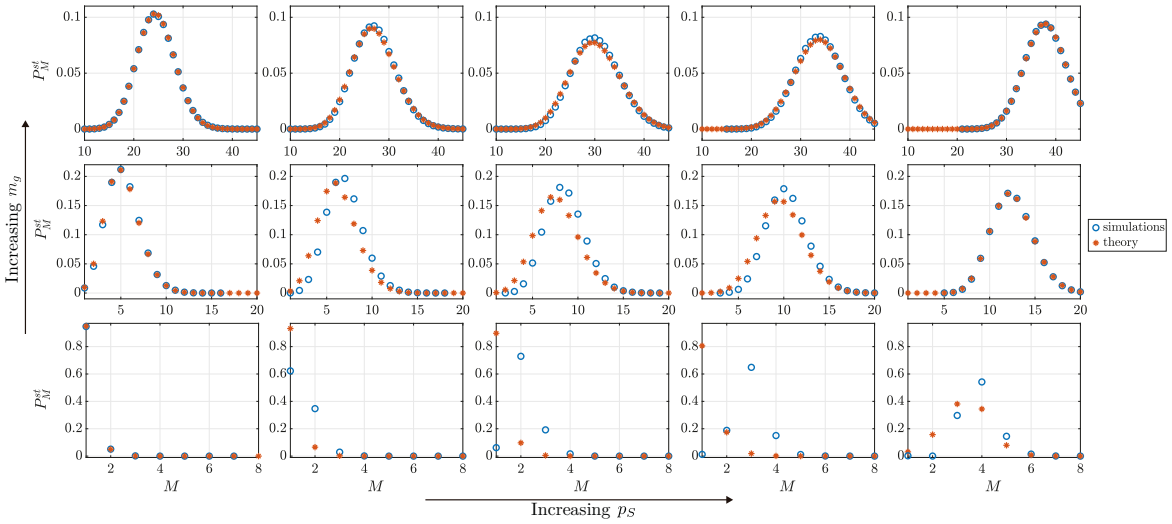

Figure 5.18: Stationary distribution $P^{\rm st}_M$ for $N = 100$ from numerical simulations of the full model with switching environment (open circles) and from the generator-matrix approach (asterisks). We fix the average cycle time to $\tau = 2$ generations throughout, and vary the fraction of time spent in the sexual environment, p_S, and the mutation rate, m_g. The values used (from left to right columns) are $p_S = 0.01, 0.25, 0.50, 0.75, 0.99$, and (from lower to upper rows) $m_g = 0.01, 1, 10$. Numerical simulations were conducted by time-averaging one single run up to time $t = 10^5$ generations, where the first 10^2 units of time are ignored to ensure stationarity

5.8.2 Theoretical prediction of $P^{\text{st}}_{M,\sigma}$ for each environment

Using the generator-matrix approach we can derive the stationary distribution $P^{\text{st}}_{M,\sigma}$. We point out that this is not the same as $P^{\text{st}}_{M|\sigma}$, instead $P^{\text{st}}_{M,\sigma}$ is the joint distribution of finding the environment in state σ and M mating types in the population in a model with switching environment. The distribution $P^{\text{st}}_{M,\sigma}$ cannot be calculated using the approaches for the slow switching and fast switching limits presented in Sections 5.3.1 and 5.3.2.

As explained in Section 5.3.3, the first N elements of $\underline{P}^{\text{st}}$ are the $P^{\text{st}}_{M,S}$, for $M = 1, \ldots, N$, while the second N entries are $P^{\text{st}}_{M,A}$ (see Eq. (5.23)). In Figure 5.19, we illustrate how the theoretical predictions for both distributions obtained from the generator-matrix approach behave for different values of p_S, i.e, when varying the fraction of time spent in each environment. These quantities cannot be obtained using the fast and slow switching approximations presented in Sections 5.3.1 and 5.3.2. As shown, the amplitude of $P^{\text{st}}_{M,S}$ increases with p_S, while the opposite occurs to $P^{\text{st}}_{M,A}$. When $p_S = 0$ or $p_S = 1$ we see the distribution of only one environment, while when $p_S = 0.5$ the amplitude is similar in both distributions.

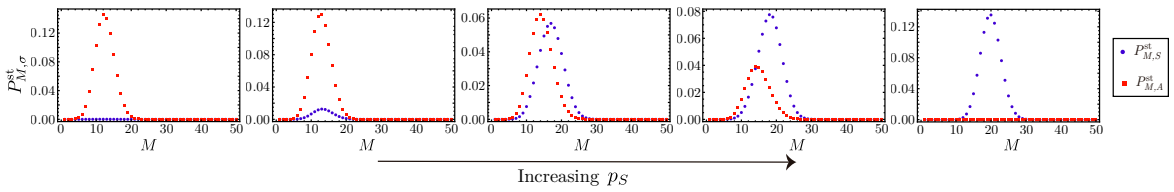

Figure 5.19: Predictions for the distributions $P^{\text{st}}_{M,S}$ and $P^{\text{st}}_{M,A}$ from the generator-matrix approach. Parameters $N = 50, m_g = 5$, and $\lambda_{A\to S} = 0.5$. The value for p_S in the different panels is $0, 0.1, 0.5, 0.66, 1$ from left to right.

5.8.3 Transition between slow and fast switching regimes for low and high p_S

In Figure 5.7 of the main text, we showed how P^{st}_{M} behaves when varying the average time cycle τ for $p_S = 0.5$, i.e. when the environment spends equal fractions of time in each of the two states A and S. The stationary distribution for M the differs in the fast and slow switching regimes (for example the distribution can be bimodal for slow switching, but unimodal for fast switching). In Figure 5.20 we show how P^{st}_{M} behaves when the environment spends most of the time in either one of the two states. As

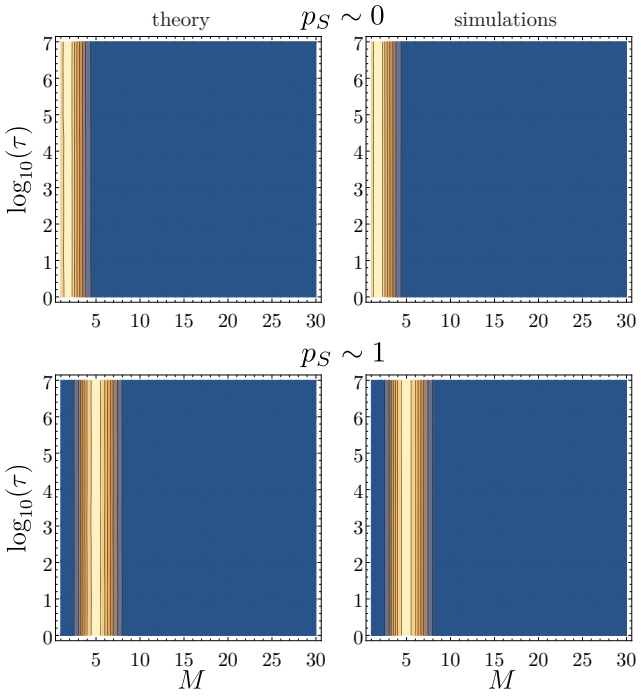

Figure 5.20: Stationary distribution P_M^{st} as a function of the cycle time τ obtained from the generator-matrix theoretical approach and simulations of the full model. The upper and lower rows represent cases of high and low p_S with values $p_S = 0.999$ and $p_S = 0.001$, respectively. Parameters: $N = 30, m_g = 0.3$ and $\lambda_{A\to S} = 1$. Numerical simulations were conducted by time-averaging one single run up to time $t = 10^7$ generations, where the first 10^6 units of time are ignored to ensure stationarity.

shown, there is then no noticeable difference between the distributions in the slow and fast regimes. This is because one of the environments dominates, irrespective of the speed of environmental switching.

5.8.4 Analytical results from the generator-matrix approach

The theoretical approach in Section 5.3.3 of the main paper makes use of the generator matrix $\underline{\underline{Q}}$ to calculate the stationary distribution $\underline{P}^{\text{st}}$. The evaluation of this is mostly numerical. We now show how analytical results can be derived from the generator-matrix approach in the slow and fast switching regimes. As we will see, this reproduces the results for the slow-switching limit in Section 5.3.1 of the main paper, while the prediction from the generator matrix in the fast-switching limit is different from the result presented in Section 5.3.2 for the full model. This disagreement originates from the use of the rates $T^-_{M|\sigma}$ and $T^+_{M|\sigma}$ in the generator-matrix approach. These rates are derived for fixed environments, and assuming a stationary state of the population in those environments, see Sections 5.6 and 5.6.2 of this Supplement. These assumptions

are not valid when the switching of the environment is fast, as the population can then not reach a stationary state between switches of the environmental state. However, as explained in Section 5.3.3, there are situations in which the fast-switching limit derived from the the generator-matrix approach approximates the predictions of the full model well (i.e., the limit presented in Section 5.3.2).

The analysis starts from the equation defining the stationary state of the reduced model,

$$\underline{P}^{\mathrm{st}}\underline{\underline{Q}} = 0. \tag{5.105}$$

This is a linear $2N \times 2N$ system, and can be written out explicitly. For the components describing environmental state $\sigma = A$ we have

$$0 = T^-_{M-1|A}P^{\mathrm{st}}_{M-1,A} + T^-_{M+1|A}P^{\mathrm{st}}_{M+1,A} - (T^-_{M|A} + T^+_{M|A})P^{\mathrm{st}}_{M,A} + \lambda_{S\to A}P^{\mathrm{st}}_{M,S} - \lambda_{A\to S}P^{\mathrm{st}}_{M,A}, \tag{5.106}$$

while for $\sigma = S$

$$0 = T^-_{M-1|S}P^{\mathrm{st}}_{M-1,S} + T^-_{M+1|S}P^{\mathrm{st}}_{M+1,S} - (T^-_{M|S} + T^+_{M|S})P^{\mathrm{st}}_{M,S} + \lambda_{A\to S}P^{\mathrm{st}}_{M,A} - \lambda_{S\to A}P^{\mathrm{st}}_{M,S}. \tag{5.107}$$

In these equations, M takes values $1, \ldots, N$. At the boundaries we have $T^-_{1|\sigma} = 0$ and $T^+_{N|\sigma} = 0$ both for $\sigma = A$ and $\sigma = S$.

Subtracting Eq. (5.107) from Eq. (5.106) we find

$$T^-_{M|A}P^{\mathrm{st}}_{M,A} + T^-_{M|S}P^{\mathrm{st}}_{M,S} = T^+_{M-1|A}P^{\mathrm{st}}_{M-1,A} + T^+_{M-1|S}P^{\mathrm{st}}_{M-1,S}. \tag{5.108}$$

Within the reduced model this relation holds for any combination of the environmental switching rates $\lambda_{A\to S}$ and $\lambda_{S\to A}$.

Before analysing the slow-switching and fast-switching regimes, we make further preparations. First, we recall that

$$\sum_{M=1}^{N} P^{\mathrm{st}}_{M,A} = 1 - p_S, \quad \text{and} \quad \sum_{M=1}^{N} P^{\mathrm{st}}_{M,S} = p_S, \tag{5.109}$$

see Section 5.2.2 of the main paper.

Secondly, by summing the first M instances of Eqs. (5.106) and (5.107) we obtain

$$P^{\mathrm{st}}_{M,A} = \frac{T^+_{M-1|A}}{T^-_{M|A}}P^{\mathrm{st}}_{M-1,A} + \frac{\lambda_{S\to A}}{T^-_{M|A}}\sum_{M'=1}^{M-1} P^{\mathrm{st}}_{M',A} - \frac{\lambda_{A\to S}}{T^-_{M|A}}\sum_{M'=1}^{M-1} P^{\mathrm{st}}_{M',S} \tag{5.110}$$

and

$$P^{\rm st}_{M,S} = \frac{T^+_{M-1|S}}{T^-_{M|S}} P^{\rm st}_{M-1,S} + \frac{\lambda_{A\to S}}{T^-_{M|S}} \sum_{M'=1}^{M-1} P^{\rm st}_{M',S} - \frac{\lambda_{S\to A}}{T^-_{M|S}} \sum_{M'=1}^{M-1} P^{\rm st}_{M',A}, \tag{5.111}$$

respectively. In these relations we have expressed $P^{\rm st}_{M,\sigma}$ in terms of $P^{\rm st}_{M',\sigma}$ up to $M' = M-1$.

Limit of slow environmental switching

In the limit of slow switching, i.e., when $\lambda_{A\to S}, \lambda_{S\to A} \ll 1$, the dominant terms in Eqs. (5.110) and (5.111) are those not proportional to any of the switching rates, so that

$$P^{\rm st}_{M,\sigma} \approx \frac{T^+_{M-1|\sigma}}{T^-_{M|\sigma}} P^{\rm st}_{M-1,\sigma} \tag{5.112}$$

both for $\sigma = A$ and $\sigma = S$. The rates $T^{\pm}_{M|\sigma}$ satisfy the following relation (see Eq. (5.13) in the main paper)

$$P^{st}_{M|\sigma} = \frac{T^+_{M-1|\sigma}}{T^-_{M|\sigma}} P^{\rm st}_{M-1|\sigma}. \tag{5.113}$$

From this we conclude

$$P^{\rm st}_{M,\sigma} \approx \frac{P^{st}_{M|\sigma}}{P^{st}_{M-1|\sigma}} P^{\rm st}_{M-1,\sigma} \tag{5.114}$$

By applying this relation successively, one then sees that

$$P^{\rm st}_{M,\sigma} \approx \frac{P^{st}_{M|\sigma}}{P^{st}_{1|\sigma}} P^{\rm st}_{1,\sigma}. \tag{5.115}$$

Summing on both sides over M from 1 to N, and using $\sum_{M=1}^{N} P_{M|\sigma} = 1$, one finds

$$\sum_{M=1}^{N} P^{\rm st}_{M,\sigma} \approx \frac{P^{\rm st}_{1,\sigma}}{P^{st}_{1|\sigma}}. \tag{5.116}$$

This holds for $\sigma = A$ and $\sigma = S$. Using Eqs. (5.109), these relations then become

$$(1-p_S) \approx \frac{P^{\rm st}_{1,A}}{P^{st}_{1|A}}, \quad \text{and} \quad p_S \approx \frac{P^{\rm st}_{1,S}}{P^{st}_{1|S}}. \tag{5.117}$$

for $\sigma = A$ and $\sigma = S$, respectively. Finally, using this in Eq. (5.115), we find

$$P^{\rm st}_{M,A} \approx (1-p_S) P^{st}_{M|A}, \quad \text{and} \quad P^{\rm st}_{M,S} \approx p_S P^{st}_{M|S}, \tag{5.118}$$

which leads to

$$P^{st}_{M} \approx (1-p_S) P^{st}_{M|A} + p_S P^{st}_{M|S}, \tag{5.119}$$

which is the result in Section 5.3.1 of the main paper.

Limit of fast environmental switching

In the limit of fast switching, the switching rates $\lambda_{A\to S}$ and $\lambda_{S\to A}$ take very large values ($\lambda_{A\to S}, \lambda_{S\to A} \gg 1$). The terms proportional to these rates in Eqs. (5.106) and (5.107) then dominate all other contributions in these equations. This leads to

$$\lambda_{A\to S} P^{\rm st}_{M,A} \approx \lambda_{S\to A} P^{\rm st}_{M,S}. \tag{5.120}$$

Using $p_S = \lambda_{A\to S}/(\lambda_{A\to S} + \lambda_{S\to A})$ this can be written as

$$P^{\rm st}_{M,A} \approx \frac{(1-p_S)}{p_S} P^{\rm st}_{M,S}. \tag{5.121}$$

This implies that the distributions $P_{M,A}$ and $P_{M,S}$ share the same mode for M in the limit of fast environments.

Using Eq. (5.121) in Eq. (5.108) yields

$$\left(T^-_{M|A}\frac{(1-p_S)}{p_S} + T^-_{M|S}\right) P^{\rm st}_{M,S} \approx \left(T^+_{M-1|A}\frac{(1-p_S)}{p_S} + T^+_{M-1|S}\right) P^{\rm st}_{M-1,S}, \tag{5.122}$$

and therefore,

$$\begin{aligned} P^{\rm st}_{M,S} &\approx \left(\frac{(1-p_S)T^+_{M-1|A} + p_S T^+_{M-1|S}}{(1-p_S)T^-_{M|A} + p_S T^-_{M|S}}\right) P^{\rm st}_{M-1,S}, \\ &= \frac{T^+_{M-1,\rm eff}}{T^-_{M,\rm eff}} P^{\rm st}_{M-1,S}. \end{aligned} \tag{5.123}$$

This resembles the stationary distribution solution for fixed environments (see Eq. (5.13) in the main paper) with rates

$$T^\pm_{M,\rm eff} = (1-p_S)T^\pm_{M|A} + p_S T^\pm_{M|S}. \tag{5.124}$$

This means that in the limit of fast environments the population behaves as if it were in an effective fixed environment with rates $T^\pm_{M,\rm eff}$.

By applying Eq. (5.123) successively one sees that

$$P^{st}_{M,S} \approx \frac{T^+_{M-1,\rm eff}\cdots T^+_{1,\rm eff}}{T^-_{M,\rm eff}\cdots T_{2,\rm eff}} P^{\rm st}_{1,S}, \tag{5.125}$$

and, by using Eq. (5.121), that

$$P^{st}_{M,A} \approx \frac{(1-p_S)}{p_S}\frac{T^+_{M-1,\rm eff}\cdots T^+_{1,\rm eff}}{T^-_{M,\rm eff}\cdots T_{2,\rm eff}} P^{\rm st}_{1,S}. \tag{5.126}$$

Finally, we obtain

$$P_M^{\rm st} \approx \frac{1}{p_S}\frac{T^+_{M-1,\rm eff}\cdots T^+_{1,\rm eff}}{T^-_{M,\rm eff}\cdots T_{2,\rm eff}}P^{\rm st}_{1,S}. \tag{5.127}$$

The term $P^{\rm st}_{1,S}$ is a normalisation factor which is determined from normalisation ($\sum_{M=1}^N P_M^{st}=1$). We find

$$P^{\rm st}_{1,S} = \left[\frac{1}{p_S}\left(1+\sum_{M=2}^{N}\prod_{i=2}^{M}\frac{T^+_{i-1,\rm eff}}{T^-_{i,\rm eff}}\right)\right]^{-1}. \tag{5.128}$$

We remark that this prediction for the limit of fast environments is different from the result in Section 5.3.2 in the main paper. In the main paper, the transition rates in the full model were approximated by the weighted average of the rates in each environment, with the weights given by the fraction spent in each environment, i.e.,

$$\mathcal{T}_{ij}^{\rm fast} = (1-p_S)\mathcal{T}_{ij}^{A} + p_S\mathcal{T}_{ij}^{S}. \tag{5.129}$$

This approximation translates into

$$T_M^{\pm,\rm fast} = (1-p_S)T^{\pm}_{M,A} + p_S T^{\pm}_{M,S} \tag{5.130}$$

in the reduced model. Since we do not know how to calculate $T^{\pm}_{M,S}$ and $T^{\pm}_{M,A}$, we use $T^{\pm}_{M|S}$ and $T^{\pm}_{M|A}$ instead as input in the generator matrix $\underline{\underline{Q}}$. This leads to what we obtained above in Eq. (5.124). Figure 5.9 in the manuscript explores the validity of this approximation. Nevertheless, we remark that although we do not calculate $T^{\pm}_{M,S}$ and $T^{\pm}_{M,A}$, we still are able to compute $T_M^{\pm,\rm fast}$ (as explained in Section 5.3.2) by using the results from Section 5.7.2.

5.9 Appendix D: Selective sweeps

In this section, we explore a model with additional selective sweeps, as described in Section 5.4 of the main text. We present the theoretical formalism to derive the stationary distribution $P_M^{\rm st}$ for this model, and compare the resulting predictions against numerical simulations. We consider situations with switching environments (so that reproduction switches between sexual and asexual), and the case of a fixed environment in which reproduction is only asexual. In the case of switching environments, selective sweeps can only occur in the asexual environment.

5.9.1 Switching environments

To estimate the distribution P_M^{st} in the presence of selective sweeps we proceed using the method explained in Section 5.3.3 of the main text. We construct the generator matrix $\underline{\underline{Q}}$ and calculate the corresponding stationary state. Throughout this section the rates $T^{\pm}_{M|\sigma}$ are always those of the model without selective sweeps. Sweeps are accounted for separately in the analysis.

As in the main text, we write the matrix $\underline{\underline{Q}}$ in block form

$$\underline{\underline{Q}} = \begin{pmatrix} Q^{(A,A)} & Q^{(A,S)} \\ Q^{(S,A)} & Q^{(S,S)} \end{pmatrix}. \tag{5.131}$$

Since selective sweeps occur only in the asexual environment, the block $Q^{(A,A)}$ is the only one affected by selective sweeps. Taking into account the process $M \xrightarrow{\nu} 1$, the block $Q^{(A,A)}$ becomes

$$Q^{(A,A)} = \begin{pmatrix} -(T^+_{1|A}+\lambda_{A\to S}) & T^+_{1|A} & 0 & \dots & \dots & 0 \\ T^-_{2|A}+\nu & -(T^+_{2|A}+T^-_{2|A}+\lambda_{A\to S}+\nu) & T^+_{2|A} & 0 & \dots & \vdots \\ \nu & T^-_{3|A} & \ddots & \ddots & \ddots & \vdots \\ \vdots & 0 & \ddots & \ddots & \ddots & 0 \\ \vdots & \vdots & \ddots & \ddots & \ddots & T^+_{N-1|A} \\ \nu & \dots & \dots & 0 & T^-_{N|A} & -(T^-_{N|A}+\lambda_{A\to S}+\nu) \end{pmatrix},$$

i.e., compared to the model without selective sweeps, we have added ν to the entries $Q^{(A,A)}_{M,1}$ and $Q^{(A,A)}_{M,M}$ for $2 < M \leq N$.

The stationary distribution P_M^{st} resulting from this generator matrix is an approximative result as the rates $T^{\pm}_{M|\sigma}$ are for fixed environments and do not account for selective sweeps. To take into account the effect of the selective sweeps on $T^{\pm}_{M|\sigma}$ it would be necessary to calculate first the stationary distribution $P^{\mathrm{st}}_{\mathbf{n},\sigma}$ from the full model, including selective sweeps. With this distribution one could then construct $T^{\pm}_{M|\sigma}$ in a similar way as explained in Section 5.6. It is difficult however to obtain $P^{\mathrm{st}}_{\mathbf{n},\sigma}$ for the full model with selective sweeps.

The generator-matrix approach still allows to capture important features that emerge from the inclusion of selective sweeps. In Figures 5.21 and 5.22, we illustrate

the behaviour of P_M^{st} for slow switching and fast switching environments, respectively, as the parameters m_g and ν are varied. Each of the graphs shows a horizontal cut in Figure 5.13 in the main text. We compare this against numerical simulations of the full model. In the simulations, the effect of selective sweeps is implemented by adding an extra transition $M \xrightarrow{\nu} 1$ in the asexual environment, independent of the state of the population. When such an event occurs, the population jumps to the state $M = 1$, and $n_1 = N$.

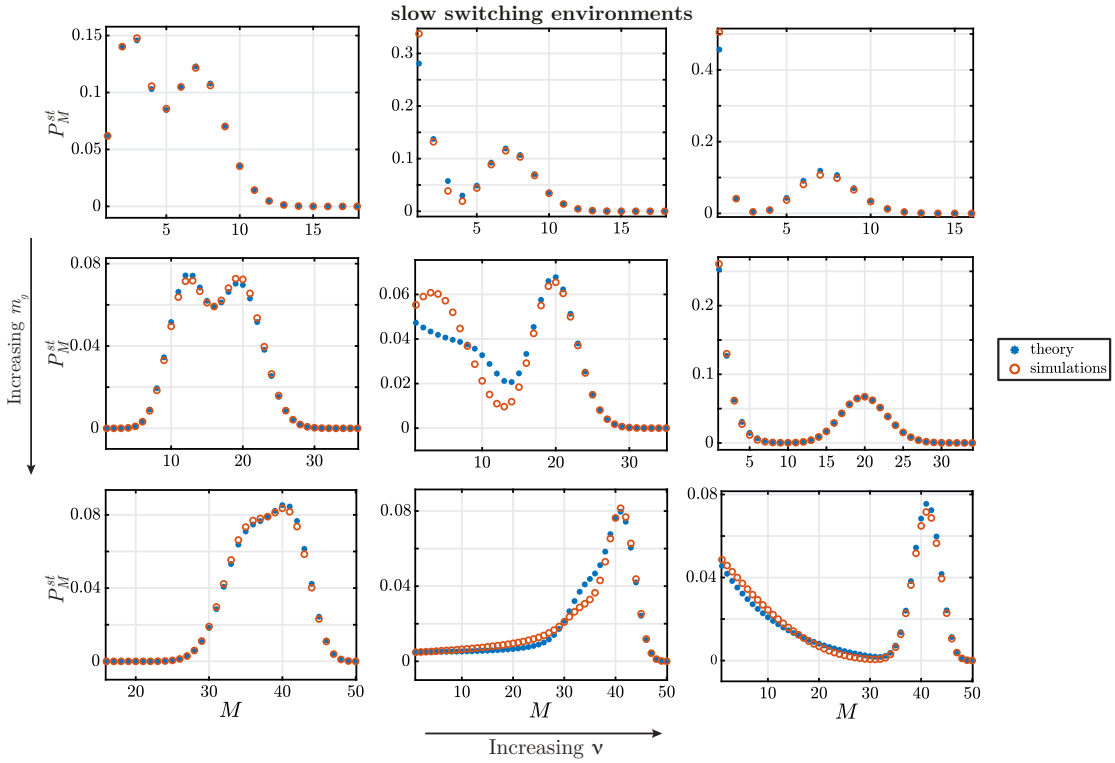

Figure 5.21: Stationary distribution of number of mating types in the model with selective sweeps and fast-switching environments. Theoretical prediction of P_M^{st} with selective sweeps as function of M for slow switching environments, population size $N = 50$, for different values of m_g and ν. From upper to lower rows: $m_g = 0.5, 5, 50$. From left to right columns: $\nu = 0, 0.5, 5$. Switching rates used: $\lambda_{S\to A} = \lambda_{A\to S} = 5 \times 10^{-4}$.

Figures 5.21 and 5.22 both show that, in general, the theoretical prediction is in good agreement with numerical simulations. As shown, the effect of selective sweeps is to increase the chance to find the system at $M = 1$, while mutations, on the contrary, have the effect of driving the population to higher numbers of mating types, reducing the probability of finding $M = 1$. When one of these effects dominates, our prediction shows good agreement with simulations. In such cases, the distribution P_M^{st} exhibits a well-defined peak given by the dominant effect (at $M = 1$ when $\nu \gg m_g$, and at $M \gg 1$

when $m_g \gg \nu$). In situations like this, the assumption of ignoring selective sweeps on the calculation of rates $T^{\pm}_{M|\sigma}$ may become less relevant: if $\nu \gg m_g$, selective sweeps are dominant in the generator matrix and the rates $T^{\pm}_{M|\sigma}$ (this includes mutations) have a small effect on $P^{\rm st}_M$; if $m_g \gg \nu$, selective sweeps have small effect on $P^{\rm st}_M$ and the stationary distribution for M is mainly determined by rates $T^{\pm}_{M|\sigma}$. When both effects are relevant, the prediction becomes less accurate (see central panels of Figures 5.21 and 5.22). In cases like this we cannot ignore the effect of selective sweeps on rates $T^{\pm}_{M|\sigma}$, neither we can ignore the effect of mutations on the stationary distribution.

As discussed in Section 5.4, for slow switching environments the distribution $P^{\rm st}_M$ is in general bimodal, with the lowest peak approaching $M = 1$ and increasing its probability as ν increases. This is also shown in Figure 5.21. The data in Figure 5.21 also show more clearly than in Figure 5.13 that the probability of the highest peak is not affected by ν. For fast switching environments (see Figure 5.22), $P^{\rm st}_M$ is always unimodal with its mode approaching $M = 1$ as ν increases.

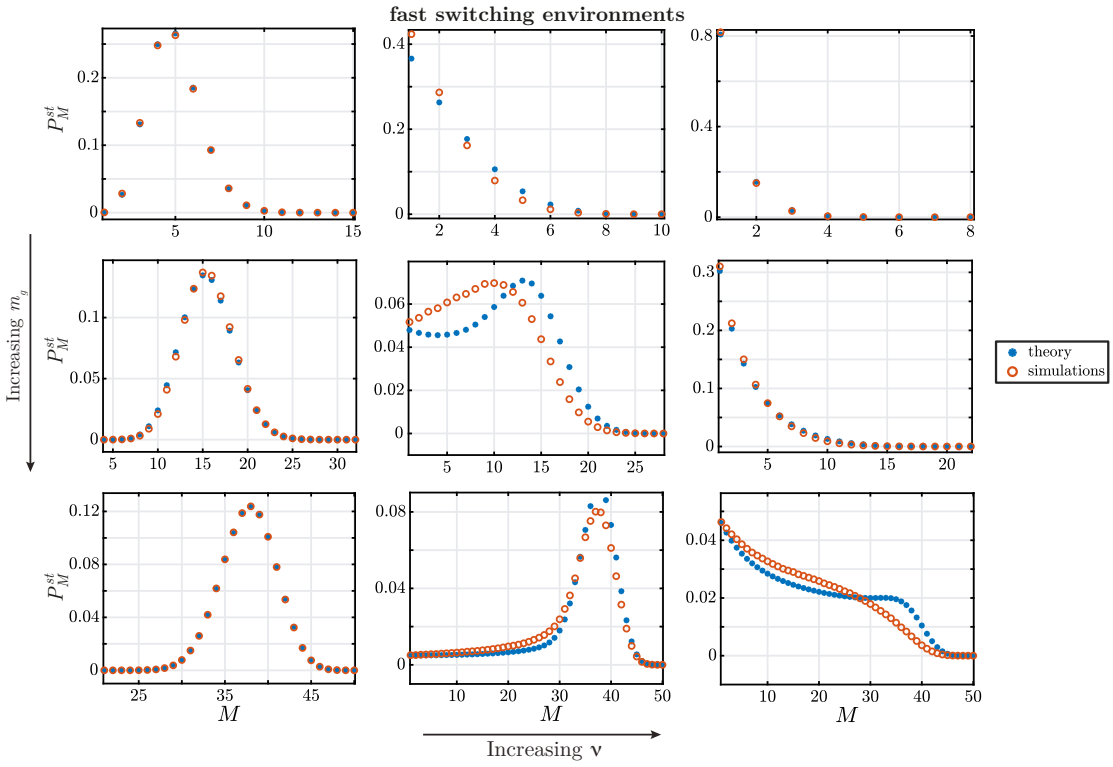

Figure 5.22: Stationary distribution of number of mating types in the model with selective sweeps and slowly switching environments. Theoretical prediction of $P^{\rm st}_M$ with selective sweeps as function of M for fast switching environments, population size $N = 50$, for different values of m_g and ν. From upper to lower rows: $m_g = 0.5, 5, 50$. From left to right columns: $\nu = 0, 0.5, 5$. Switching rates used: $\lambda_{S\to A} = \lambda_{A\to S} = 5$.

5.9.2 Fixed asexual environment

We now focus on a fixed environment with asexual reproduction, and explore how stationary distribution P_M^{st} behaves as parameters m_g and ν are varied. This can be done by calculating the eigenvector with eigenvalue zero of a generator matrix given solely by the block $Q^{(A,A)}$ in Eq. (5.131). The theoretical predictions and how they compare to numerical simulations in the full model are presented in Figure 5.23. As shown, the distribution is always unimodal for any value of m_g and ν, with the mode approaching $M = 1$ as ν increases. The fact there is only one peak is not surprising as the system has only one environment.

As stated in Section 5.4 of the main paper, the mean time until fixation of a single mutant is approximately given by $T = 2\log(N)/s$, where s the selective advantage of the mutant. Then, for a system that includes switching environments if we assume that $1/\lambda_{A\to S} \gg T$, i.e., that the time spent in the asexual environment is long enough so that the beneficial mutation sweeps through the population, and that $p_S \approx 0$, i.e., that the fraction of time spent in the sexual environment is negligible (so we can ignore any effect of the sexual environment), we can estimate the corresponding stationary distribution P_M^{st} using only the block $Q^{(A,A)}$ as the generator matrix.

Bibliography

[1] L. S. Tsimring, "Noise in Biology", Reports on Progress in Physics **77**, 026601 (2014).

[2] W. J. Ewens, *Mathematical Population Genetics* (Springer-Verlag, Berlin, 2004).

[3] M. Assaf, M. Mobilia, and E. Roberts, "Cooperation dilemma in finite populations under fluctuating environments", Physical Review Letters **111**, 238101 (2013).

[4] M. Danino, N. M. Shnerb, S. Azaele, W. E. Kunin, and D. A. Kessler, "The effect of environmental stochasticity on species richness in neutral communities", Journal of Theoretical Biology **409**, 155–164 (2016).

[5] B. Charlesworth, "Recombination Modification in a Fluctuating Environment", Genetics **83**, 181–195 (1976).

[6] B. Cloez, R. Dessalles, A. Genadot, F. Malrieu, A. Marguet, and R. Yvinec, "Probabilistic and piecewise deterministic models in biology", ESAIM: Proc. Surv. **60**, 225–245 (2018).

[7] P. Ashcroft, P. M. Altrock, and T. Galla, "Fixation in finite populations evolving in fluctuating environments", Journal Royal Society Interface **11**, 20140663 (2014).

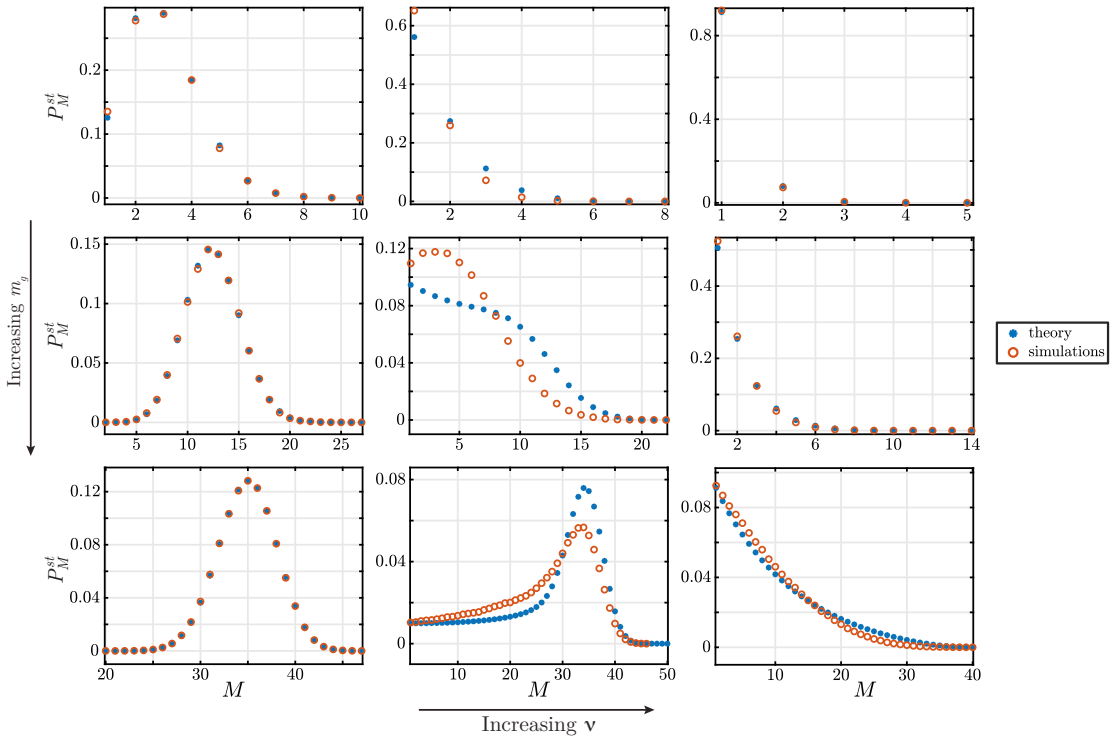

Figure 5.23: Theoretical prediction of P_M^{st} as function of M for population size $N = 50$ and $\sigma = A$ (asexual environment) for different values of m_g and ν. From upper to lower rows: $m = 0.5, 5, 50$. From left to right columns: $\nu = 0, 0.01, 0.1$.

[8] K. Wienand, E. Frey, and M. Mobilia, "Eco-evolutionary dynamics of a population with randomly switching carrying capacity", Journal of The Royal Society Interface **15**, 20180343 (2018).

[9] I. Meyer, and N. Shnerb, "Noise-induced stabilization and fixation in fluctuating environment", Sci Rep **8**, 9726 (2018).

[10] A. Taitelbaum, R. West, M. Assaf, and M. Mobilia, "Population Dynamics in a Changing Environment: Random versus Periodic Switching", Physical Review Letters **125** (2020).

[11] J. D. Van Dyken, and M. J. Wade, "The Genetic Signature of Conditional Expression", Genetics **184**, 557–570 (2010).

[12] T. Togashi, and P. A. Cox, *The Evolution of Anisogamy, A Fundamental Phenomenon Underlying Sexual Selection* (Cambridge University Press, Cambridge, 2011).

[13] S. Geng, P. De Hoff, and J. G. Umen, "Evolution of Sexes from an Ancestral Mating-Type Specification Pathway", PLoS Biology **12**, e1001904 (2014).

[14] J. Lehtonen, H. Kokko, and G. A. Parker, "What do isogamous organisms teach us about sex and the two sexes?", Philosophical Transactions of the Royal Society B: Biological Sciences **371**, 20150532 (2016).

[15] Y. Iwasa, and A. Sasaki, "Evolution of the Number of Sexes", Evolution **41**, 49–65 (1987).

[16] E. Kothe, "Tetrapolar fungal mating types: sexes by the thousands", FEMS Microbiology Reviews **18**, 65–87 (1996).

[17] Z. Hadjivasiliou, "Theoretical studies on the role and evolution of mating types and two sexes", PhD thesis (University College London (University of London), 2014).

[18] Z. Hadjivasiliou, Y. Iwasa, and A. Pomiankowski, "Cell–cell signalling in sexual chemotaxis: a basis for gametic differentiation, mating types and sexes", Journal of the Royal Society Interface **12**, 20150342 (2015).

[19] S. Billiard, M. López-Villavicencio, B. Devier, M. E. Hood, C. Fairhead, and T. Giraud, "Having sex, yes, but with whom? Inferences from fungi on the evolution of anisogamy and mating types", Biological Reviews **86**, 421–442 (2011).

[20] R. F. Hoekstra, "On the asymmetry of sex: evolution of mating types in isogamous populations", Journal of Theoretical Biology **98**, 427–451 (1982).

[21] L. D. Hurst, and W. D. Hamilton, "Cytoplasmic fusion and the nature of sexes", Proceedings of the Royal Society of London. Series B: Biological Sciences **247**, 189–194 (1992).

[22] A. G. Clark, and T.-H. Kao, "Self-incompatibility: theoretical concepts and evolution", in (Springer Netherlands, Dordrecht, 1994), pp. 220–242.

[23] Z. Hadjivasiliou, A. Pomiankowski, and B. Kuijper, "The evolution of mating type switching", Evolution **70**, 1569–1581 (2016).

[24] G. W. Constable, and H. Kokko, "The rate of facultative sex governs the number of expected mating types in isogamous species", Nature Ecology & Evolution **2**, 1168 (2018).

[25] P. Czuppon, and G. W. A. Constable, "Invasion and extinction dynamics of mating types under facultative sexual reproduction", Genetics **213**, 567–580 (2019).

[26] B. P. Nieuwenhuis, and T. Y. James, "The frequency of sex in fungi", Philosophical Transactions of the Royal Society B: Biological Sciences **371**, 20150540 (2016).

[27] J. Umen, "Evolution of sex and mating loci: an expanded view from Volvocine algae", Current Opinion in Microbiology **14**, 634–641 (2011).

[28] A. M. Nedelcu, and R. E. Michod, "Sex as a response to oxidative stress: the effect of antioxidants on sexual induction in a facultatively sexual lineage", Proceedings of the Royal Society B: Biological Sciences **270**, S136–S139 (2003).

[29] H. Kokko, "When Synchrony Makes the Best of Both Worlds Even Better: How Well Do We Really Understand Facultative Sex?", The American Naturalist **195**, 380–392 (2020).

[30] Y. Krumbeck, G. W. A. Constable, and T. Rogers, "Fitness differences suppress the number of mating types in evolving isogamous species", Royal Society Open Science **7**, 192126 (2020).

[31] G. Bell, "Experimental sexual selection in Chlamydomonas", J. Evol. Biol. **18**, 722–734 (2005).

[32] M. B. Nathanson, *Elementary methods in number theory*, Vol. 195 (Springer Science & Business Media, New York, 2008).

[33] S. Heubach, and T. Mansour, *Combinatorics of compositions and words* (CRC Press, Boca Raton, 2009).

[34] R. L. Graham, D. E. Knuth, O. Patashnik, and S. Liu, "Concrete mathematics: a foundation for computer science", Computers in Physics **3**, 106–107 (1989).

[35] L. Comtet, *Advanced Combinatorics: The art of finite and infinite expansions* (Springer Science & Business Media, Dordrecht, 2012).

[36] Y. Suhov, and M. Kelbert, *Probability and Statistics by Example: Volume 2, Markov Chains: A Primer in Random Processes and Their Applications*, Vol. 2 (Cambridge University Press, New York, 2008).

[37] D. Gillespie, "DT Gillespie, J. Comput. Phys. 22, 403 (1976).", Journal of Computational Physics **22**, 403 (1976).

[38] D. T. Gillespie, "Exact stochastic simulation of coupled chemical reactions", The Journal of Physical Chemistry **81**, 2340–2361 (1977).

[39] P. Czuppon, and D. Rogers, "Evolution of mating types in finite populations: the precarious advantage of being rare", Journal of Evolutionary Biology **32**, 1290–1299 (2019).

[40] G. J. Baxter, R. A. Blythe, and A. J. McKane, "Exact solution of the multi-allelic diffusion model", Mathematical biosciences **209**, 124–170 (2007).

[41] H. Wang, and S. Xiang, "On the convergence rates of Legendre Approximation", Mathematics of Computation **81**, 861–877 (2012).

[42] M. A. Mandel, B. M. Barker, S. Kroken, S. D. Rounsley, and M. J. Orbach, "Genomic and Population Analyses of the Mating Type Loci in Coccidioides Species Reveal Evidence for Sexual Reproduction and Gene Acquisition", Eukaryotic Cell **6**, 1189–1199 (2007).

[43] D. F. Gruchy, "The Breeding System and Distribution of Tetrahymena pyriformis", The Journal of Protozoology **2**, 178–185 (1955).

[44] M. Bakhshi, M. Arzanlou, and A. Babai-Ahari, "Uneven distribution of mating type alleles in Iranian populations of Cercospora beticola, the causal agent of Cercospora leaf spot disease of sugar beet", Phytopathologia Mediterranea **50**, 101–109 (2011).

[45] T. E. Douglas, J. E. Strassmann, and D. C. Queller, "Sex ratio and gamete size across eastern North America in Dictyostelium discoideum, a social amoeba with three sexes", J. Evol. Biol. **29**, 1298–1306 (2016).

[46] G. Wang, K. Chen, J. Zhang, X. Ma, S. Deng, J. Xiong, X. He, Y. Fu, and W. Miao, "Dynamics of the sex ratio in Tetrahymena thermophila", bioRxiv, 327544 (2018).

[47] S. C. Lee, M. Ni, W. Li, C. Shertz, and J. Heitman, "The Evolution of Sex: a Perspective from the Fungal Kingdom", Microbiology and Molecular Biology Reviews Microbiology and Molecular Biology Review **74**, 298–340 (2010).

[48] S. S. Phadke, and R. A. Zufall, "Rapid diversification of mating systems in ciliates", Biological Journal of the Linnean Society **98**, 187–197 (2009).

[49] J. A. Fraser, S. Diezmann, R. L. Subaran, A. Allen, K. B. Lengeler, F. S. Dietrich, and J. Heitman, "Convergent Evolution of Chromosomal Sex-Determining Regions in the Animal and Fungal Kingdoms", PLoS Biology **2** (2004).

[50] I. Hanski, *Metapopulation Ecology* (Oxford University Press, New York, 1999).

[51] F. P. Doerder, M. A. Gates, F. P. Eberhardt, and M. Arslanyolu, "High frequency of sex and equal frequencies of mating types in natural populations of the ciliate Tetrahymena thermophila.", Proceedings of the National Academy of Sciences of the United States of America **92**, 8715–8718 (1995).

[52] A. R. Hasan, and R. W. Ness, "Recombination Rate Variation and Infrequent Sex Influence Genetic Diversity in Chlamydomonas reinhardtii", Genome Biology and Evolution **12**, 370–380 (2020).

[53] I. J. Tsai, D. Bensasson, A. Burt, and V. Koufopanou, "Population genomics of the wild yeast Saccharomyces paradoxus: Quantifying the life cycle", Proceedings of the National Academy of Sciences **105**, 4957–4962 (2008).

[54] R. A. Ennos, and X.-S. Hu, "Estimating the number of sexual events per generation in a facultatively sexual haploid population", Heredity **122**, 729–749 (2019).

[55] M. Hartfield, and P. D. Keightley, "Current Hypotheses for the evolution of sex and recombination", Integrative Zoology **7**, 192–209 (2012).

[56] T. G. D'Souza, and N. K. Michiels, "The Costs and Benefits of Occasional Sex: Theoretical Predictions and a Case Study", Journal of Heredity **101**, S34–S41 (2010).

[57] N. Colegrave, "Sex releases the speed limit on evolution", Nature **420**, 664–666 (2002).

[58] J. Lehtonen, M. Jennions, and H. Kokko, "The many costs of sex", Trends in Ecology and Evolution **27**, 172–178 (2012).

[59] S. Eger, "Restricted weighted integer compositions and extended binomial coefficients", J. Integer Seq. **16**, 3 (2013).

[60] L. Hörmander, *An introduction to complex analysis in several variables* (Elsevier, Amsterdam, 1973).

[61] P. Butzer, and M. Hauss, "Riemann Zeta function: Rapidly converging series and integral representations", Applied mathematics letters **5**, 83–88 (1992).

Chapter 6

Beyond the adiabatic limit in systems with fast environments: a τ-leaping algorithm

Preface

This chapter constitutes an arXiv preprint[1] currently under review at Physical Review E. This work is co-authored with Tobias Galla[2,3].

E.B-C. contributed designing the study, developed the numerical methods presented here, produced all figures, and wrote the manuscript. T.G. contributed with the initial conception of the study, discussions guiding the work, and writing the manuscript.

[1] E. Berríos-Caro and T. Galla, "Beyond the adiabatic limit in systems with fast environments: a τ-leaping algorithm", *arXiv preprint*, arXiv 2011.10748 (2020). arXiv:2011.10748

[2] Theoretical Physics, Department of Physics and Astronomy, School of Natural Sciences, Faculty of Science and Engineering, The University of Manchester, Manchester M13 9PL, United Kingdom.

[3] Instituto de Física Interdisciplinar y Sistemas Complejos, IFISC (CSIC-UIB), Campus Universitat Illes Balears, E-07122 Palma de Mallorca, Spain.

Abstract

We propose a τ-leaping simulation algorithm for stochastic systems subject to fast environmental changes. Similar to conventional τ-leaping the algorithm proceeds in discrete time steps, but as a principal addition it captures environmental noise beyond the adiabatic limit. The key idea is to treat the input rates for the τ-leaping as (clipped) Gaussian random variables with first and second moments constructed from the environmental process. In this way, each step of the algorithm retains environmental stochasticity to sub-leading order in the time scale separation between system and environment. We test the algorithm on several toy examples with discrete and continuous environmental states, and find good performance in the regime of fast environmental dynamics. At the same time, the algorithm requires significantly less computing time than full simulations of the combined system and environment. In this context we also discuss several methods for the simulation of stochastic population dynamics in time-varying environments with continuous states.

The modelling of dynamical systems in biology and other disciplines necessarily requires simplifying assumptions and a level of coarse graining. If all processes we know about are included, then the model becomes so complicated that it cannot be simulated or analysed. Even if simulation or analysis is possible further study of such a model will rarely be enlightening. Excessive detail makes hard to identify the key mechanisms at work and to understand what model components are responsible for these mechanisms. At the same time, some element of realism must be maintained. The model must not be so stylised to miss the key ingredients and behaviour it is meant to capture. The principal challenge, therefore, is to find the right level of detail, given the intended purpose.

The choice between stochastic and deterministic modelling approaches is one aspect of this discussion. If more detailed stochastic models mark one end of the spectrum, then many traditional models in mathematical biology or chemistry sit at the opposite end. These models are often built on a small number of ordinary or partial differential equations (e.g. [1, 2]). This deterministic approach is valid if one can assume that the same initial conditions will always lead to the same outcome. For many applications

involving very large systems this is a perfectly sensible approach.

However, it is now also universally recognised that stochasticity in the time-evolution of many systems is key in shaping the outcome, see e.g. [3–5]. Consequently a number of analytical and computational methods has been developed for the study of stochastic systems. One focus is on systems with discrete interacting individuals. What these individuals represent depends on the context, they could be members of different species in population dynamics, individual animals or humans in models of an epidemic, or molecules in chemical reaction systems [3, 6–8].

One particular point of interest within this class of individual-based systems are models operating in a time-dependent environment. This environment is not part of the system proper, but its state has an effect on what happens in the system. In a model of a population of bacteria for example, the reproduction or death rates could depend on external conditions such as the availability of nutrients or the presence of toxins [9, 10]. In population dynamics, the carrying capacity could vary in time [11–13], and in epidemics the infection rate is subject to seasonal changes [14]. The focus of our paper is on such individual-based models in time-varying external environments.

Analytical approaches to stochastic systems with discrete individuals usually start from the chemical master equation. In limited cases direct solution is possible, for example using generating functions. However, this is the exception, and a number of approximation schemes have consequently been developed. These include Kramers–Moyal and system-size expansions, leading to Fokker–Planck equations and descriptions in terms of stochastic differential equations [8, 15]. These schemes sacrifice the granularity of a discrete-agent system, and instead describe the dynamics in terms of continuous densities. This approach can be successful in particular for large populations. Any particular event then only results in a small change in the composition of the population relative to its size. Individual-based approaches and descriptions based on deterministic differential equations have been extended to models of population dynamics in switching environments, for a selection of work see [11, 16–26].

There are however situations in which one would rather avoid giving up the discrete nature of the population. For example, granularity is crucial for extinction processes (the number of individuals of the species about to go extinct is small by definition). In other situations the population may not be large enough to warrant a description in

terms of continuous densities. For example, copy numbers in genetic circuits can be of the order of tens to hundreds (see e.g. [27]), and it is difficult to justify a continuum limit. It then becomes necessary to carry out numerical simulations of the discrete individual-based process. The method of choice is the Gillespie algorithm [28, 29], generating a statistically accurate ensemble of sample paths of the continuous-time dynamics.

In most applications the rate of events scales with the size of the population so that each individual experiences an $\mathcal{O}(1)$ number of reactions per unit time. The Gillespie method then runs into difficulties when the population is large, and with it the number of reactions per unit time. The computational cost of generating sample paths to up the desirable end point can then become very high. Similarly, a time scale separation between the dynamics in the population and the environment may make simulations challenging. If the environment is very fast compared to the population, a significant number of environmental events needs to be executed between events in the population. This aggravates the above limitations for large populations, and simulations can become problematic even for intermediate population sizes. One possible approach to this consists of assuming that the environment is 'infinitely' fast compared to the population. This is known as quasi steady state approximation [30, 31], or the 'adiabatic limit' [26, 32]. For related work see also [23, 33–36]. If this limit is taken then the environmental dynamics can be 'averaged out', and effective reaction rates can be used for the population. While computationally convenient, this approach discards any stochasticity from the environmental process. This sets another limitation, in particular when it is not valid to assume that the environment is infinitely fast compared to the population.

The objective of this work is therefore to design and test an algorithm for systems with fast environmental dynamics, but which also captures some elements of the environmental noise. We call this discrete-time algorithm τFE – τ-leaping for fast environments. It is built on the ideas of the conventional τ-leaping algorithm [37], but with modifications such as to preserve elements of the stochasticity of the environmental process. To do this, we assume that the environment is fast compared to the population, but not infinitely fast. More precisely, in each step of the algorithm we take into account sub-leading contributions in the time-scale separation.

The key new element of our algorithm is how we deal with the environment. We do not take the adiabatic limit, instead we treat the reaction rates in the population as random variables during each step. The rates are drawn from a distribution at the beginning of each step, and then remain fixed during the time step. The distribution of rates can change from one step to the next, and is constructed to reflect statistical features of the original environmental dynamics.

Each step of the τFE algorithm consists of two parts: First a realisation of reaction rates is drawn from the appropriate distribution. Then a conventional τ-leaping step is carried out with these rates. The core of our paper consists of the construction of the 'appropriate distribution' for the reaction rates. These ideas were introduced in a previous work [38] for a simple case of a two-species birth-death process in an environment which can take two discrete states. In the present paper we develop this further. We develop and test a more general algorithm for environments with more than two discrete states. As we will show, the algorithm can also be extended to continuous environmental dynamics.

The remainder of the paper is organised as follows. In Sec. 6.1 we describe the general setup of the type of system we simulate. We also outline the general principles of the τFE algorithm. In Sec. 6.2 we then make the necessary preparations for the introduction of the algorithm. In particular, we compute the statistics of reaction rates which are fed into the conventional τ-leaping step. We then describe the algorithm in detail. In Sec. 6.3, we test the τFE algorithm in different models with discrete environmental states. In Sec. 6.4, we then describe how the τFE algorithm can be used when the environment takes continuous states. Specifically, we consider an Ornstein-Uhlenbeck process. In this context we also describe how known algorithms can be adapted to simulate continuous environments. Finally, we provide a discussion of our results and overall conclusions in Sec. 6.6.

6.1 Model setup and general principles of the algorithm

6.1.1 Model definitions and notation

We look at systems composed of discrete individuals. We will refer to this synonymously as the 'system proper', or 'the population'. Each of the individuals is of one of S species (or types), labelled $i = 1, \ldots, S$. We write n_i for the number of individuals of species i in the population, and $\mathbf{n} = (n_1, \ldots, n_S)$. The system evolves in an external environment, whose state we write as σ. These states are time dependent, and can either take discrete values or be continuous.

The dynamics in the population proceeds through reactions $r = 1, \ldots, R$. Each of these reactions converts a number of individuals from one type into another. Time in the model is continuous, and we assume that the dynamics is Markovian. We then write $R_{r,\sigma}(\mathbf{n})$ for the rate of reaction r if the environment is in state σ and the population in state $\mathbf{n}$. The stoichiometric coefficient $\nu_{r,i}$ indicates how the number of individuals of type i changes when a reaction of type r occurs. Each $\nu_{r,i}$ is an integer, which can be negative, zero, or positive. We write $\boldsymbol{\nu}_r = (\nu_{r,1}, \ldots, \nu_{r,S})$. The rates $R_{r,\sigma}(\mathbf{n})$ and the stoichiometric coefficients fully specify the dynamics of the population when the environment is in state σ.

The state of the environment undergoes a Markovian stochastic process, governed by a master equation if states are discrete or by a stochastic differential equation in the case of continuous environmental states. These dynamics can depend on the state of the population $\mathbf{n}$. If the environmental states are discrete we write $q_{\sigma\to\sigma'}(\tau)$ for the probability of finding the environment in state σ' at a particular point in time, given that τ units of time earlier it was in state σ. If the environment is continuos then $q_{\sigma\to\sigma'}(\tau)$ is a probability density for σ' (at given σ). We call $q_{\sigma\to\sigma'}(\tau)$ the transition kernel of the environmental process. We write $\boldsymbol{\rho}^*$ for the stationary distribution of the environmental dynamics. For discrete environmental states the entries ρ^*_σ denote the probability of finding the system in state σ in the stationary state. For continuous environments ρ^*_σ is the stationary probability density for σ.

6.1.2 General principles of the τ-leaping algorithm for systems in fast environments

A conventional reaction system (without external environment) is governed by a chemical master equation of the form

$$\frac{\mathrm{d}}{\mathrm{d}t}P(\mathbf{n},t) = \sum_r \Big[R_r(\mathbf{n}-\boldsymbol{\nu}_r)P(\mathbf{n}-\boldsymbol{\nu}_r,t) - R_r(\mathbf{n})P(\mathbf{n},t)\Big]. \tag{6.1}$$

The notation is as in Sec. 6.1.1, the only difference is that there is no subscript σ, as there is no environment. Sample paths entail events (reactions) which can occur at any point in continuous time, separated by exponentially distributed random waiting times. In each such event the state of the system $\mathbf{n}$ changes, and accordingly the reaction rates $R_r(\mathbf{n})$ can also change. Sample paths can be generated for example using the celebrated Gillespie algorithm [28, 29]. This scheme, however, can become ineffective when the number of reactions per unit time is high. In those cases, in order to speed up the simulations one can work with an approximated method usually termed as the τ-leaping algorithm.

The τ-leaping algorithm for such conventional reaction systems is built around the idea of keeping reaction rates constant over finite time steps of length τ [37]. That is to say, if the state of the population is $\mathbf{n}$ at time t, then the assumption is made that this state $\mathbf{n}$ and the rates $R_r(\mathbf{n})$ do not change until the end of the time step. The algorithm does not account for potential changes of the rates as individual reactions occur, and instead directly 'leaps' to time $t+\tau$. This is justified provided the so-called 'leap condition' is fulfilled [37]: broadly speaking the time step τ must be sufficiently small so that the state $\mathbf{n}$ in the continuous-time system does not change significantly in a time interval of length τ. For discrete environments, using conventional exact schemes (such as the Gillespie algorithm [28, 29]) can be used as a benchmark to choose τ. For continuous environments, however, this is no longer possible as only approximated methods can be used to simulate them. We discuss this below.

Making the approximation of constant $\mathbf{n}$ in the time interval from t to $t+\tau$, the number of reactions of type r that fire in this interval follows a Poissonian distribution with parameter $\tau R_r(\mathbf{n})$. Accordingly, realisations of Poissonian random variables $m_1,\ldots,m_R$ are drawn, and the corresponding numbers of each reactions are executed simultaneously. This generates a new state $\mathbf{n}'$ at time $t+\tau$, with entries $n_i' =$

$n_i + \sum_{r=1}^{R} m_r \nu_{i,r}$. The process then repeats with updated rates $R_r(\mathbf{n}')$.

The idea of the τ-leaping algorithm we introduce for systems in external environments is similar. As in the conventional algorithm we discretise time, and keep the composition of the population $\mathbf{n}$ fixed during each iteration. It is only updated at the end of each step. From now on we use Δt for the duration of a step instead of τ.

The difference to the conventional case is the external environment. If the environmental state space is discrete then switches of the environment can in principle be simulated in continuous time along with the other reactions (using Gillespie algorithm [28, 29]). They can also be dealt with by means of the conventional τ-leaping algorithm, again along with the other reactions. These are natural simulation approaches when the environment operates on a similar time scale as the reactions in the population. Not much can then be gained by distinguishing between environmental processes and the dynamics in the system proper.

If the environment is infinitely fast compared to the reactions in the population, then the environment reaches stationarity on very short time scales. One can average over environmental states, see for example [26, 30, 31, 33, 38, 39]. If the environment is discrete, for example, we can use average rates

$$R_r^*(\mathbf{n}) \equiv \sum_{\sigma} \rho_\sigma^* R_{r,\sigma}(\mathbf{n}). \tag{6.2}$$

In the case of continuous environments the sum is to be replaced with an integral. These rates are functions of $\mathbf{n}$ only, the environmental process has been averaged out. Noise from the environmental process plays no role in the dynamics if these average rates are used. This corresponds to making a quasi-stationary state approximation for the fast-moving environment [30, 31].

The aim of this paper is to go beyond this adiabatic limit, and to construct a τ-leaping algorithm which captures some elements of extrinsic noise. We focus on the limit of a fast, but not infinitely fast environmental dynamics.

Broadly speaking the τFE algorithm is constructed around the idea of treating the reaction rates $R_r(\mathbf{n})$ as stochastic variables in each discrete time step. These random variables represent the rates one obtains when averaging the environmental process over the time step Δt. Assuming that the rate of change of the environment is finite these average rates will remain stochastic. In the limit of infinitely fast environments

the deterministic limit in Eq. (6.2) is recovered, and there is no stochasticity from the environment.

To construct the random reaction rates for each step, we make an approximation: we use a Gaussian distribution for the rates, with means as in Eq. (6.2) and with variances and correlations derived from the original combined process of the population and environment. We describe this in detail in the next section.

6.2 Construction of the τFE algorithm for systems with discrete environments

6.2.1 Preliminary analysis of the environmental process

Here we assume the environmental states are discrete, $\sigma \in \{1, \ldots, M\}$. The dynamics of the environment is governed by the rates $\lambda A_{\sigma\to\sigma'}(\mathbf{n})$ for transitions from σ to σ'. The factor λ is introduced to control the time-scale separation between reactions in the population and the switching of the environment. We use the notation $\mathbf{A}(\mathbf{n})$ for the $M \times M$ matrix with elements $A_{\sigma\to\sigma'}(\mathbf{n})$. We also set $A_{\sigma\to\sigma}(\mathbf{n}) = -\sum_{\sigma'\neq\sigma} A_{\sigma\to\sigma'}(\mathbf{n})$. The combined dynamics of population and environment are then described by the master equation

$$\begin{aligned}\frac{\mathrm{d}}{\mathrm{d}t}P(\mathbf{n},\sigma,t) = &\sum_r \Big[R_{r,\sigma}(\mathbf{n}-\boldsymbol{\nu}_r)P(\mathbf{n}-\boldsymbol{\nu}_r,\sigma,t) - R_{r,\sigma}(\mathbf{n})P(\mathbf{n},\sigma,t)\Big] \\ &+ \lambda\sum_{\sigma'}\Big[A_{\sigma'\to\sigma}(\mathbf{n})P(\mathbf{n},\sigma',t) - A_{\sigma\to\sigma'}(\mathbf{n})P(\mathbf{n},\sigma,t)\Big]. \qquad (6.3)\end{aligned}$$

The rates $\lambda A_{\sigma\to\sigma'}(\mathbf{n})$ can depend on the state of the population, $\mathbf{n}$. This means that $\mathbf{n}$ and σ do not necessarily evolve in time independently. However, as mentioned above the state $\mathbf{n}$ of the system is kept constant during each τ-leaping step. This in turn means that the transition rates for the environment also remain constant during each step.

We now focus on one such time step, starting at time t and ending at $t + \Delta t$. We assume that $\mathbf{n}$ remains constant during this time interval. For the remainder of Sec. 6.2.1 we suppress the potential dependence of $\mathbf{A}$ on $\mathbf{n}$, although it is always implied. We write $\rho_\sigma(t')$ for the probability that the environment is in state σ at time

$t \in [t, t + \Delta t]$. We then have the master equation

$$\frac{\mathrm{d}\boldsymbol{\rho}}{\mathrm{d}t'} = \lambda \mathbf{A}\boldsymbol{\rho} \tag{6.4}$$

for the environmental dynamics. The stationary distribution $\boldsymbol{\rho}^*$ for the environment is the solution of $\mathbf{A}\boldsymbol{\rho}^* = 0$. If $\mathbf{A}$ depends on $\mathbf{n}$, then ρ^* will also be a function of $\mathbf{n}$. Assuming that the environmental process is irreducible this stationary distribution is unique for any one $\mathbf{n}$.

The stochastic matrix $\mathbf{A}$ has one zero eigenvalue, which we write as $\mu_1 = 0$. The remaining eigenvalues are denoted by $\mu_2, \ldots, \mu_M$. We then have $\mu_2, \ldots, \mu_M < 0$. The corresponding (right) eigenvalues are written as $\mathbf{v}_1 = \boldsymbol{\rho}^*$ (the eigenvector corresponding to eigenvalue 0), and $\mathbf{v}_2, \ldots, \mathbf{v}_M$ respectively for the remaining eigenvectors. These are all understood to be column vectors of length M.

We note that the general solution of Eq. (6.4) can be written in the form

$$\boldsymbol{\rho}(t') = \boldsymbol{\rho}^* + \sum_{\ell=2}^{M} c_\ell e^{\lambda \mu_\ell (t'-t)} \mathbf{v}_\ell, \tag{6.5}$$

with coefficients c_ℓ determined by the initial condition at the beginning of the time step $t' = t$. More precisely these coefficients can be obtained from the linear system

$$\sum_{\ell=2}^{M} c_\ell \mathbf{v}_\ell = \boldsymbol{\rho}(t) - \boldsymbol{\rho}^*. \tag{6.6}$$

We remark that there are $M-1$ coefficients, c_ℓ ($\ell = 2, \ldots, M$). The system in Eq. (6.6) technically consists of M equations, but these are not independent due to normalisation of the probabilities on the right-hand side.

Calculating the probability $q_{\sigma \to \sigma'}(\Delta t)$ to find the environment in state σ' at the end of the time step if it was in σ at the beginning of the step is now mainly a matter of computing the coefficients c_ℓ. We write $c_{\ell,\sigma}$ for the value the coefficient c_ℓ takes when $\rho_{\sigma'}(t) = \delta_{\sigma',\sigma}$ (i.e., when the system starts in state σ at the beginning of the step).

We then have

$$q_{\sigma \to \sigma'}(\Delta t) = \rho^*_{\sigma'} + \sum_{\ell=2}^{M} c_{\ell,\sigma} e^{\lambda \mu_\ell \Delta t} v_{\ell,\sigma'}, \tag{6.7}$$

where $v_{\ell,\sigma'}$ is the σ'-entry of the eigenvector $\mathbf{v}_\ell$ of $\mathbf{A}$.

If the matrix $\mathbf{A}$ depends on the population state $\mathbf{n}$, the parameters μ_ℓ, $v_{\ell,\sigma'}$, and $c_{\ell,\sigma}$ can also depend on $\mathbf{n}$. For simplicity of notation we have not included this potential dependence in the above equations.

6.2.2 Time-averaged reaction rates as random variables

The τ-leaping algorithm proceeds in discrete time intervals of length Δt. We continue to focus on one such interval $[t, t+\Delta t]$. The state of the population at the beginning of the step is $\mathbf{n}$ and we assume that this state does not change until the end of the interval. We do however take into account the fact that the state of environment σ can undergo changes in the interval from t to $t+\Delta t$. As a consequence, $R_{r,\sigma}(\mathbf{n})$ (at fixed $\mathbf{n}$) is also a function of time.

We then introduce the time-averaged quantities

$$\overline{R_r}(\mathbf{n}) \equiv \frac{1}{\Delta t}\int_t^{t+\Delta t} \mathrm{d}t\; R_{r,\sigma(t)}(\mathbf{n}), \tag{6.8}$$

noting that the time average is *over the duration of the time step only* as opposed to a long-term asymptotic time average. Given that the time step Δt is finite ($\Delta t < \infty$) and assuming that the environment fluctuates with finite rates ($\lambda < \infty$), the quantity $\overline{R_r}(\mathbf{n})$ is a stochastic variable as it depends on the realisation of the environmental process. In one given time interval, the rates $\overline{R_r}(\mathbf{n})$ for different r will be correlated as they all derive from the same path of the environment. As we will show below, the fluctuations of the random variables $\overline{R_r}(\mathbf{n})$ in any one time step are inversely proportional to $\lambda\Delta t$ to leading order. In the limit $\lambda\Delta t \to \infty$ the $\overline{R_r}(\mathbf{n})$ become deterministic.

We assume that the distribution for σ at the beginning of the time step is the stationary distribution $\boldsymbol{\rho}^*$. This is the case for example, if then environmental state is drawn from the stationary distribution at the beginning of the simulation. The distribution for $\sigma(t')$ is then also the stationary distribution at each time $t' \in [t, t+\Delta t]$. Writing $\langle \ldots \rangle$ for the average over realisations of the environmental process, we then have

$$\left\langle \overline{R_r}(\mathbf{n}) \right\rangle = R_r^*(\mathbf{n}), \tag{6.9}$$

with $R_r^*(\mathbf{n})$ as in Eq. (6.2).

However, $\sigma(t')$ ($t' \in [t, t+\Delta t]$) will generally be correlated with $\sigma(t)$. Neglecting these means to operate in the adiabatic limit. We would like to retain some of these correlations. In order to compute second moments $\left\langle \overline{R}_r(\mathbf{n})\overline{R}_s(\mathbf{n}) \right\rangle$ we first use Eq. (6.8). This leads to averages of the type $\left\langle R_{r,\sigma(t_1)}(\mathbf{n}) R_{s,\sigma(t_2)}(\mathbf{n}) \right\rangle$, where t_1 and t_2 are two times in the interval from t to $t+\Delta t$. The second moments can then be expressed in terms

of $q_{\sigma\to\sigma'}(\cdot)$ as follows

$$\left\langle \overline{R}_r(\mathbf{n})\overline{R}_s(\mathbf{n})\right\rangle = \frac{1}{\Delta t^2}\sum_{\sigma\sigma'}\int_t^{t+\Delta t} \mathrm{d}t_1 \int_{t_1}^{t_1+\Delta t} \mathrm{d}t_2 \Big\{ \rho^*_\sigma q_{\sigma\to\sigma'}(t_2-t_1) \times \Big[R_{r,\sigma}(\mathbf{n})R_{s,\sigma'}(\mathbf{n}) + R_{r,\sigma'}(\mathbf{n})R_{s,\sigma}(\mathbf{n})\Big]\Big\}. \tag{6.10}$$

Further details are given in Appendix 6.7. Using Eq. (6.7) we find

$$\left\langle \overline{R}_r(\mathbf{n})\overline{R}_s(\mathbf{n})\right\rangle - R^*_r(\mathbf{n})R^*_s(\mathbf{n}) = \frac{1}{\Delta t^2}\sum_{\sigma\sigma'}\sum_{\ell=2}^{M}\Big\{\rho^*_\sigma c_{\ell,\sigma}v_{\ell,\sigma'} \times \Big[R_{r,\sigma}(\mathbf{n})R_{s,\sigma'}(\mathbf{n}) + R_{r,\sigma'}(\mathbf{n})R_{s,\sigma}(\mathbf{n})\Big]\int_t^{t+\Delta t}\mathrm{d}t_1\int_{t_1}^{t_1+\Delta t}\mathrm{d}t_2\; e^{\lambda\mu_\ell(t_2-t_1)}\Big\}. \tag{6.11}$$

For fixed $\ell \in \{2,\dots,M\}$ the integral in the last expression evaluates to

$$\int_t^{t+\Delta t}\mathrm{d}t_1\int_{t_1}^{t_1+\Delta t}\mathrm{d}t_2\; e^{\lambda\mu_\ell(t_2-t_1)} = -\frac{\Delta t}{\lambda\mu_\ell} + \frac{1}{(\lambda\mu_\ell)^2}\left[e^{\lambda\mu_\ell\Delta t}-1\right]. \tag{6.12}$$

For $\lambda\Delta t \gg 1$ the first term dominates after inserting into Eq. (6.11), as also observed in [40]. We are then left with

$$\left\langle \overline{R}_r(\mathbf{n})\overline{R}_s(\mathbf{n})\right\rangle - R^*_r(\mathbf{n})R^*_s(\mathbf{n}) = -\frac{1}{\lambda\Delta t}\sum_{\sigma\sigma'}\sum_{\ell=2}^{M}\left\{\frac{1}{\mu_\ell}R_{r,\sigma}(\mathbf{n})R_{s,\sigma'}(\mathbf{n})\Big[\rho^*_\sigma c_{\ell,\sigma}v_{\ell,\sigma'} + \rho^*_{\sigma'}c_{\ell,\sigma'}v_{\ell,\sigma}\Big]\right\}. \tag{6.13}$$

The main challenge in implementing the τFE algorithm is then to find the average rates from Eq. (6.9) for all r, and the second moments from Eq. (6.13) for any pair r,s of reactions affected by the environment. We stress that our algorithm relies on knowing the stationary distribution ρ^* and the rates $q_{\sigma\to\sigma'}$ of the environmental dynamics.

6.2.3 Description of the algorithm

Without loss of generality, we assume that only the rates for the reactions $r = 1,\dots,L$ ($L \le R$) depend on the environmental state σ.

The τFE algorithm with time step Δt proceeds as follows:

1. Initiate the population in state $\mathbf{n}(0)$. Set time to $t = 0$.

2. Compute $R^*_r(\mathbf{n})$ for $r = 1,\dots,L$ using Eq. (6.2), and the covariances $\Xi_{rs}(\mathbf{n}) \equiv \left\langle \overline{R}_r(\mathbf{n})\overline{R}_s(\mathbf{n})\right\rangle - R^*_r(\mathbf{n})R^*_s(\mathbf{n})$ using Eq. (6.13) for every pair $r,s \in \{1,\dots,L\}$.

3. (i) First consider the reactions with rates dependent on the environment: Draw correlated Gaussian random numbers $\ell_1, \ldots, \ell_L$ such that $\langle \ell_r \rangle = R_r^*(\mathbf{n})$, and $\langle \ell_r \ell_s \rangle - \langle \ell_r \rangle \langle \ell_s \rangle = \Xi_{rs}(\mathbf{n})$. If $\ell_r < 0$ for any $r \in \{1, \ldots, L\}$ set $\ell_r = 0$.

   (ii) For the remaining reactions $r \in \{L+1, \ldots, R\}$ set $\ell_r = R_r(\mathbf{n})$. These are the reactions with rates independent of the environment.

5. Draw independent Poissonians random numbers m_r, $r = 1, \ldots, R$, each with parameter $\ell_r \Delta t$.

6. Update the state of the population, $\mathbf{n}(t + \Delta t) = \mathbf{n}(t) + \sum_r m_r \boldsymbol{\nu}_r$.

7. Increment time by Δt and go to 2.

We note that the mean of the ℓ_r in step 3(i) is of order $(\lambda \Delta t)^0$, and their variance of order $(\lambda \Delta t)^{-1}$. Truncation of the ℓ_r will therefore only be required very rarely when $\lambda \Delta t \gg 1$.

Evaluating the expressions in Eqs. (6.2) and (6.13) in step 2 requires eigenvalues μ_ℓ of the transition matrix $\mathbf{A}(\mathbf{n})$ for the environment, the eigenvectors, $\mathbf{v}_\ell$ (including the stationary distribution $\mathbf{v}_1 = \boldsymbol{\rho}^*$), and the coefficients $c_{\ell,\sigma}$ for all σ. If the environmental process is independent of the state of the population (the $A_{\sigma \to \sigma'}$ are not functions of $\mathbf{n}$), then these quantities do not depend on $\mathbf{n}$, and only need to be calculated once at the beginning.

In Sec. 6.3 we first test the τFE algorithm on different models with discrete environments. However, we stress that the algorithm can also be extended to the case of environmental dynamics with continuous states. This will be discussed in Sec. 6.4.

6.3 Application of the τFE algorithm to models with discrete environmental states

We now consider three examples of systems with discrete environmental states.

The first example (Sec. 6.3.1) is a genetic circuit. The role of the environment is here played by a process of binding and unbinding to promoters of the genes described by the model. Gene regulatory systems can exhibit time scale separation as discussed for

example in [41–43]. Mathematically the model describes a population with two types of individuals and an environment with two states (bound/unbound). The environmental dynamics depends on the state of the population.

The second example (Sec. 6.3.2) is a toy model with two species in the population and three environmental states. The environmental process in this example is independent of the state of the population.

Sec. 6.3.3 finally focuses on a bimodal genetic switch with two species in the population, and an environmental process with three states, and with rates which depend on the state of the population.

6.3.1 Genetic circuit: two system-independent environments, two species

This system models the dynamics of two genes, which produce two different regulatory proteins: X (a transcription factor) and Y (an inhibitor that titrates X into an inactive complex). Specifically, we use the activator-titration circuit described in [32]. The reactions are as follows:

$$\begin{aligned}
&\emptyset \xrightarrow{\Omega\beta_X} X, \quad \emptyset \xrightarrow{\Omega\beta_{Y,\sigma}} Y, \quad (\sigma = 0, 1)\\
&X \xrightarrow{\delta_X} \emptyset, \quad Y \xrightarrow{\delta_Y} \emptyset,\\
&X + Y \xrightarrow{\alpha/\Omega} \emptyset,\\
&E_0 \xrightarrow{\lambda n_X \kappa_Y/\Omega} E_1, \quad \text{and,} \quad E_1 \xrightarrow{\lambda\theta_Y} E_0,
\end{aligned} \tag{6.14}$$

where the E_σ denote states of the environment ($\sigma = 0, 1$). These two environmental states represent situations in which a transcription factor X is bound to the promoter of gene Y (state E_1), or no transcription factor is bound (E_0), respectively. The first two reactions in Eq. (6.14) describe the production of the two proteins (X and Y). The production rates are β_X and $\beta_{Y,\sigma}$. The former is independent of the environmental state, the latter explicitly depends on σ (i.e., on the presence or absence of a bound transcription factor). The reactions in the second line of Eq. (6.14) describe degradation of X and Y, and the reaction in the third line captures titration. The binding and unbinding processes of the transcription factor are described by the reactions in the last line. The parameter Ω in the reaction rates determines the typical number of

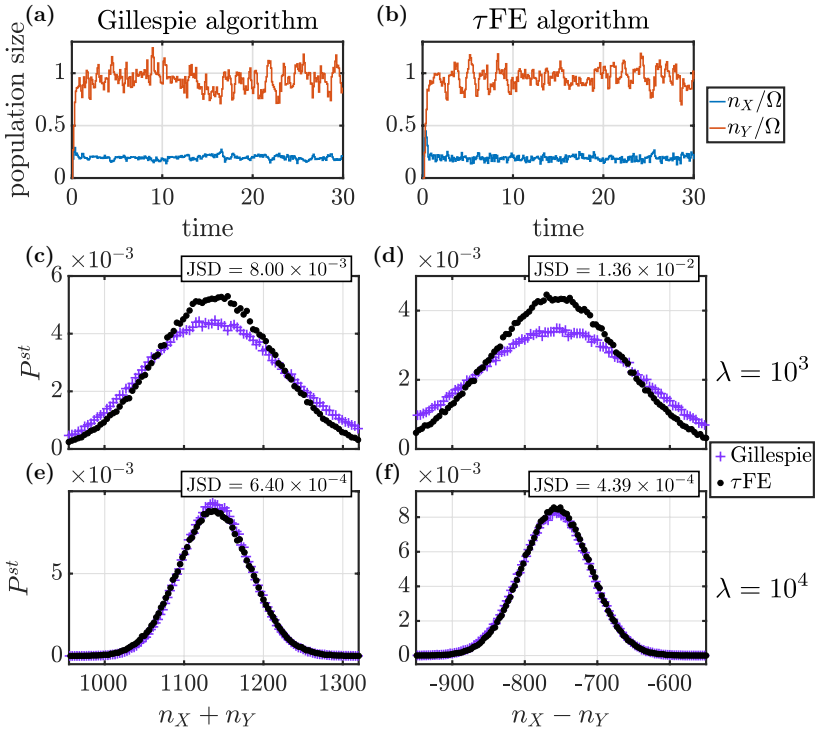

Figure 6.1: Simulation output for the model of the genetic-circuit in Eq. (6.14). Panel (a) shows a sample path obtained from Gillespie simulations of the full model. Panel (b) is a sample path from the τFE algorithm [$\lambda = 10^3$ in panels (a) and (b)]. Panels (c) and (d) show the stationary distributions of $n_X + n_Y$ and $n_X - n_Y$, respectively, for $\lambda = 10^3$, while (e) and (f) are for $\lambda = 10^4$. In each panel (c)–(f) we report the Jensen-Shannon divergence (JSD) between the distributions obtained using the two different simulation methods. Remaining parameters: $\Omega = 10^3, \beta_X = 2, \beta_{Y,0} = 0, \beta_{Y,1} = 10, \delta_X = \delta_Y = 1, \kappa_Y = 1, \theta_Y = 0.5$, and $\alpha = 10$. For the τFE we have used a time step $\Delta t = 0.1$.

particles in the system, for further details see [32]. We write n_X for the number of X-particles in the system, and similarly n_Y is the number of Y-particles. One finds $n_X, n_Y = \mathcal{O}(\Omega)$ in the stationary state.

Mathematically, the model consists of two species in the population (with numbers of particles n_X, n_Y), and two environmental states, $\sigma = 0, 1$. We therefore have $S = 2, M = 2$. Eqs. (6.9) and (6.13) can be evaluated explicitly for this case, see also [38]. The only process affected by the state of the environment is the production of Y, with rate $\beta_{Y,\sigma}$. This rate becomes a (clipped) Gaussian random variable in the τFE algorithm, with first moment

$$\left\langle \overline{\beta}_Y \right\rangle = \beta_Y^* = \frac{\theta_Y \beta_{Y,0} + n_X \kappa_Y \beta_{Y,1}/\Omega}{\theta_Y + n_X \kappa_Y / \Omega}, \tag{6.15}$$

and with variance

$$\sigma^2_{\beta_Y\beta_Y} \equiv \langle \bar{\beta}_Y^2 \rangle - {\beta_Y^*}^2 = \frac{2n_X\kappa_Y\theta_Y/\Omega}{\lambda\Delta t(n_X\kappa_Y/\Omega + \theta_Y)} \left(\beta_{Y,0} - \beta_{Y,1}\right)^2 . \tag{6.16}$$

Further details of the derivation can be found in Appendix 6.8.

Simulation results for this model are shown in Fig. 6.1. In panels (a) and (b) we illustrate typical sample paths obtained from Gillespie simulations of the full model (population and environment), and from the τFE algorithm, respectively. We also show the stationary distributions for the quantities $n_X + n_Y$ and $n_X - n_Y$ as obtained from both simulation algorithms. The distributions in panels (c) and (d) are for $\lambda = 10^3$ (i.e., moderately fast environmental dynamics), there are then remaining discrepancies between the τFE algorithm and simulations of the full model. In panels (e) and (f) the time-scale separation is larger ($\lambda = 10^4$). The agreement improves as indicated by the Jensen-Shannon divergence (JSD) [44, 45] given in the figure.

We note at this point that the average CPU time to run a sample path up to time $t = 10^3$ with parameters as in Fig. 6.1 (e) and (f) is 2.94 seconds for the Gillespie algorithm, and 0.03 seconds for the τFE algorithm (with a time step $\Delta t = 0.1$). These average simulation times are obtained from ten runs. They indicate that the τFE algorithm can significantly increase efficiency while producing results of the quality shown in Fig. 6.1. We stress that our primary interest is the relative comparison of computing times, and not on absolute simulation times [4].

6.3.2 Birth-death process: three environments, two species

Next, we consider a two-species birth-death process subject to an external environment which can be in one of three different states. This is a toy model chosen for illustration and does not represent any specific natural system. However, it captures elements of models of population dynamics.

The species in the population are labeled A and B, and the environmental states $\sigma = 0, 1, 2$. Particles of type A are produced with rate $\Omega\alpha_\sigma$, and particles of type B with rate $\Omega\beta_\sigma$. The subscript σ indicates explicit dependence on the state of the environment.

[4] For completeness, we add that simulations were performed on a MacBook Pro (Mid 2014), with processor 2.6 GHz Dual-Core Inter Core i5, and memory 8 GB 1600 MHz DDR3.

Particles are removed with constant per capita rates d_A and d_B respectively. The parameter Ω again sets the typical size of the population. We write n_A and n_B for the number of individuals of either species. The environmental states cycle stochastically through the sequence $\sigma = 0, 1, 2, 0, \ldots$, with rate constants λk_1, λk_2 and λk_0 for the three transitions. Mathematically, the reactions in this model are

$$\begin{aligned} &\emptyset \xrightarrow{\Omega\alpha_\sigma} A, \quad \emptyset \xrightarrow{\Omega\beta_\sigma} B, \quad (\sigma = 0, 1, 2) \\ &A \xrightarrow{d_A} \emptyset, \quad B \xrightarrow{d_B} \emptyset, \\ &E_0 \xrightarrow{\lambda k_1} E_1, \quad E_1 \xrightarrow{\lambda k_2} E_2, \quad E_2 \xrightarrow{\lambda k_0} E_0, \end{aligned} \tag{6.17}$$

where as before E_σ denotes the environment. The rates k_0, k_1, and k_2 are constant parameters, independent of the population state.

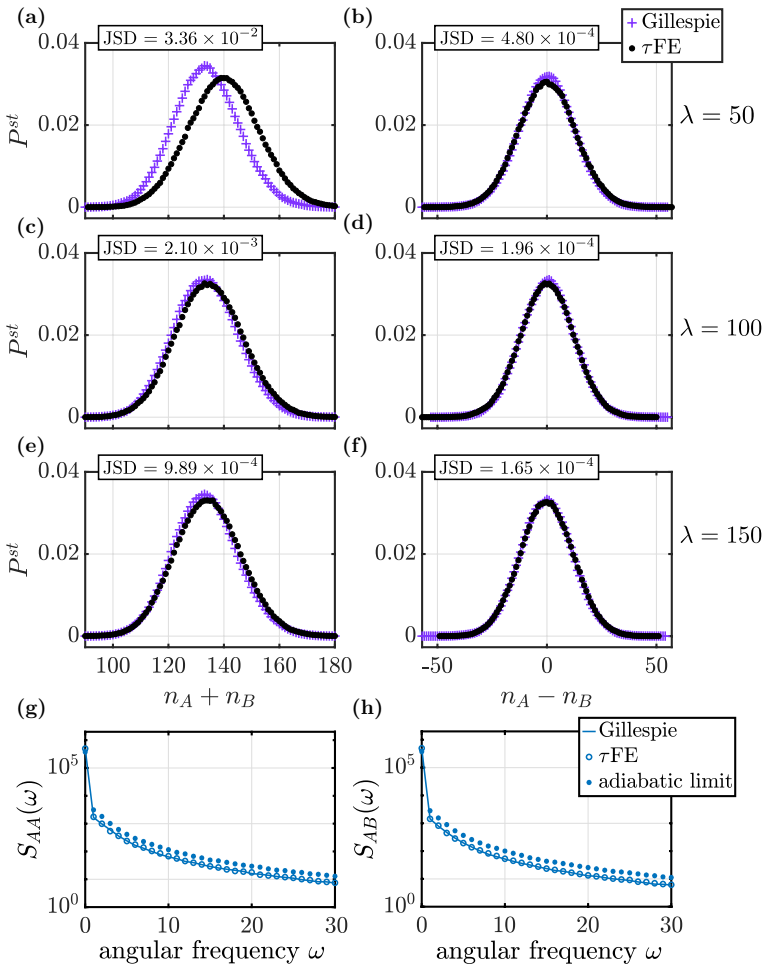

Figure 6.2: Simulation output of the two-species birth-death process in an environment with three states [Eq. (6.17)]. Panels (a), (c), and (e) show the stationary distribution of $n_A + n_B$ obtained using the Gillespie algorithm for the full model, and the τFE algorithm. Data is shown for different values of λ. Panels (b), (d), and (f) show the stationary distribution of $n_A - n_B$. Parameters used: $k_0 = k_1 = k_2 = 1, \Omega = 20, d_A = d_B = 0.1$, $\alpha_0 = \beta_0 = \beta_1 = \alpha_2 = 0$, and $\alpha_1 = \beta_2 = 1$. In each panel (a)–(f) we report the Jensen-Shannon divergence (JSD) between the two distributions obtained from Gillespie simulations of the full model and from the τFE algorithm. Panels (g) and (h): Spectral densities $S_{AA}(\omega)$ and $S_{AB}(\omega)$ [Eq. (6.21)] obtained from simulations using the Gillespie algorithm (full line), the τFE algorithm (open circles), and from conventional τ-leaping simulations of the model in the adiabatic limit (asterisks). Parameters in (g) and (h) are as in panels (e) and (f), i.e., $\lambda = 150$. The time step for the τFE algorithm and for conventional τ-leaping in the adiabatic limit is $\Delta t = 0.1$.

Details of the calculation of the average rates and their second moments can be

found in Appendix 6.9. The average production rates for the two types of particles are

$$\begin{aligned} \alpha^* &= \frac{k_0\alpha_0 + k_1\alpha_1 + k_2\alpha_2}{k_0 + k_1 + k_2}, \\ \beta^* &= \frac{k_0\beta_0 + k_1\beta_1 + k_2\beta_2}{k_0 + k_1 + k_2}, \end{aligned} \tag{6.18}$$

while the covariance $\sigma_{\alpha\beta} = \sigma_{\beta\alpha} \equiv \langle\bar{\alpha}\bar{\beta}\rangle - \alpha^*\beta^*$ takes the form

$$\begin{aligned} \sigma_{\alpha\beta} = \frac{\theta^2}{\lambda\Delta t}\Big\{ &(\alpha_0 - \alpha_1)(\beta_0 - \beta_1)\left(3k_0^2 - k_{0,1}k_{0,2}\right) \\ &+ (\alpha_1 - \alpha_2)(\beta_1 - \beta_2)\left(3k_1^2 - k_{1,0}k_{1,2}\right) \\ &+ (\alpha_0 - \alpha_2)(\beta_0 - \beta_2)\left(3k_2^2 - k_{2,0}k_{2,1}\right)\Big\}, \end{aligned} \tag{6.19}$$

with

$$\theta^2 \equiv \frac{k_0k_1k_2}{(k_0k_1 + k_1k_2 + k_2k_0)^3}, \tag{6.20}$$

and $k_{\sigma,\sigma'} = k_\sigma - k_{\sigma'}$, for $\sigma, \sigma' \in \{0, 1, 2\}$. The variance $\sigma_{\alpha\alpha} \equiv \langle\bar{\alpha}\bar{\alpha}\rangle - (\alpha^*)^2$, is obtained by replacing all instances of β_σ on the right-hand side of Eq. (6.19) with α_σ. The analog $\sigma_{\beta\beta}$ is obtained similarly by replacing α_σ with β_σ.

In Fig. 6.2 we report results from numerical simulations for this model, both from conventional Gillespie algorithm of the full systems of environment and population, and using the τFE algorithm. Panels (a)–(f) show the stationary distributions of $n_A + n_B$ and $n_A - n_B$. As seen from the data for example in panel (a) the τFE algorithm displays deviations from Gillespie simulations of the full model when the environmental process is not sufficiently fast. We quantify these deviations again through the Jensen–Shannon divergence between the two distributions. The deviations reduce as the time scale separation λ is increased, i.e., when the environmental process becomes faster relative to the dynamics within the population.

In order to examine if the τFE algorithm accurately reproduces dynamical features (i.e., properties of the system beyond the stationary distribution), we show spectral densities of the time series for n_A and n_B in Fig. 6.2(g) and (h). The spectral densities are defined as

$$\begin{aligned} S_{AA}(\omega) &= \langle|\hat{n}_A(\omega)|^2\rangle, \\ S_{AB}(\omega) &= \langle\hat{n}_A^\dagger(\omega)\hat{n}_B(\omega)\rangle, \end{aligned} \tag{6.21}$$

where $\hat{n}_A(\omega)$ and $\hat{n}_B(\omega)$ are the Fourier transforms of $n_A(t)$ and $n_B(t)$, respectively. The dagger denotes complex conjugation. The data from the τFE algorithm (open

symbols) in Fig. 6.2(g) and (h) compares well with spectra obtained from direct Gillespie simulations of the full model (solid lines). This shows the τFE method indeed captures the dynamics of n_A and n_B. We also provide a comparison against the spectral densities obtained from conventional $\tau-$leaping simulations in the adiabatic limit, i.e., simulations with constant rates α^* and β^* for the production events [Eq. (6.18)]. These are shown as full markers in Fig. 6.2(g) and (h). One then finds more substantial systematic deviations. This is because environmental fluctuations are discarded in the adiabatic limit. The τFE algorithm on the other hand captures the stochasticity of the environment to sub-leading order in λ^{-1} in each iteration step.

6.3.3 Bimodal genetic switch: three system-state dependent environments, two species

We now consider a model studied in [26, 46], describing a single gene G with a promoter site which can bind to a total of up to N molecules of protein. The number of protein molecules bound, σ, plays the role of the environment in this setting. The rate for transitions from σ to $\sigma+1$ depends on the number of protein molecules. The reactions in this model can be summarised as follows,

$$\begin{aligned} G_\sigma + P &\underset{\lambda k_-}{\overset{\lambda k_+/\Omega}{\rightleftharpoons}} G_{\sigma+1}, \quad \text{for} \quad \sigma < N, \\ G_\sigma &\xrightarrow{\Omega b_\sigma} G_\sigma + M, \\ M \xrightarrow{d} \emptyset, \quad M &\xrightarrow{\beta} M + P, \quad P \xrightarrow{\delta} \emptyset, \end{aligned} \tag{6.22}$$

where M and P refer to molecules of mRNA and protein, respectively. The production rate b_σ for mRNA depends on the number of protein molecules bound to the promoter. We refer to [26, 46] for further details. In the following we write n_M and n_P for the numbers of particles of either type. One interesting feature of this model is that the distribution of the protein and mRNA populations can become bimodal, as illustrated in Fig. 6.3. This leads to bistability, with trajectories transitioning between the two modes of the joint distribution of n_P and n_M. Hence, the model describes a genetic switch.

In this model only the production rate of mRNA molecules is affected by the state

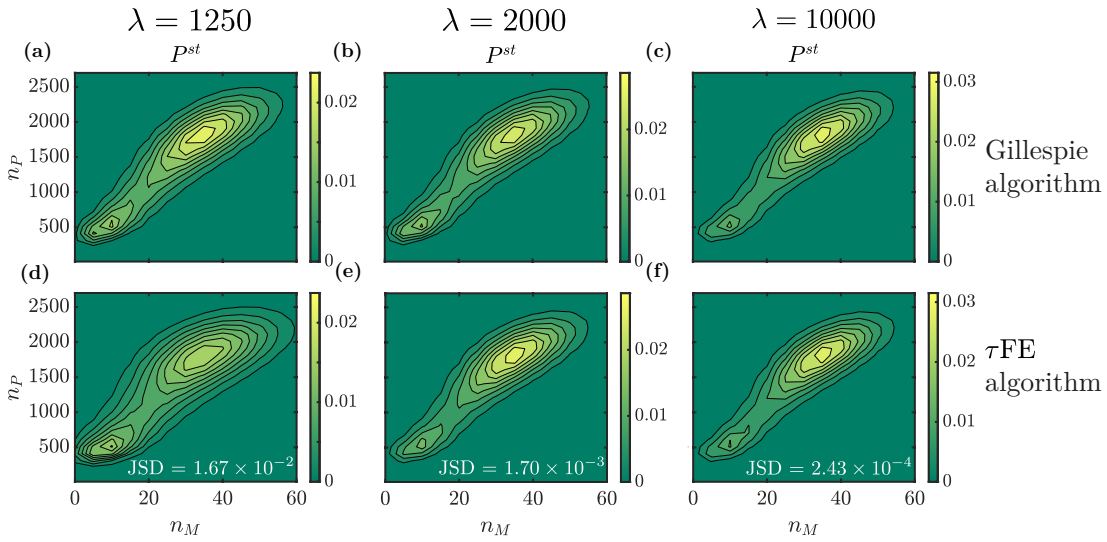

Figure 6.3: Stationary distribution for the numbers of mRNA and protein molecules (n_M and n_P, respectively) in the model of a genetic switch [Eq. 6.17]. Data is shown for different values of λ and for simulations of the full model by means of the Gillespie algorithm, and the τFE algorithm. Parameters: $N = 2, \Omega = 50, b_0 = b_1 = 1, b_2 = 20, d = 9.2, \beta = 50, \delta = 1, k_+ = 0.025, k_- = 1$. The stationary distribution is obtained from a long run up to time $t = 10^5$. For the τFE algorithm we use $\Delta t = 100/\lambda$. For each of the three values of λ we report the Jensen-Shannon divergence (JSD) between the distributions obtained from the two simulation methods.

of the environment. The average mRNA-production rate is found as

$$b^* = \frac{k_-^2 b_0 + k_- \tilde{k}_+ b_1 + \tilde{k}_+^2 b_2}{k_-^2 + k_- \tilde{k}_+ + \tilde{k}_+^2}, \tag{6.23}$$

with $\tilde{k}_+ = k_+ n_P/\Omega$. The second moment of the production rate takes the form

$$\begin{aligned}\sigma_{bb}^2 &\equiv \langle \bar{b}^2 \rangle - b^{*2} \\ &= \frac{\theta^2}{\lambda \Delta t}\Big\{(b_0 - b_1)^2 k_- \left(k_-^2 + \tilde{k}_+ k_- - \tilde{k}_+^2\right) \\ &\quad + (b_0 - b_2)^2 2 k_- \tilde{k}_+ \left(k_- + \tilde{k}_+\right) \\ &\quad + (b_1 - b_2)^2 \tilde{k}_+ \left(\tilde{k}_+^2 + \tilde{k}_+ k_- - k_-^2\right)\Big\},\end{aligned} \tag{6.24}$$

with

$$\theta^2 = \frac{2 k_- \tilde{k}_+}{\left(k_-^2 + k_- \tilde{k}_+ + \tilde{k}_+^2\right)^3}. \tag{6.25}$$

Details of the calculation leading to Eqs. (6.23) and (6.24) can be found in Appendix 6.10.

Figure 6.3 shows the stationary joint distribution of the number of mRNA and protein molecules for different values of the time-scale separation parameter λ. The figure shows data from Gillespie simulations of the full model [panels (a)–(c)], and data

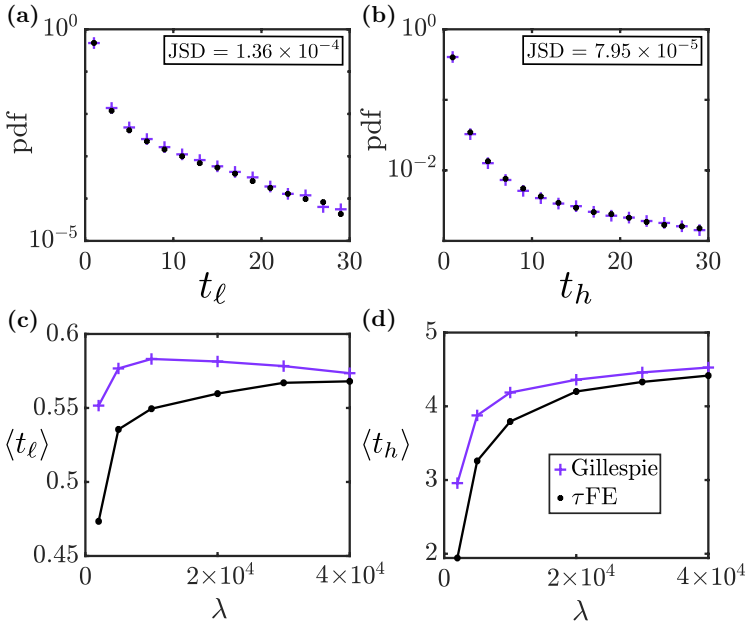

Figure 6.4: Sojourn times t_ℓ and t_h near the two modes of the bistable genetic switch (see also Fig. 6.3). Panels (a) and (b) show the distribution of the time spent in the vicinity of each mode (see text for details); data obtained from τFE algorithm is shown along with results from exact Gillespie simulations of the full model ($\lambda = 2000$). In each panel we report the Jensen–Shannon distance between the two distributions. Panels (c) and (d) show the mean sojourn times as a function of the time-scale parameter λ. The parameters are as in Fig. 6.3, the lower mode is $(n_M, n_P) = (10, 500)$, and the upper mode $(n_M, n_P) = (30, 1800)$. For the τFE algorithm we use a time step of $\Delta t = 100/\lambda$.

from the τFE algorithm [panels (d)–(f)]. The τFE algorithm captures the distribution profile with two local maxima. For low values of λ (i.e., a relatively slow environmental process) the distribution obtained from τFE tends to be wider than those from the Gillespie algorithm. The agreement improves for faster environments, as indicated again by the Jensen–Shannon distances in Fig. 6.3.

In Fig. 6.4, we show the distribution and means of the sojourn times t_ℓ and t_h near the lower and higher modes of the stationary distribution. More precisely this is the time between entering and leaving a designated region around each of the modes. The lower maximum of the stationary distribution is sharper than the upper maximum (Fig. 6.3). Accordingly, we have chosen a smaller region at the lower mode than at the upper mode. For the lower mode, we use the region $0 \leq n_M \leq 20$, $0 \leq n_P \leq 1100$ which encloses the mode at $(n_M, n_P) = (10, 500)$. For the higher mode we use the region $20 \leq n_M \leq 80$, $1100 \leq n_P \leq 2700$ enclosing the mode at $(n_M, n_P) = (30, 1800)$.

The data shown in the figure is constructed from one long sample path (run until $t = 10^6$), recording the points in time at which the system enters or leaves either

region. Gillespie simulations operate in continuous time and the τFE algorithm in discrete time. In order to remove any artefacts resulting from this difference, the same time resolution (0.05) is used in both algorithms for the measurement of arrival and departure times. Because the lower mode is sharper than the upper maximum and because the sizes of the two detection regions are different the sojourn time t_ℓ at the lower mode is found to be smaller than that at the higher mode, t_h.

The distributions of sojourn times in Figs. 6.4 (a) and (b) indicate that the τFE algorithm captures this dynamic quantity, provided the environmental process is sufficiently fast. This is confirmed in panels (c) and (d), where we show the mean sojourn times as a function of the relative speed λ of the environment compared to the population dynamics. As seen in both panels, the τFE algorithm generates accurate measurements of the mean sojourn times $\langle t_\ell \rangle$ and $\langle t_\mathrm{h} \rangle$ in the limit $\lambda \gg 1$.

At the same time, stochastic effects due to the random environmental process are captured for large but finite λ. This can be seen in Fig. 6.4 (d): the mean sojourn time $\langle t_\mathrm{h} \rangle$ drops significantly as the environmental process becomes slower, and hence additional noise is injected into the population (there is no environmental noise in the adiabatic limit). While there are quantitative differences compared to exact simulations, the τFE algorithm captures this reduction of $\langle t_h \rangle$. Panel (c) reveals that there are also limitations to the precision of the τFE algorithm. The mean sojourn time $\langle t_\ell \rangle$ near the lower mode is affected much less by a reduction of the time-scale separation parameter λ than the mean sojourn time at the upper mode. This indicates that the escape from this region is driven mostly by intrinsic noise rather than by environmental stochasticity. While the data from the two algorithms remains within approximately 10% for sufficiently fast environmental dynamics ($\lambda \gtrsim 10^4$) the τFE algorithm is unable to capture the small rise of $\langle t_\ell \rangle$ observed in Gillespie simulations for intermediate values of λ.

In Table 6.1 we compare the the computing time required for both the Gillespie algorithm and the τFE method for different values of λ. The data in the table is the CPU time required to generate one sample path up to time $t = 10^3$, averaged over ten runs. The model parameters are as in Figs. 6.3 and 6.4.

The full model comprises the reactions in the population and the environmental switching. The rates for the former reactions are independent of λ, the rates for the

latter scale linearly in λ. Accordingly, one expects the computing time for Gillespie simulations of the full model to be linear in λ, with a non-zero intercept. The data in the table is consistent with this. We note that Gillespie algorithm does not require any time discretisation.

The running time for the τFE algorithm depends on the choice of the time step. The time step in turn affects the accuracy of the outcome. If Δt is large, then τFE simulations are fast, but the approximation to the continuous-time full model becomes less good. On the other hand the time step must not be too small, as the construction of the algorithm requires sufficient averaging of the environmental process in each step [Eqs. (6.11)–(6.13)]. The time step for the τFE algorithm in Figs. 6.3 and 6.4, and in Table 6.1 is chosen inversely proportional to λ. This is to ensure that each time step captures a sufficient number of switches of the environmental state. Accordingly, we expect the computing time for the τFE algorithm to scale linearly in λ, with no intercept. Again, the running times we measured in our simulations are consistent with this expectation. Overall, Table 6.1 shows that the τFE algorithm is able to generate data of the accuracy as in Figs. 6.3 and 6.4 while reducing the computing effort approximately ten fold compared to full Gillespie simulations.

λ	Gillespie	τFE
1250	1.35	0.04
2500	1.89	0.08
5000	2.62	0.17
10000	4.30	0.31
20000	7.77	0.57

Table 6.1: Mean computation time (in seconds) required to simulate one sample path up to $t = 10^3$ of the bimodal genetic-switch system defined in Eq. (6.22). Measurements are from ten independent sample runs, using Gillespie simulations of the full model, and the τFE algorithm respectively. Parameters are as in Fig. 6.3. For the τFE algorithm we set $\Delta t = 100/\lambda$. The values of λ used here are in the range of fast switching environments in which there is a good agreement between both algorithms. The data shown in this table shows how faster the τFE algorithm can be in comparison to the Gillespie algorithm.

6.4 Numerical simulation of continuous-environmental systems

6.4.1 Setup

We turn now to systems which are subject to an environment with continuous states. Specifically, we follow [20] and assume that the environmental state σ follows an Ornstein–Uhlenbeck process (see also [22, 47]),

$$\frac{\mathrm{d}\sigma}{\mathrm{d}t} = \lambda(m-\sigma) + \sqrt{2\lambda v^2}\,\eta(t), \tag{6.26}$$

where $\eta(t)$ is Gaussian white noise of unit amplitude, in particular $\langle \eta(t)\eta(t')\rangle = \delta(t-t')$. The parameter m is the average value of σ in the long run, whilst v controls the magnitude of noise. As before, the parameter $\lambda > 0$ indicates how quickly the environment changes relative to the dynamics in the population; λ is the equivalent of $1/\tau_c$ in the notation of [20].

The probability distribution of finding the environment in state σ at time t, given that was in state σ' at time t', can be obtained from the Fokker–Planck equation for the Ornstein–Uhlenbeck process, and is given by (see e.g. [48, 49])

$$q_{\sigma'\to\sigma}(t-t') = \sqrt{\frac{1}{2\pi v^2(1-e^{-2\lambda(t-t')})}}\exp\left[-\frac{\left(\sigma-\sigma' e^{-\lambda(t-t')} - m\left(1-e^{-\lambda(t-t')}\right)\right)^2}{2v^2\left(1-e^{-2\lambda(t-t')}\right)}\right]. \tag{6.27}$$

For $t\to\infty$ (and t' fixed) this quantity tends to the stationary distribution

$$\rho^*_\sigma = \sqrt{\frac{1}{2\pi v^2}}\exp\left[-\frac{(\sigma-m)^2}{2v^2}\right]. \tag{6.28}$$

We note that it is not a requirement for the τFE algorithm that the environment follows an Ornstein–Uhlenbeck process. However, both functions $q_{\sigma'\to\sigma}(t-t')$ and ρ^*_σ are required, as discussed in more detail below.

We proceed to describe how the τFE algorithm can be implemented for models with continuous environments (Sec. 6.4.2).

In the case of discrete environments, continuous-time sample paths of the full model can be generated using the conventional Gillespie algorithm. This is an exact procedure: the ensemble of these sample paths faithfully describes the statistics of the full model.

In Sec. 6.3 we have used this as a benchmark to test the τFE algorithm and choose the time discretisation Δt. We are not aware of any analogous exact simulation method for models of discrete populations in a stochastic environment with continuous states. In order to test the τFE algorithm we therefore compare outcomes against those from approximation methods to generate paths of the combined set of the population and the environment. Several such methods exist, we describe these in Sec. 6.4.3. The tests of the τFE algorithm against the baseline of these methods are described in Sec. 6.5. We stress that since the schemes employed for continuous environments are approximations, using them as benchmark to choose Δt requires careful attention depending on the system under study. We explore below this in more detail.

6.4.2 Implementation of the τFE algorithm for continuous environments

We proceed similar to discrete case in Sec. 6.2, replacing the sums over σ in Eqs. (6.2) and (6.10) with integrals. We then have

$$R_r^*(\mathbf{n}) = \int_{-\infty}^{\infty} \mathrm{d}\sigma \rho_\sigma^* R_{r,\sigma}(\mathbf{n}), \tag{6.29}$$

and the relation for the second moments turns into

$$\begin{aligned}\left\langle \overline{R}_r(\mathbf{n})\overline{R}_s(\mathbf{n})\right\rangle &= \frac{1}{\Delta t^2}\int_{-\infty}^{\infty}\mathrm{d}\sigma\int_{-\infty}^{\infty}\mathrm{d}\sigma'\int_t^{t+\Delta t}\mathrm{d}t_1\int_{t_1}^{t+\Delta t}\mathrm{d}t_2 \\ &\times\left\{\rho_\sigma^* q_{\sigma\to\sigma'}(t_2-t_1)\Big[R_{r,\sigma}(\mathbf{n})R_{s,\sigma'}(\mathbf{n}) + R_{r,\sigma'}(\mathbf{n})R_{s,\sigma}(\mathbf{n})\Big]\right\}.\end{aligned} \tag{6.30}$$

Depending on the form of the stationary distribution ρ_σ^*, the kernel $q_{\sigma\to\sigma'}(t_2-t_1)$ and the rates $R_{r,\sigma}(\mathbf{n})$ the integrals in Eqs. (6.29) and (6.30) can be carried out, and closed-form analytical expressions can be obtained. In Sec. 6.5 we explore a number of different examples, further scenarios are also discussed Appendix 6.12. Once the average rates and the second moments are calculated, the τFE algorithm is implemented as described in Sec. 6.2.3.

6.4.3 Conventional simulation approaches for discrete populations in continuous environments

In this section we summarise 'conventional' approaches to simulating discrete Markovian systems subject to environmental dynamics with continuous states. By 'conventional' we

mean methods which produce explicit (approximate) sample paths of the environmental process. This is in contrast to the τFE algorithm, which generates paths only of the system proper.

Gillespie algorithm with discretised environmental states (GADE)

This approach is based on a discretisation of the space of environmental states, time remains continuous. Once such a discretisation for the environmental states is carried out, the combined states of the population and environment are also discrete. Simulations can be carried out using the conventional Gillespie method. We will refer to this method as GADE (Gillespie approach with discretised environment).

The key step in this approach is to find an appropriate dynamics in the space of discretised environmental states. We describe this in the context of the Ornstein–Uhlenbeck process in Eq. (6.26). We discretise the environmental state into integer multiples of $\Delta\sigma$, i.e., the environment takes states $\ldots, -2\Delta\sigma, -\Delta\sigma, 0, \Delta\sigma, 2\Delta\sigma, \ldots$. Transitions from one state $k\Delta\sigma$ can only occur to states $(k \pm 1)\Delta\sigma$. The transition rates are constructed such that this discrete process recovers the continuous Ornstein–Uhlenbeck dynamics in the limit $\Delta\sigma \to 0$. The details of the construction are described in Appendix 6.11, we here only report the main outcome. Specifically, the rates to transition from state $k\Delta\sigma$ to $(k \pm 1)\Delta\sigma$ can be chosen as

$$T_k^{\pm} = \frac{\lambda}{2\Delta\sigma}\left[\pm(m - k\Delta\sigma) + \frac{2v^2}{\Delta\sigma}\right]. \tag{6.31}$$

This process can then be simulated using the standard Gillespie algorithm, along with the events in the population. We note that the rates $T_k^{\pm}$ need to be non-negative, i.e., we require $|m - k\Delta\sigma| < 2v^2/\Delta\sigma$, for all k. In practice, this can be achieved by truncating the set of possible states $k\Delta\sigma$. More precisely, we disallow transitions out of the region $\{k : |m - k\Delta\sigma| \leq K\}$, with a given cutoff K. Provided that K is sufficiently large truncations will only be required rarely. Once a cutoff K is chosen we must require $\Delta\sigma \leq 2v^2/K$ to guarantee non-negativity of the $T_k^{\pm}$. The variance of the Ornstein–Uhlenbeck process for σ is given by v^2 in the long run [Eq. (6.28)], so $K \propto v$ is a sensible choice. This results in maximum value for $\Delta\sigma$ which is also proportional to v.

Discrete-time simulation with explicit environmental dynamics (DEED)

Approximate sample paths of the combined system of population and environment can also be generated in a discrete-time simulation. We refer to this as DEED (discrete-time simulation with explicit environmental dynamics). The time step Δt needs to be sufficiently small to capture the details of the environmental process with characteristic time scale $\tau_c = \lambda^{-1}$. We therefore require $\Delta t \lesssim \lambda^{-1}$. One possible implementation is as follows:

1. Suppose we have arrived at time t, and the state of the population is $\mathbf{n}(t)$ and that of the environment $\sigma(t)$. Obtain $\sigma(t + \Delta t)$ from Eq. (6.26) using the Euler-Maruyama method [50].

2. Use $\sigma(t)$ and $\mathbf{n}(t)$ to calculate the rates $p_r(t) = \Delta t \times R_{r,\sigma(t)}[\mathbf{n}(t)]$ for $r = 1, \ldots, R$.

3. Provided Δt is small enough, the $p_r(t)$ are all less than one. To lowest order in Δt they are the probabilities that a reaction of type r occurs in the next Δt. For each $r = 1, \ldots, R$ implement one reaction of this type with probability $p_r(t)$. With probability $1 - p_r(t)$ no reaction of type r occurs. Executing all reactions that fire, one obtains $\mathbf{n}(t + \Delta t)$.

4. Increment time by Δt, and go to step 1.

Step 3 disregards the possibility that a particular reaction fires multiple times during one time step. This is a valid approximation, provided that the $p_r(t) = \Delta t \times R_{r,\sigma(t)}$ are much smaller than one. As an alternative step 3 could be replaced by a conventional τ-leaping step. The number of reactions of type r that fire is then a Poissonian random variable with parameter $p_r(t)$.

Thinning algorithm by Lewis

A population subject to a dynamic external environment with continuous state space can also be simulated using the so-called thinning algorithm by Lewis [51]. This algorithm generates a statistically faithful ensemble of sample paths for Markovian systems with discrete states and transition rates with explicit external time dependence.

In the context of our model the population is such a system. If the environmental dynamics is independent of the population then realisations $\sigma(t)$ for the environment

can be generated in advance independently from the population. For instance, sample solutions of the Ornstein-Uhlenbeck process in Eq. (6.26) could be generated. Each such realisation $\sigma(t)$ then determines a realisation of time-dependent rates $R_r(\mathbf{n}, t) \equiv R_{r,\sigma(t)}(\mathbf{n})$ for the population. The Lewis algorithm can then be used to produce sample paths for the population dynamics.

In practice, numerical approximation schemes are required to generate realisations for the environment. For example, Eq. (6.26) can be solved numerically using the Euler–Maruyama method, with time step Δt. As discussed above this time step needs to be sufficiently small ($\Delta t \lesssim \lambda^{-1}$) to resolve the short-time features of the environmental process. The Lewis algorithm then uses this as an input and generates sample paths for the population in continuous time.

6.5 Application of the τFE to continuous-environmental models

In this section we test the τFE algorithm on a number of different examples of models with continuous environmental states. Simulation outcomes are compared against those from the algorithms described in Sec. 6.4.3.

6.5.1 Toy model: Population dynamics with production and removal rates proportional to σ^2

We first consider a production-removal process for a single species. The environmental state $\sigma(t)$ follows the Ornstein–Uhlenbeck process in Eq. (6.26). The corresponding transition kernel $q_{\sigma\to\sigma'}(\tau)$ is given in Eq. (6.27), and the stationary distribution ρ^*_σ in Eq. (6.28). The production rate in the population is assumed to be $R_{b,\sigma} = \beta\sigma^2$, and the removal rate $R_{d,\sigma} = \delta\sigma^2$. These are not chosen with any particular natural system in mind, instead this example serves as an illustration (see also Appendix 6.12 for similar calculations for two related examples).

From (6.29) we obtain

$$\begin{aligned} R^*_b &= \beta(m^2 + v^2), \\ R^*_d &= \delta(m^2 + v^2). \end{aligned} \tag{6.32}$$

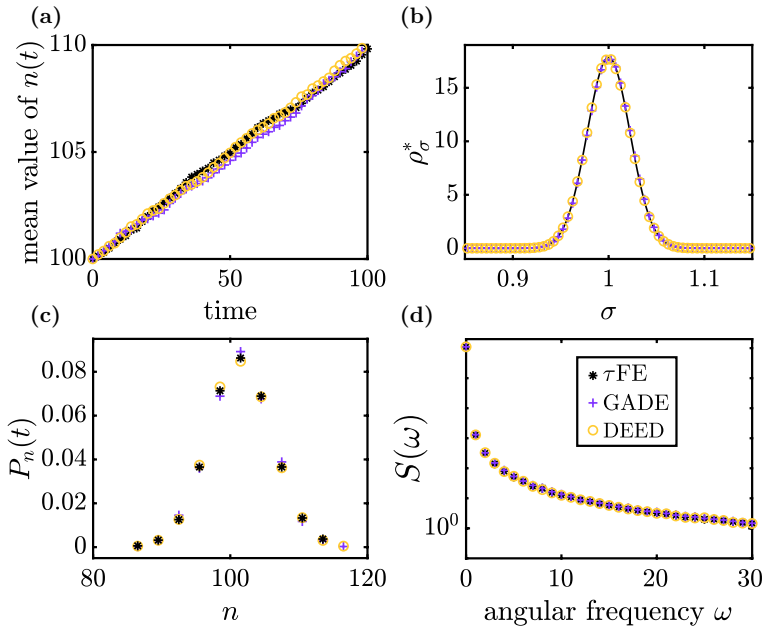

Figure 6.5: Simulation results for a production-removal process with rates $b = \beta\sigma^2$ and $d = \delta\sigma^2$ (Sec. 6.5.1), for the different algorithms described in Sec. 6.4. Parameters used: $\beta = 1.1$ and $\delta = 1.0$, $m = 1$, $\lambda = 10^3$, and $v^2 = 5 \times 10^{-4}$. Panel (a): mean value of the number of individuals as function of time, obtained from 10^3 runs. Panel (b): stationary distribution of the environmental state, ρ^*_σ, for the GADE method and the DEED approach (the τFE algorithm does not simulate the environment). The solid line in panel (b) is the analytical solution from Eq. (6.28). Panel (c): distribution of the number of particles n in the population at time $t = 10$. Panel (d): spectral density [Eq. (6.21)] obtained from 10^3 runs. We use $\Delta\sigma = 10^{-3}$ for the GADE simulations, and $\Delta t = 1/(100\lambda) = 10^{-5}$ for DEED. For the τFE algorithm, we set $\Delta t = 10/\lambda = 10^{-2}$.

The second moments of the rates $\overline{R}_b(n)$ and $\overline{R}_d(n)$ can be calculated from Eq. (6.30). We find

$$\left\langle \overline{R}_b(n)\overline{R}_d(n) \right\rangle - R^*_b(n)R^*_d(n) = \\ \frac{\beta\delta v^2 e^{-2\lambda\Delta t}}{\lambda^2\Delta t^2}\left[8m^2 e^{\lambda\Delta t} + e^{2\lambda\Delta t}\left(8m^2(\lambda\Delta t - 1) + v^2(2\lambda\Delta t - 1)\right) + v^2\right]. \tag{6.33}$$

for the covariance. The expressions for the variances are similar, with suitable replacements $\beta\delta \to \beta^2$ and $\beta\delta \to \delta^2$ in the prefactor in Eq. (6.33). This covariance matrix and the means in Eq. (6.32) are then used in the τFE algorithm.

Figure 6.5 shows simulation results from the τFE algorithm, as well as from the GADE and DEED schemes (Secs. 6.4.3 and 6.4.3 respectively). Panel (a) shows that all simulation methods result in linear growth (parameters are such that $\beta > \delta$, i.e., the growth rate is always larger than the death rate). Panel (b) confirms that GADE and DEED both generate the correct statistics for the stationary distribution of the environmental process [the solid line is the Gaussian distribution in Eq. (6.28)]. In

panel (c) we focus on a fixed time $t = 10$, and show that all three simulation methods results in very similar distributions for the number of individuals in the population n at that time. Panel (d) finally shows a dynamic quantity, the Fourier spectrum $S(\omega)$ of the time series $n(t)$, or equivalently the Fourier transform of the correlation function of n. Again, all three simulation methods produce very similar results.

In Table 6.2 we compare the average computing time required by the different algorithms to generate a trajectory up to time $t = 10^3$. We show data for varying values of the typical time scale λ^{-1} of the environmental process. GADE does not require any discretisation of time. For the DEED approach we use $\Delta t = 1/(100\lambda)$. For the τFE method we choose $\Delta t = 10/\lambda$. This is in-line with the requirements $\Delta t \lesssim \lambda^{-1}$ for DEED, and $\Delta t \gtrsim \lambda^{-1}$ for τFE. The choice of time steps will be discussed in further detail below.

The data in the table indicates that the simulation time scales approximately linearly with λ for all three algorithms tested, provided λ is sufficiently large. This is to be expected: The rates for the environmental events in the GADE simulations (Sec. 6.4.3) scale as λ, and therefore dominate the events in the population for $\lambda \gg 1$. Each typical Gillespie step then advances time by an amount proportional to λ^{-1}, and $\mathcal{O}(\lambda)$ such steps are required to reach the designated end time. A similar argument applies to the DEED algorithm (Sec. 6.4.3) and for the τFE algorithm: For both of these we use time steps $\Delta t \propto \lambda^{-1}$, so again the number of iteration steps required scales as λ.

The key message from Table 6.2 is that, for the choice of time steps made in the

λ^{-1}	GADE	DEED	τFE
1×10^{-2}	28.47	3.84	0.79 $\times 10^{-2}$
5×10^{-3}	53.20	7.88	0.16 $\times 10^{-1}$
1×10^{-3}	288.30	40.91	0.08
5×10^{-4}	576.69	82.78	0.15
1×10^{-4}	3022.47	397.63	0.79

Table 6.2: Mean computing time (in seconds) required for one simulation run of the model described in Sec. 6.5.1 until $t = 10^3$. Data is from ten independent runs, parameters are as in Figure 6.5, i.e., $\beta = 1.1, \delta = 1.0, m = 1$, and $v^2 = 5 \times 10^{-4}$. For GADE we set $\Delta\sigma = 10^{-3}$; for the DEED approach we set $\lambda\Delta t = 1/100$; for the τFE algorithm we set $\lambda\Delta t = 10$. The values of λ used here are in the range of fast switching environments in which there is a good agreement between all the algorithms. The data shown in this table shows how faster the τFE algorithm can be in comparison to the others schemes.

table, the computing time required by the τFE algorithm is substantially lower than that for the other two simulation methods. Given the linear dependence on λ, this increase in efficiency can be extrapolated to environments operating on time scales faster than the smallest time scale shown in the table (i.e., to the range $\lambda > 10^4$). We note that, due to the smaller time step, DEED produces a finer resolution of sample paths in time than τFE. When we make our comparison we have average macroscopic quantities in mind (such as those in Fig. 6.5), and not necessarily the generation of individual paths with the highest possible resolution in time.

We now briefly discuss the choice of time steps for the τFE method and for DEED. In principle, we could have increased or decreased the step for either method. This would then reduce or increase the computing time required to reach the designated end point. It might also affect the accuracy of the outcome. Our choice of $\Delta t = 10/\lambda$ for τFE is motivated by the good agreement with GADE in Fig. 6.5, noting that GADE does not require any discretisation of time. Similarly, for the example discussed below in Sec. 6.5.2 good agreement with analytical predictions is found for this choice, see the regime of small λ^{-1} in Fig. 6.6. Our conclusion is therefore that the τFE algorithm is able to produce results of the accuracy as in Fig. 6.5 with computing times as reported in Table 6.2.

The DEED algorithm requires $\Delta t \lesssim \lambda^{-1}$ to be able to resolve the environmental dynamics. Our choice $\Delta t = 1/(100\lambda)$ in Table 6.2 is well below this requirement, and the algorithm can in principle be speed up by choosing a larger time step. If we were to exhaust the limit and used $\Delta t = \lambda^{-1}$ for DEED then this would reduce the computing time by about a factor of one hundred in Table 6.2. For for $\lambda^{-1} = 10^{-3}$ this would mean a reduction from approximately 40 seconds to 0.4 seconds per sample path. Using this larger time step also results in noticeable deviations in measurements of the quantities in Fig. 6.5 from continuous-time GADE simulations. But even if we accept this and use the hundred fold larger time step for DEED the τFE algorithm would remain approximately five times faster, requiring 0.08 seconds per sample path at $\lambda^{-1} = 10^{-3}$, see Table 6.2.

We have also conducted tests with Lewis' thinning algorithm. To do this we have first generated sample paths of the Ornstein–Uhlenbeck process for the environment [Eq. (6.26)] using an Euler–Maruyama scheme. This is then fed into the Lewis'

algorithm for systems with time dependent rates. Given that the typical time scale of the environment is λ^{-1}, the largest sensible time step for the Euler–Maruyama scheme is $\Delta t = \lambda^{-1}$, similar to DEED. This choice minimises the computing time for the Lewis' approach. We therefore use this time step to compare the efficiency of the Lewis' approach with that of τFE. We find that the thinning algorithm is considerably slower than the τFE approach. For $\lambda^{-1} = 10^{-3}$, for example, we obtain a simulation time of approximately 13 seconds per run up to $t = 10^3$ compared to 0.08 seconds for τFE (see Table 6.2).

6.5.2 Genetic switch with Hill-like regulatory function

As a final example we consider a model of protein production subject to a continuous environment discussed in [20]. The model entails positive feedback, in that the presence of protein has the potential to increase production of protein. There is one single species in the model (protein), we write the number of protein molecules as n. We also define $x = n/\Omega$, where Ω is again a model parameter setting the typical size of the system. The production rate of protein is given by

$$f(x, \sigma) = \alpha_0 + (1 - \alpha_0 + \sigma)\Theta(x - x_0), \tag{6.34}$$

where $0 < \alpha_0 < 1$ and $x_0 > 0$ are constants, and where $\Theta(x)$ is the Heaviside function. Protein molecules also decay with unit rate. In the absence of environmental influence ($\sigma \equiv 0$), the production rate is thus unity when $x > x_0$, and $\alpha_0 < 1$ when $x < x_0$. For $\sigma \equiv 0$ the mean re-scaled number of protein follows the rate equation

$$\dot{\bar{x}} = f(\bar{x}) - \bar{x}, \tag{6.35}$$

where time is measured in units of generations. We choose $\alpha_0 < x_0 < 1$. Eq. (6.35) has three fixed points $x_1^* < x_2^* < x_3^*$, where $x_1^* = \alpha_0$ and $x_3^* = 1$ are attractors, and $x_2^* = x_0$ is a repeller. Similar to [20], we refer to x_1^* and x_3^* as the 'low' and 'high' states, respectively.

The environmental process $\sigma(t)$ modulates the production rate when $x > x_0$. As in [20] we asssume that σ follows an Ornstein-Uhlenbeck process of the form given in Eq. (6.26). The noisy system has the potential to switch between the 'high' and 'low' states. To test the performance of the τFE algorithm, we focus on the mean switching

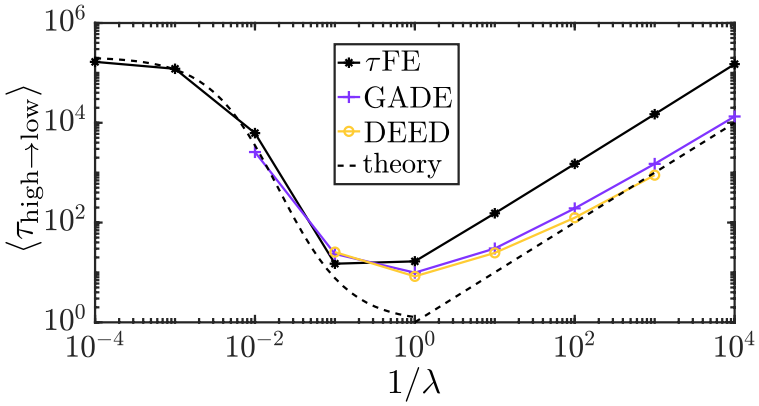

Figure 6.6: Mean switching time (MST) from the high to the low state in the model described in Sec. 6.5.2. For the τFE algorithm we used $\Delta t = 10/\lambda$, for GADE $\Delta\sigma = 0.01$, and for DEED $\Delta t = 10^{-4}$. Theory curves are from Eqs. (8) and (10) in [20]. Model parameters are as in the top right panel of Fig. 2 in [20] ($\Omega = 5000, v = 0.1, \alpha_0 = 0.01, x_0 = 0.93$).

time (MST) to transit from the high state to the low state. This time is studied and calculated in [20], we denote it by $\langle \tau_{\text{high}\to\text{low}} \rangle$. In simulations we start the system in the high state, and measure the first time the system reaches the low state.

Only the production of protein is affected by the state σ of the environment, we write $R_{\text{prod},\sigma}(\mathbf{n}) = f(x, \sigma)$, with f as in Eq. (6.34). Inserting this in Eqs. (6.29) and (6.30), and after straightforward calculations, we obtain

$$R^*_{\text{prod}}(n) = \alpha_0 + (1 - \alpha_0)\Theta(n/\Omega - x_0), \tag{6.36}$$

and the second moment

$$\left\langle (\overline{R}_{\text{prod}}(n))^2 \right\rangle - [R^*_{\text{prod}}(n)]^2 = \frac{2v^2}{\lambda^2 \Delta t^2} \left[\lambda \Delta t + (e^{-\lambda \Delta t} - 1)\right] \Theta(n/\Omega - x_0). \tag{6.37}$$

In Fig. 6.6 we show the MST measured in simulations using the different approaches described in in Sec. 6.4. Assaf et al. [20] report non-monotonous behaviour of the MST as a function of $\tau_c = \lambda^{-1}$. As seen in Fig. 6.6 the τFE algorithm reproduces this behaviour. For fast environmental dynamics (low λ^{-1}) the MST obtained from the τFE algorithm is in good agreement with measurements obtained from the other simulation methods, and with the analytical approximations from [20]. The agreement extends over several decades of values of $\tau_c = \lambda^{-1}$.

At the same time we observe that the τFE algorithm requires significantly less computing time than the GADE or DEED approaches. For $\lambda^{-1} = 10^{-1}$ for example, we measured an average computing time of 2×10^{-3} seconds to generate one run of

the system up to time 10^3 with the τFE algorithm ($\Delta t = 10/\lambda$). GADE required 0.674 seconds, and DEED 4.2 seconds (for a time step $\Delta t = 10^{-4}$).

We note that we have implemented DEED as described in Sec. 6.4.3. In particular at most one reaction of each type can fire in each time step (step 3 of the algorithm). This requires a sufficiently small time step Δt to ensure $p_r(t) < 1$ for all r. This is achieved by our choice $\Delta t = 10^{-4}$. Alternatively step 3 of the DEED algorithm could be replaced by a (conventional) τ-leaping step. Larger choices of the time step Δt are then possible, up to the limit of $\Delta t \approx \lambda^{-1}$ to ensure that the environmental dynamics are captured appropriately. Focusing on $\lambda^{-1} = 10^{-1}$ we expect that increasing the time step by a factor of a thousand (from 10^{-4} to 10^{-1}) would reduce the simulation time by at most a factor of a thousand for a τ-leaping version of DEED. This would result in a computing time of approximately 4×10^{-3} for one simulation run up to $t = 10^3$ instead of the 4.2 seconds reported for DEED in the previous paragraph. This is comparable with the CPU time required by the τFE algorithm (2×10^{-3} seconds), but would resolve environmental fluctuations with lower accuracy. For example one observes systematic deviations for the stationary distribution of the environment in Fig. 6.5(b).

6.6 Discussion and conclusions

In summary, we have presented τFE, a variant of the τ-leaping stochastic simulation algorithm for systems subject to fast environmental dynamics. Just like conventional τ-leaping the algorithm operates in discrete time. The rates of the reactions in the system proper are treated as constant during each time step, and the numbers of different reactions firing in one step have Poissonian statistics.

The key difference compared to conventional τ-leaping is the external environment. In the full continuous-time model reaction rates which depend on the environmental state fluctuate in time even when the state of the population does not change. An adiabatic approximation would consist of assuming an infinitely fast environment and of replacing the reaction rates by their means with respect to the stationary distribution of the environmental process. This is justified if the relaxation time scale of the environmental process is infinitely shorter than the time step of the simulation.

The τFE algorithm goes beyond this approximation, and is based on time averages of reaction rates over the *finite* time step. For finite speeds of the environment these average rates are random variables. If the environmental dynamics is fast we can make a Gaussian approximation. The rates feeding into the τ-leaping step are clipped Gaussian random numbers designed to retain the first and second moments of the actual environmental dynamics. It is important to note that this not the same as drawing an environmental state σ from the stationary distribution ρ^*_σ, and then using the rates $R_{r,\sigma}(\mathbf{n})$ for the next τ-leaping step. Instead, the covariance matrix of the rates $\overline{R}_r(\mathbf{n})$ in Eq. (6.8) is calculated as described in Eqs. (6.10) for discrete environments, and in Eq. (6.30) for continuous environmental states.

The choice of time step for the τFE algorithm requires careful consideration. On the one hand the time step must be long enough to justify the averaging procedure over the environmental dynamics and the Gaussian assumption for the reaction rates in the τ-leaping step. Broadly speaking $\lambda\Delta t$ must be sufficiently large ($\lambda\Delta t \gg 1$). At the same time the so-called leap condition for the τ-leaping part of the algorithm must be fulfilled [37]. This means that the state of the system must not change significantly in each iteration step, as a constant state $\mathbf{n}$ of the population is an assumption made in setting up the τ-leaping. Mathematically, this means that the change of the number of particles in the system in a time step must be much smaller than the typical number of particles in the system. Assuming that the stoichiometric coefficients do not scale with the system size Ω this means that $\Delta t \times R_{r,\sigma}(\mathbf{n})$ must be much smaller than Ω. Noting that $R_{r,\sigma}(\mathbf{n})$ is of order Ω in many applications we thus require that Δt is much smaller than one. For $\lambda \gg 1$ and Δt proportional to λ^{-1} this condition is often relatively easy to meet in practice.

We have tested the τFE algorithm on a number of systems with discrete and continuous environments. This includes examples of systems which can be addressed analytically and models motivated by applications in biology. Our tests focus on stationary distributions, but also dynamic features such as Fourier spectra of fluctuations or first-passage time distributions. In all cases we have tested the τFE method produces good agreement with results from conventional simulation methods in the regime of fast environmental dynamics. This is the regime for which τFE is designed. Naturally, quantitative deviations are found when the time scales of the environmental dynamics

and system proper are insufficiently separated.

We stress that τFE goes beyond simulations in the adiabatic limit, and is able to capture the dependence of macroscopic observables on the time scale separation, provided this dependence is sufficiently strong [see e.g. Figs. 6.4(d) and 6.6)]. At the same time our analysis also reveals limitations of the algorithm. If the dependence of observables on the time scale separation is weak such as in Fig. 6.4(c), then τFE may not be able to fully resolve these dependencies. When the environment is fast the quantitative agreement with simulations of the full system is however still within approximately 10% in the example in Fig. 6.4(c).

The computing time required for the τFE algorithm to generate sample paths up to a designated end time is proportional to the inverse time step. The time step on the other hand is typically a multiple of the characteristic time scale λ^{-1} of the environmental dynamics. This means that the computational effort scales approximately linearly in the time scale separation λ. In all cases we have tested we found that τFE is considerably more efficient for the measurement of macroscopic quantities than alternative simulation algorithms.

In summary, we think the τFE algorithm has passed the initial selection of tests presented in this paper. It provides an promising approach to probing the regime of fast environmental dynamics, and captures effects induced by extrinsic noise beyond the adiabatic limit. The algorithm is particularly valuable for systems in which the regime of intermediate time scale separation can be accessed with conventional simulation methods. The accuracy of the τFE algorithm can then be assessed in this regime (an example can be found in Fig. 6.6). If the comparison is favourable, then it is justified to use τFE in the regime of increasing time scale separation.

Acknowledgements

We would like to thank Yen Ting Lin (Los Alamos) for useful discussions and feedback on earlier versions of the manuscript. EBC acknowledges a President's Doctoral Scholarship (The University of Manchester). TG acknowledges funding from the Spanish Ministry of Science, Innovation and Universities, the Agency AEI and FEDER (EU) under the grant PACSS (RTI2018-093732-B-C22), and the Maria de Maeztu

program for Units of Excellence in R&D (MDM-2017-0711).

6.7 Appendix A: Second moments of rates

In this Appendix we calculate the second moments of the quantities $\overline{R}_r(\mathbf{n})$ ($r = 1, \ldots, R$) defined in Eq. (6.8). Without loss of generality we assume that the time interval in question starts at $t = 0$, the end point is then Δt. Assuming the space of environmental states is discrete, we have

$$\begin{aligned}
\left\langle \overline{R}_r(\mathbf{n})\overline{R}_s(\mathbf{n})\right\rangle &= \frac{1}{\Delta t^2}\int_0^{\Delta t} \mathrm{d}t_1 \int_0^{\Delta t} \mathrm{d}t_2 \left\langle R_{r,\sigma(t_1)}(\mathbf{n}) R_{s,\sigma(t_2)}(\mathbf{n})\right\rangle \\
&= \frac{1}{\Delta t^2}\int_0^{\Delta t} \mathrm{d}t_1 \int_{t_1}^{\Delta t} \mathrm{d}t_2 \left\langle R_{r,\sigma(t_1)}(\mathbf{n}) R_{s,\sigma(t_2)}(\mathbf{n})\right\rangle \\
&+ \frac{1}{\Delta t^2}\int_0^{\Delta t} \mathrm{d}t_2 \int_{t_2}^{\Delta t} \mathrm{d}t_1 \left\langle R_{r,\sigma(t_1)}(\mathbf{n}) R_{s,\sigma(t_2)}(\mathbf{n})\right\rangle \\
&= \frac{1}{\Delta t^2}\sum_{\sigma\sigma'}\int_0^{\Delta t} \mathrm{d}t_1 \int_{t_1}^{\Delta t} \mathrm{d}t_2 \; \rho^*_\sigma q_{\sigma\to\sigma'}(t_2 - t_1) R_{r,\sigma}(\mathbf{n}) R_{s,\sigma'}(\mathbf{n}) \\
&+ \frac{1}{\Delta t^2}\sum_{\sigma\sigma'}\int_0^{\Delta t} \mathrm{d}t_2 \int_{t_2}^{\Delta t} \mathrm{d}t_1 \; \rho^*_{\sigma'} q_{\sigma'\to\sigma}(t_1 - t_2) R_{r,\sigma}(\mathbf{n}) R_{s,\sigma'}(\mathbf{n}) \\
&= \frac{1}{\Delta t^2}\sum_{\sigma\sigma'}\int_0^{\Delta t} \mathrm{d}t_1 \int_{t_1}^{\Delta t} \mathrm{d}t_2 \; \rho^*_\sigma q_{\sigma\to\sigma'}(t_2 - t_1) R_{r,\sigma}(\mathbf{n}) R_{s,\sigma'}(\mathbf{n}) \\
&+ \frac{1}{\Delta t^2}\sum_{\sigma\sigma'}\int_0^{\Delta t} \mathrm{d}t_1 \int_{t_1}^{\Delta t} \mathrm{d}t_2 \; \rho^*_\sigma q_{\sigma\to\sigma'}(t_2 - t_1) R_{r,\sigma'}(\mathbf{n}) R_{s,\sigma}(\mathbf{n}).
\end{aligned} \tag{6.38}$$

In the first step we have applied the definition of the over-bar average [Eq. (6.8)]. In the third step we have carried out the average over realisations of the environmental process. In the last step we have renamed $t_1 \leftrightarrow t_2$ and $\sigma \leftrightarrow \sigma'$ in the second term. Therefore

$$\begin{aligned}
\left\langle \overline{R}_r(\mathbf{n})\overline{R}_s(\mathbf{n})\right\rangle &= \frac{1}{\Delta t^2}\sum_{\sigma\sigma'}\int_0^{\Delta t} \mathrm{d}t_1 \int_{t_1}^{\Delta t} \mathrm{d}t_2 \; \rho^*_\sigma q_{\sigma\to\sigma'}(t_2 - t_1) \\
&\quad \times \Big[R_{r,\sigma}(\mathbf{n}) R_{s,\sigma'}(\mathbf{n}) + R_{r,\sigma'}(\mathbf{n}) R_{s,\sigma}(\mathbf{n})\Big].
\end{aligned} \tag{6.39}$$

Up to a shift of the start point of the time step, this is identical to Eq. (6.10).

As explained in Section 6.4.2, the sums over σ become integrals when the environment takes continuous states. We then find Eq. (6.30).

When the environmental space is discrete, we can use Eq. (6.7) and find

$$\begin{aligned}\left\langle \overline{R}_r(\mathbf{n})\overline{R}_s(\mathbf{n})\right\rangle =&\frac{1}{\Delta t^2}\sum_{\sigma\sigma'}\int_0^{\Delta t}\mathrm{d}t_1\int_{t_1}^{\Delta t}\mathrm{d}t_2\ \rho^*_\sigma\rho^*_{\sigma'}\Big[R_{r,\sigma}(\mathbf{n})R_{s,\sigma'}(\mathbf{n})+R_{r,\sigma'}(\mathbf{n})R_{s,\sigma}(\mathbf{n})\Big]\\ &+\frac{1}{\Delta t^2}\sum_{\sigma\sigma'}\sum_{\ell=2}^{M}\int_0^{\Delta t}\mathrm{d}t_1\int_{t_1}^{\Delta t}\mathrm{d}t_2\ \rho^*_\sigma c_{\ell,\sigma}v_{\ell,\sigma'}e^{-\lambda\mu_\ell(t_2-t_1)}\\ &\times\Big[R_{r,\sigma}(\mathbf{n})R_{s,\sigma'}(\mathbf{n})+R_{r,\sigma'}(\mathbf{n})R_{s,\sigma}(\mathbf{n})\Big]\\ =&R_{r,\mathrm{avg}}(\mathbf{n})R_{s,\mathrm{avg}}(\mathbf{n})\\ &+\frac{1}{\Delta t^2}\sum_{\sigma\sigma'}\sum_{\ell=2}^{M}\rho^*_\sigma c_{\ell,\sigma}v_{\ell,\sigma'}\Big[R_{r,\sigma}(\mathbf{n})R_{s,\sigma'}(\mathbf{n})+R_{r,\sigma'}(\mathbf{n})R_{s,\sigma}(\mathbf{n})\Big]\\ &\times\int_0^{\Delta t}\mathrm{d}t_1\int_{t_1}^{\Delta t}\mathrm{d}t_2\ e^{\lambda\mu_\ell(t_2-t_1)}.\end{aligned}\tag{6.40}$$

6.8 Appendix B: Further details for systems with two species and two environmental states

The case of two species and two environmental states ($S=2, M=2$) was studied in [38], and a simple version of the τFE algorithm was presented for this restricted case. We assume σ switches from state 0 to state 1 with rate λk_1, and from 1 to 0 with rate λk_0. The environmental transition matrix then becomes

$$\mathbf{A}=\begin{pmatrix}-k_1 & k_0\\ k_1 & -k_0\end{pmatrix},\tag{6.41}$$

whose eigenvalues are $\mu_1=0$ and $\mu_2=-(k_0+k_1)$. The respective eigenvectors take the form

$$\mathbf{v}_1=\boldsymbol{\rho}^*=\frac{1}{k_0+k_1}\begin{pmatrix}k_0\\ k_1\end{pmatrix}\quad\text{and}\quad\mathbf{v}_2=\begin{pmatrix}1\\ -1\end{pmatrix},\tag{6.42}$$

where $\boldsymbol{\rho}^*$ has been normalised to represent the stationary distribution for σ. The coefficients $c_{2,0}$ and $c_{2,1}$ are obtained from Eq. (6.6), for the initial conditions $\boldsymbol{\rho}(0)=(1,0)$ and $\boldsymbol{\rho}(0)=(0,1)$. We find

$$c_{2,0}=\frac{k_1}{k_0+k_1}\quad\text{and}\quad c_{2,1}=\frac{-k_0}{k_0+k_1}.\tag{6.43}$$

Putting all together in Eq. (6.13), and after straightforward calculations we arrive at

$$\Xi_{rs}\equiv\left\langle \overline{R}_r(\mathbf{n})\overline{R}_s(\mathbf{n})\right\rangle-R^*_r(\mathbf{n})R^*_s(\mathbf{n})=\frac{\theta^2}{\lambda\Delta t}\left[R_{r,1}(\mathbf{n})-R_{r,0}(\mathbf{n})\right]\left[R_{s,1}(\mathbf{n})-R_{s,0}(\mathbf{n})\right],\tag{6.44}$$

where $\theta^2 = 2k_0k_1/(k_0+k_1)^3$. The indices r and s stand for reactions affected by the environment. As explained in Section 6.2.3, to simulate the τFE algorithm we need to draw correlated Gaussian random numbers $\overline{R}_r$ with means

$$R_r^*(\mathbf{n}) = \frac{k_0 R_{r,0} + k_1 R_{r,0}}{k_0 + k_1}, \tag{6.45}$$

for $r = 1, 2$, and covariance matrix

$$\mathbf{\Sigma} = \begin{pmatrix} \Xi_{11} & \Xi_{12} \\ \Xi_{21} & \Xi_{22} \end{pmatrix}. \tag{6.46}$$

One way to do this is by drawing independent Gaussian random numbers z_1 and z_2 with mean zero and unit variance, and then to set

$$\begin{pmatrix} \overline{R}_1(\mathbf{n}) \\ \overline{R}_2(\mathbf{n}) \end{pmatrix} = \begin{pmatrix} R_1^*(\mathbf{n}) \\ R_2^*(\mathbf{n}) \end{pmatrix} + \mathbf{C} \begin{pmatrix} z_1 \\ z_2 \end{pmatrix}, \tag{6.47}$$

with a matrix $\mathbf{C}$ that fulfils $\mathbf{C}\mathbf{C}^T = \mathbf{\Sigma}$, where T denotes the transpose. This matrix is not unique. We use

$$\mathbf{C} = \frac{\mathbf{\Sigma}}{\sqrt{\theta^2/(\lambda\Delta t)\left\{\left[R_{1,1}(\mathbf{n}) - R_{1,0}(\mathbf{n})\right]^2 + \left[R_{2,1}(\mathbf{n}) - R_{2,0}(\mathbf{n})\right]^2\right\}}}. \tag{6.48}$$

6.9 Appendix C: Birth-death process with two species and three environmental states

In the example in Sec. 6.3.2 we have the following transition matrix for the environmental process

$$\mathbf{A} = \begin{pmatrix} -k_1 & 0 & k_0 \\ k_1 & -k_2 & 0 \\ 0 & k_2 & -k_0 \end{pmatrix}. \tag{6.49}$$

The eigenvalues of this matrix are

$$\mu_1 = 0, \quad \mu_2 = -\frac{1}{2}\left(k_0 + k_1 + k_2 + \Gamma\right), \quad \text{and,} \quad \mu_3 = -\frac{1}{2}\left(k_0 + k_1 + k_2 - \Gamma\right), \tag{6.50}$$

with $\Gamma = \sqrt{k_0^2 + k_1^2 + k_2^2 - 2(k_0k_1 + k_1k_2 + k_2k_0)}$. The associated eigenvectors take the form

$$\mathbf{v}_1 = \boldsymbol{\rho}^* = \frac{1}{k_0k_1 + k_1k_2 + k_2k_0} \begin{pmatrix} k_2k_0 \\ k_0k_1 \\ k_1k_2 \end{pmatrix}, \tag{6.51}$$

and

$$\mathbf{v}_2 = \begin{pmatrix} (-k_0+k_1-k_2+\Gamma)/(2k_2) \\ (k_0-k_1-k_2-\Gamma)/(2k_2) \\ 1 \end{pmatrix}, \qquad \mathbf{v}_3 = \begin{pmatrix} (-k_0+k_1-k_2-\Gamma)/(2k_2) \\ (k_0-k_1-k_2+\Gamma)/(2k_2) \\ 1 \end{pmatrix}. \tag{6.52}$$

Using Eq. (6.6) and three sets of initial conditions (each concentrated on one environmental state) we find

$$c_{2,0} = \frac{k_1k_2\,(k_0+k_1+k_2-\Gamma)}{2\Gamma(k_0k_1+k_1k_2+k_2k_0)}, \quad c_{3,0} = -\frac{k_1k_2\,(k_0+k_1+k_2+\Gamma)}{2\Gamma(k_0k_1+k_1k_2+k_2k_0)}, \tag{6.53}$$

as well as

$$c_{2,1} = -\frac{k_2\,(k_0(k_1+2k_2)+k_1\,(-k_1+k_2+\Gamma))}{2\Gamma(k_0k_1+k_1k_2+k_2k_0)}, \tag{6.54}$$

$$c_{3,1} = \frac{k_2\,(k_0(k_1+2k_2)+k_1\,(-k_1+k_2-\Gamma))}{2\Gamma(k_0k_1+k_1k_2+k_2k_0)}, \tag{6.55}$$

and finally

$$c_{2,2} = \frac{k_0\,(-k_1^2-k_2^2+k_0(k_1+k_2)+k_1\Gamma+k_2\Gamma)}{2\Gamma(k_0k_1+k_1k_2+k_2k_0)}, \tag{6.56}$$

$$c_{3,2} = \frac{k_0\,(k_1^2+k_2^2-k_0(k_1+k_2)+k_1\Gamma+k_2\Gamma)}{2\Gamma(k_0k_1+k_1k_2+k_2k_0)}. \tag{6.57}$$

Putting all together in Eqs. (6.2) and (6.13) and after further tedious but straightforward calculations, we arrive at the expressions in Eqs. (6.18) and (6.19).

In order to draw the correlated Gaussian random numbers $\bar{\alpha}$ and $\bar{\beta}$ required for the τ-leaping step, we proceed as in Appendix 6.8. We construct the covariance matrix $\mathbf{\Sigma}$ [Eq. (6.46)] and then find a matrix $\mathbf{C}$ such that $\mathbf{C}\mathbf{C}^T = \mathbf{\Sigma}$. We then draw independent Gaussian random numbers z_1 and z_2 with mean zero and unit variance, and use an expresion analogous to that in Eq. (6.47) to obtain $\bar{\alpha}$ and $\bar{\beta}$. The matrix $\mathbf{C}$ we use is

$$\mathbf{C} = A \begin{pmatrix} \dfrac{\sigma_{\alpha\alpha}+B}{\sigma_{\alpha\beta}} & 1 \\ 1 & \dfrac{\sigma_{\beta\beta}+B}{\sigma_{\alpha\beta}} \end{pmatrix}, \tag{6.58}$$

with $\sigma_{\alpha\alpha}$ and $\sigma_{\alpha\beta}$ as given in Eq. (6.19), and

$$A = \frac{\sigma_{\alpha\beta}}{\sqrt{\sigma_{\alpha\alpha}+\sigma_{\beta\beta}+B}}, \tag{6.59}$$

and

$$B = \frac{\sqrt{3}k_0k_1k_2}{\lambda\Delta t(k_0k_1+k_1k_2+k_2k_0)^2} \times |\alpha_0(\beta_2-\beta_1)+\alpha_1(\beta_0-\beta_2)+\alpha_2(\beta_1-\beta_0)|. \tag{6.60}$$

6.10 Appendix D: Bimodal genetic switch

For the model in Sec. 6.3.3 the rates of the environmental transitions depend on the number of proteins n_P in the population. We assume that n_P remains constant during each τ-leaping step. The environmental transition matrix then becomes

$$\mathbf{A} = \begin{pmatrix} -\tilde{k}_+ & k_- & 0 \\ \tilde{k}_+ & -\tilde{k}_+ - k_- & k_- \\ 0 & \tilde{k}_+ & -k_- \end{pmatrix}, \tag{6.61}$$

with $\tilde{k}_+ = k_+ n_P/\Omega$. The eigenvalues of this matrix are

$$\mu_1 = 0, \quad \mu_2 = -k_- - \tilde{k}_+ - \sqrt{k_-\tilde{k}_+}, \quad \mu_3 = -k_- - \tilde{k}_+ + \sqrt{k_-\tilde{k}_+}, \tag{6.62}$$

while the associated eigenvectors take the form

$$\mathbf{v}_1 = \boldsymbol{\rho}^* = \frac{1}{k_-^2 + k_-\tilde{k}_+ + \tilde{k}_+^2} \begin{pmatrix} k_-^2 \\ k_-\tilde{k}_+ \\ \tilde{k}_+^2 \end{pmatrix},$$

$$\mathbf{v}_2 = \begin{pmatrix} \sqrt{k_-/\tilde{k}_+} \\ \left(-\sqrt{k_-} - \sqrt{\tilde{k}_+}\right)/\sqrt{\tilde{k}_+} \\ 1 \end{pmatrix}, \quad \text{and,} \quad \mathbf{v}_3 = \begin{pmatrix} -\sqrt{k_-/\tilde{k}_+} \\ \left(\sqrt{k_-} - \sqrt{\tilde{k}_+}\right)/\sqrt{\tilde{k}_+} \\ 1 \end{pmatrix}. \tag{6.63}$$

Applying Eq. (6.6) for different initial conditions as above, we obtain

$$c_{2,0} = \frac{\tilde{k}_+^{3/2}}{2\sqrt{k_-}\left(k_- + \sqrt{k_-\tilde{k}_+} + \tilde{k}_+\right)}, \quad c_{3,0} = -\frac{\tilde{k}_+^{3/2}}{2\sqrt{k_-}\left(k_- - \sqrt{k_-\tilde{k}_+} + \tilde{k}_+\right)}, \tag{6.64}$$

as well as

$$c_{2,1} = -\frac{\tilde{k}_+ + \sqrt{k_-\tilde{k}_+}}{2\left(k_- + \sqrt{k_-\tilde{k}_+} + \tilde{k}_+\right)}, \quad c_{3,1} = -\frac{\tilde{k}_+ - \sqrt{k_-\tilde{k}_+}}{2\left(k_- - \sqrt{k_-\tilde{k}_+} + \tilde{k}_+\right)}, \tag{6.65}$$

and finally

$$c_{2,2} = \frac{k_-}{2\left(k_- + \sqrt{k_-\tilde{k}_+} + \tilde{k}_+\right)}, \quad c_{3,2} = \frac{k_-}{2\left(k_- - \sqrt{k_-\tilde{k}_+} + \tilde{k}_+\right)}. \tag{6.66}$$

Putting this together in Eqs. (6.2) and (6.13) and after straightforward calculations, we arrive at the expressions in Eqs. (6.23) and (6.24).

Since only one reaction is affected by the environmental state, it is only necessary to drawn one Gaussian random number with mean b^* and variance σ_{bb} in each step of the τFE algorithm, with b^* and σ_{bb} given in Eqs. (6.23) and (6.24) respectively.

6.11 Appendix E: Gillespie algorithm with discretised environmental dynamics (GADE)

In this Appendix we briefly describe the constructions of the rates given in Eq. (6.31). They define a continuous-time dynamics on a discrete state space approximating the Ornstein–Uhlenbeck process in Eq. (6.26).

Matching the first moments of movements. We first look at the mean drift of σ, i.e., the mean change of σ per unit time. Suppose the environment is in a given state σ. The mean drift in the Ornstein–Uhlenbeck process [Eq. (6.26)] is then $\lambda(m-\sigma)$.

Suppose now the above discrete-σ process is in state $\sigma = k\Delta\sigma$. Then σ increases to $\sigma + \Delta\sigma$ with rate T_k^+ and decreases to $\sigma - \Delta\sigma$ with rate T_k^-. The expected change (per unit time) is therefore $\Delta\sigma \times (T_k^+ - T_k^-)$.

We conclude that we need to impose

$$\Delta\sigma \times (T_k^+ - T_k^-) = \lambda(m - k\Delta\sigma). \tag{6.67}$$

Matching the variance of movements. Next we look at the variance of movements of σ. For the Ornstein–Uhlenbeck process in Eq. (6.26) the second moment of movements (per unit time) is given by $2\lambda v^2$. In the discrete-σ process, the second moment of movements is $(\Delta\sigma)^2 \times (T_k^+ + T_k^-)$. To match the Ornstein–Uhlenbeck process, we then need to impose

$$(\Delta\sigma)^2 \times (T_k^+ + T_k^-) = 2\lambda v^2. \tag{6.68}$$

Overall solution. Simultaneously solving Eqs. (6.67) and (6.68) for T_k^+ and T_k^- we arrive at Eq. (6.31).

6.12 Appendix F: Additional examples of production-removal processes in continuous environments

In this Appendix we include results for the variances and covariances $\left\langle \overline{R}_r(n)\overline{R}_s(n)\right\rangle - R_r^*(\mathbf{n})R_s^*(n)$ for two further exemplar systems in which the environment follows the Ornstein–Uhlenbeck process in Eq. (6.26). We set $m = 0$ for both examples. Both systems describe production and removal dynamics of a single species. In the first

example, production and removal rates are proportional to σ when $\sigma > 0$ and zero otherwise. In the second example the rates are each proportional to $|\sigma|$. These examples are not used in the main paper, we report them here for completeness, as they may prove useful for future applications of the τFE algorithm.

6.12.1 Rates $R_{r,\sigma}(n) = \alpha_r \sigma \Theta(\sigma)$

We look at the example $R_{r,\sigma}(n) = \alpha_r \sigma \Theta(\sigma)$, where $\Theta(\sigma)$ is the Heaviside function, $\Theta(\sigma) = 1$ for $\sigma > 0$ and $\Theta(\sigma) = 0$ otherwise. For $m = 0$, we find

$$R_r^*(n) = \alpha_r \frac{v}{\sqrt{\pi}}, \tag{6.69}$$

and

$$\begin{aligned}
&\left\langle \overline{R}_r(n)\overline{R}_s(n)\right\rangle - R_r^*(n)R_s^*(n) = \\
&\frac{\alpha_r\alpha_s v^2}{24\pi\Delta t^2}\Bigg\{\frac{1}{\lambda^2}\left[24\pi\left(\lambda\Delta t - 1\right) - \pi^2 + 12\log^2(2)\right] + \frac{4e^{-\lambda\Delta t}}{\lambda^2}\Bigg[3\left(6\sqrt{e^{2\lambda\Delta t}-1}+\pi\right) \\
&- 4e^{\lambda\Delta t}\log\left(\sqrt{e^{2\lambda\Delta t}-1}+e^{\lambda\Delta t}\right) + 6\tan^{-1}\left(\frac{1}{\sqrt{e^{2\lambda\Delta t}-1}}\right)\Bigg] - \frac{32}{\lambda^2}\mathrm{Re}\left(i\sin^{-1}\left(e^{\lambda\Delta t}\right)\right) \\
&- 6\Bigg[\frac{1}{\lambda^2}\log^2\left(\sqrt{1-e^{-2\lambda\Delta t}}+1\right) + \frac{4\Delta t}{\lambda}\log\left(\sqrt{1-e^{-2\lambda\Delta t}}+1\right) - \frac{4\Delta t\log(2)}{\lambda} \\
&- \frac{\log(4)}{\lambda^2}\log\left(\sqrt{1-e^{-2\lambda\Delta t}}+1\right) - \frac{4\Delta t}{\lambda}\tanh^{-1}\left(e^{-\lambda\Delta t}\sqrt{e^{2\lambda\Delta t}-1}\right) \\
&- \frac{2}{\lambda^2}\mathrm{Li}_2\left(\frac{1}{2}\left(1-\sqrt{1-e^{-2\lambda\Delta t}}\right)\right) + \frac{\log^2(2)}{\lambda^2} + 2\Delta t^2\Bigg] - 24\Bigg\},
\end{aligned} \tag{6.70}$$

where $\mathrm{Re}(\cdot)$ denotes the real part, and $\mathrm{Li}_2(\cdot)$ is the polylogarithm of order 2.

6.12.2 Rates $R_{r,\sigma}(n) = \alpha_r |\sigma|$

For this case (and setting again $m = 0$), we find

$$R_r^*(n) = \alpha_r \frac{2v}{\sqrt{\pi}}, \tag{6.71}$$

and

$$\left\langle \overline{R}_r(n)\overline{R}_s(n)\right\rangle - R_r^*(\mathbf{n})R_s^*(n) =$$
$$\frac{\alpha_r\alpha_s v^2}{6\pi\Delta t^2}\Bigg\{\frac{12\Delta t}{\lambda}\left[-2\log\left(\sqrt{1-e^{-2\lambda\Delta t}}+1\right)+2\tanh^{-1}\left(\sqrt{1-e^{-2\lambda\Delta t}}\right)+\pi+\log(4)\right]$$
$$+\frac{1}{\lambda^2}\Bigg[72e^{-\lambda\Delta t}\sqrt{e^{2\lambda\Delta t}-1}-6\log^2\left(\frac{1}{2}\left(\sqrt{1-e^{-2\lambda\Delta t}}+1\right)\right)$$
$$+24e^{-\lambda\Delta t}\tan^{-1}\left(\frac{1}{\sqrt{e^{2\lambda\Delta t}-1}}\right)-48\tanh^{-1}\left(e^{-\lambda\Delta t}\sqrt{e^{2\lambda\Delta t}-1}\right)$$
$$+12\mathrm{Li}_2\left(\frac{1}{2}\left(1-\sqrt{1-e^{-2\lambda\Delta t}}\right)\right)-\pi^2-12\pi+12\log^2(2)\Bigg]-12\left(\Delta t^2+2\right)\Bigg\}. \tag{6.72}$$

Bibliography

[1] J. D. Murray, *Mathematical Biology I. An Introduction*, 3rd ed., Vol. 17, Interdisciplinary Applied Mathematics (Springer, New York, 2002).

[2] J. D. Murray, *Mathematical Biology II: Spatial Models and Biomedical Applications*, Vol. 18, Interdisciplinary Applied Mathematics (Springer, New York, 2003).

[3] N. S. Goel, and N. Richter-Dyn, *Stochastic Models in Biology* (The Blackburn Press, 2004).

[4] W. Ewens, *Mathematical Population Genetics 1* (Springer-Verlag, New York, 2004).

[5] A. Traulsen, and C. Hauert, "Stochastic Evolutionary Game Dynamics", in *Reviews of Nonlinear Dynamics and Complexity* (Wiley-VCH Verlag GmbH and Co. KGaA, 2010), pp. 25–61.

[6] C. Castellano, S. Fortunato, and V. Loreto, "Statistical physics of social dynamics", Reviews of Modern Physics **81**, 591–646 (2009).

[7] M. J. Keeling, and P. Rohani, *Modeling Infectious Diseases in Humans and Animals* (Princeton University Press, 2008).

[8] N. V. Kampen, *Stochastic processes in physics and chemistry* (North Holland, 2007).

[9] M. Acar, J. T. Mettetal, and A. Van Oudenaarden, "Stochastic switching as a survival strategy in fluctuating environments", Nature Genetics **40**, 471–475 (2008).

[10] P. Patra, and S. Klumpp, "Emergence of phenotype switching through continuous and discontinuous evolutionary transitions", Physical Biology **12**, 046004 (2015).

[11] K. Wienand, E. Frey, and M. Mobilia, "Evolution of a Fluctuating Population in a Randomly Switching Environment", Physical Review Letters **119**, 158301 (2017).

[12] E. Wienand, K .and Frey and M. M., "Eco-evolutionary dynamics of a population with randomly switching carrying capacity", Journal of The Royal Society Interface **15**, 20180343 (2018).

[13] A. Taitelbaum, R. West, M. Assaf, and M. Mobilia, "Population Dynamics in a Changing Environment: Random versus Periodic Switching", Physical Review Letters **125**, 048105 (2020).

[14] A. J. Black, and A. J. McKane, "Stochastic amplification in an epidemic model with seasonal forcing", Journal of Theoretical Biology **267**, 85–94 (2010).

[15] C. W. Gardiner, *Handbook of stochastic methods for physics, chemistry and the natural sciences*, Third, Vol. 13, Springer Series in Synergetics (Springer-Verlag, Berlin, 2004).

[16] E. Kussell, and S. Leibler, "Phenotypic diversity, population growth, and information in fluctuating environments", Science **309**, 2075–2078 (2005).

[17] T. B. Kepler, and T. C. Elston, "Stochasticity in transcriptional regulation: origins, consequences, and mathematical representations", Biophysical Journal **81**, 3116–3136 (2001).

[18] M. Thattai, and A. Van Oudenaarden, "Stochastic gene expression in fluctuating environments", Genetics **167**, 523–530 (2004).

[19] P. S. Swain, M. B. Elowitz, and E. D. Siggia, "Intrinsic and extrinsic contributions to stochasticity in gene expression", Proceedings of the National Academy of Sciences (USA) **99**, 12795–12800 (2002).

[20] M. Assaf, E. Roberts, Z. Luthey-Schulten, and N. Goldenfeld, "Extrinsic Noise Driven Phenotype Switching in a Self-Regulating Gene", Physical Review Letters **111**, 058102 (2013).

[21] A. Duncan, S. Liao, T. Vejchodský, R. Erban, and R. Grima, "Noise-induced multistability in chemical systems: Discrete versus continuum modeling", Physical Review E **91**, 042111 (2015).

[22] M. Assaf, M. Mobilia, and E. Roberts, "Cooperation Dilemma in Finite Populations under Fluctuating Environments", Physical Review Letters **111**, 238101 (2013).

[23] P. Ashcroft, P. M. Altrock, and T. Galla, "Fixation in finite populations evolving in fluctuating environments", Journal Royal Society Interface **11**, 20140663 (2014).

[24] R. West, M. Mobilia, and A. M. Rucklidge, "Survival behavior in the cyclic Lotka-Volterra model with a randomly switching reaction rate", Physical Review E **97**, 022406 (2018).

[25] M. Assaf, A. Kamenev, and B. Meerson, "Population extinction in a time-modulated environment", Physical Review E **78**, 041123 (2008).

[26] P. G. Hufton, Y. T. Lin, and T. Galla, "Model reduction methods for population dynamics with fast-switching environments: Reduced master equations, stochastic differential equations, and applications", Physical Review E **99**, 032122 (2019).

[27] A. Eldar, and M. Elowitz, "Functional roles for noise in genetic circuits", Nature **467**, 167–173 (2010).

[28] D. T. Gillespie, "A general method for numerically simulating the stochastic time evolution of coupled chemical reactions", Journal of Computational Physics **22**, 403–434 (1976).

[29] D. T. Gillespie, "Exact stochastic simulation of coupled chemical reactions", The Journal of Physical Chemistry **81**, 2340–2361 (1977).

[30] J. Bowen, A. Acrivos, and A. Oppenheim, "Singular perturbation refinement to quasi-steady state approximation in chemical kinetics", Chemical Engineering Science **18**, 177–188 (1963).

[31] L. A. Segel, and M. Slemrod, "The Quasi-Steady-State Assumption: A Case Study in Perturbation", SIAM Review **31**, 446–477 (1989).

[32] Y. T. Lin, and N. E. Buchler, "Efficient analysis of stochastic gene dynamics in the non-adiabatic regime using piecewise deterministic Markov processes", Journal of The Royal Society Interface **15**, 20170804 (2018).

[33] J. M. Newby, and P. C. Bressloff, "Quasi-steady State Reduction of Molecular Motor-Based Models of Directed Intermittent Search", Bulletin of Mathematical Biology **72**, 1840–1866 (2010).

[34] P. C. Bressloff, "Stochastic Fokker-Planck equation in random environments", Physical Review E **94**, 042129 (2016).

[35] P. C. Bressloff, "Stochastic Liouville equation for particles driven by dichotomous environmental noise", Physical Review E **95**, 012124 (2017).

[36] P. C. Bressloff, "Feynman-Kac formula for stochastic hybrid systems", Physical Review E **95**, 012138 (2017).

[37] D. T. Gillespie, "Approximate accelerated stochastic simulation of chemically reacting systems", The Journal of Chemical Physics **115**, 1716–1733 (2001).

[38] P. G. Hufton, Y. T. Lin, and T. Galla, "Classical stochastic systems with fast-switching environments: Reduced master equations, their interpretation, and limits of validity", Physical Review E **99**, 032121 (2019).

[39] P. C. Bressloff, and J. M. Newby, "Path integrals and large deviations in stochastic hybrid systems", Physical Review E **89**, 042701 (2014).

[40] P. G. Hufton, Y. T. Lin, T. Galla, and A. J. McKane, "Intrinsic noise in systems with switching environments", Physical Review E **93**, 052119 (2016).

[41] J. Gunawardena, "Time-scale separation – Michaelis and Menten's old idea, still bearing fruit", The FEBS Journal **281**, 473–488 (2014).

[42] N. E. Buchler, U. Gerland, and T. Hwa, "On schemes of combinatorial transcription logic", Proceedings of the National Academy of Sciences (USA) **100**, 5136–5141 (2003).

[43] Y. T. Lin, and N. E. Buchler, "Efficient analysis of stochastic gene dynamics in the non-adiabatic regime using piecewise deterministic Markov processes", Journal Royal Society Interface **15** (2018).

[44] B. Fuglede, and F. Topsoe, "Jensen-Shannon divergence and Hilbert space embedding", in International Symposium on Information Theory, 2004. Proceedings. (2004), p. 31.

[45] J. Lin, "Divergence measures based on the Shannon entropy", IEEE Transactions on Information Theory **37**, 145 (1991).

[46] Y. T. Lin, P. G. Hufton, E. J. Lee, and D. A. Potoyan, "A stochastic and dynamical view of pluripotency in mouse embryonic stem cells", PLOS Computational Biology **14**, 1–24 (2018).

[47] E. Roberts, S. Be'er, C. Bohrer, R. Sharma, and M. Assaf, "Dynamics of simple gene-network motifs subject to extrinsic fluctuations", Physical Review E **92**, 062717 (2015).

[48] F. C. Klebaner, *Introduction to stochastic calculus with applications* (World Scientific Publishing Company, Singapore, 2005).

[49] H. Risken, "Fokker-planck equation", in *The Fokker-Planck Equation* (Springer, 1996), pp. 63–95.

[50] G. Maruyama, "Continuous Markov processes and stochastic equations", Rendiconti del Circolo Matematico di Palermo **4**, 48 (1955).

[51] P. W. Lewis, and G. S. Shedler, "Simulation of nonhomogeneous Poisson processes by thinning", Naval Research Logistics Quarterly **26**, 403–413 (1979).

Chapter 7

Conclusions

7.1 Overview of the thesis

Throughout this thesis, we have explored several biological scenarios subject to different types of changing environments. We have studied these systems using methods from stochastic processes, applying tools from mathematics and physics by using a number of theoretical, numerical and experimental frameworks.

Broadly speaking, the study carried out in this thesis can be divided into two main groups: the first one, composed of Chapters 3 and 4, focused on the study of the evolution of resistance in cell populations subject to drug therapies of one or two drugs. The environment in these systems (which specified the drug concentrations applied) varied deterministically. The second group, composed of Chapters 5 and 6, focused on the study of fluctuating environments in different biological contexts. We explored both discrete and continuous environments.

Although the focus on each chapter was similar, i.e., the study of the effect of environments on biological systems, the approach used in each of them was different. In Chapter 3, we analysed experimental data by comparing it against numerical simulations of a stochastic model we developed. In Chapters 4 and 5, we adopted a more theoretical point of view, focussing on developing methods to formulate theoretical predictions. In Chapter 6, the focus was on the optimisation of simulations of stochastic systems.

All in all, the stochastic methods we developed allowed us to deduce relevant features of the different contexts we studied. The results from Chapters 3 and 4, for example, are of potential interest in clinical treatments to prevent the spread

of resistance. The findings from Chapter 5 are pertinent in evolutionary biology to understand the evolution of mating types in isogamous species with synchronous sex. Lastly, the results from Chapter 6 allow a more effective numerical studies of biological systems in fast fluctuating environments.

We present below a summary of the results of each Chapter, focusing on achievements obtained with the different methods we employed, the challenges each system presented, and the relevance of our findings.

7.2 Summary of results

Chapter 3: Mutators drive evolution of multi-resistance to antibiotics

In this chapter, the approach employed was to develop a stochastic model that could capture the main features of an experimental setup of bacterial populations in single-drug and combination therapies. The experiments included several properties that were relevant in the emergence of resistance, such as diauxic growth, dilutions, and competition. Our model incorporated these through a framework based on the competitive Lotka-Volterra equations and individual-based variants representing these equations. Since the bacterial populations in the experiments could become large, the numerical simulations of our model became considerably slow when using standard continuous-time algorithms (e.g., Gillespie algorithm) for these cases. This occurs given the large number of events per unit time when populations are large. To deal with this problem, we developed a discrete-time numerical scheme using binomial distributions that sped up the simulations without losing significant precision.

Overall, the predictions of our approach showed a good agreement with experimental observations. The proportion of resistant bacteria, for example, was qualitatively similar to experiments. Both experiments and simulations showed that the presence of mutators allows multi-drug resistance to evolve during single-drug and combination therapies, suggesting that direct selection is not necessary for multi-drug resistance to occur during both therapies. These results are of potential clinical relevance as they suggest that combination therapy may not necessarily prevent the emergence of resistance in infections with higher mutation rates, which are fairly common in real-life situations.

The implementation of stochastic modelling in this study brought an additional

perspective of the behaviour of the system in terms of interactions between individuals. Our model, for example, does not consider the possibility of mutating directly from sensitive to double resistant strains, showing that sequential acquisition of multi-drug resistance can be a valid mechanism of resistance evolution. Besides, the numerical scheme developed here may allow us to design additional experimental setups by previously exploring the system evolution for different parameters in a fast way.

Chapter 4: Competition delays multi-drug resistance evolution during combination therapy

In this chapter, the approach we employed was to develop a theoretical framework to calculate the probability of resistance of a population in combination therapy of two drugs assuming three growth models: exponential, logistic, and competitive logistic. Our approach was based on multi-branching non-homogeneous processes, using as starting point the work by Foo and Michor for an exponential growth model [1]. In our analysis, we achieved to deduce analytical results for exponential growth models that had not been previously reported. We adapted Foo and Michor's framework for the logistic models, which required the calculation of their extinction probabilities of simple birth-death processes. The computation of the probabilities of resistance required the developing of strategies to calculate numerically the integrals involved in a fast way. The predictions of our model were tested against numerical simulations carried out using the Gillespie algorithm for constant drug treatments, and the Lewis' thinning algorithm for time-dependent drug treatments.

Our theoretical/numerical framework allowed us to show the delaying effect of competition on the emergence of resistance. We were able to not only to explore a wide range of parameters of the system, but also to explore the effect of clinical-based dosing schedules. Our results showed that the optimum treatment, i.e., the one that maximises the typical time of emergence of resistance, depends on the type of the growth model chosen. In particular, we showed that when competition is present, the optimum treatment is found when both drugs are completely out of phase. This result has been reported in similar contexts (see e.g., [2]). These results suggest that how a particular infection grows and competes with others could have important implications for designing clinical treatments aimed at combatting resistance evolution

Chapter 5: Switching environments, synchronous sex, and the evolution of mating types

In this chapter, we adopted a theoretical approach that combined calculations from branching processes and methods from number theory in the estimation of the stationary distribution of the number of mating types in different environmental switching regimes. As a starting point, we used a model developed by Constable and Kokko [3]. The first focus of this study was the case of non-switching environments in which we exploited properties of partitions of integer numbers for the estimation of the production and removal rates of the number of mating types. Our method allowed us to deduce exact analytical solutions by assuming the system was in its stationary state. These results had not been previously reported. The production and annihilation rates were then inserted in a switching environmental framework of two environments: sexual and asexual reproduction. For the different switching regimes we studied, we found that our approach was appropriate for slow and fast switching environments. For the former regime, the distribution of mating types was estimated as the weighted average of the non-switching distributions in each environment; for the latter, we found the system behaves as if it was in an effective non-switching environment. For intermediate switching environments, however, we found limitations in our approach due to the slow relaxation to the stationary state in the asexual environment. This meant we could not assume an stationary regime for this environment.

Our findings are of relevance for the study of mating types in evolutionary biology. Our results show that the consideration of synchronous sex can show significant differences in the expected number of mating types with respect to asynchronous sexual cases which most of studies assume. In particular, we proved that both cases are only equivalent in the fast switching regime. Our model, on the other hand, allows the accounting of other scenarios such as the inclusion of selective sweeps, which are pertinent in the mating type extinction of some facultatively sexual species (i.e., species that are able to reproduce both sexually and asexually).

Chapter 6: Beyond the adiabatic limit in systems with fast environments: a τ-leaping algorithm

In this chapter, we focused on the design of a numerical scheme to simulate systems in fast fluctuating environments in regimes beyond the adiabatic limit. Both discrete and continuous environments were studied. We based our scheme on the well-known $\tau-$leaping algorithm [4], using as starting point the approach developed in [5] for a simple case of two environments. In our study, we extended this approach to a general case of an arbitrary number of environments and reactions. Our algorithm requires the calculation of first and second moments of Gaussian random variables that work as input rates for the reactions coupled to the environmental process. Analytical solutions were found for these quantities in all the models we studied, both for discrete and continuous environmental spaces. For the latter case, we assumed the environment followed an Ornstein–Uhlenbeck process. This is not a requirement for our algorithm, but we chose it given the usefulness of this process in biological systems. We tested our algorithm against standard algorithms. For discrete environments we used the Gillespie algorithm. For continuous environments, we designed a number of algorithms based on well-known approaches. These algorithms required special attention on the discretisation used for the environmental states and time in order to find a balance between simulation speed and precision. In all the cases we studied, our algorithm proved to be faster.

Having an algorithm to simulate systems in fast fluctuating environments in a fast way is a useful tool for the study of biological systems. Our algorithm can be implemented in an easy way, only requiring to previously have calculated the first and second moments for the input rates which does not suppose in itself a major challenge. In fact, the cases we studied could be adapted to other similar biological scenarios without having to calculate the rates again.

7.3 Future research and final remarks

In this thesis we have characterised several biological systems using stochastic processes. Our findings open new interesting possible research directions in the different scenarios we have studied. Our study of multi-drug resistance in Chapters 3 and 4, for example,

has shown the relevance of accounting high mutation rates within a population as well as competition between strains, two factors that are relevant in common infections [6–9]. This study could improve the design of combination treatment strategies to effectively suppress the emergence of resistance. The study of the probability of resistance in Chapter 4 also opens the question about the role of more realistic situations in the emergence of resistance, e.g., heterogeneous competition [10] or heterogeneity of the mutation rate [11], or the effect of therapies with more than two drugs. Other possible direction of this study is the accounting for other mechanisms of resistance such as plasmids [12]. On a related subject, the modelling of the experimental setup used in Chapter 3 leaves some interesting questions about the effect of dilutions (i.e., population bottlenecks) on the growth of populations. Dilutions are commonly used in experiments and also occur due to natural effects [13]. Progress has been done in this direction [14] in simple models, which could serve as a starting point for the types of models we have studied.

The results from Chapter 5 left some unanswered questions about the characterisation of systems in intermediate switching environments. Our study puts in evidence the challenge of studying these regimes and the need of developing a theoretical framework to fully understanding evolution of facultatively sexual species. On the other hand, the methods developed using number theory in this Chapter could contribute to the study of other similar systems. Such is the case of the voter model whose structure resembles our model of mating types evolution [15]. Our methods provide a useful way to calculate the reduced transition rates of between its states in more complex cases, for example, that include mutations (i.e., new types added). The alternative methods presented in Sec. 5.3.3 could contribute to the developing of strategies for the studying of similar systems in switching environments.

The different algorithms for continuous environments in fluctuating environments we constructed in Chapter 6 (see GADE and DEED in Sec. 6.4.3) could serve as a starting point of the design of other algorithms in more complicated systems. Our algorithms do not necessarily require the fluctuating environment to be fast so they could be adapted to diverse situations.

On the whole, this thesis illustrates the utility of stochastic processes for studying biological populations in changing environments. Generally speaking, developing

strategies for studying the effect of environments is not restricted to a particular collection of methods but rather depends on the system under study and the type of description we want to make about it. Normally one does not approach a problem of changing environments using a standard procedure but uses methods from diverse disciplines, sometimes being able to obtain analytical results, or requiring to perform experiments, or being able to characterise a system only through simulations. This thesis promotes the utility of diverse tools in the study of biological systems. We have approached this by not limiting ourselves to one particular type of methods but have exploited tools from mathematics, physics, experimental biology, and computer simulations.

The study of the effect of deterministic and stochastic environments carried out in this thesis has resulted in a better understanding of the effect of surroundings in biological populations. Changing environments are complex but must be taken into account when trying to understand the behaviour of a biological population. Whether they vary deterministically or stochastically, or whether they are better described using discrete or continuous spaces, their effect is not something we can ignore. Given the complexity of changing environments and the diversity of their effect on biological populations, much of the mathematical modelling of them is a work in progress. It is my hope that the methods and approaches developed here will contribute to this progress and prove useful in applications of systems in changing environments.

Bibliography

[1] J. Foo, and F. Michor, "Evolution of resistance to anti-cancer therapy during general dosing schedules", Journal of Theoretical Biology **263**, 179–188 (2010).

[2] R. Peña-Miller, D. Lähnemann, H. Schulenburg, M. Ackermann, and R. Beardmore, "The optimal deployment of synergistic antibiotics: a control-theoretic approach", Journal of The Royal Society Interface **9**, 2488–2502 (2012).

[3] G. W. Constable, and H. Kokko, "The rate of facultative sex governs the number of expected mating types in isogamous species", Nature Ecology & Evolution **2**, 1168 (2018).

[4] D. T. Gillespie, "Approximate accelerated stochastic simulation of chemically reacting systems", The Journal of Chemical Physics **115**, 1716–1733 (2001).

[5] P. G. Hufton, Y. T. Lin, and T. Galla, "Model reduction methods for population dynamics with fast-switching environments: Reduced master equations, stochastic differential equations, and applications", Physical Review E **99**, 032122 (2019).

[6] I. Chopra, A. J. O'Neill, and K. Miller, "The role of mutators in the emergence of antibiotic-resistant bacteria", Drug Resistance Updates **6**, 137–145 (2003).

[7] K. Miller, A. J. O'Neill, and I. Chopra, "*Escherichia coli* mutators present an enhanced risk for emergence of antibiotic resistance during urinary tract infections", Antimicrobial Agents and Chemotherapy **48**, 23–29 (2004).

[8] N. Mideo, "Parasite adaptations to within-host competition", Trends in Parasitology **25**, 261–268 (2009).

[9] F. Wang, Z. Ma, and Y. Shag, "A competition model of HIV with recombination effect", Mathematical and Computer Modelling **38**, 1051–1065 (2003).

[10] M. E. Hibbing, C. Fuqua, M. R. Parsek, and S. B. Peterson, "Bacterial competition: surviving and thriving in the microbial jungle", Nature Reviews Microbiology **8**, 15 (2010).

[11] H. K. Alexander, S. I. Mayer, and S. Bonhoeffer, "Population heterogeneity in mutation rate increases the frequency of higher-order mutants and reduces long-term mutational load", Molecular Biology and Evolution **34**, 419–436 (2017).

[12] M. Santer, and H. Uecker, "Evolutionary rescue and drug resistance on multicopy plasmids", Genetics (2020).

[13] T. Wein, and T. Dagan, "The effect of population bottleneck size and selective regime on genetic diversity and evolvability in bacteria", Genome biology and evolution **11**, 3283–3290 (2019).

[14] L. M. Wahl, P. J. Gerrish, and I. Saika-Voivod, "Evaluating the impact of population bottlenecks in experimental evolution", Genetics **162**, 961–971 (2002).

[15] F. Herrerías-Azcué, and T. Galla, "Consensus and diversity in multistate noisy voter models", Physical Review E **100**, 022304 (2019).